Small scale motors : fabrication, characterizations, motions studies and applications

Zhao, Guanjia

2014

Zhao, G. (2014). Small scale motors : fabrication, characterizations, motions studies and applications. Doctoral thesis, Nanyang Technological University, Singapore.

https://hdl.handle.net/10356/62258

https://doi.org/10.32657/10356/62258

NANYANG TECHNOLOGICAL UNIVERSITY

SMALL SCALE MOTORS: FABRICATION, CHARACTERIZATIONS, MOTIONS STUDIES AND APPLICATIONS

ZHAO GUANJIA

SCHOOL OF PHYSICAL AND MATHEMATICAL SCIENCES

NANYANG TECHNOLOGICAL UNIVERSITY

2014

SMALL SCALE MOTORS: FABRICATION, CHARACTERIZATIONS, MOTIONS STUDIES AND APPLICATIONS

ZHAO GUANJIA

2014

SMALL SCALE MOTORS: FABRICATION, CHARACTERIZATIONS, MOTIONS STUDIES AND APPLICATIONS

ZHAO GUANJIA

School of Physical and Mathematical Sciences

A thesis submitted to the Nanyang Technological University
in partial fulfillment of the requirement for the degree of
Doctor of Philosophy

2014

Acknowledgement

This thesis is not possible without the guidance and help from many people, and I would like to take this opportunity to express my sincere thanks to them.

First of all, I would like to express my deepest gratitude to my supervisor, Nanyang Assistant Professor Martin Pumera, for his abundant support and invaluable guidance all along the way. Deepest gratitude is also due to his persistent spirit to difficulties, rigorous attitude to work, and great passion to research, which inspired me to aggressively pursue knowledge and truth in Chemistry. His contagious scientific optimism is both refreshing and inspiring; his trust, concerns and encouragements allowed me to devote all my energy into research.

I would also like to express my deepest appreciation to Dr. Adriano Ambrosi and Dr. Alessandra Bonanni, for their patience and helpful discussions and advices.

It is also a great chance for me to show my gratefulness to people offered me with generous and invaluable help, both in life and in research. I would like to express my appreciation first to Dr. Chua Chun Kiang, for his solid friendship, patient and important help in life as well as in research; it has always been an enjoyable experience to work with Dr. Chua. My gratitude also goes to Miss Elaine Chng, for her truly and warm kindness in daily life, and for bringing all the happiness and joy in work. Thanks also to Miss Hwee Ling Poh for her help in research and experiments as well as the invaluable discussions in the projects, and of course for offering me a memorable experience in my Ph.D. studies.

I would also like to thank my colleagues working together with me on the small motors projects, Elijah, Wang Hong, and James. It is their abundant help and support, collaboration as well as understanding that allowed me to make achievements and enjoy the process of research. I am grateful for having such nice people to work with.

Meanwhile, I wish to take this chance to thank all other colleagues and friends too: Adeline, Rou Jun, Colin, Alex, Wei Zhe, Wang Lu, Shu Min, Zafir, for their kind assistance, suggestions and collaborations. Special thanks to Luo Jingshan, Chen Renjie and Wu Bo as well, for their help in SEM during my first year PhD study as well as the abundant collaborations and discussions in research, which were really of high importance to me. I also appreciate very much the help from the technical and academic staff from general office and teaching lab in our division.

I would like to express my deep gratitude to Assoc. Prof. Li Tianhu for opening the door of research and scientific exploration for me and for offering me the chance to see what research is about. Special thanks to Dr. Long Yi, who delivered to me generously his knowledge and skills and helped me to learn my first step in research.

Finally, my deepest gratitude goes to my beloved family, for their warm and continuous support and encouragement.

Table of Content

Abstract

In this thesis, the author describes the research work done during the four years Ph.D. study, focusing on the fabrication, motion study and possible applications of small motors, ranging from millimeter scale polymer motors to microscale and nanoscale catalytic motors.

The millimeter scale capsule motors were made from polysulfone, and a series of studies were carried out on such motors, including the factors influencing the motion, motion manipulation with magnet, cooperative behaviors, and induced motion of oil droplets. Moreover, running of such motors in water/oil interface and the maze channel was studied. Additionally, the enhanced diffusion of pollutants in the natural environment was also investigated.

The studies on the microscale and nanoscale catalytic motors were also carried out. Fabrication and characterizations of the tubular motors were realized, and magnetization was achieved for both nanomotors and micromotors. Upon magnetization, such microtubes can pick up the paramagnetic cargoes for possible delivery. Moreover, the effects of the running medium on the motion of the micromotors were also investigated.

List of Publications

1. Zhao, G.; Pumera, M., Reynolds numbers exhibit dramatic influence on directionality of movement of self-propelled systems. *Phys. Chem. Chem. Phys.* **2012**, *14*, 6456-6458.
2. Zhao, G.; Pumera, M., Liquid–liquid interface motion of a capsule motor powered by the interlayer Marangoni effect. *J. Phys. Chem. B* **2012**, *116*, 10960-10963.
3. Zhao, G.; Pumera, M., Macroscopic self-propelled objects. *Chem. – Asian J.* **2012**, *7*, 1994-2002.
4. Zhao, G.; Stuart, E. J. E.; Pumera, M., Enhanced diffusion of pollutants by self-propulsion. *Phys. Chem. Chem.Phys.* **2011**, *13*, 12755-12757.
5. Zhao, G.; Seah, T. H.; Pumera, M., External-energy-independent polymer capsule motors and their cooperative behaviors. *Chem. – Euro. J.* **2011**, *17*, 12020-12026.
6. Zhao, G.; Pumera, M., Marangoni Self-propelled capsules in a maze: pollutants 'sense and act' in complex channel environments. *Lab Chip* **2014**, *14*, 2818-2823.
7. Seah, T. H.; Zhao, G.; Pumera, M., Surfactant capsules propel interfacial oil droplets: an environmental cleanup strategy. *ChemPlusChem* **2013,** *78*, 395-397.
8. Zhao, G.; Ambrosi, A.; Pumera, M. Clean room-free rapid fabrication of roll-up self-powered catalytic microengines. *J. Mater. Chem. A.* **2014, 2**, 1219-1223.
9. Zhao, G.; Pumera, M., Concentric bimetallic microjets by electrodeposition. *RSC Advances* **2013,** *3*, 3963-3966.
10. Zhao, G.; Ambrosi, A.; Pumera, M., Self-propelled nanojets via template electrodeposition. *Nanoscale* **2013**, *5*, 1319-1324.
11. Zhao, G.; Pumera, M., Magnetotactic artificial self-propelled nanojets. *Langmuir* **2013,** 29, 7411–7415.
12. Zhao, G.; Pumera, M. Geometric asymmetry driven Janus micromotors. *Nanoscale* **2014,** *6*, 11177-11180.
13. Zhao, G.; Sanchez, S.; Schmidt, O. G.; Pumera, M., Micromotors with built-in compasses. *Chem. Commun.* **2012,** *48*, 10090-10092.
14. Zhao, G.; Wang, H.; Sanchez, S.; Schmidt, O. G.; Pumera, M. Artificial micro-cinderella based on self-propelled micromagnets for the active separation of paramagnetic particles. *Chem. Commun*. **2013,** *49*, 5147-5149.
15. Zhao, G.; Wang, H.; Khezri, B., Sanchez, S.; Schmidt, O. G.; Webster, R. D.; Pumera, M. Corrosion of self-propelled catalytic microengines. *Chem. Commun.*, **2013,** *49*, 9125-9127.
16. .Zhao, G.; Khezri, B., Webster, R. D.; Pumera, M. Influence of real-world environments on the motion of catalytic bubble-propelled micromotors. *Lab Chip* **2013,** *13*, 2937-2941.

17. Zhao, G.; Viehrig, M.; Pumera, M., Challenges of the movement of catalytic micromotors in blood. *Lab Chip* **2013,** *13*, 1930-1936.

18. Zhao, G.; Sanchez, S.; Schmidt, O. G.; Pumera, M., Poisoning of bubble propelled catalytic micromotors: the chemical environment matters. *Nanoscale* **2013,** *5*, 2909-2914.

19. Zhao, G.; Nguyen, N. T.; Pumera, M. Reynolds numbers influence the directionality of self-propelled macrojet engines in the 10^{-4} regime. *Nanoscale* **2013,** *5*, 7277-7283.

20. Bonanni, A.; Chua, C. K.; Zhao, G.; Sofer, Z.; Pumera, M., Inherently electroactive graphene oxide nanoplatelets as labels for single nucleotide polymorphism detection. *ACS Nano* **2012,** 6, 8546–8551.

21. Scott, C. L.; Zhao, G. J.; Pumera, M., Stacked graphene nanofibers doped polypyrrole nanocomposites for electrochemical sensing. *Electrochem. Commun*. **2010**, *12*, 1788-1791.

22. Wang, H.; Zhao, G.; Pumera, M., Blood electrolytes exhibit a strong influence on the mobility of artificial catalytic microengines. *Phys. Chem. Chem. Phys.* **2013,** *15*, 17277-17280.

23. Moo, J. G. S.; Wang, H.; Zhao, G.; Pumera. M., Biomimetic artificial inorganic enzyme-free self-propelled microfish robot for selective detection of Pb^{2+} in water. *Chem. Eur. J.* **2014,** *20*, 4292-4296.

24. Wang, H.; Zhao, G.; Pumera, M., Crucial role of surfactants in bubble-propelled microengines. *J. Phys. Chem. C.* **2014,** *118*, 5268-5274.

25. Wang, H.; Zhao, G.; Pumera, M., Blood metabolite strongly suppresses motion of electrochemically deposited catalytic self-propelled microjet engines. *Electrochem. Commun*. **2014,** *38*, 128-130.

26. Wang, H.; Zhao, G.; Pumera, M., Beyond Platinum: Bubble-propelled micromotors based on Ag and MnO_2 catalysts. *J. Am. Chem. Soc.* **2014,** *136*, 2719-2722.

27. Chng, E. L. K.; Zhao, G.; Pumera, M., Towards biocompatible nano/microscale machines: self-propelled catalytic nanomotors not exhibiting acute toxicity. *Nanoscale* **2014,** *6*, 2119-2124.

28. Wang, H.; Zhao, G.; Pumera, M., Blood proteins strongly reduce the mobility of artificial self-propelled micromotors. *Chem. – Euro. J.***2013,** *19*, 16756-16759.

CHAPTER ONE: INTRODUCTION

1.1 Significance of Small Scale Motors

Our Mother Nature has her smart, simple and yet powerful way of creating running stuff. From as small as protein molecules[1-4], to small insets like ants, all the way to animals, including us human beings; we are moving around busily and lively, making the world more and more efficient and organized.

It is the dream and fantasy of human being to learn from our Mother Nature and create our own moving devices that can help out with our business and errands. Starting from the bulk machines, we have built airplanes that fly like birds, we have built ships and submarines that swim like sharks, and we have built cars and trains that run out horses and leopards. But what if we wish to go down? What if we wish to perform some task that has to be done at the millimeter, micrometer, and even smaller to nanometer scales?

Let us think about an ant. This little guy has been walking around happily because he can walk as fast or slow as he wishes, he can walk to any direction assigned, he can sense the

presence of high temperature or unpleasant chemicals, and he can carry a relatively heavy cargoes back home to feed his family. But, if we are to build some motor of a size similar to this ant, are we going to be happy with it?

The research in Nanomotors and micromotors, as described by Prof. Joseph Wang in his book *Nanomachines: Fundamentals and Applications*, is at its infancy.[5] We can so much easily crush an ant into nothing but we are not able to build it. Human creatures are not that Pessimistic, on the other hand, because so far we are able to construct a wide variety of motors. Scientists have carried out the biomimetic study of cytoskeletal motor protein kinesin and their work led us to the production of nanomtors.[6] Scientists have also carried out the biomimetic of insets and such work led us to the production of moving objects at millimeter scales.[7] Showcases of such biomemmic work can be seen in Figure 1-1.

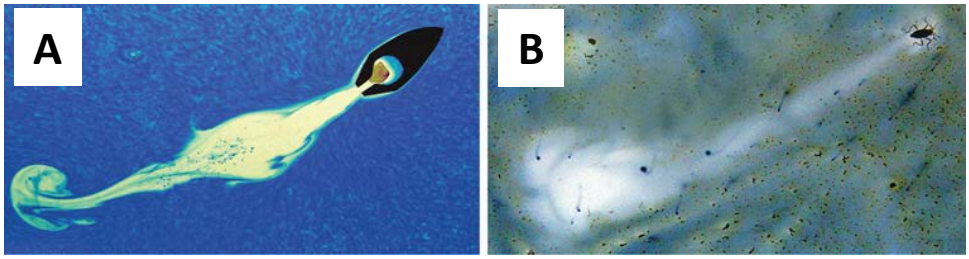

Figure 1-1 Self-propulsion for (A) a "soap boat," and (B) Microvelia. The inset microvelia can release some little amount of surface active molecules, and thus be propelled forward due to the resulted surface tension gradient. The presence of surface tension gradient in both systems can be seen in the clearing of the dye molecules from the free surface. Reprinted with permission from ref 7. Copyright (2006) from Annual Reviews.

To date, the self-propelled nano-, micro-, and millimeter scale devices are in the forefront of materials and nanotechnology research.[5,8-13] Such devices are referred to as motors

because they are able to navigate in complex environments while converting energy into mechanical motion. And due to their intrinsic small size, such motors are collectively named as small scale motors in this thesis.

For many years, it has been the perusal of scientific community to design, fabricate, and apply the self-propelled nano-, micro-, and millimeter scale devices. These devices have been proposed as potential tools for delivery of drug payloads,[14-17] transportation of cargoes,[18-20] autonomous wireless detection, sensing and biosensing,[21-24] manipulation of cells and biomolecules,[25-28] environment detection and cleaning,[13,22,29-31] and microsurgery[32]. In order for better performance of the tasks, the small motors are required not only to generate sufficient power thrust, but also to have their motion manipulated as desired. The manipulation of motion at the small scale is still a challenging and yet promising facet for the research in this field.

1.2 Aspects of Motion at Small Scales

1.2.1 Energy Sources for Small Motors

In order for the motors run, there must be some sources of energy input into the system, which is converted into mechanical motion and forces. There are two parts of destination for such input energy, namely the energy lost during the process of overcoming the frictional forces from the environment, and the kinetic power for these small motors to run. The sources of energy are possible from three origins, including input external physical energy, energy from chemical fuels, and the energy from the chemical gradient through the physicochemical processes. [29]

The externally powered motors are also referred to as “fuel-free” motors as this class of motors is powered completely by the external physical energy supplied, which is

transformed into mechanical energy.[8] The external physical energy can originate from an electric field gradient,[33-35] light,[36,37] a magnetic field,[38,39] ultrasound,[40,41] or thermal gradient.[42] Motors rely on this kind of energy supply are quite diversified in size. For example, there are magnetically powered motors whose dimensions are at the nanometer to micrometer scales,[43] as shown in Figure 1-2, and there are also macroscopic motors, with a size of around 20 mm, run with the presence of light,[37] as shown in Figure 1.3. Motors powered through this approach of energy supply usually require devices that generate and focus the external physical energy on the motors, and thus leading to a high cost for the propulsion of motion.

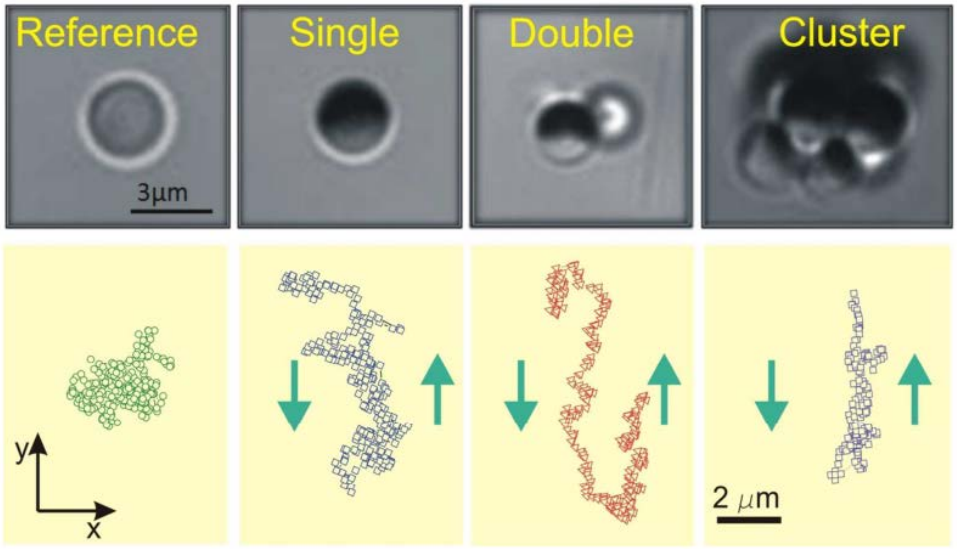

Figure 1-2 Trajectories of thermophoretic magnetic Janus motors. Plain silica particle is used to compare propulsion of single Janus motor, doubled particle and large cluster consisting of Janus motors. Plain silica particle reveals Brownian motion. Janus motors move deterministically. Direction of motion of the all tracked objects (single particles, particles carrying cargo and clusters is changed over the time, as shown by blue arrows, because of the changing in the input magnetic field's polarity. Reprinted with permission from ref 43. Copyright (2006) from Annual Reviews.

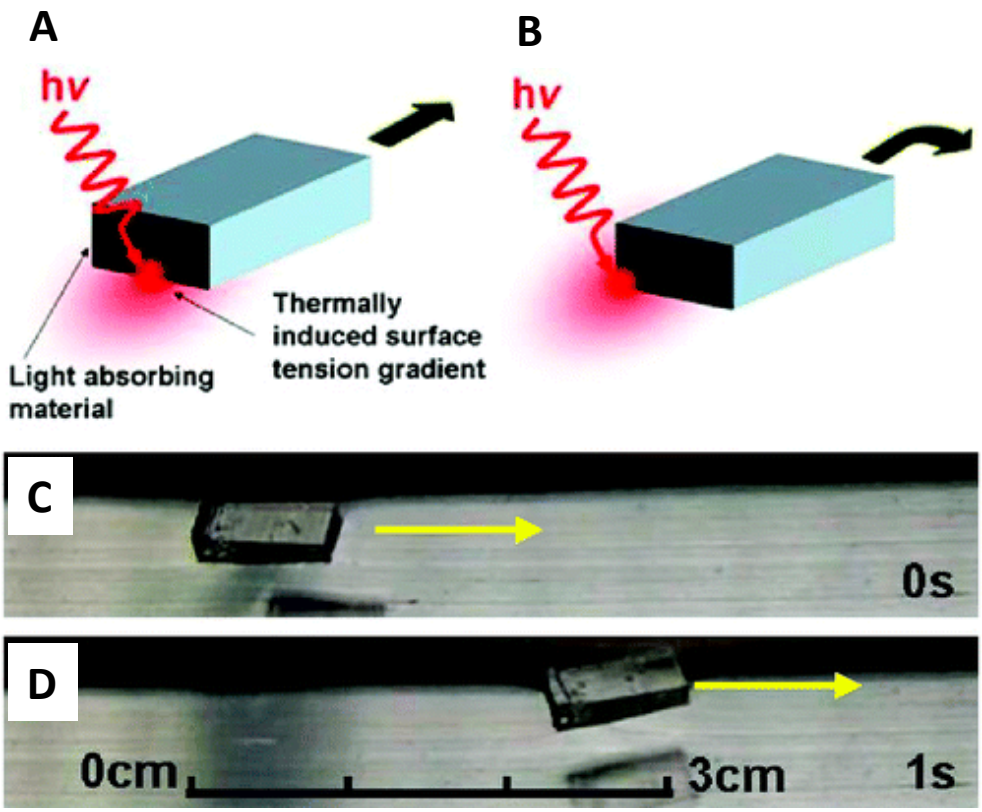

Figure 1-3 Power and manipulation of the moving object with photo energy. (A) When light was on, there is a reduce in surface tension around the back of the object, and the object is subsequently pulled forward. (B) By changing the location of the light spot, the back-left of the device is heated selectively, and a force of asymmetry can be generated, which in turn makes the device to turn right while moving forward. This effect offers a potential to produce and control the motion in a remote manner. (C-D) Optical images of such a device flowing on the surface of water in a trough. The linear motion of the abovementioned system can be seen by irradiating the device for a short time with the focus light (near-IR light of 450 mW power), at the middle point on the back, which is the face that absorbing the photo energy. The source of the laser is put roughly 13 cm from the device, and the laser is nearly grazing the water surface. The laser beam focus was set to coincide with the back of the device. Reprinted with permission from ref 37. Copyright (2009) from American Chemical Society.

Artificial motors can also be powered through the utilization of chemical energy from the environment they operate in. A pioneering work reported by Whitesides *et al.* described a millimetre scale obstruct that catalysed the disproportionate reaction of H_2O_2, from which bubbles were generated at the Pt/solution interface.[44] A subsequent motion of this plate including its self-assembling behaviour with other plates were observed, as shown in Figure 1-4.

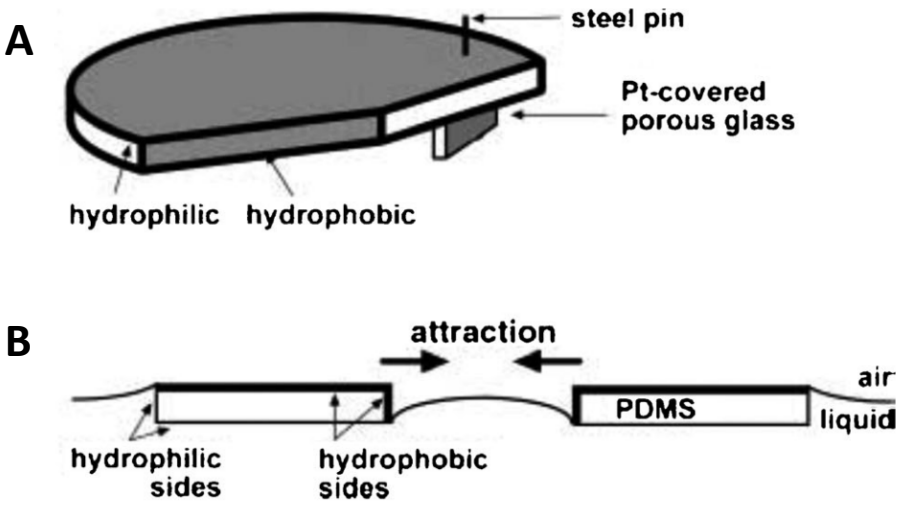

Figure 1-4 (A) A plate of around 1±2 mm thick and 9 mm in diameter was made from PDMS, and the hydrophilic faces were generated by plasma oxidation in air. Pinned at the corner of the plate, a glass filter (2×2 mm^2) covered with Pt served as the catalytic site for hydrogen peroxide decomposition. (B) Schematic showing the interactions between different plates through the capillary interactions. Reprinted with permission from ref 44. Copyright (2002) from Wiley-VCH Verlag GmbH & Co.

Since this report, the utilization of chemical energy from hydrogen peroxide has become the most common energy source for nanomotors and micromotors, and this evident that

chemical fuel powered motors can not only run at the macroscale, but also at the nanometer/micromotor scales. One of the examples is shown in Figure 1-5.[45]

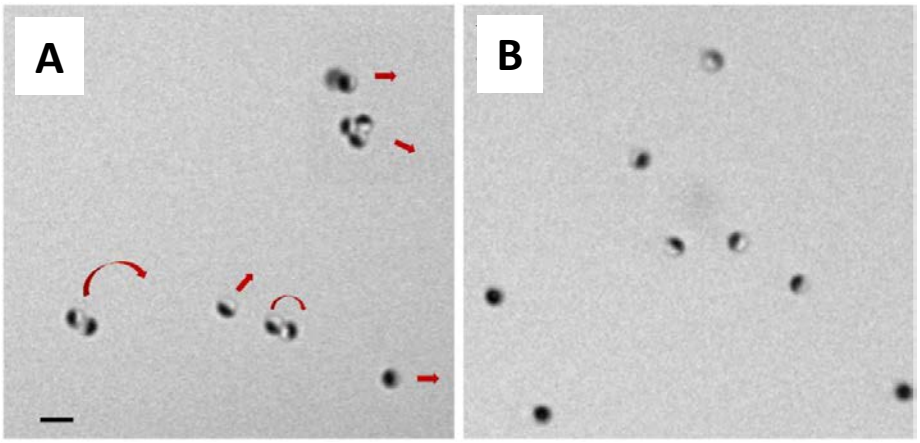

Figure 1-5 Running of Janus micromotors. (A) motors with hydrophobic coating, which makes the motors run as single, doublets, or motor assemblies; (B) motors without hydrophobic coating. The scale bar indicates 2 μm. Reprinted with permission from ref 45. Copyright (2013) from American Chemical Society.

Small motors powered by chemical fuels have received considerable attention in recent years, and hydrogen peroxide has been the most commonly used fuel for the chemical power. Such fuel molecules offer a sufficiently strong thrust to power the motor, but it is also biohazardous. Man-made small motors, unlike the naturally occurred protein motors that utilize ATP as the chemical fuel[46], are operating so far mostly in biologically toxic environments and it is a great challenge to power the small motors with biocompatible fuels. One successful example showed that artificial macroscopic objects could use D-glucose as fuel for their motion on the water/air interface.[47] As illustrated in Figure 1-6, a millimetre scale carbon fibre was modified with the enzyme, glucose oxidase, at one end of the device, and bilirubin oxidase at the other end of the device. Glucose oxidase is able

to oxidize glucose to gluconic acid, and bilirubin oxidase is able to reduce oxygen to water. A net flow of electrons can be generated from this reaction, from the end modified with glucose oxidase towards the end with the incorporation of bilirubin oxidase. The migration of hydronium ion (H_3O^+) can thus be induced at the surface the fibre, and eventually a self-electrophoretic propulsion of the fibre in the direction opposite the glucose oxidase end can be observed (Figure 1-6).

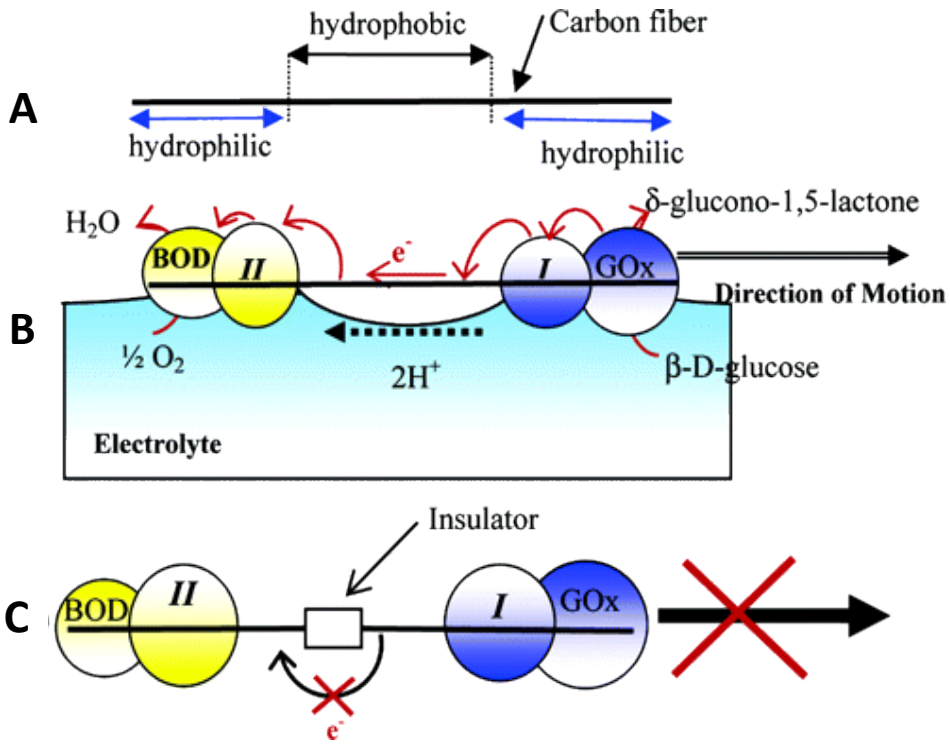

Figure 1-6 (A) By exposure to a one torr oxygen plasma, both ends of the device are ensured to be hydrophilic. (B) The enzyme glucose oxidase (GOx) was incorporated at the right hand side of the carbon fiber device, through the electrostatic adduct interaction. The redox polymer *I* was attached by the side consequently. The enzyme bilirubin oxidase (BOD) was incorporated at the left hand side of the carbon fiber device, also through the electrostatic adduct interaction. The redox polymer *II* was attached at its side. The device is placed on the surface of a buffer solution (pH 7) with glucose concentration of 10 mM. The electron flow follows the direction glucose → GOx → *I* → carbon fiber

→ *II* → BOD → O_2. Motion of the device is observed at the solution-oxygen interface due to the flow of ions accompanying the flow of electrons. (C) No motion can be triggered when the middle part of the device was made non-conductive. Reprinted with permission from ref 47. Copyright (2005) from American Chemical Society.

Other than the abovementioned sources of energy, some of the small motors are able to move due to the presence of a chemical gradient in their environment, which usually results into an imbalance in surface tension and thus a motion can be generated. From the energy point of view, the autonomous motions of such motors are resulted from free-energy minimization through physicochemical processes. [48,49] Such "chemical gradient"-induced movement can originate from 1) movement on designed surfaces and 2) the release of some molecules from the motors that changes the surface tension in their surroundings.

For the first type, although the movement is independent on the fuel-holding capacity of motors, the surface on which the motors move on has to be carefully designed (Figure 1-7).[49]

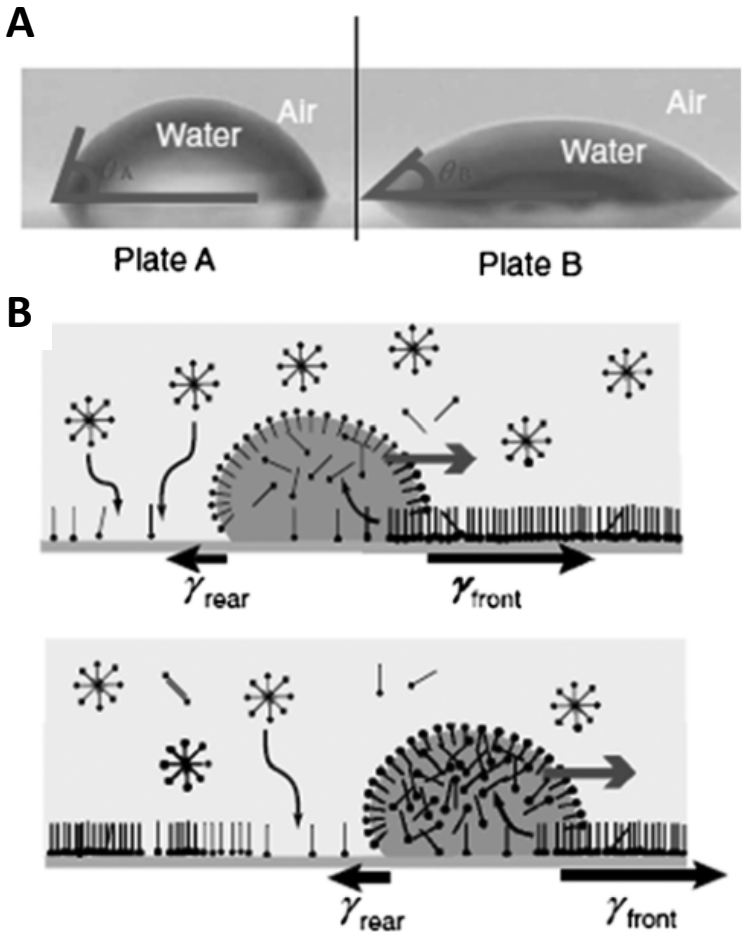

Figure 1-7 (A) Movement of a droplet of water on the solid/air interface modified with surfactant molecules due to the Marangoni effect. The surface tension difference is quantified to be around 14 mN m^{-1}. (B) Illustration on the surface tension difference. The direction of the movement for a droplet of oil is shown with the arrows. The polar heads and hydrophobic tails represent stearyl trimethyl ammonium ions (STA^+). As there is a tendency for the STA^+ ions to assemble with the I_3^- present in the oil, such STA^+ ions can dissolve into the oil from the glass surface. Subsequently, the presence of concentration difference of such ions results in a surface tension gradient, and $\gamma_{front} > \gamma_{rear}$. The hydrophobicity property of the surface can be restored when the oil droplet left, as the ions of STA^+ in water will adhere back onto the solid surface. Reprinted with permission from ref. 49. Copyright (2005) from American Physical Society.

For the second type, because the surface tension-changing chemical molecules are being released directly from the motor itself, the design of running surface is not necessary and the motors can run on a wide range of solutions. As will be shown in Chapter 2, the polymer capsule motors studied in my research work are observed to move on both artificially made different aqueous solutions and natural water samples.[29] a similar mechanism is used by the insect Mesovelia for fast movement/escape on the water surface.[7] The disadvantage for this type of motors is also obvious: the capacity of the motors is limited since the self-contained molecules that alter the surface tension will be exhausted at a certain point, and the motion will cease when the release of such molecules is not sufficient to overcome the frictional forces. A typical example of such a type is a camphor boat, as shown in Figure 1-8.[50]

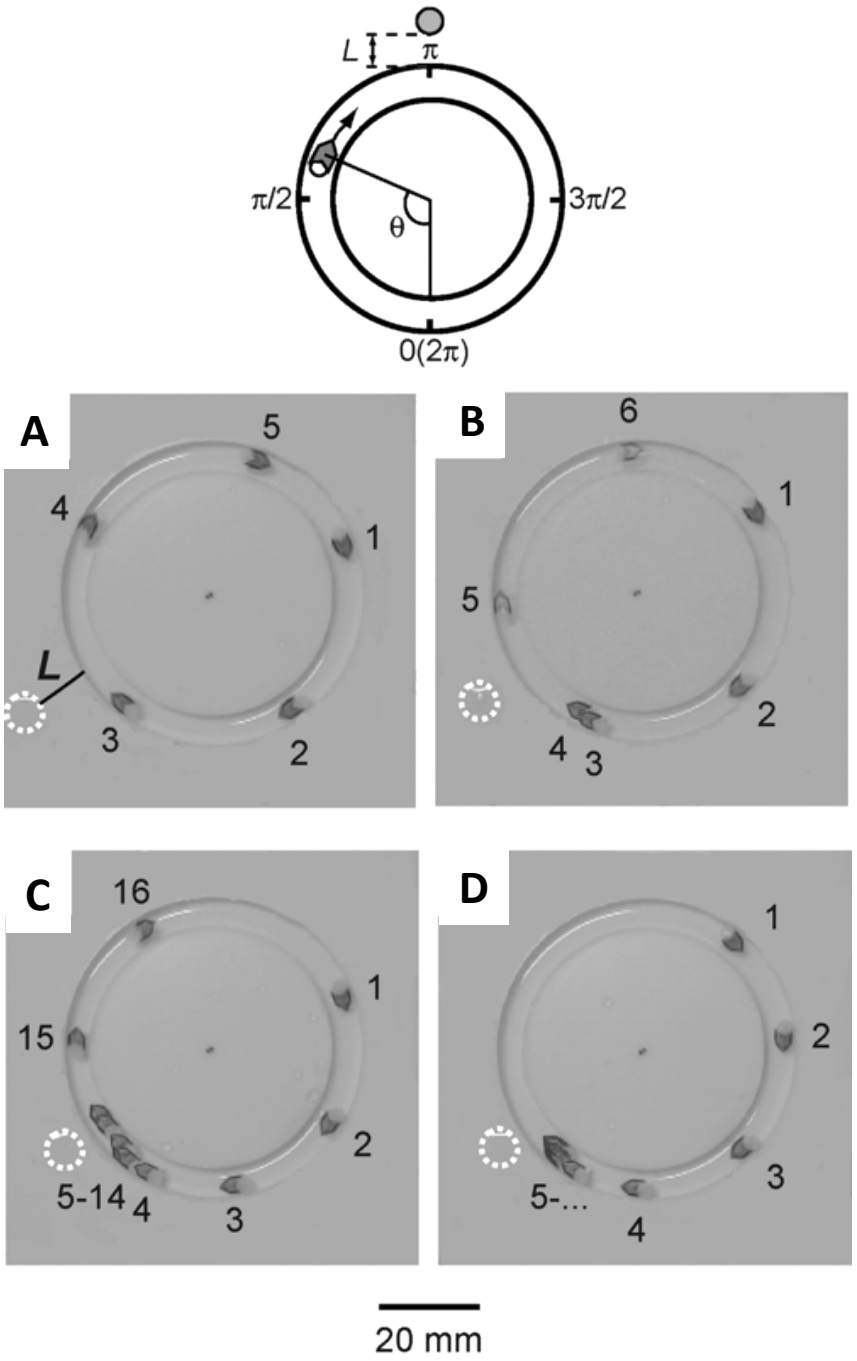

Figure 1-8 Self-propelled movement of a "camphor boat" on the surface of water in a channel for L = (A) 10, (B) 5, (C) 3, and (D) 2 mm with the placing of a methyl n-butyrate droplet, which is surrounded by a dotted white circle (top view, time interval 1/3 s). At the top of the image is an illustration showing the polar coordinates used to analyze the motion. The angle, θ, is defined as π when the running camphor runs by the droplet, which is shown as a gray circle. Reprinted with permission from ref. 50. Copyright (2005) from American Chemical Society.

1.2.2 Mechanism and Driving Forces

When one is to study the motion mechanism for a specific motor, a most important aspect to consider is the medium in which the motor runs in. To date, the running mediums for small scale motors fall into two categories: motors either run at the interfaces, or they run in the bulk liquid.

For motors running at the interface, which can be a liquid/air interface,[29] a liquid/liquid interface,[51] or a solid/air interface,[49] the driving force for their motion arises from the interfacial gradient. With the supply of physical or chemical energy, a surface tension gradient can be generated and the motors are thus running towards a direction with higher surface tension. Most of the macroscopic small motors are running based on this mechanism of propulsion. Figure 1-9 shows an example of motors running under such mechanism.[29]

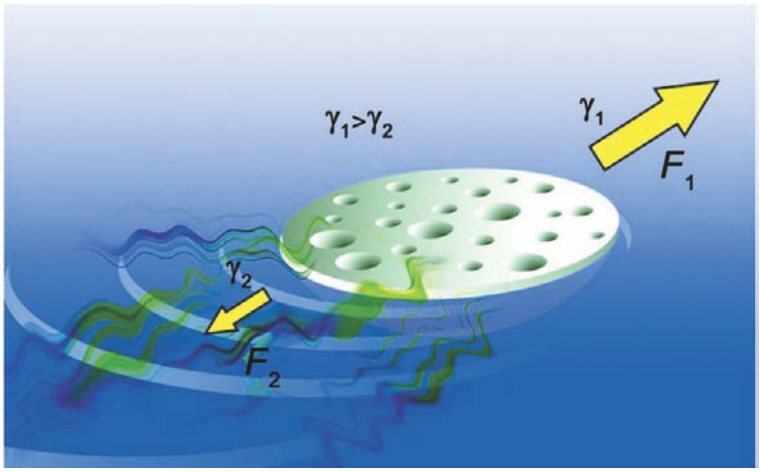

Figure 1-9 Movement of a polymer capsule. The molecules of DMF are slowly released out from the device in an asymmetric manner. The back vicinity of higher concentration of DMF possesses a lower surface tension than that of the front vicinity of the capsule, and thus the force at the front is higher, pulling the device to move forward. Reprinted with permission from ref. 29. Copyright (2011) from Wiley-VCH Verlag GmbH & Co.

For motors running inside the bulk liquid, different kinds of mechanisms are adapted for motors of different designs. For examples, nanomotors or micromotors running in the hydrogen peroxide solutions are propelled by self-diffuosiophoresis as shown in Figure 1-10,[52] self-electrophoresis as shown in Figure 1-11,[53] or bubble-propulsion mechanisms as shown in Figure 1-12.[17]

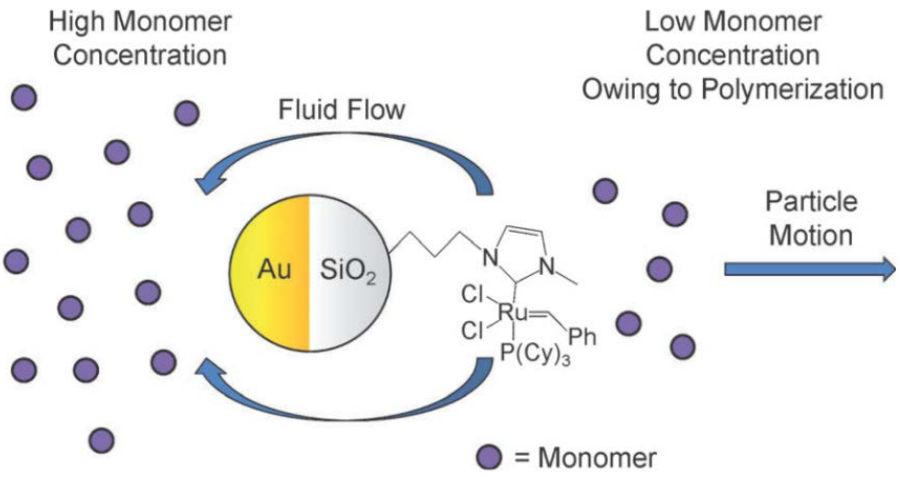

Figure 1-10 Schematic illustration of a catalytic micromotor. The silica surface of the motor was modified with catalyst, which facilitates the polymerization reaction of the monomers, and a less amount and lower concentration of the monomer molecules are created. As a result, the surround liquid molecules move from the silica side towards the gold side, where a higher concentration of monomers is present. The device moves subsequently towards the silica side, which is in an opposite direction of the fluid flow. Reprinted with permission from ref. 52. Copyright (2011) from Wiley-VCH Verlag GmbH & Co.

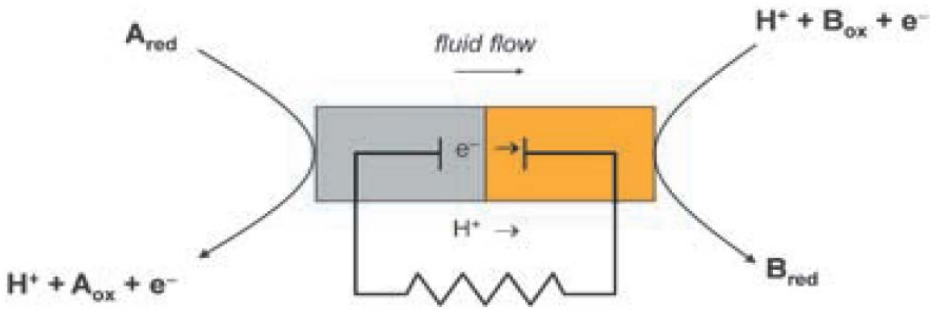

Figure 1-11 Schematic illustration of the local electric field generated surrounding a redox-active device. The oxidation of species A and reduction of species B proceed at opposite ends of the device, and the asymmetric generation and reaction of such ions leads to a difference in concentration, and consequently an electric field is induced. This process is driven by the net reduction in the system's free energy. Reprinted with permission from ref. 53. Copyright (2005) from Wiley-VCH Verlag GmbH & Co.

To date, one of the most important mechanism for powering the nano-/micromotors is the bubble-propulsion mechanism, which is adapted by the microjets and they possess the advantages of ease of control over the motion, high power output, as well as straight in motion trajectories, as shown in Figure 1-12. [17]

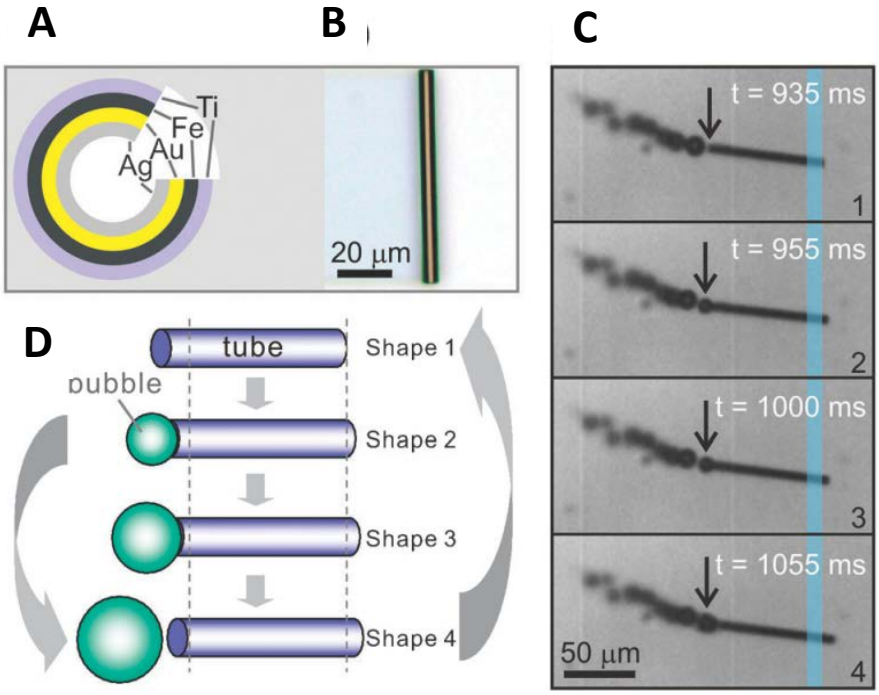

Figure 1-12 (A) Structure of the multi-metallic micromtors. (B) Top view of the multi-metallic tube. (C) Snap shots of a running microtubular motor at different time frames. (D) Corresponding scheme illustrations of the snap shot images for the bubble-propelled motion. Reprinted with permission from ref. 17. Copyright (2011) from the Royal Society of Chemistry.

1.2.3 Motion Description and Manipulation

In order to describe the motion of small scale motors, different physical concepts are considered, and by varying these aspects of the motion, we can potentially realize the manipulation of the motors. Such physical concepts include the start/stop of motion, the velocity of the motion (including direction and speed), as well as the motion styles.

One of the most important observations for the motion is its on/off status, which indicates if the motors are still running. To control this parameter of motion, we need to look into the energy sources for the motors. If the motors are powered by external physical energy sources, this aspect of motion is simply controlled by the on/off of energy supply. If the

motors are running due to the chemical reactions, in most cases motion can only be stopped when the fuel concentration is no longer sufficiently high to provide the driving force and overcome the resistance forces. If the motors are running based on the releasing of molecules which lower the surrounding surface tension, the motion can only be stopped when the release rate is lower, which generates a driving force weaker than the resistance forces. However, there is another possibility that we can control the start/stop of motors with external magnet. As shown in Figure 1-12, with the application of a magnet, the speed of the capsule motor was zero – the motion was stopped. It resumed motion with the removal of the magnet.[51]

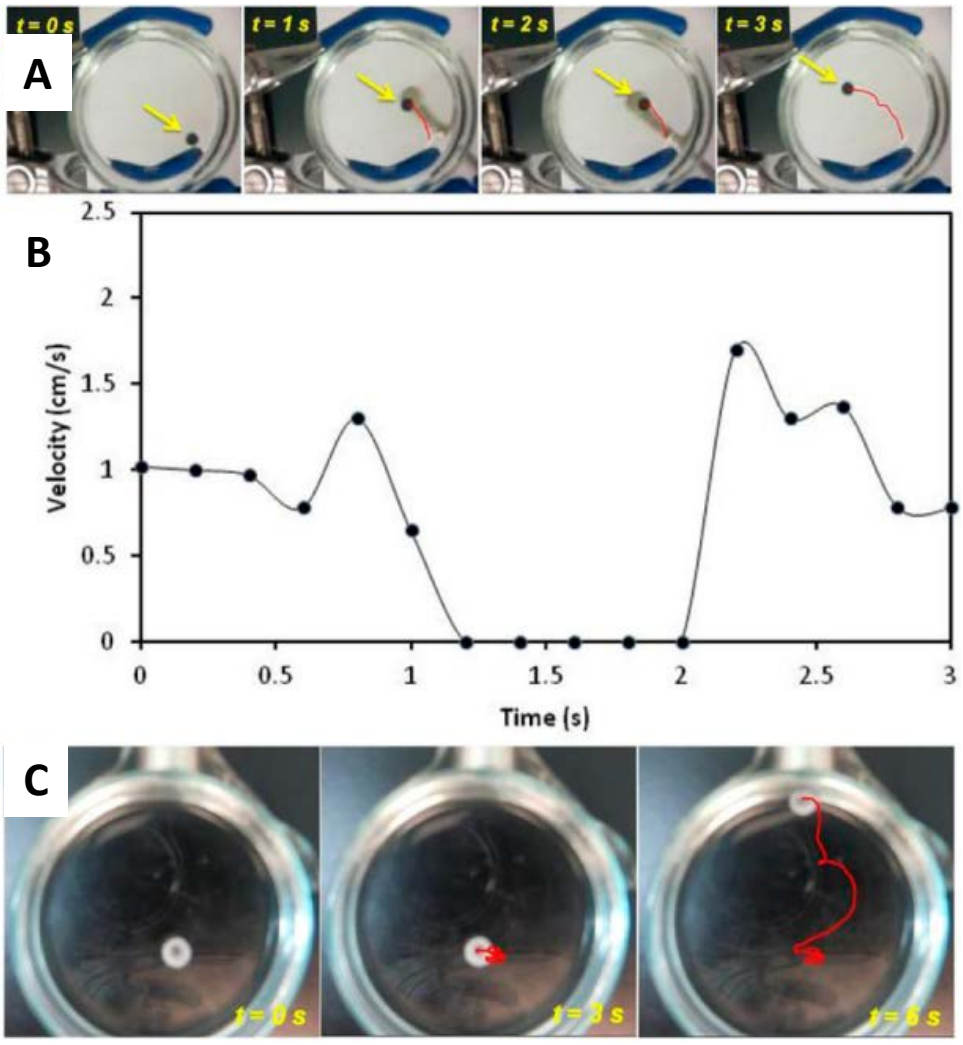

Figure 1-12 Magnetic manipulation of the running polymer capsule. (A) Snap shots of the running capsule incorporated with Ni nanoparticles; the time interval is 1 s. (B) Velocity profile of the capsule; zero velocity indicates that the capsule motor actually stopped motion. (C) With the presence of magnet at the side, the motion direction of the capsule motor can be controlled. Reprinted with permission from ref. 51. Copyright (2012) from the American Chemical Society.

The velocity of the motion, including the direction and speed, is a most important factor for the motors and their applications. We would like the motors to run at a high speed, and with their motion directions within our control, so that they can reach the desired location fast to facilitate the realization of desired applications. With the same resistance force, motion velocity can be determined by different means, depending also on the energy source. For external physical energy powered motors, the control over speed/direction is usually by altering the input energy. As shown in the example in Figure 1-13, a reversible movement of a droplet can be observed under partial illumination at different edge of the droplet, leading to a reverse in motion direction.[36]

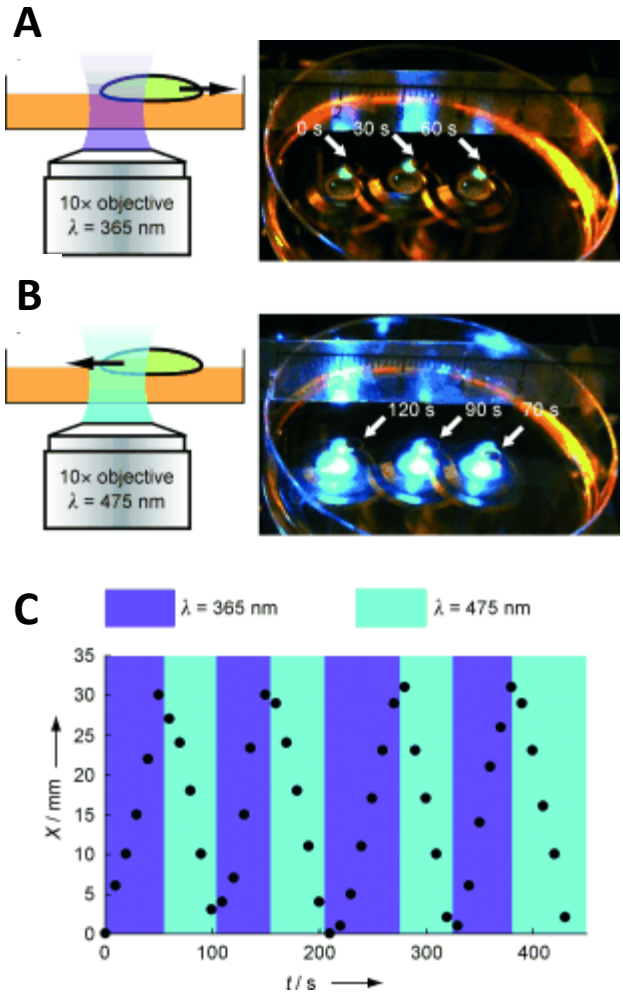

Figure 1-13 Movement of a liquid drop powered by light energy. Such movement is dependent on the wavelength of the light. The left image shows a schematic illustration of the movement under partial illuminate, and the right image is snap shots for the motion. Wavelengths are (A) λ=365 nm, and (B) λ=475 nm. The objective lens of the microscope was set to move along with the motion of droplet to keep it partially illuminated. The length scale was determined by placing a ruler over the Petri dish. (C) The position (denoted x) of the moving particle with relative to the Petri dish is shown against time. A total number of 4 repeats of changing wavelength between 365 and 475 nanometers were carried out. Reprinted with permission from ref. 36. Copyright (2009) from Wiley-VCH Verlag GmbH & Co.

For motors running due to the chemical reactions, motion speed can be altered by varying the fuel concentration, and in most cases a higher fuel concentration leads to a higher speed of the motors. External magnet has to be applied to change the motion direction, provided that the motor itself contains paramagnetic materials in its structure. Sometimes magnetic field can not only affect motion direction, but also the speed of the motors. This is observed also in my study and introduced in Chapter 4 in details.

For motors running based on the releasing of molecules which lower the surrounding surface tension, the speed of the motors are always lower and lower as the molecules are being released into the bulk solution. The speed can be altered by changing the environment, and different magnitudes of speed can be observed for different solutions and concentrations. This is also evident from my study and illustrated in Chapter 2 in details.

The speed of motion can also be utilized to indicate the concentration of certain molecules in the solution, offering the possible of applications for sensing and biosensing. Figure 1-14 gives an example.[24]

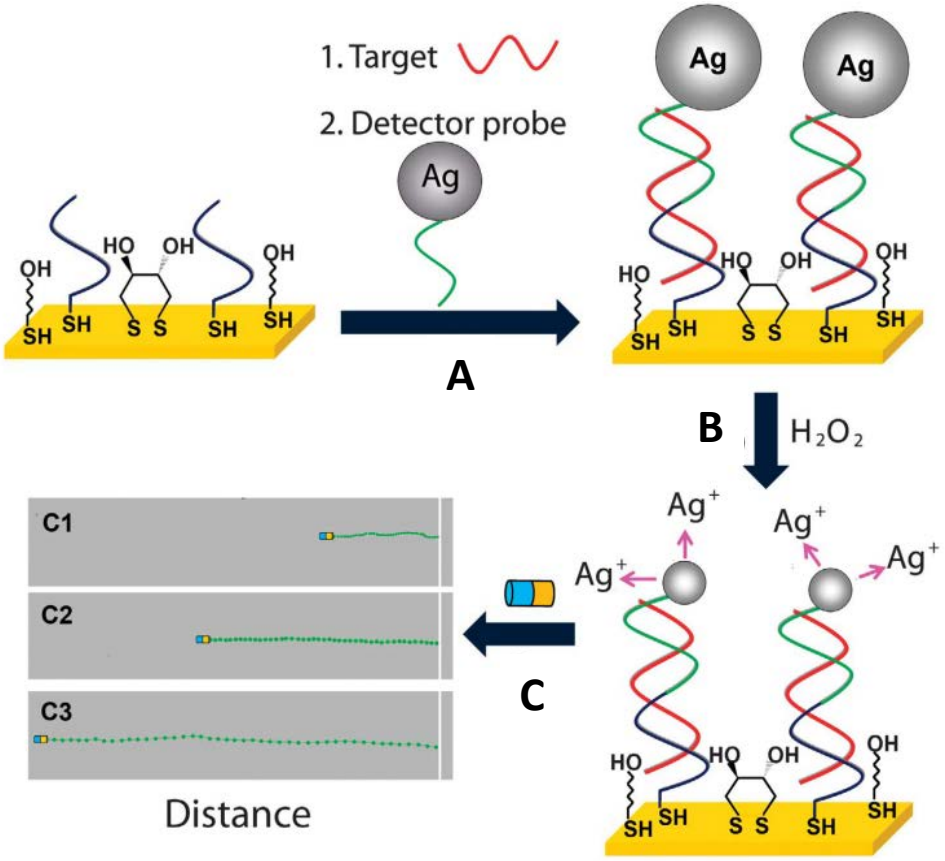

Figure 1-14 Motion based detection of nucleic acid. (A) Hybridization of the target and bound of the Ag NP-tagged detector probe in a typical sandwich assay on the ternary SH-CP/DTT + MCH surface. The removal of not captured SH-DP-Ag nanoparticles is also included. (B) The dissolving of Ag nanoparticle tags in the H_2O_2 solution resulting into a higher concentration of silver ions in the solution. (C) Visual detection of the running of the nanomotors in the solution of higher silver ion concentration. The running lengths of different motors corresponding to higher concentrations of the target DNA concentrations are also illustrated. Reprinted with permission from ref. 24. Copyright (2010) from Nature Publishing Group.

The third physical concept to describe the motion is the motion style. In fluid mechanics, for a rigid motor to run in the bulk solution or at the interface, its trajectory can be linear,

circular or a combination of those two. The abovementioned three different styles of motion are interchangeable and can be affected by different factors.

One of the most deterministic factors is the intrinsic shape of the motor. For those with asymmetric shapes, the motors can only adapt a circular motion, due to the frictional force off the axis of the motors. Figure 1-15 gives an example.[54]

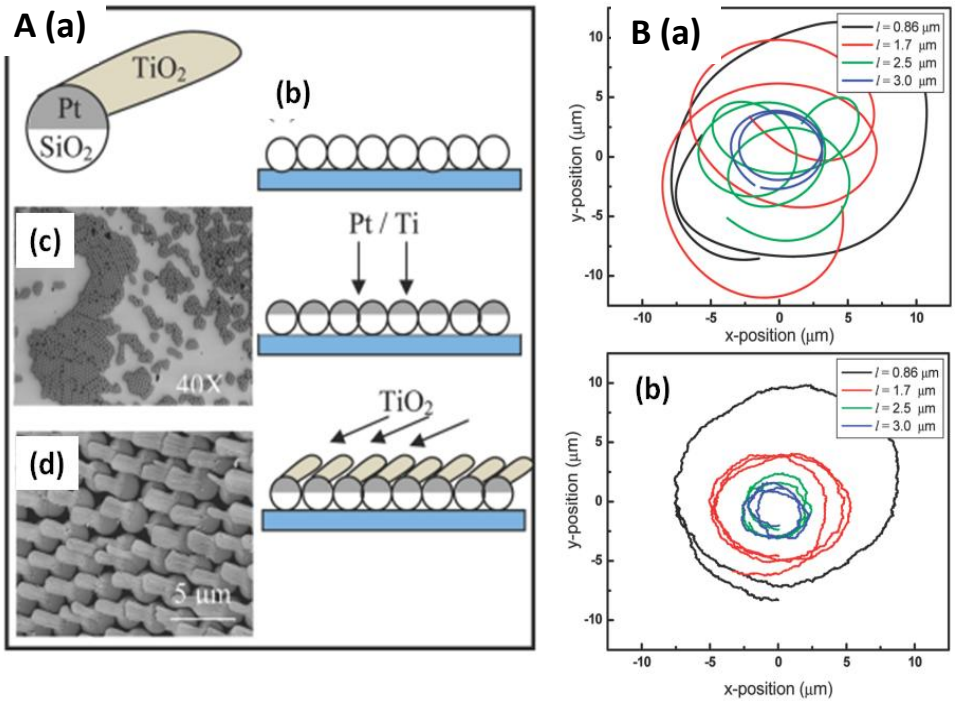

Figure 1-15 (A, a) Illustration of platinum-covered microspheres with an arm of titanium dioxide. (A, b) Illustration of a single layer of the microspheres, titanium and platinum metals are coated onto these beads, and the arm is deposited. (A, c) A normal microscope image of the microspheres is shown and the spheres are magnified at 40×; (A, d) SEM top-view of the single layer of the beads with titanium dioxide arms. B, a) The image indicates the running paths of the running particles with 4 varied sizes of arms ranging from 0.86, 1.7, 2.5, to 3.0 μm. With the increment of such sizes, smaller running paths can be observed. In every plot, the time interval is 10 s, and central point of every path are placed intentionally at a common center point. (B, b) Similar running paths can be seen

from the simulation result under the same condition shown in (B, a). Reprinted with permission from ref. 54. Copyright (2011) from American Chemical Society.

For motors with symmetric shapes, their style of motion is influenced greatly by the environment it runs in. Detailed discussion of motion style will be presented in Chapter 2 for millimeter scale motors and Chapter 5 for micromotors, respectively.

1.2.4 Applications of Small Scale Motors

Nature utilized biological motors to perform a broad range of physiological tasks, and artificial synthetic motors are designed and fabricated not only to further understand their motion at the small scale, but also to fulfill the ultimate destination of applying them in real applications. Small motors with the physical, biological, as well as chemical functionalizations have been reported extensively in the literature in the recent decades. Such state-of-the-art motors and applications represent highly integrated systems. Here I would like to introduce a few applications of small scale motors in environmental remediation, drug delivery, transportation of cargoes, autonomous wireless sensing and biosensing, manipulation of cells, and microsurgery.

Application of small scale motors in environmental remediation

The ability of the small scale motors to carry out tasks in environment remediation has been illustrated extensively in recent literature. The motors are reported to be able to sense the presence of certain chemicals, collect to facilitate removal of oil droplets in water, or to enhance the degradation of pollutant molecules. These small scale self-propelled motors equipped with remediation functionality opens up a promising direction for the cleaning of water in small pipes or channels that is hard to be reached with conventional methods.[13] Figure 1-16 gives an example of biocatalytic degradation of polluting molecules by small motors that can release enzymes.[55]

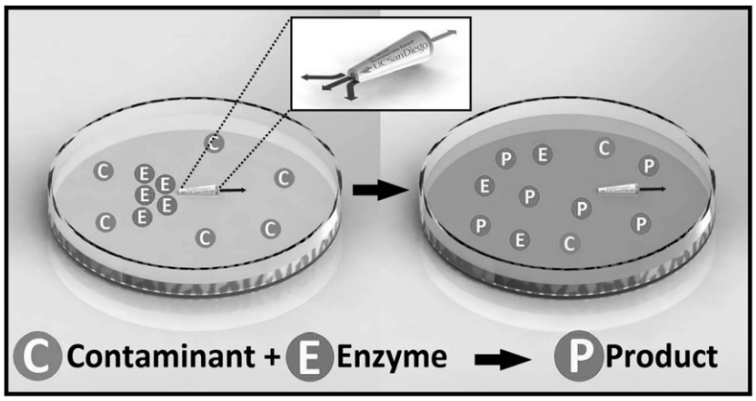

Figure 1-16 Illustration of the idea in motion dependent biocatalytic pollution removal due to the slow release of enzyme molecules. The solution of surfactant (SDS, 90%) and enzyme (10%) was put inside a pipette tip, which is placed on a polluted water surface and allowed to move for half an hour. The pollutant molecules are eliminated by the enzyme. The inset shows a larger image of the motor. Reprinted with permission from ref. 55. Copyright (2009) from Wiley-VCH Verlag GmbH & Co.

Figure 1-17 gives an example of effective removal of oil in water facilitated by the super hydrophobic alkanethiol-coated micromotors.[31]

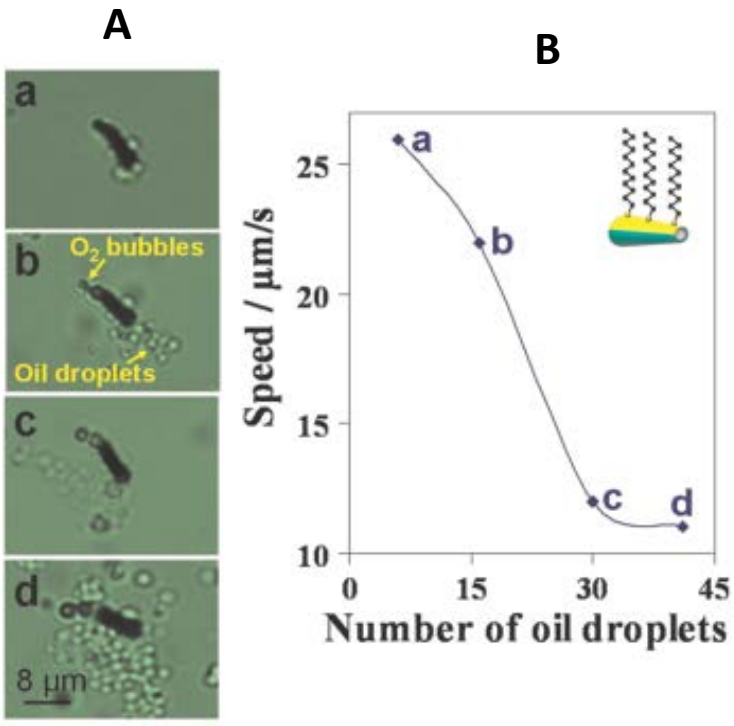

Figure 1-17 Microtubular motors functionalized with super hydrophobic Dodecanethiol (C12-SAM) can catch the oil droplets. (A) Snap shots of running in the mixture of oil in water with 10% hydrogen peroxide for a time interval of 5, 12, 66, and 80 s, respectively (B) Relationship between of the motor speed and the amount of oil droplets captured. Inset: illustration of the dodecanethiol-incorporated micromotors. Reprinted with permission from ref. 31. Copyright (2010) from American Chemical Society.

Figure 1-18 gives an example of enhanced cleaning of rhodamine 6G (Rh6G) contaminated water with the catalytically active Fe/Pt micromotors.[56]

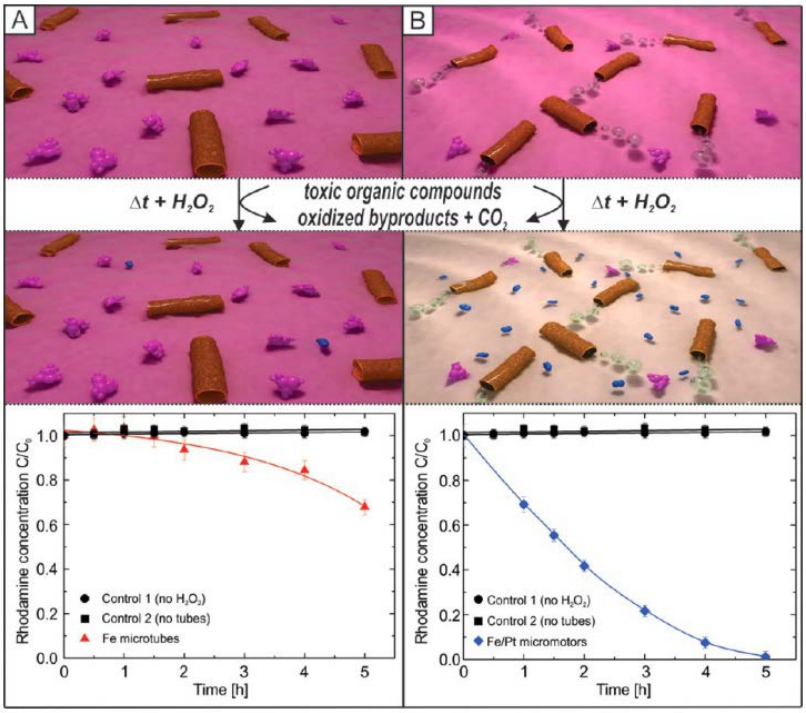

Figure 1-18 Remediation of pollutant chemicals from water using Fe-micromotors (column A images) and running Fe/Pt micromotors (column B) in H_2O_2 suspension. The rhodamine 6G, or Rh6G, is shown in pink color. The products from the oxidation of Rh6G are shown in blue color. Such Rh6G molecules are oxidized faster with the presence of catalytic running micromotors compared the pure Fe tubes. Also

demonstrated here is the quantified comparison of Rh6G oxidation under these two different conditions in 5 hours. The reagents were prepared at pH 2.5. Initial concentration of Rh6G is 45 mg/L, in the presence of 15% hydrogen peroxide, 0.5% of SDS, and a number of ~440±10 micromotors. The volume was topped up to 1 mL with water. Control experiments with no hydrogen peroxide and no motors were also prepared for comparison. Reprinted with permission from ref. 56. Copyright (2009) from Wiley-VCH Verlag GmbH & Co.

Application of small scale motors in transportation of cargoes and bimolecules

In order to achieve a significant targeting and transport of cargoes, the small scale motors should be equipped with a high power thrust as well as a precise guidance and control over its motion. Recent progress in the design and development of small scale motors have led to a great improvement in the power thrust and velocity, motion manipulation, as well as the functionalizations of motors to realize the transportation of therapeutic cargoes. There is of high importance to utilize the small scale motors for cargo-delivery as it holds the potential to improve the curing efficiency and reduce the adverse effects of toxic molecules by delivering the payloads to predetermined body locations, and such kind of small motors can also be further functionalized with the imaging moieties and desired legends to confer tissue specificity.[57] So far, state-of-the-art transportation capabilities of small motors have emerged and developed greatly. [15,16,58] Figure 1-19 showcases the catalytic nanowire motors readily picking up the poly (D,L-lactic-co-glycolic acid) (PLGA) particles loaded with therapeutic agents and deliver such cargoes following a desired path to the desired destination.[15]

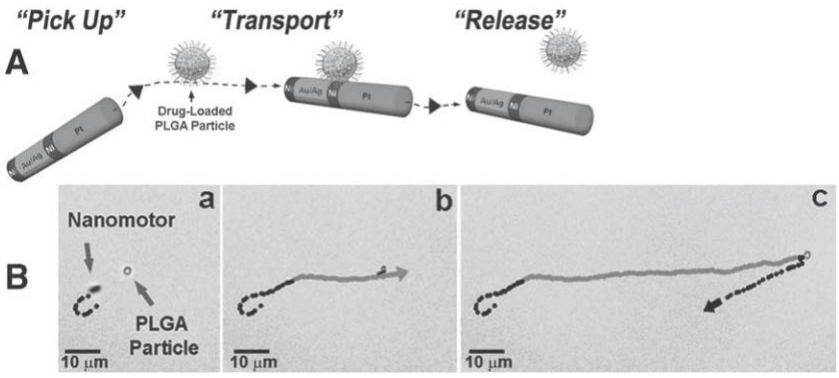

Figure 1-19 Transportation of therapeutic agents by paramagnetic nanoscale motors. (A) Illustration of the real-time pick-up, transport, and release of PLGA that is incorporated with therapeutic agents using a nanomotor. (B) Snap shots of drug-loaded PLGA particle being picked-up and transported by a catalytic alloy (Ni/(Au_{50}/Ag_{50})/Ni/Pt) nanoscale motor. Figure (B, a) demonstrates the direction motion of the nanoscale motor with external magnet running to the paramagnetic PLGA particle, while (b) and (c) respectively, show the real-time pick-up, transport, and finally release of the cargo by the nanoscale motor in a 5 wt% H_2O_2 medium. Reprinted with permission from ref. 15. Copyright (2010) from Wiley-VCH Verlag GmbH & Co.

Other than the transport of cargo and drug payloads, the small motors are also reported to be able to isolate specific biomolecules, including proteins, peptides and sugar molecules. Figure 1-20 shows a selective, sensitive and fast pick-up of targeted protein molecules from raw body liquids.[59]

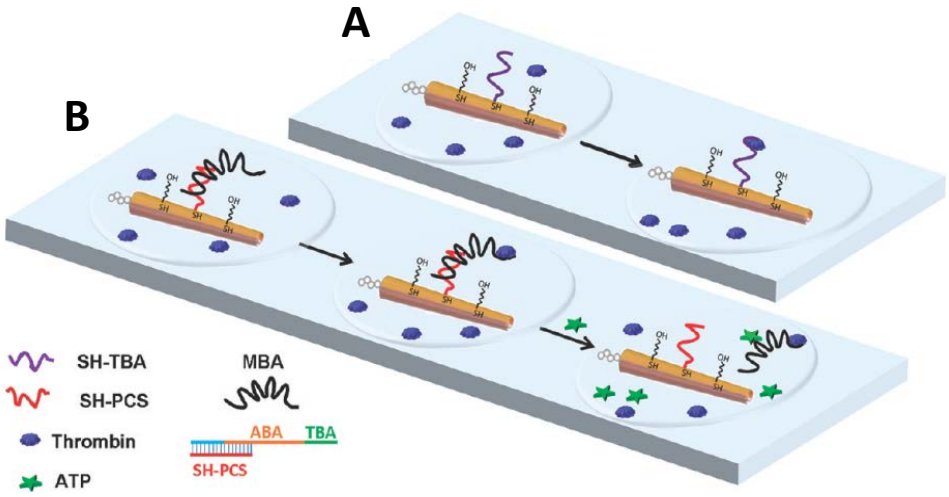

Figure 1-20 Illustration of the specified separation of the desired protein molecules using the aptamer-incorporated micromotors. (A) Selective capture and delivery of desired molecule from a raw body fluid using a TBA-functionalized micromotor. (B) Selective capture, delivery as well as dropping of the protein molecules with a MBA-functionalized micromotors. The left bottom image shows the structure of MBA. Reprinted with permission from ref. 59. Copyright (2011) from American Chemical Society.

Application of small scale motors in sensing

The abilities to detect the presence of certain factors in the environment, including chemicals, light or heat, is based on the pre-requisite for them to run, and the sensing is reflected in the motion change of the motors. In other words, sensing ability has to do with the motion control of small motors with the presence of analyte molecules or targeted detection entities. Specific interactions between the physical or chemical factors have to be translated into observable signals in the forms of speed. For example, some motors are able to sense the presence of certain molecules both qualitatively and semi-quantitatively, by increasing their velocities or travel-distance;[24] some motors stopped or slowed down due to the "toxic" effect of molecules in the running solution, as shown in

Figure 1-21;[30] some motors demonstrate an enhanced motion speed upon the irradiation with laser, indicating a sensing capability toward light.[21]

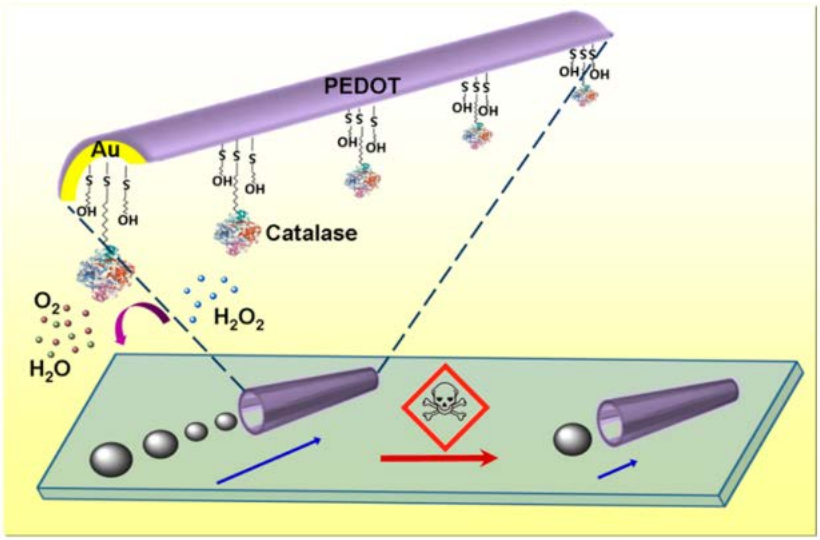

Figure 1-21 Reduction of the performance of microtubular motors by the toxic molecules in the running medium, which can show harmful effect on the catalase enzyme. The catalase molecules were attached to the inner side of the microtubular motor. Reprinted with permission from ref. 30. Copyright (2013) from Wiley-VCH Verlag GmbH & Co.

Similar to the living systems, another ability for the man-made small motors to respond to the external environment is their chemotactic capability, which is seen from microorganisms to move towards or away from the higher concentration of some molecules.[60] The Bacterium was observed to accumulate in the oxygen rich environment,[61] and the catalytic micromotors were also reported to run towards a higher concentration of H_2O_2, as seen in Figure 1-22.[62]

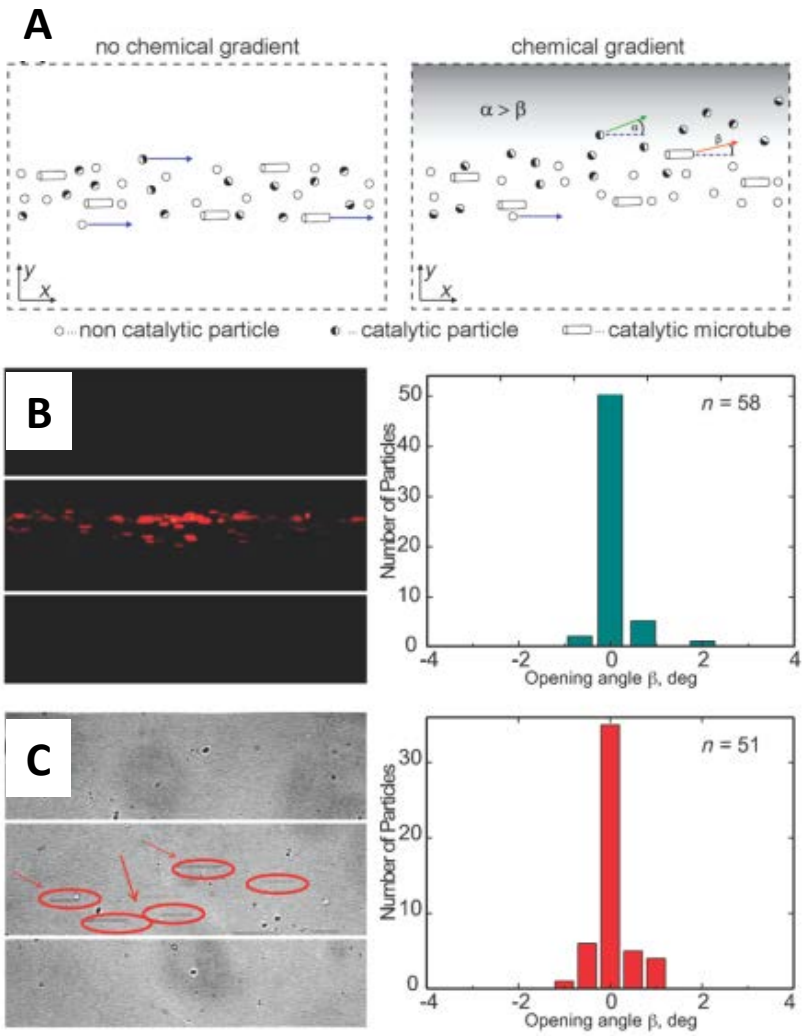

Figure 1-22 Observation and quantification of chemotactic behaviors. (A) Chemotactic motion of the micromotors is determined by the opening angle β. Negative control experiments: (B) non-catalytic fluorescent polystyrene particles in the gradient of H_2O_2 (10 wt% hydrogen peroxide in i1, no hydrogen peroxide is present in i3) do not show chemotactic migration towards the place of higher H_2O_2 concentration; Plotting-image indicates histogram from the opening-angle study for the non-catalytic particles, which gives 0 opening-angle. (C) Catalytic micromotors, placed into the system from the middle inlet do not migrate (0% hydrogen peroxide in i1, 0% hydrogen peroxide in i3) when no hydrogen peroxide is present in the liquid. Histogram indicates that most of the tubular micromotors do not show any migration. The input flow speeds are made to be 140 μL

per hour. Reprinted with permission from ref. 62. Copyright (2013) from Wiley-VCH Verlag GmbH & Co.

Application of small scale motors in microsurgery and manipulation of cells

It is one of the ultimate desires to utilize the small scale motors for biological and medical applications. In order to achieve *in vitro* and *in vivo* tasks, the motors are supposed be biological non-toxic, and run with biocompatible fuels. It has been shown by Elaine *et al* that the catalytic nanomotors are non-toxic. [63]However, unfortunately the only efficient chemical fuel to be used by the catalytically small motors so far is hydrogen peroxide, which is biologically toxic.

While on the way of searching for possible biocompatible fuels, it is meaningful to study the motion behavior as well as the functionality of small motors for various biological applications. Even with the availability of such ideal power source, it is still challenging for applications at such small scales. A continuous motion with a powerful thrust and remote manipulation is desired, and up to now, magnetic control over the direction is the most efficient manner. As can be seen from Figure 1-23, a precise manipulation of motion with external magnetic field can not only position the microtubular motor to the desired location, but also drill a hole at the site of interest.[64]

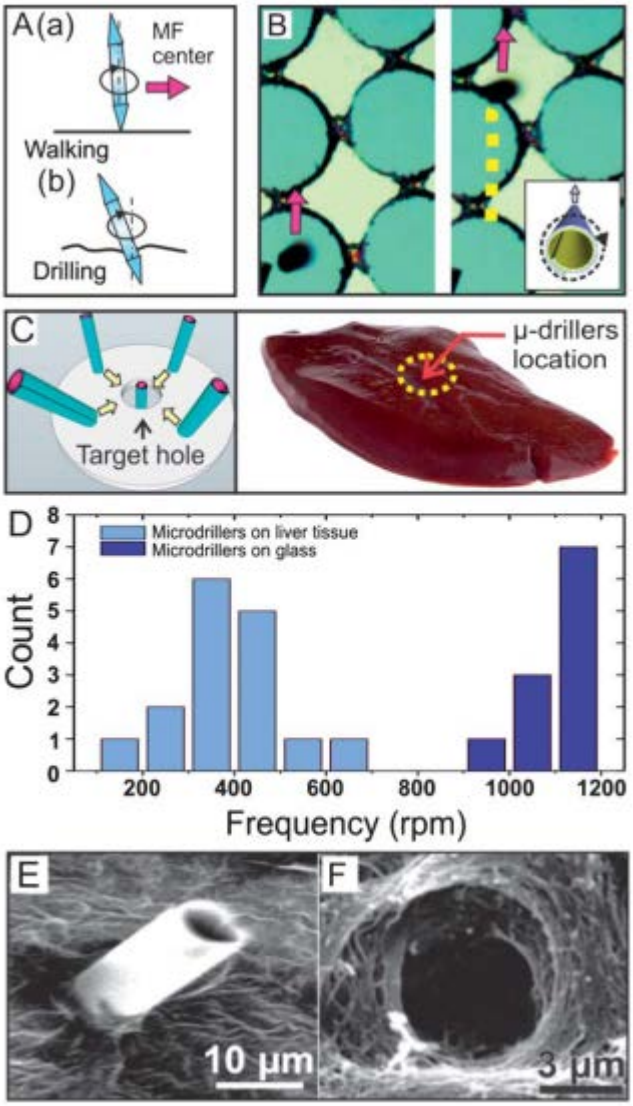

Figure 1-23 (A) Running and drilling ability of the microscale drillers. (a) Fuel independent movement of ferromagnetic microtubes in standing up position moving towards the middle point of the magnetic field where the material that is to be drilled is located. (b) Illustration of a microscale device drilling at the interested position. (B) Microscopic picture of tracked path of a drilling device under the rotating magnetic field of 20 mT and motion towards the middle point of the field. (C) Illustration image showing the fuel-free movement of the device towards the center of the field and the drilling action on pig liver tissue. (D) The allocation of the stabilized rotation frequency of microdevices on the pig liver and on a rigid glass surface with the same selected magnetic frequency of

1,150 rounds per minute. (E) Observation with SEM for a device that stays partially in the tissue. (F) A hole can be seen under SEM after the device is removed by a strong external magnet (500 mT). Reprinted with permission from ref. 64. Copyright (2012) from the Royal Society of Chemistry.

Selectivity is also one of the major challenges while we deploy the small motors for biological applications. The manipulation of specific cells can be realized with the modification of the motors with antibody. Figure 1-24 gives an example.[27]

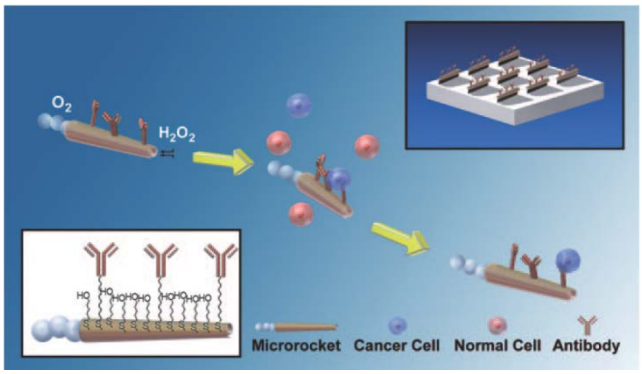

Figure 1-24 Selectively pick-up and delivery of cancer cells with tubular micromotors. The anti-CEA mAb-incorporated micromotors can bind to the CEA cell surface antigens, offering the capability for them to be selectively captured. Fabrication of the Ab-incorporated micromotors and functionalization of such motors are shown in the top-right and bottom-left images, respectively. Reprinted with permission from ref. 27. Copyright (2011) from Wiley-VCH Verlag GmbH & Co.

1.3 Motivation of This Work and Thesis Structure

The target of this research work is to further understand the motion of the small scale motors to facilitate the realization of potential applications.

The framework of this thesis is organized as follows. Chapter One has provided an overview on the definition and aspects of small scale motors. My own research projects during PhD study are exhibited from Chapter Two to Chapter Five. Firstly, a novel and highly efficient millimeter scale polymer capsule motor is introduced, and an extensive study on its motion and application is given in Chapter Two. Next, different routes for the fabrication of nanomotors and micromotors are illustrated in Chapter Three. In Chapter Four, magnetic manipulation over the motion of such nanomotors and micromotors is discussed. Finally, in Chapter Five, I am going to show the motion of such nanomotors/micromotors in real environments, ranging from deionized water to natural water samples and blood samples. The effects of certain chemicals on the corrosion of micromotors as well as on the poisoning of such motors are also discussed. Lastly, Chapter Six points out the remaining challenges faced by current research in small motors, and it also provides an outlook for the research in this field.

1.4 References

(1) Schliwa, M.; Woehlke, G.: Molecular motors. *Nature* **2003**, *422*, 759-765.

(2) Rayment, I.; Rypniewski, W. R.; Schmidt-Base, K.; Smith, R.; Tomchick, D. R.; Benning, M. M.; Winkelmann, D. A.; Wesenberg, G.; Holden, H. M.: Three-dimensional structure of myosin subfragment-1: a molecular motor. *Science* **1993**, *261*, 50-8.

(3) Gelles, J.; Landick, R.: RNA polymerase as a molecular motor. *Cell* **1998**, *93*, 13-6.

(4) Sambongi, Y.; Iko, Y.; Tanabe, M.; Omote, H.; Iwamoto-Kihara, A.; Ueda, I.; Yanagida, T.; Wada, Y.; Futai, M.: Mechanical rotation of the c subunit oligomer in ATP synthase (F0F1): direct observation. *Science* **1999**, *286*, 1722-4.

(5) Wang, J.: *Nanomachines: Fundamentals and Applications*; Wiley-VCH Verlag GmbH & Co. KGaA: Weinheim, Germany, 2013.

(6) Böhm, K. J.; Stracke, R.; Mühlig, P.; Unger, E.: Motor protein-driven unidirectional transport of micrometer-sized cargoes across isopolar microtubule arrays. *Nanotechnology* **2001**, *12*, 238.

(7) Bush, J. W. M.; Hu, D. L.: Walking on water: Biolocomotion at the Interface. *Ann. Rev. Fluid Mech.* **2006**, *38*, 339-369.

(8) Zhao, G.; Pumera, M.: Macroscopic self-propelled objects. *Chem. Asian. J.* **2012**, *7*, 1994-2002.

(9) Sanchez, S.; Pumera, M.: Nanorobots: the ultimate wireless self-propelled sensing and actuating devices. *Chem. Asian.J.* **2009**, *4*, 1402-1410.

(10) Gao, W.; Wang, J.: The Environmental Impact of Micro/Nanomachines: A Review. *ACS Nano* **2014**, *8*, 3170-3180.

(11) Gao, W.; Sattayasamitsathit, S.; Wang, J.: Catalytically propelled micro-/nanomotors: how fast can they move? *Chem. Rec.* **2012**, *12*, 224-231.

(12) Sengupta, S.; Ibele, M. E.; Sen, A.: Fantastic Voyage: Designing Self-Powered Nanorobots. *Angew. Chem. Int. Ed.* **2012**, *51*, 8434-8445.

(13) Soler, L.; Sanchez, S.: Catalytic nanomotors for environmental monitoring and water remediation. *Nanoscale* **2014**, *6*, 7175-7182.

(14) Campuzano, S.; Orozco, J.; Kagan, D.; Guix, M.; Gao, W.; Sattayasamitsathit, S.; Claussen, J. C.; Merkoci, A.; Wang, J.: Bacterial isolation by lectin-modified microengines. *Nano letters* **2012**, *12*, 396-401.

(15) Kagan, D.; Laocharoensuk, R.; Zimmerman, M.; Clawson, C.; Balasubramanian, S.; Kang, D.; Bishop, D.; Sattayasamitsathit, S.; Zhang, L.; Wang, J.: Rapid delivery of drug carriers propelled and navigated by catalytic nanoshuttles. *Small* **2010**, *6*, 2741-7.

(16) Solovev, A. A.; Sanchez, S.; Pumera, M.; Mei, Y. F.; Schmidt, O. G.: Magnetic Control of Tubular Catalytic Microbots for the Transport, Assembly, and Delivery of Micro-objects. *Adv. Func. Mater.* **2010**, *20*, 2430-2435.

(17) Mei, Y.; Solovev, A. A.; Sanchez, S.; Schmidt, O. G.: Rolled-up nanotech on polymers: from basic perception to self-propelled catalytic microengines. *Chem. Soc. Rev.* **2011**, *40*, 2109-2119.

(18) Baraban, L.; Tasinkevych, M.; Popescu, M. N.; Sanchez, S.; Dietrich, S.; Schmidt, O. G.: Transport of cargo by catalytic Janus micro-motors. *Soft Matter* **2012**, *8*, 48-52.

(19) Gao, W.; Kagan, D.; Pak, O. S.; Clawson, C.; Campuzano, S.; Chuluun-Erdene, E.; Shipton, E.; Fullerton, E. E.; Zhang, L.; Lauga, E.; Wang, J.: Cargo-Towing Fuel-Free Magnetic Nanoswimmers for Targeted Drug Delivery. *Small* **2012**, *8*, 460-467.

(20) Burdick, J.; Laocharoensuk, R.; Wheat, P. M.; Posner, J. D.; Wang, J.: Synthetic nanomotors in microchannel networks: directional microchip motion and controlled manipulation of cargo. *J. Am. Chem. Soc.* **2008**, *130*, 8164-5.

(21) Liu, Z.; Li, J.; Wang, J.; Huang, G.; Liu, R.; Mei, Y.: Small-scale heat detection using catalytic microengines irradiated by laser. *Nanoscale* **2013**, *5*, 1345-52.

(22) Zhao, G.; Pumera, M.: Marangoni self-propelled capsules in a maze: pollutants 'sense and act' in complex channel environments. *Lab. Chip.* **2014**, 14, 2818-23.

(23) Kagan, D.; Calvo-Marzal, P.; Balasubramanian, S.; Sattayasamitsathit, S.; Manesh, K. M.; Flechsig, G.-U.; Wang, J.: Chemical Sensing Based on Catalytic Nanomotors: Motion-Based Detection of Trace Silver. *J. Am. Chem. Soc.* **2009**, *131*, 12082-12083.

(24) Wu, J.; Balasubramanian, S.; Kagan, D.; Manesh, K. M.; Campuzano, S.; Wang, J.: Motion-based DNA detection using catalytic nanomotors. *Nat. Commun.* **2010**, *1*, 36.

(25) Kagan, D.; Campuzano, S.; Balasubramanian, S.; Kuralay, F.; Flechsig, G. U.; Wang, J.: Functionalized micromachines for selective and rapid isolation of nucleic acid targets from complex samples. *Nano letters* **2011**, *11*, 2083-7.

(26) Sanchez, S.; Solovev, A. A.; Schulze, S.; Schmidt, O. G.: Controlled manipulation of multiple cells using catalytic microbots. *Chem. Commun.* **2011**, *47*, 698-700.

(27) Balasubramanian, S.; Kagan, D.; Jack Hu, C.-M.; Campuzano, S.; Lobo-Castañon, M. J.; Lim, N.; Kang, D. Y.; Zimmerman, M.; Zhang, L.; Wang, J.: Micromachine-Enabled Capture and Isolation of Cancer Cells in Complex Media. *Angew. Chem. Int. Ed.* **2011**, *50*, 4161-4164.

(28) Kuralay, F.; Sattayasamitsathit, S.; Gao, W.; Uygun, A.; Katzenberg, A.; Wang, J.: Self-Propelled Carbohydrate-Sensitive Microtransporters with Built-In Boronic Acid Recognition for Isolating Sugars and Cells. *J. Am. Chem. Soc.* **2012**, *134*, 15217-15220.

(29) Zhao, G.; Seah, T. H.; Pumera, M.: External-energy-independent polymer capsule motors and their cooperative behaviors.*Chem. Euro. J.* **2011**, *17*, 12020-12026.

(30) Orozco, J.; Garcia-Gradilla, V.; D'Agostino, M.; Gao, W.; Cortes, A.; Wang, J.: Artificial enzyme-powered microfish for water-quality testing. *ACS Nano* **2013**, *7*, 818-824.

(31) Guix, M.; Orozco, J.; Garcia, M.; Gao, W.; Sattayasamitsathit, S.; Merkoci, A.; Escarpa, A.; Wang, J.: Superhydrophobic alkanethiol-coated microsubmarines for effective removal of oil. *ACS Nano* **2012**, *6*, 4445-51.

(32) Solovev, A. A.; Xi, W.; Gracias, D. H.; Harazim, S. M.; Deneke, C.; Sanchez, S.; Schmidt, O. G.: Self-propelled nanotools. *ACS Nano* **2012**, *6*, 1751-6.

(33) Chang, S. T.; Paunov, V. N.; Petsev, D. N.; Velev, O. D.: Remotely powered self-propelling particles and micropumps based on miniature diodes. *Nat. Mater*.**2007**, *6*, 235-240.

(34) Loget, G.; Kuhn, A.: Propulsion of Microobjects by Dynamic Bipolar Self-Regeneration. *J. Am. Chem. Soc.* **2010**, *132*, 15918-15919.

(35) Loget, G.; Kuhn, A.: Electric field-induced chemical locomotion of conducting objects. *Nat. Commun.* **2011**, *2*, 535.

(36) Diguet, A.; Guillermic, R.-M.; Magome, N.; Saint-Jalmes, A.; Chen, Y.; Yoshikawa, K.; Baigl, D.: Photomanipulation of a Droplet by the Chromocapillary Effect. *Angew. Chem. Int. Ed.* **2009**, *48*, 9281-9284.

(37) Okawa, D.; Pastine, S. J.; Zettl, A.; Fréchet, J. M. J.: Surface Tension Mediated Conversion of Light to Work. *J. Am. Chem. Soc.* **2009**, *131*, 5396-5398.

(38) Gao, W.; Sattayasamitsathit, S.; Manesh, K. M.; Weihs, D.; Wang, J.: Magnetically powered flexible metal nanowire motors. *J. Am. Chem. Soc.* **2010**, *132*, 14403-5.

(39) Tottori, S.; Zhang, L.; Qiu, F.; Krawczyk, K. K.; Franco-Obregón, A.; Nelson, B. J.: Magnetic Helical Micromachines: Fabrication, Controlled Swimming, and Cargo Transport. *Adv. Mater.* **2012**, *24*, 811-816.

(40) Wang, W.; Castro, L. A.; Hoyos, M.; Mallouk, T. E.: Autonomous motion of metallic microrods propelled by ultrasound. *ACS Nano* **2012**, *6*, 6122-32.

(41) Garcia-Gradilla, V.; Orozco, J.; Sattayasamitsathit, S.; Soto, F.; Kuralay, F.; Pourazary, A.; Katzenberg, A.; Gao, W.; Shen, Y.; Wang, J.: Functionalized Ultrasound-Propelled Magnetically Guided Nanomotors: Toward Practical Biomedical Applications. *ACS Nano* **2013**, *7*, 9232-9240.

(42) Brzoska, J. B.; Brochard-Wyart, F.; Rondelez, F.: Motions of droplets on hydrophobic model surfaces induced by thermal gradients. *Langmuir* **1993**, *9*, 2220-2224.

(43) Baraban, L.; Streubel, R.; Makarov, D.; Han, L.; Karnaushenko, D.; Schmidt, O. G.; Cuniberti, G.: Fuel-free locomotion of Janus motors: magnetically induced thermophoresis. *ACS Nano* **2013**, *7*, 1360-7.

(44) Ismagilov, R. F.; Schwartz, A.; Bowden, N.; Whitesides, G. M.: Autonomous Movement and Self-Assembly. *Angew. Chem. Int. Ed.***2002**, *41*, 652-654.

(45) Gao, W.; Pei, A.; Feng, X.; Hennessy, C.; Wang, J.: Organized self-assembly of Janus micromotors with hydrophobic hemispheres. *J. Am. chem. Soc.* **2013**, *135*, 998-1001.

(46) Cabezon, E.; Lanza, V. F.; Arechaga, I.: Membrane-associated nanomotors for macromolecular transport. *Curr. Opin. Chem. Biol.* **2012**, *23*, 537-544.

(47) Mano, N.; Heller, A.: Bioelectrochemical Propulsion. *J. Am. Chem. Soc.* **2005**, *127*, 11574-11575.

(48) Chaudhury, M. K.; Whitesides, G. M.: How to Make Water Run Uphill. *Science* **1992**, *256*, 1539-1541.

(49) Sumino, Y.; Magome, N.; Hamada, T.; Yoshikawa, K.: Self-Running Droplet: Emergence of Regular Motion from Nonequilibrium Noise. *Phys. Rev. Lett.* **2005**, *94*, 068301.

(50) Nakata, S.; Matsuo, K.: Characteristic Self-Motion of a Camphor Boat Sensitive to Ester Vapor. *Langmuir* **2004**, *21*, 982-984.

(51) Zhao, G.; Pumera, M.: Liquid–Liquid Interface Motion of a Capsule Motor Powered by the Interlayer Marangoni Effect. *The J. Phy. Chem. B* **2012**, *116*, 10960-10963.

(52) Pavlick, R. A.; Sengupta, S.; McFadden, T.; Zhang, H.; Sen, A.: A Polymerization-Powered Motor. *Angew. Chem. Int. Ed.* **2011**, *50*, 9374-9377.

(53) Paxton, W. F.; Sen, A.; Mallouk, T. E.: Motility of catalytic nanoparticles through self-generated forces. *Chem. Eur. J.* **2005**, *11*, 6462-70.

(54) Gibbs, J. G.; Kothari, S.; Saintillan, D.; Zhao, Y. P.: Geometrically designing the kinematic behavior of catalytic nanomotors. *Nano letters* **2011**, *11*, 2543-50.

(55) Orozco, J.; Vilela, D.; Valdés-Ramírez, G.; Fedorak, Y.; Escarpa, A.; Vazquez-Duhalt, R.; Wang, J.: Efficient Biocatalytic Degradation of Pollutants by Enzyme-Releasing Self-Propelled Motors. *Chem. Euro. J.* **2014**, *20*, 2866-2871.

(56) Soler, L.; Magdanz, V.; Fomin, V. M.; Sanchez, S.; Schmidt, O. G.: Self-propelled micromotors for cleaning polluted water. *ACS Nano* **2013**, *7*, 9611-20.

(57) Wang, J.; Gao, W.: Nano/Microscale motors: biomedical opportunities and challenges. *ACS Nano* **2012**, *6*, 5745-51.

(58) Petit, T.; Zhang, L.; Peyer, K. E.; Kratochvil, B. E.; Nelson, B. J.: Selective trapping and manipulation of microscale objects using mobile microvortices. *Nano letters* **2012**, *12*, 156-60.

(59) Orozco, J.; Campuzano, S.; Kagan, D.; Zhou, M.; Gao, W.; Wang, J.: Dynamic isolation and unloading of target proteins by aptamer-modified microtransporters. *Anal. Chem.* **2011**, *83*, 7962-9.

(60) Adler, J.: Chemoreceptors in Bacteria. *Science* **1969**, *166*, 1588-1597.

(61) Berg, H. C.: Chemotaxis in Bacteria. *Annu. Rev. Biophys. Bioeng.* **1975**, *4*, 119-136.

(62) Baraban, L.; Harazim, S. M.; Sanchez, S.; Schmidt, O. G.: Chemotactic Behavior of Catalytic Motors in Microfluidic Channels. *Angew. Chem. Int. Ed.* **2013**, *52*, 5552-5556.

(63) Khim Chng, E. L.; Zhao, G.; Pumera, M.: Towards biocompatible nano/microscale machines: self-propelled catalytic nanomotors not exhibiting acute toxicity. *Nanoscale* **2014**, *6*, 2119-2124.

(64) Xi, W.; Solovev, A. A.; Ananth, A. N.; Gracias, D. H.; Sanchez, S.; Schmidt, O. G.: Rolled-up magnetic microdrillers: towards remotely controlled minimally invasive surgery. *Nanoscale* **2013**, *5*, 1294-1297.

CHAPTER TWO: MILLIMETER SCALE CAPSULE MOTORS

The work discussed in this chapter resulted in the following publications:

1. Zhao, G.; Pumera, M., Reynolds numbers exhibit dramatic influence on directionality of movement of self-propelled systems. Phys. Chem. Chem. Phys. 2012, 14, 6456-6458.
2. Zhao, G.; Pumera, M., Liquid–liquid interface motion of a capsule motor powered by the interlayer Marangoni effect. J. Phys. Chem. B 2012, 116, 10960-10963.
3. Zhao, G.; Pumera, M., Macroscopic self-propelled objects. Chem. – Asian J. 2012, 7, 1994-2002.
4. Zhao, G.; Stuart, E. J. E.; Pumera, M., Enhanced diffusion of pollutants by self-propulsion. Phys. Chem. Chem.Phys. 2011, 13, 12755-12757.
5. Zhao, G.; Seah, T. H.; Pumera, M., External-energy-independent polymer capsule motors and their cooperative behaviors. Chem. – Euro. J. 2011, 17, 12020-12026.

6. Zhao, G.; Pumera, M., Marangoni Self-propelled capsules in a maze: pollutants 'sense and act' in complex channel environments. Lab Chip, accepted.
7. Seah, T. H.; Zhao, G.; Pumera, M., Surfactant capsules propel interfacial oil droplets: an environmental cleanup strategy. ChemPlusChem 2013, 78, 395-397.

2.1 Introduction

We live in a lively world, where small creatures of all kinds are trying their best to move around, either in water, in air, or at the water/air or solid/air interfaces. Such swimming, flying or walking of small biological "motors" are powered by the consumption of food, and the control over the motion is precise in terms of start/stop, speed and direction. The "motors" in most cases are also able to respond to external stimuli and alter their movement accordingly, indicating a highly intelligent moving system.

It has also been the effort of scientific community to study the motion of small animals and construct the artificial biomimetic motors. The millimeter-scale motors occurred in the literature can be found in different forms and categories.

Based on the type of energy sources, such small motors are divided into three different categories, namely: system *I* whereby the energy stored in the fuel is converted into mechanical movements, utilizing the "chemical fuels" ranging from hydrogen peroxide,[1] hydrazine[2] to glucose[3], as can be seen in Figure 1-6 for an example;[3] system *II* whereby externally supplied power source is converted into motions, and an example of light powered devices can be seen in Figure 1-3;[4] system *III* whereby self-propelled locomotion of devices on the interfaces between air/solid or air/liquid due to the process of free energy minimization *via* physicochemical reactions,[5,6] and an example can be find in Figure 1-7.[6] For motors whose motion is dependent on the supply of external physical

energy or chemical fuels, a higher requirement for the powering facilities or a large amount of chemical fuel in the environment is usually expected. Thus my Ph. D. work in the millimetre-scale motors was focused on the development of type *III* motors.

Based on the material state of the motors and the medium they are running inside, the millimetre-scale small motors can also be categorized into different groups. There are liquid motors running at the air/liquid interface,[7-9] liquid motors running at the air/solid interface,[10-14] as well as solid motors running at the air/liquid interface[15-19] or in the bulk liquid[20-22]. In order to achieve an easier functionalization, solid motors of capsule shapes running at the air/liquid surface were extensively studied in my Ph. D. work. Moreover, a novel kind of solid motor running at the liquid/liquid interface was also discovered and presented in the following text.

In this chapter, I wish to demonstrate a millimetre-scale polymer motor with a capsule shape. Running at a wide variety of air/liquid interfaces, the motor exhibited a high velocity. The liquid medium for the motor to run can be pure deionized water, sea water, organic solvents/water solutions or acidic aqueous liquids. External supply of physical energy or chemical fuel to power the motor is omitted, and the motion mechanism is attributed to the well-known phenomenon called the Marangoni effect, which indicates that solid particles or liquid droplets can migrate from locations of a weaker interfacial energy towards a direction of location that possesses a stronger interfacial energy. The manipulation of the speed and direction of the motion was investigated, and the interactions between the normal and SDS-incorporated motors were also demonstrated. Based on this, we step further to explore the possibility to utilize such motors for the clean-up of aqueous solution that contains some oil drops on the surface, which are the pollutants.

2.2 External-Energy-Independent Polymer Capsule Motors

2.2.1 Preparation and Characterization of the Polymer Capsule Motors

Experimental Procedures

The polymer solution for the motor was made by mixing PSf (Sigma-Aldrich) with DMF (Merck) and was allowed to dissolve into a transparent mixture in the ultrasonic condition for 30 minutes. For the study of relationship between plain and SDS-loaded motors, the concentrations of PSf and SDS in the DMF solution was made to be 7 wt% and 4 wt%, respectively. PSf crystals were mixed with SDS powders, and followed by the addition of liquid DMF into the mixture, which was ultrasonicated for half an hour. Similarly, Ni nanoparticles loaded polysulfone motors were prepared (Nickel NPs (size <50 nm) bought from Sigma-Aldrich). The PSf/DMF mixture was freshly made for every trial. Mineral-oil (Singer do Brasil) was transparent and was enhanced with visibility using 1 wt% of the dye diazobenzene. Surface morphologies of the capsules were determined by scanning electron microscope.

Motion studies of the millimetre-scale polymer motors were done in a glass trough with a size of 20 cm × 20 cm × 5.5 cm. An amount of 200 mL of aqueous liquid (water or water/solvent mixtures) was put into this trough. To run the polymer capsule motors, a drop of the mixture of polysulfone and DMF was placed on the surface of the liquid inside the trough. Polysulfone became solid immediately *via* a phase-inversion mechanism upon interaction with water and motion emerged subsequently.

The videos and images were studied with the software Nikon NIS-Elements™ and the mean values of speeds for the first five seconds were calculated. For every set of data, the standard deviation and mean value of the tracked speeds (n=6; six independent trials with

the same experiment setup) were calculated with the standard deviations shown as error bars.

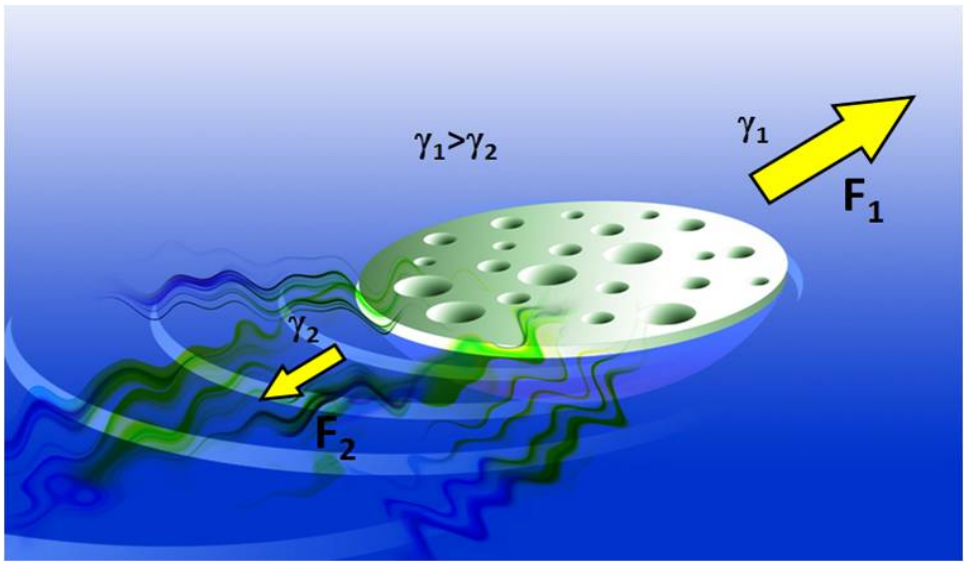

Figure 2-1 Movement of a polymer capsule. The molecules of DMF are slowly released out from the device in an asymmetric manner. The back vicinity of higher concentration of DMF possesses a lower surface tension than that of the front vicinity of the capsule, and thus the force at the front is higher, pulling the device to move forward.

Characterizations of the Motors

The self-propelled polymeric capsule-shaped motors shown in this section were prepared by placing an amount of 5 μL mixture of PSf in DMF on water surface. Immediately upon interaction with the aqueous liquid, PSf dissolved in DMF became solid through a phase-inversion process, creating a round-shape Polysulfone motor with a large quantity of tiny holes on the surface (size ~130 nm) at the side underneath the water surface while showing significantly larger holes (in the order of around 20 micrometers) at the top surface of the capsule motor. Characterization of the capsules with scanning electron microscope is seen in Figure 2-2. The molecules of DMF in the capsule were out from the structure slowly (the releasing process lasted for up to 20 min) and distributed

asymmetrically around the motor to the liquid surface *via* these large holes. The interfacial gradient (γ) of water/solvent mixture (typically water, γ=72.0 mN/m and DMF γ=35.2 mN/m) resulted into the fast motion of the motor (Figure 2-1).

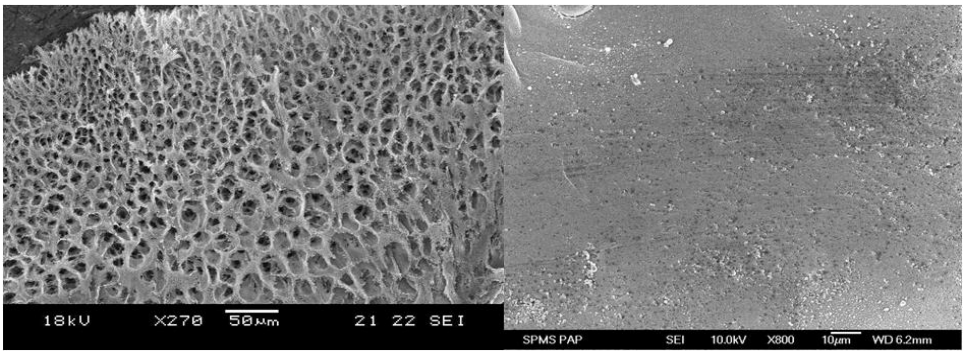

Figure 2-2 Scanning electron microscopy (SEM) images of the surfaces of the polysulfone capsules at the solid/air interface (left) and capsule/water interface (right). The magnifications are 270× and 800×, scale bars 50 µm and 10 µm, respectively.

2.2.2 Factors Affecting the Motion

Motions of the capsules were based on Marangoni effect. When DMF molecules molecules are released out, the rate of release around the capsule at the capsule/air interface is not symmetrical, leading to an asymmetric distribution of DMF at the water surface. Since the interfacial tension of DMF is lower than that of water, the imbalance of DMF concentration results in an imbalance of surface tension, and more DMF gives a lower surface tension. As depicted in Figure 2-1, there is lower amount of DMF at the front of the capsule, thus the surface tension γ_1 is higher than that at the rear γ_2. A net pulling force **F** can thus be generated to drive the capsule to move forward.

From the motion mechanism, one can determine that the driving force arises from the difference in surface tension between the bulk aqueous solution (γ_1) and the released molecules (γ_1). If the surface tension γ_1 is altered by changing the composition of surrounding solution, the net pulling force **F** will be changed, leading to a higher or lower

velocity depending on the increase or decrease of the surface tension difference. To study this hypothesis, the following experiment was carried out: Various concentrations of acetic acid were made, and according to the database, the solution of acetic acid in water at 60 wt% possesses an interfacial energy of 36.1 mN/m. This surface tension is quite close to that of DMF, which is 35.2 mN/m. Indeed, upon changing the amount of molecules of acetic acid from 0 to 90 wt% in a 30 wt% steps, the speed of the motors was reduced and became zero at 60 wt% of acetic acid (Fig. 2-3, c). On the contrary, when the surface energy of the surrounding liquid was increased, the interfacial energy gradient between that of DMF released from the motors and the surface of the aqueous solution increased as well. Such higher difference in surface tension resulted into an increment in the speed of the motors, as shown in the Figure 2-3a. When we increased the amount of KCl in the solution, the interfacial energy of the surrounding environment increased, resulting in higher interfacial energy gradient in the interfacial energies between the released molecules and the surrounding liquid. Such increment in surface tension led to a rise of the average speed of the polymer motors from 11.4 cm s^{-1} to 15.7 cm $^{-1}$.

Next, the effect of the concentration of various surface tension-reducing organic molecules in the water solution on the speed of the motors was investigated for EtOH, acetonitrile and DMF (Figures 2-3, d-f). In each of the studies, the speed of the motor was determined to decrease significantly as the concentration of such molecules in the aqueous phase was made higher; such increment could be attributed to the higher concentrations of the surface tension-reducing molecules in the water phase, which can dramatically lower the interfacial energy of the aqueous phase. Meanwhile, one of the important observations was that, even when the concentration of DMF in water was increased to be 80 wt%, motion can still be observed for the motors. Besides such molecules, the presence of surface active molecules in the system could also lead to a

reduction of the surrounding interfacial energy. In our study, SDS molecules were utilized for the reduction of the interfacial energy. It was observed that similar to the case of abovementioned organic molecules, the speed of the motors was reduced with higher amount of surfactant in the system (Fig 2-3, b).

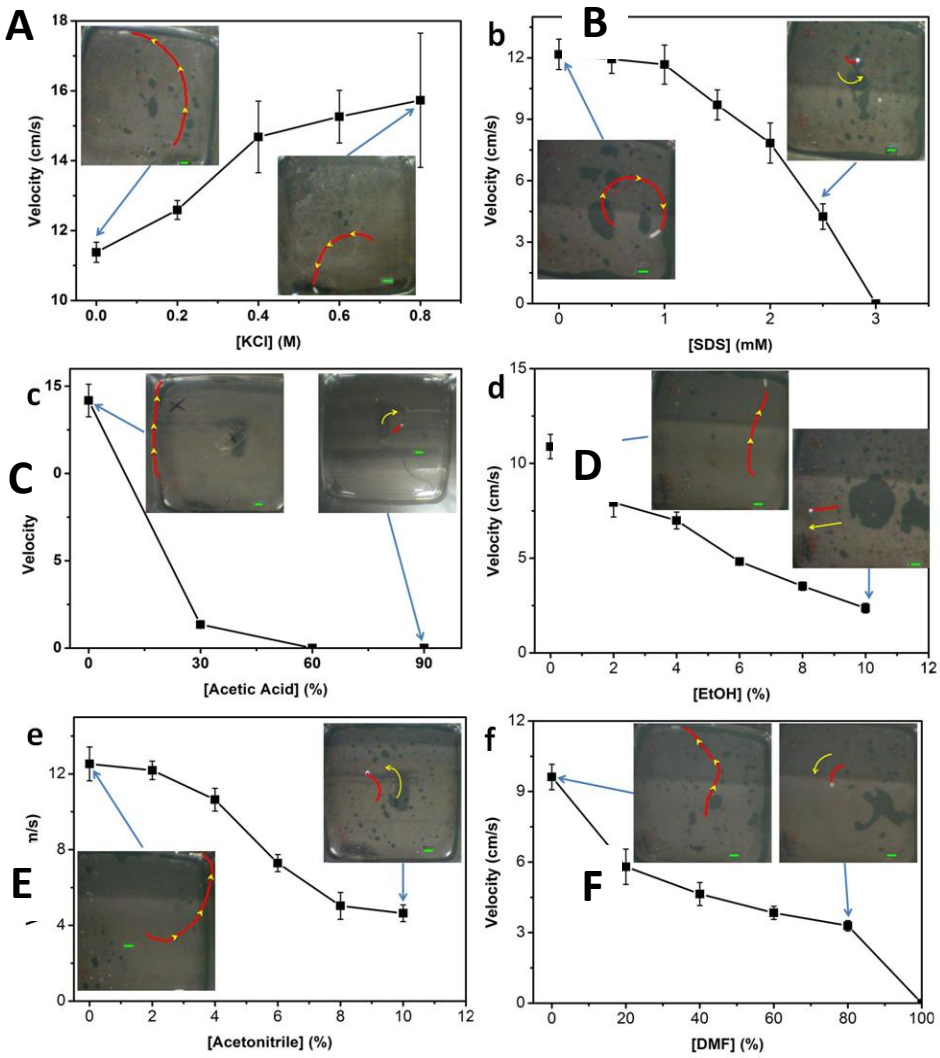

Figure 2-3. Video-tracking and plots of average-velocity of the motors as a change according to increment in amount of different salts or solvents in water solution: **(A)** KCl; (B) surfactant (SDS); **(C)** acetic acid; **(D)** EtOH; **(E)** acetonitrile and **(F)** Dimethylformamide in water mixture (*n*=6 for all data sets; relative standard deviation is at 95% confidence levels and shown by error bars). In every experiment, the volume of the motor precursor was 5 µL. The motion track-images were for a time length of 1 s and the scale-bars in all images represent five centimetre.

Our focus of study was then made to determine the effect of the motors' diameter and concentration of PSf on the motors' speed. It was hypothesized that with higher and higher amount of precursor solution placed on water surface, the side area of the running motors should also become larger, leading to a stronger resistance on the motion of the motors. As predicted by this hypothesis, a reduction in the running speed of the motors from 13.4 to 8.8 centimetres per second was recorded when the input size of the PSf/DMF mixture was made higher from 5 to 15 µL (Figure 2-4). A stepwise reduction of the running speed of the motors was seen from 11.8 to 6.5 centimetres per second as the concentration of PSf was getting higher and higher from 5 wt% to 10 wt % in a 1 wt % changing step.

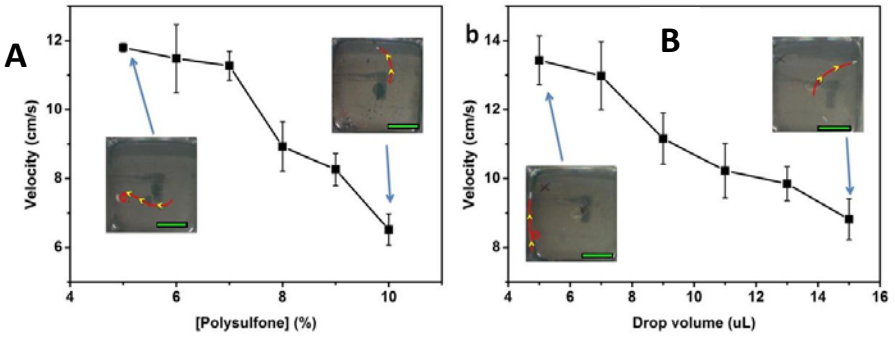

Figure 2-4 Video-tracking and plots of average-velocity of the motors as a change according to: (A) Concentration of PSf in the precursor mixture. (B) Amount of the precursor mixture placed on the water surface. In every study, amount of H_2O in the container was 200 mL, and distance of placing the precursor was roughly 2.5 cm away from the H_2O surface. For every set of the study, totally six different recordings and tracking were carried out. The tracking figures were done for a time length of 1 s and the scale bars in all images indicate five centimetre.

As shown in Chapter One, the fashion of movement, same as speed and direction of the motion, is also one of the important parameters in describing the movement. In general,

motion of an autonomously running artificial device can be linear-fashion, rotation or a mix of these two. All these categories of movements were recorded for the polymer motors in this study, as illustrated in Figure 2-5.

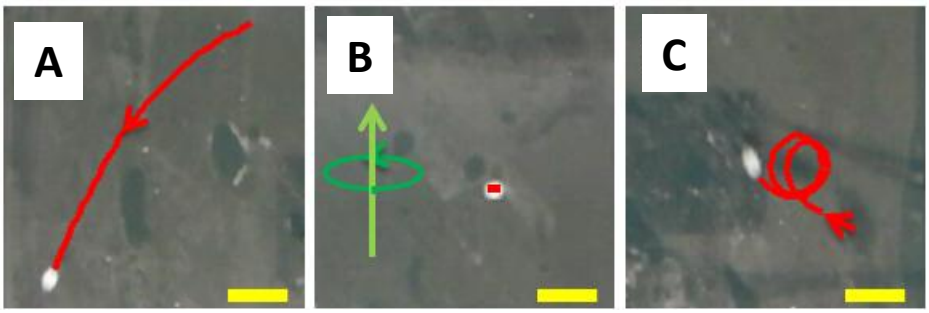

Figure 2-5 Tracking snapshots of moving motors with various styles of motions: (A) linear directional; (B) rotation on a fixed location and (C) a mixed style of motion of the above two. Scales are two centimeters and the tracking duration was 1 second for all situations.

The style of motion can be determined by 3 aspects, including (i) intrinsic aspects, that is the geometry of the device;[23,24] (ii) factors that arises from the surrounding medium that the motors operate in (viscosity, density)[25,26] or (iii) outside factors that can affect the motion (i.e. an electromagnetic field)[23,26,27]. While the motion style for the motors manipulated by an outside factors or intrinsic geometry of the devices was investigated in the literature,[23] specific investigations on the effects of the surrounding mediums that the motors are running inside on the motion styles of the motors have not been done.[28] Here it should be noted that Sanchez *et al.* recently showed that the environment temperature alters the viscosity of the H_2O_2 that serves as chemical power source for the catalytic motion and that the styles of motion for the microtubular motors transforms from linear-fashion to curvilinear fashion.[29] We would like to illustrate here in a systematic way that the motion style of a small scale autonomously running motor is significantly affected by the Reynolds numbers of the entire running-system.

Reynolds number (Re) is a dimensionless factor which determines the ratio of effects of inertia to viscosity for any situation. The Reynolds number can be calculated from the following parameters of the surrounding medium:

$$Re = \frac{\rho v l}{\mu}$$

where v is the mean running speed of the motor, ρ is the density of the liquid, l is the characteristic size of the motor and μ is the dynamic viscosity.

The movement of a motor in the fluid is determined on the net effect of its accelerating force (***Fa***) and drag force (***Fd***) from the fluid. The dragging of a running device in general is determined non-linearly on the speed of the device itself. For the systems with a low Reynolds number (that is Re is far less than 1), $\boldsymbol{F_d}$ can be estimated to a directional linear form (Stokes equation) while for high Reynolds number system (Re far higher than 1), the frictional force is determined by the running speed in non-linear form. The motion of a symmetrical device at a low Reynolds shows a perfectly linear directional movement. It is well known that very small particles (in less than one mm) running at very low Re ($R \approx 10^{-6}$)[30] and thus if the geometry of such particles are symmetrical, their motions are translational. On the other hand, running of motors at a high Reynolds number leads to the generation of slow drift eddy currents which produces a non-linear and off-axis part to the frictional force, which leads to non-linear movements. With current focus on small-scale polymer devices (cross section at the millimetre-scales), it is important to take consideration that the Re for such devices are in the "intermediate level" ($Re \approx 1–600$).[31,32] In this section I would like to demonstrate that the motion styles of the movement of millimetre-scale devices are observed be transformed from linear to non-linear by increasing the Reynolds number of the motors.

Different concentrations of glycerol and dimethylacetamide (DMAc) in water mixtures were made by mixing thoroughly with H_2O, and these mixtures were placed without disturbance to become stable before dropping the PSf/DMF mixture on the surface. To change the Reynolds number of the systems, we prepared glycerol aqueous solutions with 0, 20, 40, 60 and 80% weight concentrations. Glycerol was selected for this purpose due to its large viscosity. Moreover, glycerol can be easily dissolved in H_2O to form solutions of desired concentrations. While changing the Reynolds numbers for the capsule motors, we determined two categories of motion styles, namely the linear movement (case A) and rotation or non-linear movement (case B) (n = 10 for each situation). Figure 2-6 illustrates the effect of the concentration of glycerol in H_2O on the Reynolds number of the system. With a higher concentration of glycerol in the solution, the Reynolds number significantly reduced from 566 for no glycerol to 2.3 for 80 wt% of glycerol. The number of rotational or non-linear movements (case B) reduced from 100% for the 0% glycerol condition to 10% in an 80 wt% glycerol condition. Therefore, the possibility of non-linear or rotational motion becomes higher, from 10% to 100% upon increasing the Reynolds number from 2.3 to 566.

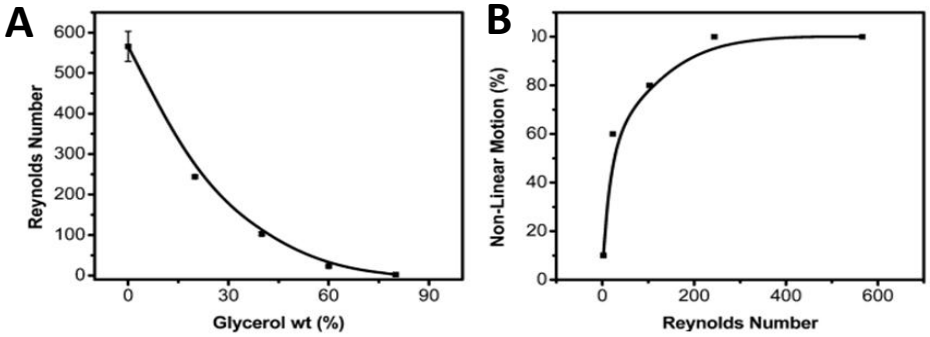

Figure 2-6 Effect of Reynolds number on the possibility of linear/rotational movement of the motor running in the glycerol aqueous solution. (A) With higher concentration of glycerol in H_2O, the Reynolds number was reduced; (B) possibility of non-translation movement got higher with higher Reynolds numbers. Experiment situation: 7 wt%

PSf/DMF precursor solution, radius of the capsule semisphere is 2 mm; temperature, 22^{o}C.

To show that the observation for glycerol solution is not a single-isolated situation which is special to aqueous glycerol solutions, experiments were also carried out to looked further into the motion of the self-running motors in a water–dimethylacetamide (DMAc) solution. By changing the concentration of dimethylacetamide from 0 to 80%, the Re of the capsule motors was reduced from 566 to 22 (Figure 2-7). With higher concentrations of dimethylacetamide in the system, the number of cases of non-linear motions was reduced from 100% to no non-linear motion at all. Thus, the possibility of non-linear motions got higher and higher from 0 to 100% as the Reynolds number of the system was made higher from 22 to 566.

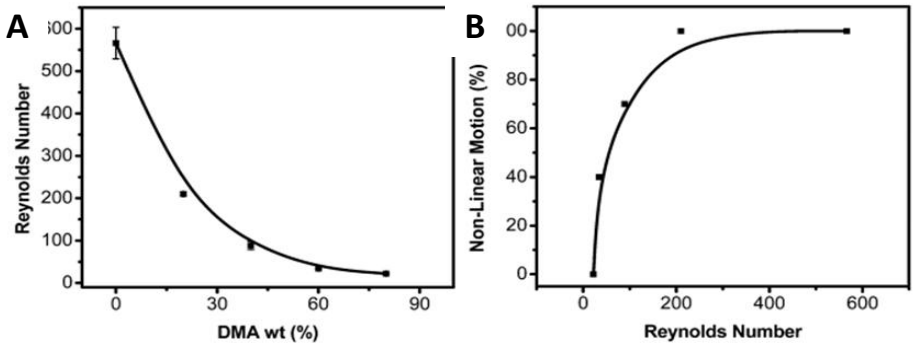

Figure 2-7 Effect of Reynolds number on the possibility of linear/rotational movement of the motor running in the DMAc aqueous solution. (A) With higher concentrations of DMAc in H_2O, the Reynolds number of the motors was reduced; (B) Possibility of non-linear movement was higher with higher Reynolds number of the motors. Experiment situation: 7 wt% PSf/DMF precursor solutions. Radius of the capsule is 2 mm; temperature, 22^{o}C.

2.2.3 Manipulation of Motion with Magnet

Ni powder of nanometer sizes was mixed into the polymer motor with a weight percentage of 4% to facilitate the manipulation of movement with the presence of external magnet. The Ni-incorporated motor was then fixed at certain spots by placing the magnet underneath the trough. The motion of the motor with the absence of magnet gives a relatively higher linear mobility with changing degree of motion (^{o}) between 0 to 25° over a 0.2 s time length. However, by placing the external magnet underneath the trough, the motor started to circulate near the spot where the magnet was located in small rounds of diameters around 0.5 centimetres. Deflection angle of the motors became higher, measured to be 130 to 180° over a 0.2 s time length. Such manipulation with external magnet offers a potential to "dock" the motors prior to their starting of running off for various tasks or purposes (see Figure 2-8).

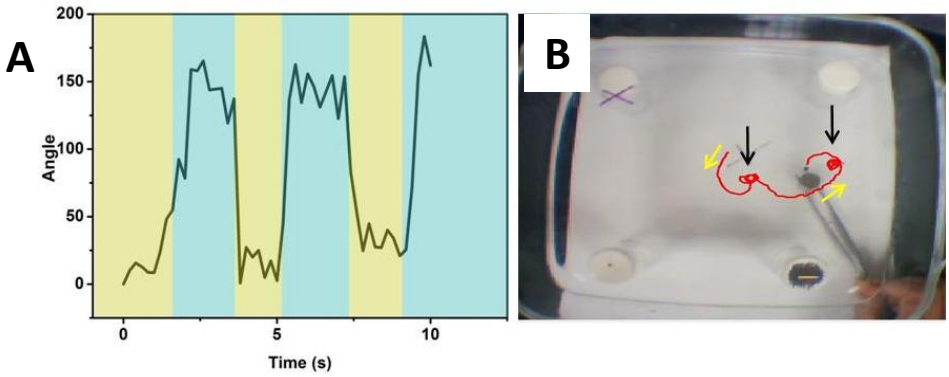

Figure 2-8 Effect of external magnet on the deflection angle of the motion (α) of the Ni-incorporated motor. (A) Quantification of the angle for the motors with the presence (blue) and absence (yellow) of magnetic field. The magnitude was low with the absence of external magnet bar, which shows that a translational movement of the motor dominates in this case. By placing the external magnet underneath the motor, the deflection angle of the motor significantly promoted to a large degree, which suggests that the motion of the motor transformed into a rotational fashion; (B) Video-tracking of the Ni-incorporated

motor. The motion transformed from a nearly translational and small angle fashion to a rotational fashion with short radius ("docking") manipulated by the external magnet which was placed and taken away 2 times at the places indicated by arrows. Scale bar: 1 cm.

2.2.4 Interactions between Plain and SDS-Loaded Capsules

Group interaction of the motors is also of high importance in order to carry out collective jobs or reduce collisions of motors.[33] The interactions of two normal polysulfone motors were investigated and long-distance effects were not seen for such motors. However, the significant interactions could be recorded in the case of an SDS-incorporated polysulfone motor and another normal polysulfone motor. The SDS-incorporated polysulfone motor (SDS/PSf) pushed-away the normal (SDS-free) polysulfone motor due to the altering (reducing) of the surrounding fluid interfacial energy by the surface active agents released. Because of the fact that these motors possess different motions and velocities, the long-distance cooperative observation of these 2 motors would show interesting tracking paths. With the absence of any restriction/boundaries in the system for the motors [6], the polysulfone motor changed its direct running path and run along the SDS/PSf motor, as seen in Figure 2-9. When a restriction/boundary exists near the paths of the motors (Figure 2-10), the repulsive phenomenon from the SDS/PSf motor resulted into the temporary pause and backward motion of the polysulfone motors. When the SDS/PSf motor was gone and away from the polysulfone motor, its normal capsule motor reversed its direction of motion for a second time and its first motion direction was readapted.

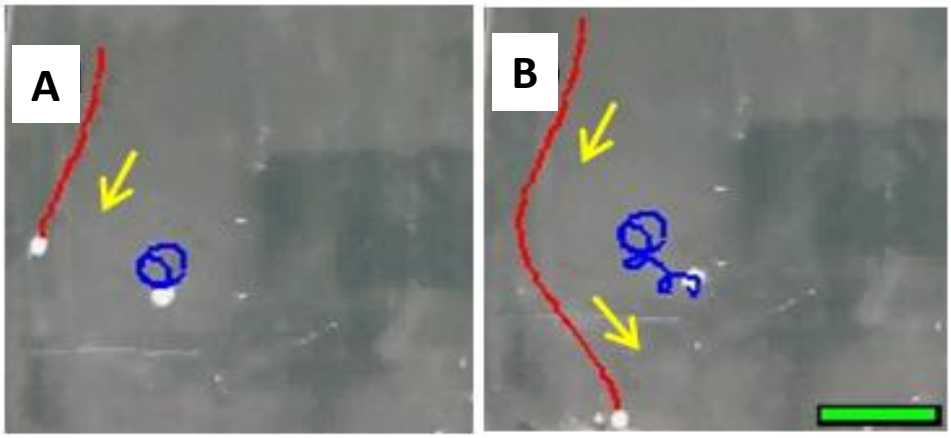

Figure 2-9 Cooperative interactions between normal polysulfone and SDS-incorporated polysulfone motors for the situation of a polysulfone motor (red color) passing by a SDS-incorporated polysulfone motor (5% wt) (blue color), the polysulfone motor "detours" SDS-incorporated polysulfone motor by letting out of the surface active SDS molecules it contained and thus reducing of interfacial energy surrounding the SDS-incorporated polysulfone motors. The snapshots taken from the recorded videos were from different time-spots and the interval is 1.2 seconds.

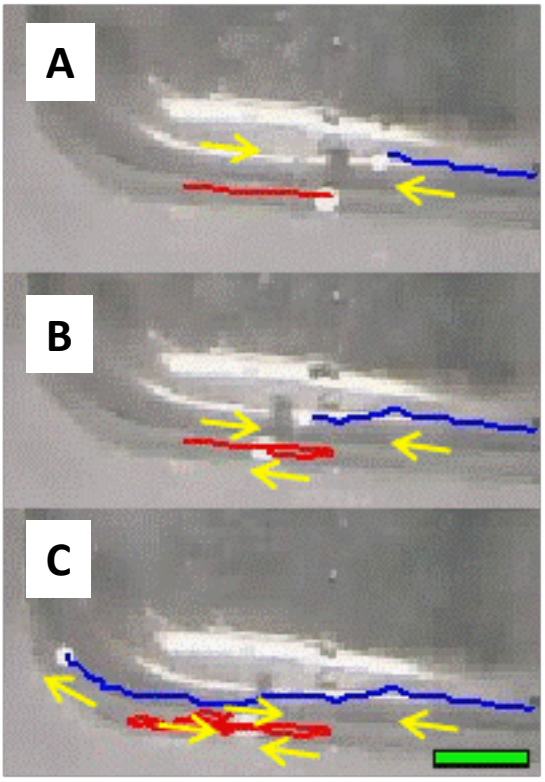

Figure 2-10 Cooperative interactions between normal polysulfone and SDS-incorporated polysulfone motors for the situation of the two motors moving head on towards one another with the presence of boundaries. (A) The normal polysulfone motor reversed its initial direction and adapted a direction along with that of the SDS-incorporated motor. (B) When the SDS-incorporated motor passed by the normal polysulfone motor, the normal polysulfone motor changed motion direction for a second time, facing away from the SDS-incorporated motor and adapted its initial direction of movement again. The time lengths between A and B is 0.4 seconds and between B and C is 0.9 seconds.

2.2.5 Induced Motion of Oil Droplets

The capability of long-distance interactions induced by the SDS-incorporating polysulfone motor on "shepherding" targets was also investigated. The effect of the motors on the motion of the oil floating on H_2O surface was also studied. The SDS-incorporated motors were able to push away the oil droplets over a long range of a few centimetres and induced the motion of oil droplets so that they move away from the SDS-incorporated motors, because of the Maragoni effect, while the normal polysulfone motors was not able to induce the motion of oil droplets (Figure 2-11). The SDS-incorporated motors wouldn't touch the oil droplets, and when the two of them got closer, the concentration of SDS molecules was higher, which resulted into a stronger repulsive force on the oil droplet. But for the normal motors, since they were not able to push away the oil droplets, collision was observed between them and the oil droplets. Moreover, the speed of the oil droplet was slower for the larger droplets, higher when the size of the SDS-incorporated motors was increased, and also higher when more amount of SDS were mixed in the motors.

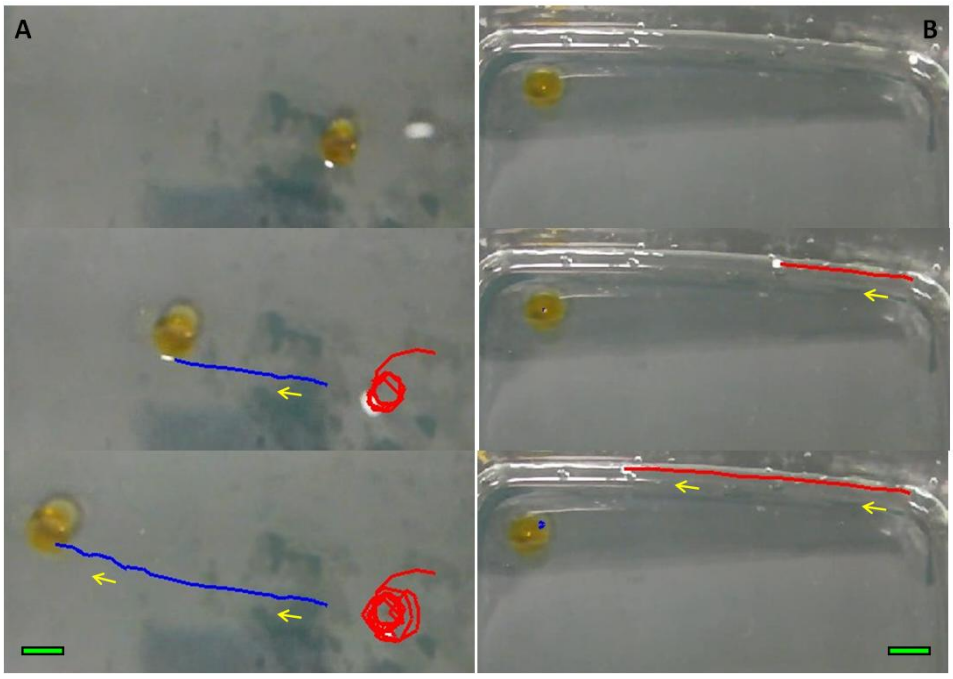

Figure 2-11 Interactions between SDS-incorporated motors with the oil droplets and the normal SDS-free motors with the oil droplets. Red color indicates the tracking of motors and blue color indicates the tracking of the oil droplets. (A) SDS-incorporating motors (4 wt% of SDS), and (B) normal polysulfone motors. A repulsive effect can be seen on the oil droplets by the SDS-incorporated motors, which gives the oil droplet an obvious motion. Scale bars indicate 1 cm. Images taken in 1 second time intervals.

2.2.6 Cleaning of Water Surface with Oil

The long-range repulsive force between SDS-incorporated motors and oil droplets may be utilized to shepherd multiple oil droplets and to accumulate such droplets, efficiently remediating the contaminated water resources. Here it is shown that such shepherding phenomenon of SDS-incorporating motors can merge 3 oil droplets (Figure 2-12). Such oil droplets, each of size of 200 µL were stabilized on the H_2O surface. When the SDS-incorporated motors were not introduced in the system, the droplets kept isolated and stationary. However, when SDS-incorporated motor was introduced, obvious motion of oil droplets could be recorded at velocity of around 2 cm/s, induced by the SDS-

incorporated motors. The motion of such oil droplets in different directions and speeds resulted into the collision and merging of two oil droplets in about 5 seconds and ultimately merging with the last droplet in 7 seconds. The deployment of such SDS-incorporating motors shepherding could have strong affection on the application of such motors for removing the pollutant from water surfaces, especially as polysulfone is biocompatible material.

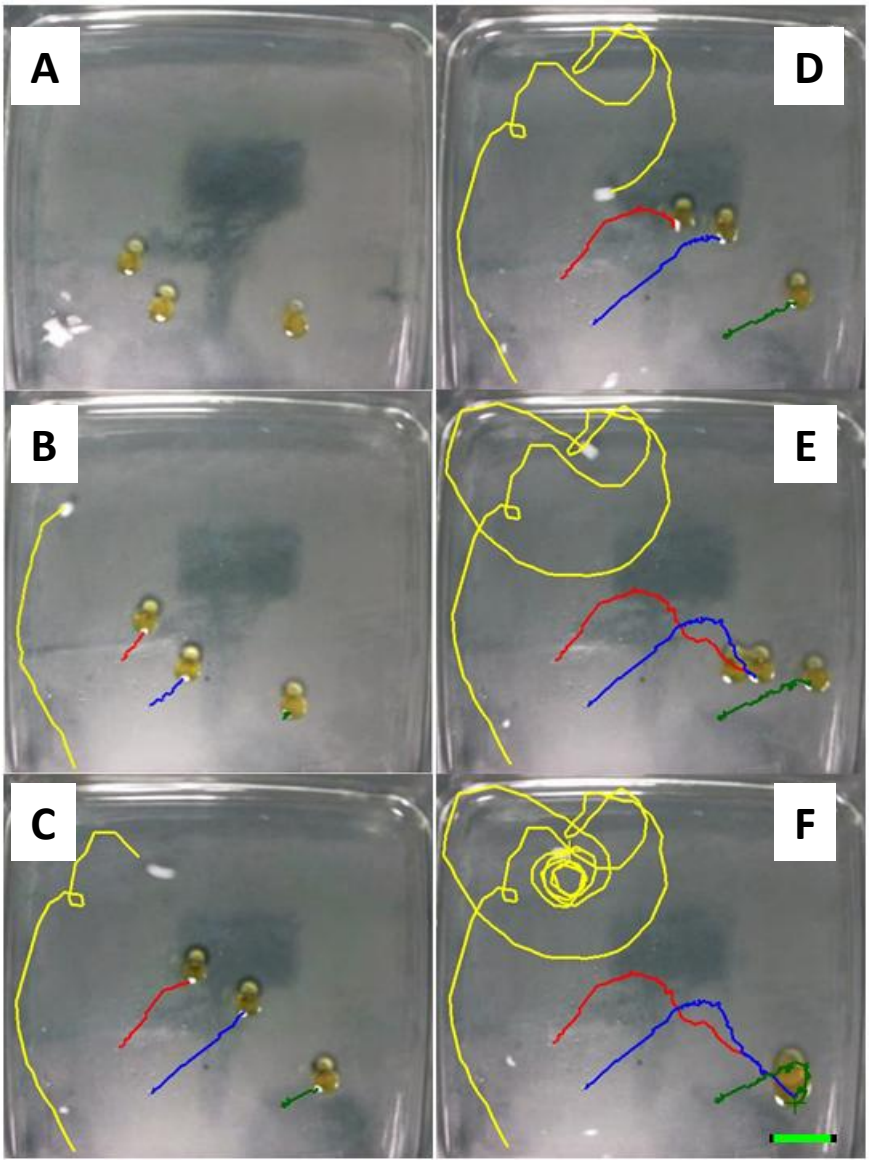

Figure 2-12 Shepherding three oil droplets by one SDS/PSf capsule. Moving SDS/PSf droplets induces movement onto oil droplets. Images taken at (a) t=0, (b) 0.8, (c) 2.3, (d)

3.5, (e) 4.7and (f) 7.0 s. Oil droplets are shepherded and in 5.8 s from the beginning two of them merge (blue and red lines); the third oil droplet merges with the rest in 7.0 seconds (green line). Scale bar, 1 cm.

2.3 Running of the Capsule Motors in Oil-Water Interface

One of the most important aspects about the motion of millimeter-scale motors is the types of medium they are able to operate within. So far, artificial small motors are able to operate in the bulk liquid[28,34,35], or at the air/liquid,[4,8,36] liquid/solid,[37,38] or air/solid interfaces.[6,39] It is interesting to wonder if they are able to move at the interface between two different liquids, and yet a study to run the motors in such an environment is lacking. In this section, I wish to show a novel system where our millimeter-scaled polymer capsule motors can identify the oil and water interface and run at this layer. It is also the hope to demonstrate here that the intrinsic and environmental aspects can alter the running of such motors.

Experimental Procedures

The fabrication procedure of such capsule motors is similar to the motors reported in Section 2.2. To study the motion of the polymer motors at the oil and water interfacial layer, a 50 mm diameter Petri dish was used. An amount of 10 mL of transparent oil was poured gently on top of 10 mL of H_2O. A drop of Polysulfone in DMF mixture with or without the containing of nickel nanoparticles was dropped on the oil/air interface using a pipette, and such precursor solution slowly went into the oil layer and became solid at the oil-water interfacial layer. Motion of the polymer motor emerged immediately when the solid capsule structure could be seen. A magnetic bar was put around the Petri dish to

control the movement of the motors incorporated with nickel nanoparticles. A Casio HD camera was fixed over the oil surface to record the videos of the movement.

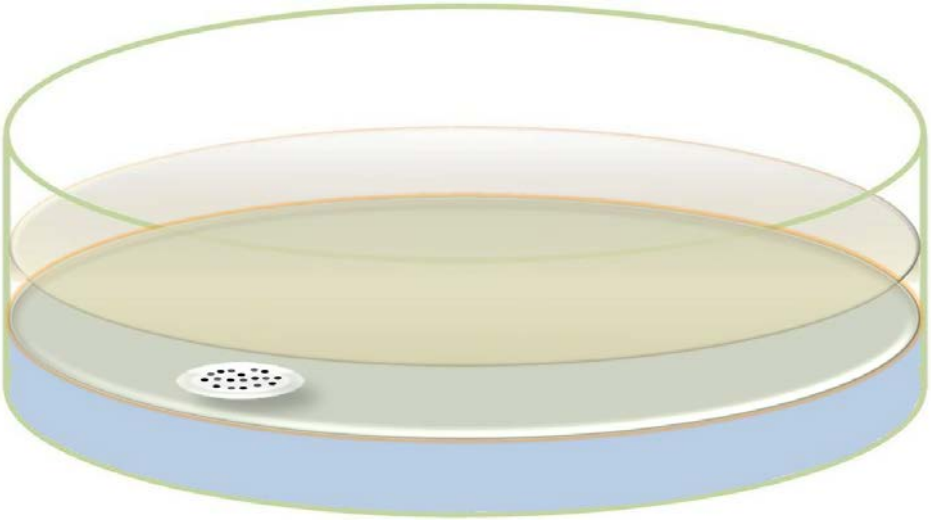

Figure 2-13 Schematic showing the motion of the polymer motor running at the interfacial layer between water and oil.

Results and Discussion

The experiment was carried out by constructing water and oil interfacial layer due to incompatibility of H_2O and oil molecules. The system was contained in a Petri dish as shown in Figure 2-13. Water has a higher density, and is not miscible with oil, thus the oil layer interfaced with both water and air. A PSf/DMF mixture of 7 wt% polysulfone was made by ultrasonication, and an amount of 5 μL of such precusor was placed on top of the oil of the system. The solution of polysulfone in DMF went into the oil layer because of its incompatibility with such mineral oil and also its heavier density than the density of oil. Once in touch with the underlying water molecules at the oil/water interfacial layer, polysulfone became solid in no time via a phase inversion process,[40] leaving a thin polymer and capsule-shaped structure. This procedure is shown in Figure 2-14.

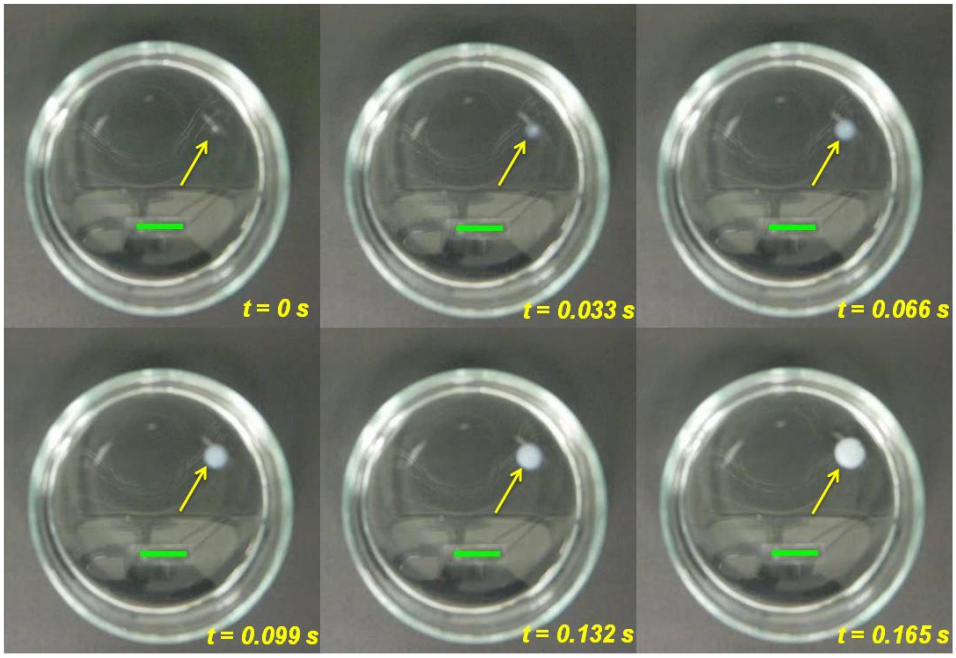

Figure 2-14 Appearing procedure of the polymer capsule structure. Images were obtained with a time difference of 0.033 s. Scale bars show 1 cm.

In total, roughly 0.165 s is required for the polysulfone to thoroughly react with H_2O and show the solidified structure of the polymer. The gradually bigger in diameter of the structure evidence the solidification and enlargement progress of the capsule motor. The self-propelled motion of the motor started immediately after the solid structure was readily constructed at the oil/water interfacial layer. The motion of the polymer motor was powered by the asymmetric leaking of DMF molecules from the motor *via* an interlayer Marangoni effect. The DMF molecules come out from the motor, and they are dissolved in H_2O. As DMF/water mixture has a much reduced interfacial energy (γ = 35.2 mN/m) than water (γ = 72.0 mN/m), the motor is propelled toward the place of liquid with higher surface tension. Motion of these motors is affected by the dragging force raised from not only the bulk water but also the oil part. Tracking of movement is shown in Figure 2-15. As the polymer motor releases molecules of DMF asymmetrically to the

water part, the interfacial energy gradient at the opposite ends of the motor leads to the running of the capsule itself.

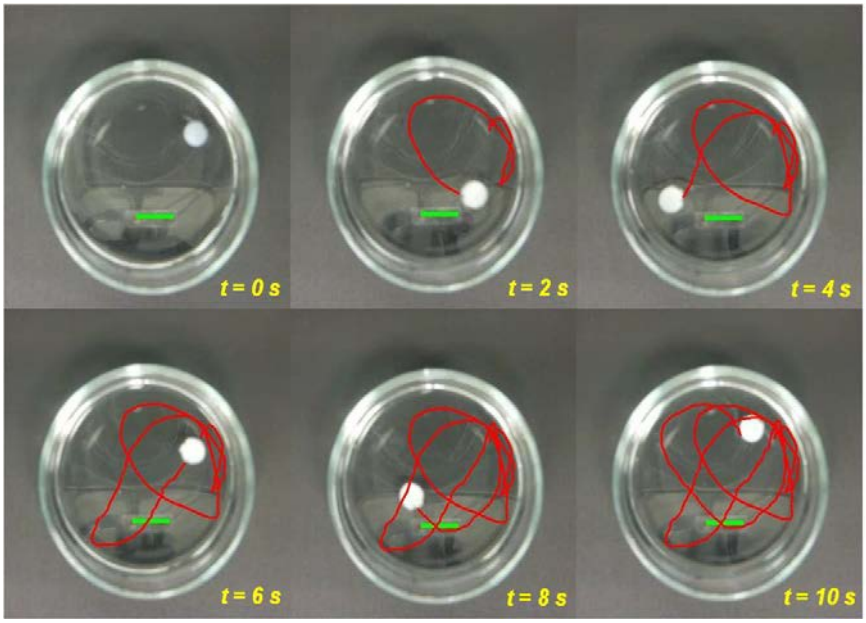

Figure 2-15 Running of the polymer capsule motor with a time frame of 2 s. The scale bars are 1 cm. The motor showed only linear movement, and rotation or circularization of the motor wouldn't be seen.

The polymer structures showed a diameter of 6 millimeter with a thickness of 830 μm and demonstrated a maximum speed of 7.5 cm/s, which corresponded to a velocity of 12.5 body lengths in each second (bd/s). The motion of such linear motion of the motor at the oil/water interfacial layer was 0.5 −1.5 minutes, covering a maximum traveled path of 57 cm. After looking at the morphology of the capsule polymer structure by scanning electron microscopy (SEM), it is determined that the surface of the capsule inside to the oil bulk liquid had large diameter of holes of ∼35 micrometer while the surface inside H_2O, in contrary, did not show any big holes but has a compact solid appearance instead, even at a high magnification (Figure 2-16). Such observation can be attributed to the process that when polysulfone became solid at the oil/water interfacial layer, it underwent

a quick phase-inversion with interaction with H_2O, and when polysulfone became solid while it penetrated through the oil part, the change of phase did not happen. The morphology of the motors is similar to that of the motors we previously seen at the aqueous surface as described in previous section. The movement of the polymer motor was realized by an asymmetric release of the encapsulated DMF molecules in the polysulfone structure which came out slowly into the aqueous phase at the interfacial layer and thus generated a surface tension gradient in the vicinity the motor body.

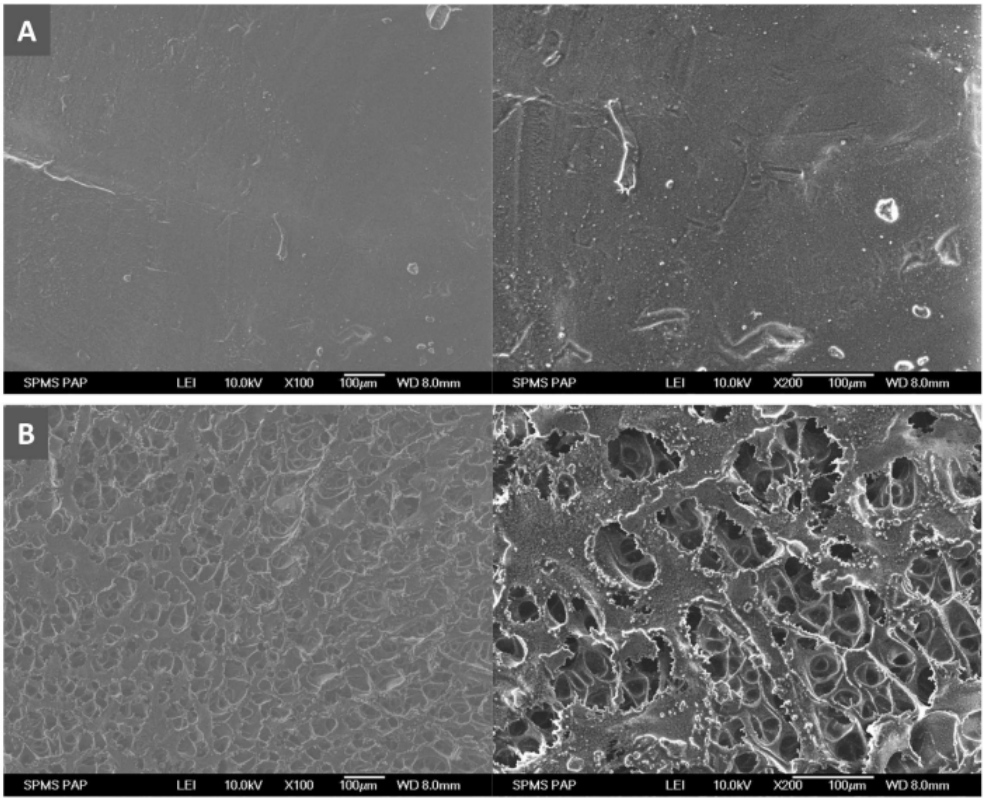

Figure 2-16 Scanning electron microscopy characterization of the surface of polysulfone motor (A) at the solid/water interface and (B) solid/oil interface. All scale bars 100 µm.

Different aspects that affect the movement of the polymer motors were investigated in this study. Two main aspects have to be studied, namely (i) the driving force and (ii) the friction force. With respect to the driving force, movement of the capsule motors at the water/oil interface is induced by the dissolution of DMF molecules with H_2O molecules, and this process is determined by the rate at which DMF molecules are being released out

of the motor. In our study, amount of polysulfone in DMF was changed with a fixed total amount of the precursor solution, which is the polysulfone in DMF solution (5 μL). The recorded speed of the motors was reduced with more polysulfone dissolved in the solution of DMF. Such decrement can be attributed to a reduced leaking of DMF molecules and thus a lower interfacial gradient surrounding the motors. Simultaneously during the movement, frictional or dragging forces were exerted on the motors from both the oil and the water parts. Through increasing the total amount of the polysulfone in DMF solution, the final size of the motors became larger, which resulted into a bigger cross section area for the dragging forces to take effect. Indeed as the sizes of the motors became bigger, the recorded velocity was reduced (Figure 2-17). From these observations, it is conclude that by changing the amount of polysulfone in DMF or the amount of the precursor solution, one can engineer the polymer motors and obtain some extend of manipulation over the speed of the motors.

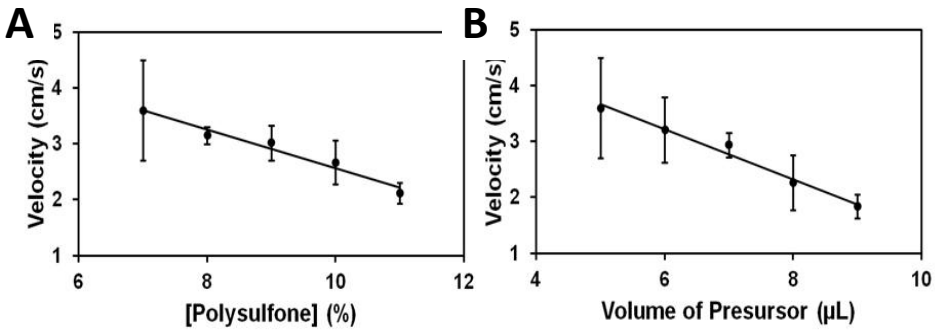

Figure 2-17 Speed of the polymer motor changes with (A) concentration of PSf in the precursor, (B) Total amount of the polysulfone and DMF mixture.

The variation on the interfacial energy of the water phase could also affect the motion of the motors. The motion of the polymer capsules is powered by the interfacial tension gradient between the released DMF (γ = 35.2 mN/m) and that of water, and thus the speed of the polymer motor is expected to be lower with a reduction in such interfacial energy.

In the case when interfacial energy of the water phase is reduced to be equivalent to that of the released DMF, no motion is to be observed for the motors since no more or no sufficient driving force is available. We changed the interfacial energy of the water part by the mixing acetic acid into the aqueous phase; the interfacial energy of aqueous part is reduced with higher concentrations of acetic acid in the mixture, i.e., to 36.1 mN/m at 60% and 33.5 mN/m at 70% (v/v). In agreement to the expected situation, it was seen that the average speed of the polymer motors was reduced with more amount of acetic acid in water. The motion of the polymer motor ceased when the concentration of acetic acid is 60%, indicating that the force generated from the interfacial energy gradient is not able to overcome the frictional force of the system (Figure 2-18).

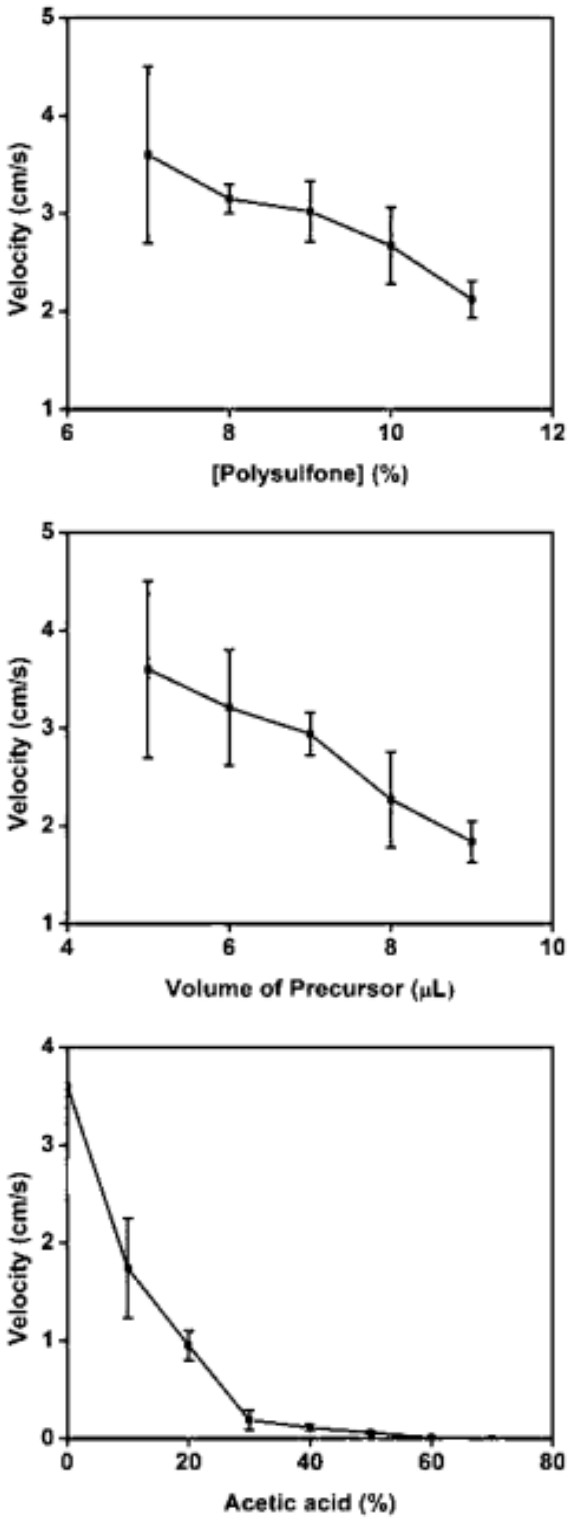

Figure 2-18 Speed of the polymer motor changes with (A) concentrations of PSf in the precursor mixture, and (B) total amount of the precursor mixture and (C) concentration of acetic acid in water.

Along with self-propelled motion, the capability for the manipulation of such motion is of high interest for the development of small motors, and the start/stop of the motion is one of the key aspects for such manipulation. As can be seen in Figure 2-19, it was illustrated that the polymer motors incorporated with Ni NPs could be docked and freed with the application and removal of the magnet bar. From t =0s tot = 1 s, no external magnetic field was applied and movement of the motor was tracked and analyzed. From *t* =1 s to *t* = 2 s, an external magnetic field was applied by placing a permanent magnet underneath the system, and the motion of the polymer motor was stopped and the motor was docked at the intended spot. From *t* =2 s to *t* = 3 s, the external magnetic field was off and the motion of the capsule motor resumed. Moreover, manipulation of direction for the motion was also illustrated by fixing the permanent magnet at the outside part of the Petri dish. The motor showed a directional motion towards the location of the permanent magnet. As seen in Figure 2-19C, with the magnet bar located at one side (top of the image), the overall direction of the motor was oriented parallel the external magnet, rather than without any preferred direction.

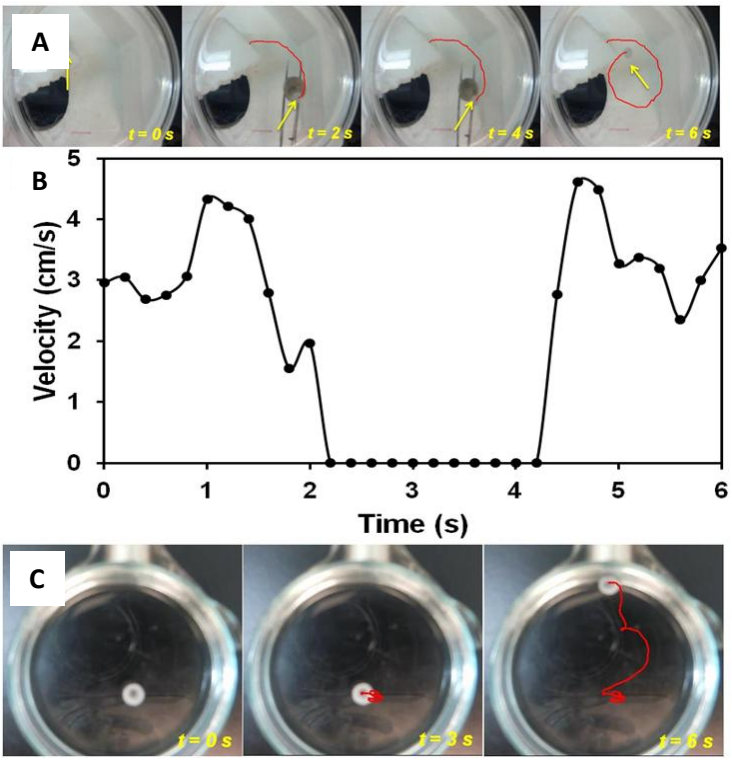

Figure 2-19 Control over the movement of the polymer motor with application of external magnetic field: (A) running of a Ni NPs loaded polymer motor with a time period of one second, (B) instant velocity to demonstrate the manipulation over the start/stop of the movement, and (C) manipulation of the direction of the motor with a magnetic bar.

2.4 Running of the Capsule Motors in a Maze

In this section, I wish to show that the Marangoni effect propelled small motors are able to run not only in an open environment, but also in a constrained channel network, or a maze. Figure 2-20 illustrates the design for the maze, which is an inter-connected running pathway in a Teflon plate.

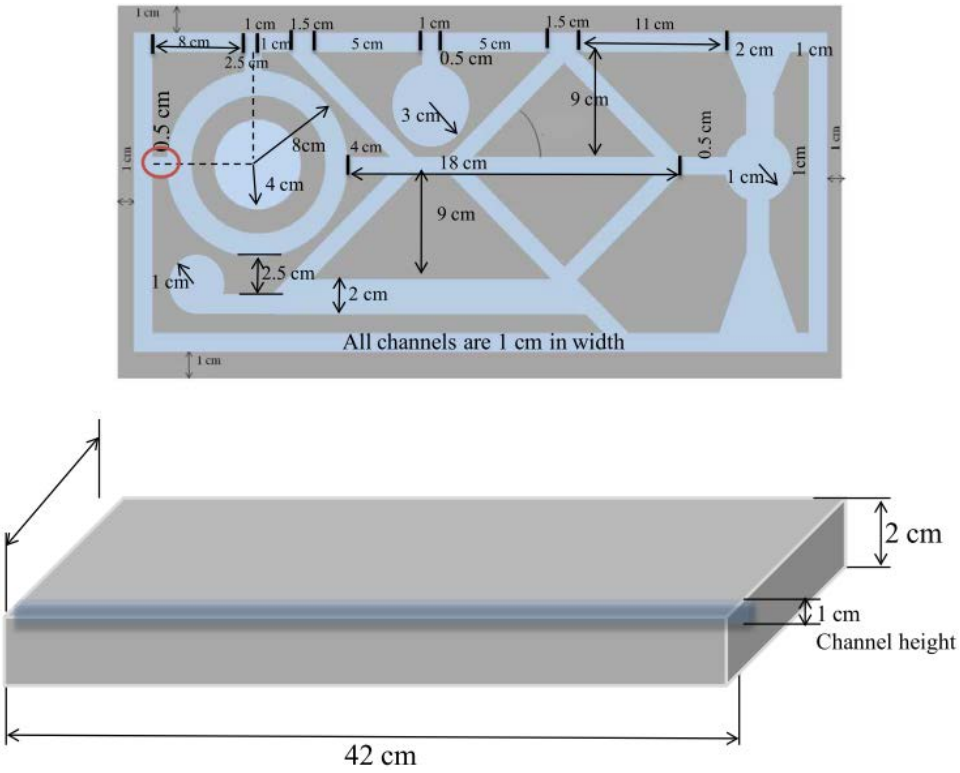

Figure 2-20 Drawing of the design of the channel maze used in this work.

The running of the millimeter-scale motors in such a maze brings up some basic requirements for the motor design. Firstly, the motors must be self-propelled and independent on external supply of physical energy or chemical fuels, as such kinds of energy/fuel supply can lead to high costs, complexity, and danger of chemical spills; secondly, motion of such motors are supposed to be long-lasting, with a capability to cover the entire length of the plate channels; thirdly, ease of modification and functionalization of the motors shall be expected, so as to achieve possible tasks and applications facilitated by the running pathways.

The millimeter-scale polymer capsule motors that we made can fit just perfectly for this purpose of study. Such autonomously running devices require no supply of power sources or chemical fuels, and they have demonstrated the ability to travel over large distances, surpassing several tens of meters. Incorporation of nickel nanoparticles, SDS molecules,

or pH indicators can be easily realized in a quantitative manner, allowing possible applications to be carried out by such motors.

Experimental Procedures

The experiments were carried out in a Teflon maze with most of its running pathways possessing a width of 1 cm and a depth of 1 cm. The dimensions of the Teflon plate were 42 cm × 26 cm × 2 cm. 200 mL of solution was put into the maze channel. After each individual experiment, the liquid was taken out with a pump and the channels were cleaned twice with 200 mL deionized water. A Casio HD camera was put over the maze. The videos and images were analysed with Nikon NIS-Elements™ software and the mean speeds or angles were calculated. For every experiment carried out, the standard deviation and average value of the recorded angles (n = 5; five independent experiments with the same conditions) were calculated with the standard deviations shown as error bars. The motor precursor solutions were made by dissolving polysulfone (PSf, Sigma-Aldrich) into N,N ′-dimethylformamide (DMF, Merck) to form a clear solution using an ultrasonic bath for 30 minutes.

For experiments utilizing sodium dodecyl sulfate (SDS) containing polysulfone capsules, the amount of PSf and SDS in DMF was 7 wt % and 4 wt %, respectively. Nickel nanoparticles (1 wt %) were incorporated into the capsules to enhance the visibility. DMF was added to the mixture and ultrasonicated for 30 minutes. Solutions were freshly prepared for each experiment. For the SDS solutions, methyl red (0.5 wt %) was mixed into the solution to enhance the visibility of the diffusion of the liquid, and the control experiment showed that there was no interaction between the methyl red containing solution and the capsules (0 mM SDS). The artificial flocculation of “pollutant” was made by mixing 40 mL of $FeCl_3$ solution (~10 mM), KI (1 M) and bleach with a ratio of

40: 2: 1.5 and the mixtures were immediately placed into the maze channel. The imidazole incorporated capsules were made by dissolving PSf (7 wt %) and imidazole (4.5 wt %) in DMF after 30 min of ultrasonication. Solutions of pH indicators were all 1 wt % and fresh solutions were made before use in the maze channel.

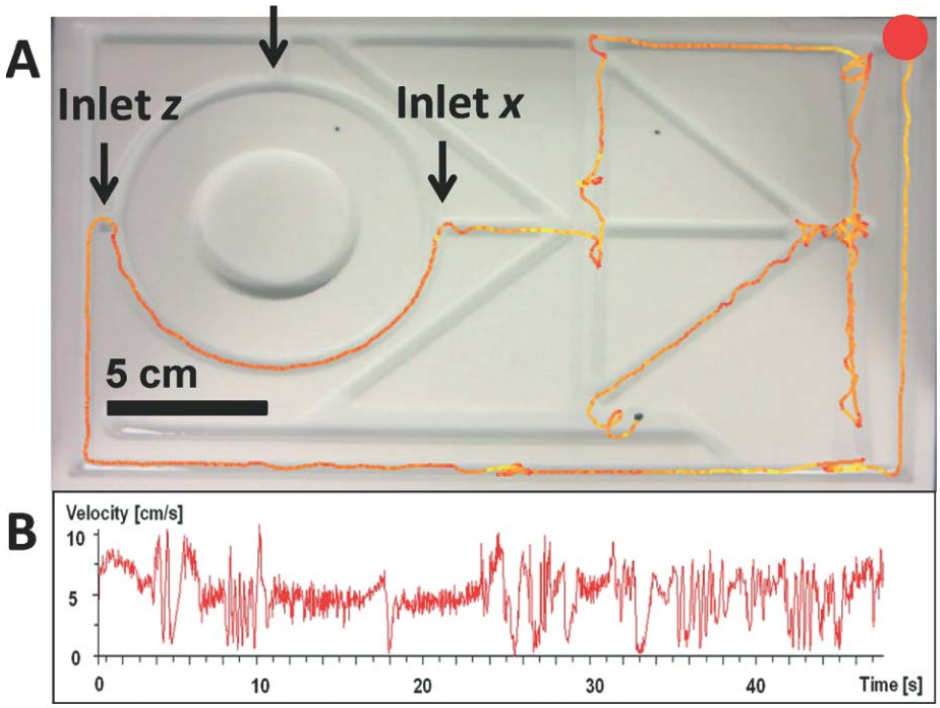

Figure 2-21 Motion of the PSf capsule in a complex channel environment. (A) Tracking of the PSf capsule in the channel of the maze. Color code: yellow to orange, the darker shade means faster velocity. The red dot indicates the place of origin of the capsule. The inlets to the main circular channel are marked "x", "y" and "z" for their better identification in the text. Scale bar 5 cm. (B) Velocity profile of the running capsule. A total path length of 2.5 meters was travelled by the motor and the average velocity was 5.1 cm s^{-1}.

Results and Discussion

I wish to demonstrate that the millimetre sized capsules are capable of sensing chemicals, signal their presence and ultimately remove them from the environment. These capsules

are made from a solution of polysulfone in DMF and the loaded cargo of chemicals can be systematically released to the surroundings. When the PSf/DMF mixture (5 µL) is introduced into an aqueous solution, it immediately solidifies upon contact with water based on phase inversion. Upon solidification, the pore size at the PSf/water interface is ~130 nm, while pores at the PSf/air interface are ~20 µm large. This leads to the slow release of DMF at the edges of the capsule. Given the volume of the capsule (5 µL) and the running time of the capsule (20 min), one can establish the DMF release rate as ~4 nL per second. Residual DMF is slowly asymmetrically released into the aqueous phase, changing the interfacial energy of its vicinity, which leads to its propulsion by the Marangoni effect. Since the surface tension (γ) of DMF-water mixture (γ DMF = 35.2 mN m^{-1}) is lower than that of water (γ_{water} = 72.0 mN m^{-1}), the capsule is "pulled" towards the region of higher surface tension. In order to study the motion of millimetre size PSf capsules in a complex channel environment, we fabricated a "maze" of channels in a Teflon slab of dimensions 42 cm × 26 cm × 2 cm. The typical channels have a width of 1 or 2 cm. First, we introduced the PSf capsule into the solution-filled channel systems. The PSf capsule moved in the channel in a singular direction and when the intersections of the interconnected channels were reached, it randomly selected its path on the crossroads. The motion of the capsule was shown to be random but when the capsules were incorporated with Ni nanoparticles, their motion direction can be controlled with external magnet (data not shown).

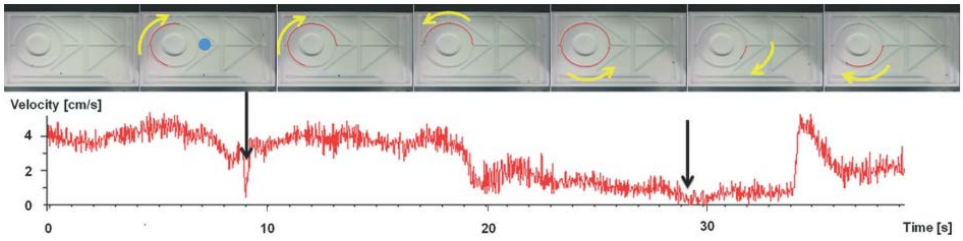

Figure 2-22 Top: interaction between the PSf capsule and the SDS containing solution. When the capsule runs near the SDS containing solution, it is "repelled" and it reverses its direction of motion. The reversing and running of the capsule showed several cycles of back and forward motion. The blue dot indicates the place where SDS solution is applied. Bottom: the velocity profile. The arrows show the time when the capsule reached its turning point, giving an instantaneous zero velocity.

To test how the PSf capsule responds to the presence of chemicals in the environment, we added SDS solution (0.1 mM, 5 μL) to the straight channel in close proximity to the inlet "x", as shown in Figure 2-21. The other outlets (labelled "y", "z") were temporally tampered so that the PSf capsule could only move within the circular channel and exit over the SDS containing entrance/outlet "x". Since the SDS/water mixture exhibits a significantly lower surface tension than water and the water/DMF mixture, the capsule is repelled away from the SDS containing solution (effectively, it is actually pulled outwards from SDS containing solution by surface tension of pure water) *via* the Marangoni effect. Figure 2-22 shows that when the capsule approached close to the SDS containing solution, it was repelled and its direction of motion was reversed. The reversing of the capsule direction showed several cycles of backward and forward motion within the circular channel. The blue dot in Figure 2-22 indicates the location of SDS solution being applied. In the velocity-time profile, the arrows show the time when the capsule reached its turning point, giving an instantaneous zero velocity at the turning point. A similar experiment was conducted to investigate whether the PSf capsule can sense the presence of surfactant and its concentration and it is demonstrated in Figure 2-23. A solution of surfactant (SDS) at different concentrations was introduced at a distance of ~20 cm from the entrance of circular channel (Figure 2-23A, black arrow with label "s" shows at the point where the SDS solution was introduced). The outlets "y" and "z" were

closed and only outlet “x” was left open. For better visibility, the SDS solution was pre-mixed with methyl red (0.5 wt %). The SDS solution spreads by convection and diffusion, reaching the entrance of the circular channel. Since the solution containing SDS exhibits a lower surface tension than water, the polysulfone capsule, whose movement is based on the difference in surface tension of water and DMF, is pulled towards the place where the surface tension is the highest (water). Therefore when it reaches the SDS containing solution, it will appear that the PSf capsule is repulsed by it. If no boundaries are applied to the system, the strength of the repulsion is difficult to quantify as the direction of the motion is largely random. However, if the motion of PSf capsule is restricted by the walls of the channel, one can quantify the concentration of SDS. In order to follow a measurable quantity, we used the circular channel for the motion of the PSf capsule with one inlet where SDS can flow in and influence the motion symmetrically. The motion of the PSf capsule in the circular channel is then restricted in the above noted “back-and-forth” style. With increasing the concentration from 2 to 8 mM SDS, the difference in the surface tension of the water and the solution containing SDS increases and this difference leads into the larger apparent repulsion of the PSf capsule from the inlet of the circular channel. Figure 2-23 shows the portion of the channel to which PSf is limited as a dashed line. We postulate the angle (α) between the two turning points of the PSf capsule as measure to quantify the repulsion strength and hence the concentration of SDS. It can be clearly observed that α increases as the concentration of SDS increases in a linear fashion. This demonstrates that the capsules are not only able to sense the presence/absence of surfactant, but also its concentration.

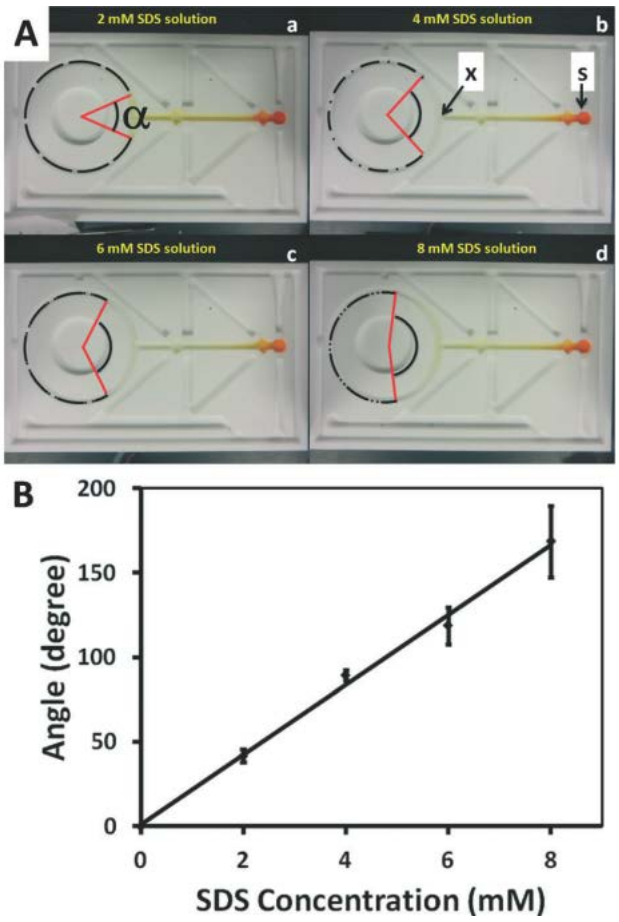

Figure 2-23 The PSf capsule is able to sense SDS-containing solutions and their concentrations and transfer it to changes in its motion. (A) The SDS-containing solution is applied at the reservoir "s" when the capsule is reaching the point normal to the reservoir channel. As the capsule is moving in the circular channel, it encounters the SDS containing solution flowing into the circular channel through inlet "x" and reverses its direction. The zero-velocity points give an angle shown by the red lines. The path along which the droplets moved is shown as dashed line. The reservoir channel was formed by blocking selected openings of the maze. (B) Plot showing the relationship between the angle (α) and SDS concentration (n = 5).

The PSf capsule is not only able to sense chemicals in its environment, but also effectively spread them, while performing its role as a chemical sensor. Figure 2-24 shows the channels filled with water containing pH indicators. When we introduced a

solid NaOH pellet to the “maze” system, the pH of the solution started to slowly change as the NaOH was being dispersed by convection and diffusion, extending into two arms of the channel after 5 min, as indicated by the colour change of phenolphthalein. This pH change took place in 16.7% (RSD 3.7%; n = 4) of the channel volume in 5 min, based on the indicator colour change. When five PSf capsules loaded with imidazole were introduced at a distance of ~20 cm from the entrance of the circular channel, the liquid in the whole maze changed pH within 5 minutes (Figure 2-24b; pH indicator, methyl red). The pH changed in 92.8% (RSD 3.4%; n = 4) of the total channel volume of the channels when using PSf to disperse the imidazole (indicated by the colour change).

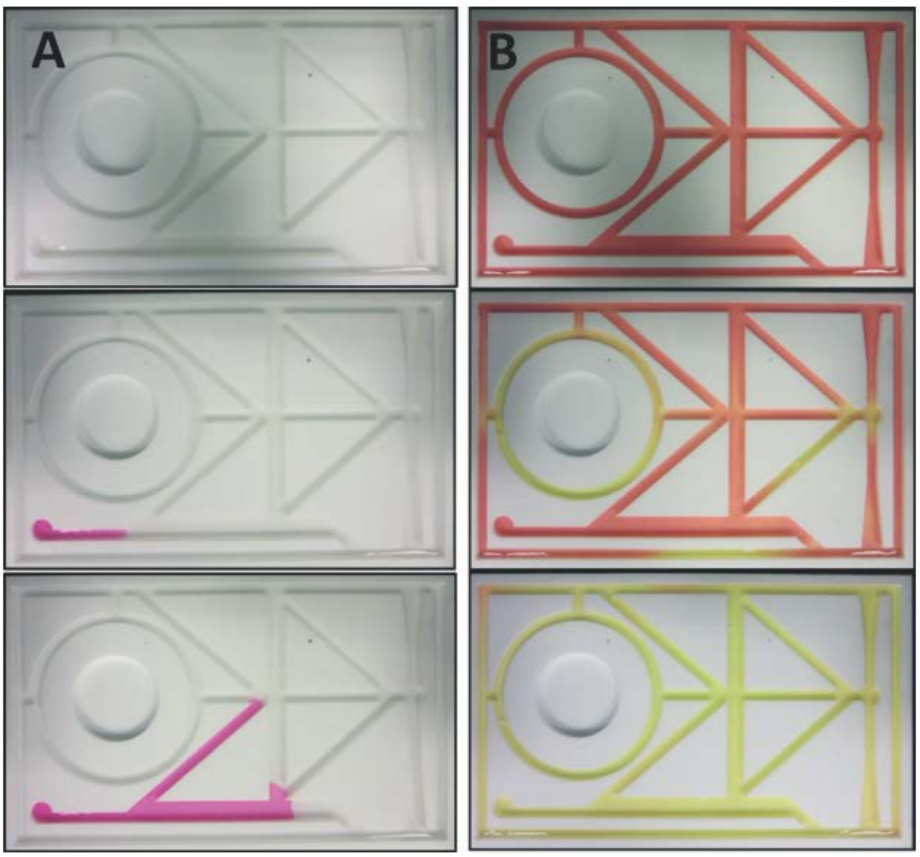

Figure 2-24 Act-and-Sense by the PSf capsule. (A) 3 g NaOH (s) is placed in the reservoir (top); it takes 5 min to diffuse to the junction (bottom). The solution contains the pH indicator, phenolphthalein. (B) The PSf capsule spreads chemicals much faster. Five

PSf capsules incorporating 4.5 wt% of imidazole can spread the chemical across the whole maze within 5 min. The pH indicator methyl red was used to visualize this. Top: t = 0, middle: t = 10 s; bottom: t = 5 min.

In a similar system, if we allowed the imidazole to enter the circular channel only by diffusion (Figure 2-25), the solution in circular channel didn't change pH even after 1 h due to the slow diffusion/convection of the imidazole molecules (note that diffusion in liquids is, in general, a slow process). More specifically, the pH changed only in 47.3% (RSD 14.3%; n = 4) of the total channel volume (as indicated by the colour change of the indicator) after one hour. However, when a PSf capsule loaded with imidazole was introduced to the entrance of the channel and allowed to run, the pH of the liquid in the circular channel changed within 1 min due to the fact that the PSf capsule released imidazole on the move. The change of pH was in this case almost complete: 94.35% (RSD 1.9%, n = 4) of the total channel volume underwent a pH change within 1 min when the PSf capsules were used, as indicated by the colour change.

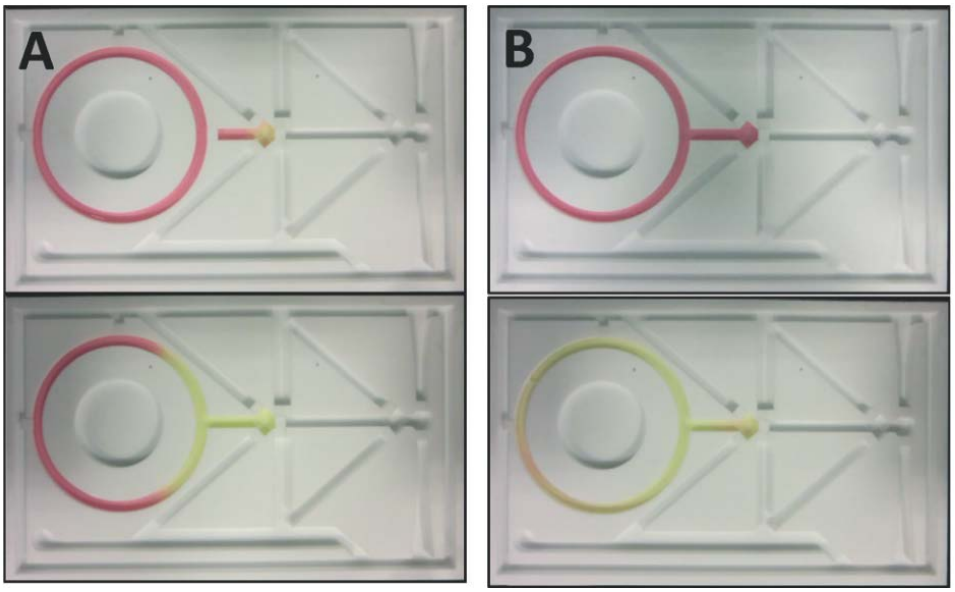

Figure 2-25 Enhanced diffusion of a basic compound into the maze channel. (A) Only diffusion takes place: 100 µL of 4.5 wt % imidazole was placed in the reservoir, and the

base solution was never able to diffuse through the whole channel. (B) The self-propelled PSf capsule induced enhanced diffusion: with the application of one capsule incorporated with 4.5 wt % of imidazole, it took 1 min for the whole channel of the maze to change colour. The pH indicator methyl red was premixed in the water.

Environmental remediation is an important issue. It has been previously demonstrated that bubble-powered micro-machines can remove oil droplets by attaching them to their surface[41] or that they can catalyse on their surface chemical transformations.[42] However, it has not yet been demonstrated that self-propelled autonomous millimetre sized device can spread chemicals that decontaminate the solution. Here we show such an example where the PSf capsule can be loaded with chemicals that serve to aggregate pollutant flocculation. Firstly, we placed Fe^{3+} and flocculants into the channels (Figure 2-26). The uniformly brown solution of flocculated Fe^{3+} is homogenously dispersed in the polluted solution. Upon the introduction the plain PSf capsule, the solution does not change its state. However, when we introduce a PSf capsule loaded with SDS, this capsule is capable of inducing the aggregation of the pollutant flocculation. The PSf capsule loaded with SDS moves over the polluted solution and “sweeps” the flocculated pollutant. We employed three PSf/SDS capsules and within 2 minutes, the flocculation aggregates were swept by capsules and accumulated by the capsule and most of the aqueous solution was cleared of pollutant, which had been previously flocculated. More specifically, the average pollutant coverage after the application of the capsules is 37.2% (RSD 10.2, n = 5). The enhanced aggregation and gathering of the flocculation resulted in easier removal of the pollutant from the solution. Such “smart” removal of the coagulated pollutants offers an interesting alternative to the current passive method of coagulated pollutant removal by filtration, which is the standard method in this field.

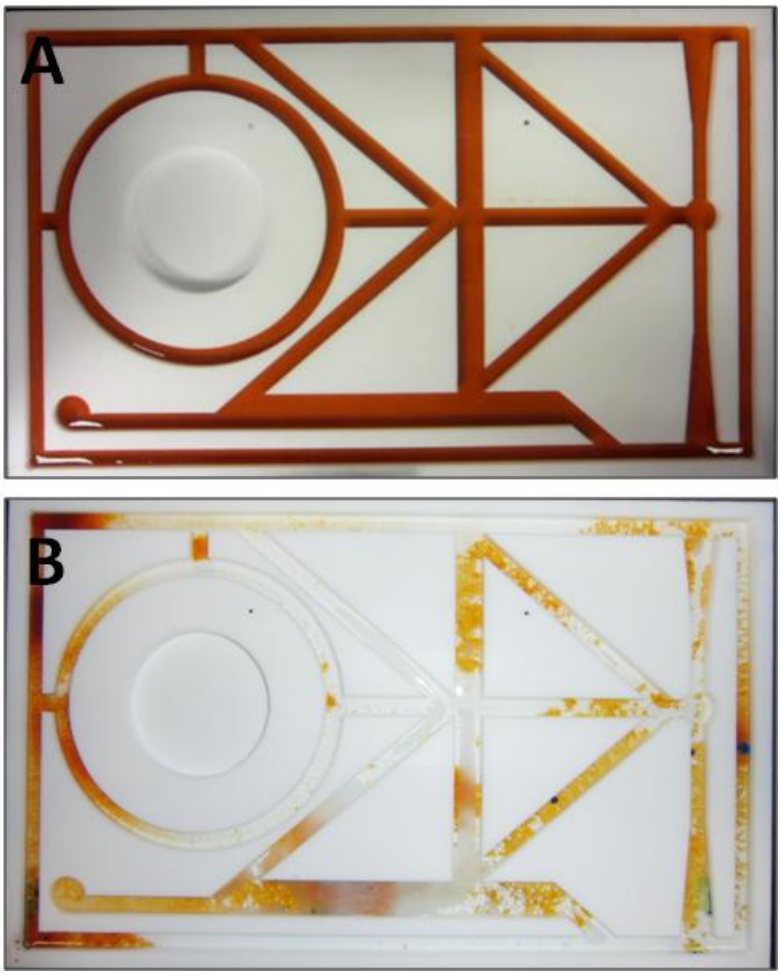

Figure 2-26 Environmental clean-up using SDS-incorporated capsule motors. (A) The maze channel was filled with pollutant. (B) After application of the capsules, the flocculated pollutant was gathered for easier removal.

2.5 Enhanced Diffusion of Pollutant

The human society is now facing more and more challenges in sustainability and environment protection, as the growth in the amount of pollutants into the environment. The distribution of such pollutants have been investigated in different models, and yet these models are only ascribing the propagation and distribution of pollutants *via* fluxes of air and fluid,[43-46] complex chemical equilibriums between water/air,[47,48] and

water/solid interfaces,[49,50] or *via* living creatures or food chains. [51-53] The propagation and distribution of pollutants in such model systems are considered to be very slow, because of the very small diffusion coefficients of molecules in the liquid environments, which suggest rates of propagation in the magnitude of a few centimeters per day (for a typical diffusion coefficient of 5×10^{-6} cm^2/s). In some cases even though turbulent flows are involved, the rate of distribution expansion of such molecules is still low. For instance, merging rivers keep their initial chemical composition even after several tens of kilometers from the merging position.[54] These studies focus their interests on the environmental flow and passive delivery of molecules or clusters, but the study on the self-propulsion of polluting materials has not been taken into account. In this section, I would like to illustrate the necessity to take into consideration the self-propulsion of the polluting materials due to the induced capability for such materials to engage in an enhanced diffusion by thousands of times.

Experimental Procedures

Experiments were carried out in a 20 × 20 × 5.5 mm glass trough filled with 25 ml of aqueous liquid at room temperature. Agglomerates of 1,1-diphenylhydrazine (Alfa Aesar) were gently placed on the liquid surface and motion initiated spontaneously. A Casio HD video recorder was placed over the trough to record motion. Video sequences, path lengths and the MDS of each time spot were analyzed using Nikon NIS-Elements™ software. The standard deviations and average values of the recorded velocities calculated were taken from five independent experiments.

Results and Discussion

The system that I would like to illustrate here is the self-propelled hydrazine-based polluting materials that can propagate at a much higher speed than that expected by the

conventional diffusing models, giving enhanced diffusion coefficients that can be ~100,000 times higher than standard molecular diffusion coefficients. The powering source for enhanced diffusion of such self-propelled hydrazine clusters is attributed to the Marangoni effect, which is induced by the asymmetric allocation of interfacial energy gradient surrounding the particles. Such a gradient in interfacial energy leads to a net driving power for the movement of the particle towards a place of higher interfacial energy. In this section, it is demonstrated that the hydrophobic agglomerates of molecules, in this study 1, 1-diphenylhydrazine, experience asymmetric mixing with water, which leads to the asymmetric variation of interfacial energy surrounding the agglomerates.

The weight of the agglomerates of 1, 1-diphenylhdrazine was determined prior to running such agglomerates by putting them on the surface of aqueous phase. Movement started immediately upon contact with water. The speed of the running particles can be as fast as a few centimetres per second, and in the process of the motion, the clusters was slowly dissolved in the water, leading to a direct spread of the polluting materials. Figure 2-27 gives a tracking profile of a 1, 1-diphenyl-hydrazine cluster running on the fluid surface.

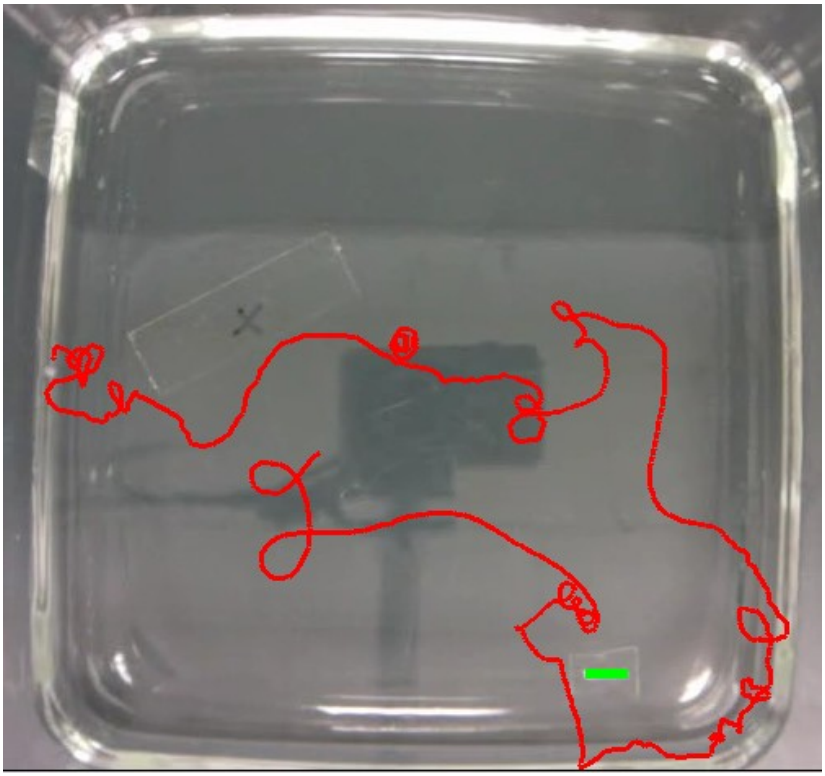

Figure 2-27 Tracking profile for the running of a 1,1-diphenylhydrazine cluster on the fluid surface over a 60 s time span. A random pathway, with both linear and rotational movements, was seen. Scale bar indicates 1 cm.

It can be determined that the agglomerates show not only linear but also circular motions, leading to a random motion or “diffusion” tracking of movement. Such random walk can be quantitatively investigated using the concept of mean squared displacement (MSD) of the agglomerates as a function of time. In this study, a total of 4 different kinds of fluid were used in order to determine their impact on the MSD of the agglomerates. Figure 2-28 demonstrates the MSD of pollutant agglomerates on (A) DI water surface, (B) sea water surface, (C) lake water surface and (d) surface of 5% SDS solution. It can be seen clearly that the mean square displacement of 1, 1-diphenylhydrazine of the sea water surface is larger than that on the surface of DI water. Such higher MSD is because of the stronger interfacial energy of sea water than the interfacial energy of DI water (λ_{water} =72.0 mN m) owing to the escalated concentration of electrolyte in sea water. The mean

square displacement of agglomerates on the surface of lake water is a bit less than that of DI water, possibly because of the reduced interfacial energy of lake water with the presence of biological molecules. It should be noted that the agglomerates show an obviously high speed and mean square displacement even on the surface of 5% of SDS solution, which possesses a much lower interfacial energy than that of DI water (72.0 mN m). The diffusion coefficients of agglomerates on different kinds of fluid measured from the experiments shown in Figure 2-28 are listed as follows: 0.51, 0.63, 0.32 and 0.10 cm^2/s for DI water, sea water, lake water and 5% SDS solution respectively. It is noteworthy that the diffusion coefficients of molecules with similar molecular weights to that of 1, 1-diphenylhydrazine are in the order of $\sim 5\times10^{-6}$ cm^2/s, specifically for diphenylhydrazine of 7.3×10^{-6} cm^2/s. Thus, owing to the Marangoni effect, the enhanced diffusion coefficients can be around hundreds of thousands of times higher than that of the standard molecular diffusion coefficients without considering the self-propulsion of the particles. Such observation indeed can enhance the propagation as well as distribution of polluting materials in the environment, if such materials are allocated on the surface of fluids, which can be the case for many of the hydrophobic solid chemicals.

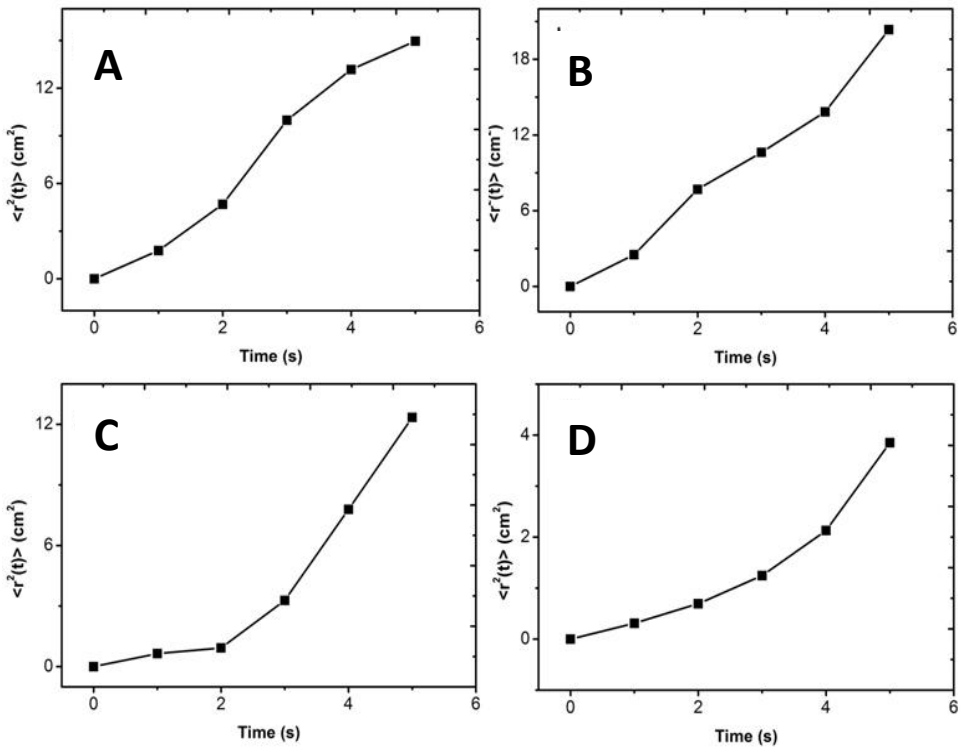

Figure 2-28 Measured MSD of 1, 1-diphenylhydrazine agglomerates on the surface of (A) DI water, (B) seawater, (C) lake water and (D) 5 wt% of SDS solution. A total of 5 independent experiments were done for each time spot in order to get the measurement for displacements.

Next, the time interval for the running agglomerates before they were totally dissolved into the aqueous fluid was also studied. The correlation between the speed of the agglomerates and their weights was also investigated. Figure 2-29A illustrates that the time before totally dissolve into the bulk fluid of the agglomerates is higher for heavier ones, from 33 seconds for a 1.5 mg agglomerate, to 447 s for a 20.1 mg agglomerate, making the latter agglomerate able to cover a path of several meters before being completely dissolved and directly spread such harmful molecules into the bulk fluid along its trace of motion. Moreover, Figure 2-29B illustrates the effect of the weight of aggregates on their mean speed. For agglomerates of bigger sizes, some with a weight of ~20 mg, motion speed are generally slower than those with smaller sizes, possibly due to

the bigger cross section of the particles, which is responsible for the dragging force from the bulk liquid. It was recorded that agglomerates of less weight showed speeds of about 4–5 cm/s. When a boundary is present for the motion of the agglomerates, such as limited room for expansion of the hydrazine particles in lateral dimensions and also in depth of the fluid, the saturation of fluid surface could happen. However, since molecules of hydrazine are miscible with water, the dissolved molecules from the agglomerates move into the bulk fluid and thus this boundary effect is not expected to show some impact on the motion. In the circumstance of a massive leak of chemicals into the environment, the presence of boundary is not expected also as a higher amount of water would be involved in this situation, such as lakes or ponds. On such types of natural water the ‘‘boundary’’ can be considered to be semi-infinite. We have carried out the experiments using multiple agglomerates of a large variety of weights, and not any stalling of the agglomerates was seen and the self-propelled motion of the agglomerates was still on even in the presence of large numbers of particles (～20).

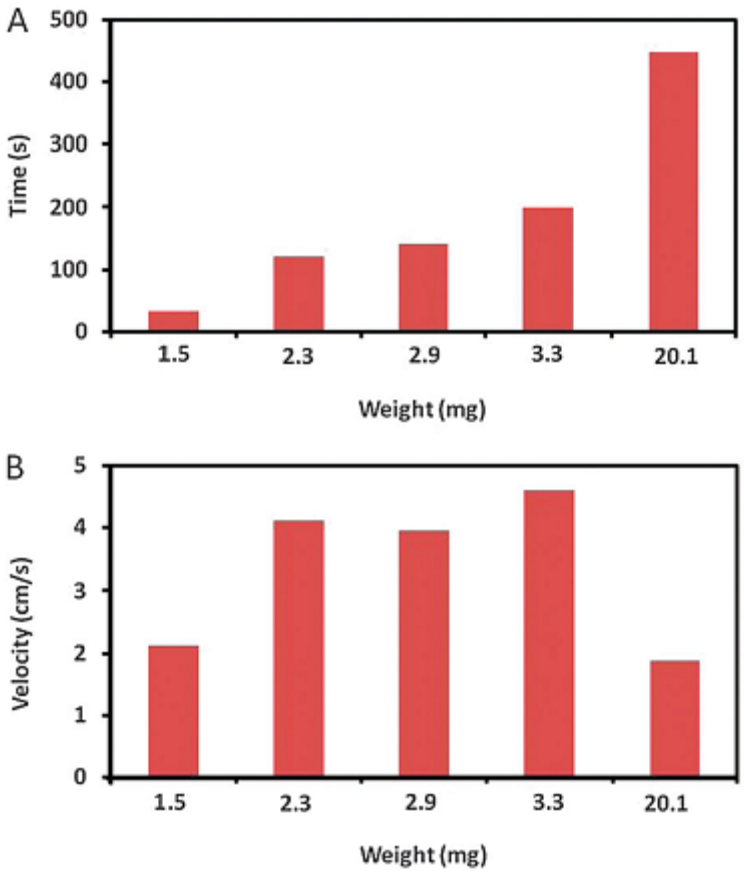

Figure 2-29 The plots of (A) running time and (B) mean velocities for the agglomerates of 1, 1-diphenylhydrazine of different weights running on the surface of DI water.

2.6 References

(1) Ismagilov, R. F.; Schwartz, A.; Bowden, N.; Whitesides, G. M.: Autonomous Movement and Self-Assembly. *Angew. Chem. Int. Ed.* **2002**, *41*, 652-654.

(2) Kline, T. R.; Paxton, W. F.; Wang, Y.; Velegol, D.; Mallouk, T. E.; Sen, A.: Catalytic Micropumps: Microscopic Convective Fluid Flow and Pattern Formation. *J. Am. Chem. Soc.* **2005**, *127*, 17150-17151.

(3) Mano, N.; Heller, A.: Bioelectrochemical Propulsion. *J. Am. Chem. Soc.* **2005**, *127*, 11574-11575.

(4) Okawa, D.; Pastine, S. J.; Zettl, A.; Fréchet, J. M. J.: Surface Tension Mediated Conversion of Light to Work. *J. Am. Chem. Soc.* **2009**, *131*, 5396-5398.

(5) Chaudhury, M. K.; Whitesides, G. M.: How to Make Water Run Uphill. *Science* **1992**, *256*, 1539-1541.

(6) Sumino, Y.; Magome, N.; Hamada, T.; Yoshikawa, K.: Self-Running Droplet: Emergence of Regular Motion from Nonequilibrium Noise. *Phys. Rev. Lett.* **2005**, *94*, 068301.

(7) Velev, O. D.; Prevo, B. G.; Bhatt, K. H.: On-chip manipulation of free droplets. *Nature* **2003**, *426*, 515-516.

(8) Diguet, A.; Guillermic, R.-M.; Magome, N.; Saint-Jalmes, A.; Chen, Y.; Yoshikawa, K.; Baigl, D.: Photomanipulation of a Droplet by the Chromocapillary Effect. *Angew. Chem. Int. Ed.* **2009**, *48*, 9281-9284.

(9) Rybalko, S.; Magome, N.; Yoshikawa, K.: Forward and backward laser-guided motion of an oil droplet. *Phys. Rev. E* **2004**, *70*, 046301.

(10) Lee, S.-W.; Laibinis, P. E.: Directed Movement of Liquids on Patterned Surfaces Using Noncovalent Molecular Adsorption. *J. Am. Chem. Soc.* **2000**, *122*, 5395-5396.

(11) Pollack, M. G.; Fair, R. B.; Shenderov, A. D.: Electrowetting-based actuation of liquid droplets for microfluidic applications. *Appl. Phys. Lett.* **2000**, *77*, 1725-1726.

(12) Ichimura, K.; Oh, S.-K.; Nakagawa, M.: Light-Driven Motion of Liquids on a Photoresponsive Surface. *Science* **2000**, *288*, 1624-1626.

(13) Berna, J.; Leigh, D. A.; Lubomska, M.; Mendoza, S. M.; Perez, E. M.; Rudolf, P.; Teobaldi, G.; Zerbetto, F.: Macroscopic transport by synthetic molecular machines. *Nat. Mater.* **2005**, *4*, 704-710.

(14) Brzoska, J. B.; Brochard-Wyart, F.; Rondelez, F.: Motions of droplets on hydrophobic model surfaces induced by thermal gradients. *Langmuir* **1993**, *9*, 2220-2224.

(15) Bassik, N.; Abebe, B. T.; Gracias, D. H.: Solvent driven motion of lithographically fabricated gels. *Langmuir* **2008**, *24*, 12158-63.

(16) Nakata, S.; Doi, Y.; Kitahata, H.: Synchronized motion of a mobile boundary driven by a camphor fragment. *J. Colloid. Interf. Sci.* **2004**, *279*, 503-8.

(17) Nakata, S.; Kirisaka, J.; Arima, Y.; Ishii, T.: Self-motion of a camphanic acid disk on water with different types of surfactants. *J. Phys. Chem. B.* **2006**, *110*, 21131-4.

(18) Chang, S. T.; Paunov, V. N.; Petsev, D. N.; Velev, O. D.: Remotely powered self-propelling particles and micropumps based on miniature diodes. *Nat. Mater.* **2007**, *6*, 235-240.

(19) Nakata, S.; Murakami, M.: Self-motion of a camphor disk on an aqueous phase depending on the alkyl chain length of sulfate surfactants. *Langmuir* **2010**, *26*, 2414-7.

(20) Loget, G.; Kuhn, A.: Propulsion of Microobjects by Dynamic Bipolar Self-Regeneration. *J. Am. Chem. Soc.* **2010**, *132*, 15918-15919.

(21) Loget, G.; Kuhn, A.: Electric field-induced chemical locomotion of conducting objects. *Nat. Commun.* **2011**, *2*, 535.

(22) Loget, G.; Kuhn, A.: Bipolar electrochemistry for cargo-lifting in fluid channels. *Lab Chip* **2012**, *12*, 1967-71.

(23) Gibbs, J. G.; Kothari, S.; Saintillan, D.; Zhao, Y. P.: Geometrically designing the kinematic behavior of catalytic nanomotors. *Nano lett.* **2011**, *11*, 2543-50.

(24) Wang, Y.; Fei, S.-t.; Byun, Y.-M.; Lammert, P. E.; Crespi, V. H.; Sen, A.; Mallouk, T. E.: Dynamic Interactions between Fast Microscale Rotors. *J. Am. Chem. Soc.* **2009**, *131*, 9926-9927.

(25) Faltinsen, O. M.; Sortland, B.: Slow drift eddy making damping of a ship. *Appl. Ocean Res.* **1987**, *9*, 37-46.

(26) Sanchez, S.; Solovev, A. A.; Schulze, S.; Schmidt, O. G.: Controlled manipulation of multiple cells using catalytic microbots. *Chem. Commun.* **2011**, *47*, 698-700.

(27) Dhar, P.; Cao, Y.; Kline, T.; Pal, P.; Swayne, C.; Fischer, T.; Miller, B.; Mallouk, T.; Sen, A.; Johansen, T.: Autonomously Moving Local Nanoprobes in Heterogeneous Magnetic Fields. *J. Phys. Chem. C.* **2007**, *111*, 3607-3613.

(28) Sanchez, S.; Solovev, A. A.; Mei, Y.; Schmidt, O. G.: Dynamics of biocatalytic microengines mediated by variable friction control. *J. Am. Chem. Soc.* **2010**, *132*, 13144-5.

(29) Sanchez, S.; Ananth, A. N.; Fomin, V. M.; Viehrig, M.; Schmidt, O. G.: Superfast motion of catalytic microjet engines at physiological temperature. *J. Am. Chem. Soc.* **2011**, *133*, 14860-3.

(30) Purcell, E. M.: Life at low Reynolds number. *Am. J. Phys.* **1977**, *45*, 3-11.

(31) Tal, R.; Sirignano, W. A.: Cylindrical cell model for the hydrodynamics of particle assemblages at intermediate reynolds numbers. *AIChE. J.* **1982**, *28*, 233-237.

(32) McHenry, M. J.; Azizi, E.; Strother, J. A.: The hydrodynamics of locomotion at intermediate Reynolds numbers: undulatory swimming in ascidian larvae (Botrylloides sp.). *J. Experim. Bio.* **2003**, *206*, 327-43.

(33) Ibele, M.; Mallouk, T. E.; Sen, A.: Schooling Behavior of Light-Powered Autonomous Micromotors in Water. *Angew. Chem. Int. Ed.* **2009**, *48*, 3308-3312.

(34) Sanchez, S.; Solovev, A. A.; Harazim, S. M.; Schmidt, O. G.: Microbots Swimming in the Flowing Streams of Microfluidic Channels. *J. Am. Chem. Soc.* **2010**, *133*, 701-703.

(35) Zhang, H.; Duan, W.; Liu, L.; Sen, A.: Depolymerization-Powered Autonomous Motors Using Biocompatible Fuel. *J. Am. Chem. Soc.* **2013**, *135*, 15734-15737.

(36) Qiao, L.; Luo, C.: Propulsion of a microsubmarine using a thermally oscillatory approach. *J. Micromech. Microeng.* **2013**, *23*, 105011.

(37) Paxton, W. F.; Sen, A.; Mallouk, T. E.: Motility of catalytic nanoparticles through self-generated forces. *Chemistry.* **2005**, *11*, 6462-70.

(38) Valadares, L. F.; Tao, Y.-G.; Zacharia, N. S.; Kitaev, V.; Galembeck, F.; Kapral, R.; Ozin, G. A.: Catalytic Nanomotors: Self-Propelled Sphere Dimers. *Small* **2010**, *6*, 565-572.

(39) Schmid, A. K.; Bartelt, N. C.; Hwang, R. Q.: Alloying at surfaces by the migration of reactive two-dimensional islands. *Science* **2000**, *290*, 1561-4.

(40) Sánchez, S.; Roldán, M.; Pérez, S.; Fàbregas, E.: Toward a Fast, Easy, and Versatile Immobilization of Biomolecules into Carbon Nanotube/Polysulfone-Based Biosensors for the Detection of hCG Hormone. *Anal. Chem.* **2008**, *80*, 6508-6514.

(41) Guix, M.; Orozco, J.; Garcia, M.; Gao, W.; Sattayasamitsathit, S.; Merkoci, A.; Escarpa, A.; Wang, J.: Superhydrophobic alkanethiol-coated microsubmarines for effective removal of oil. *ACS Nano* **2012**, *6*, 4445-51.

(42) Soler, L.; Magdanz, V.; Fomin, V. M.; Sanchez, S.; Schmidt, O. G.: Self-propelled micromotors for cleaning polluted water. *ACS Nano* **2013**, *7*, 9611-20.

(43) Stevenson, D. S.: Atmospheric science: Putting the wind up ozone. *Nature. Geosci* . **2009**, *2*, 677-679.

(44) Desai, A. R.; Austin, J. A.; Bennington, V.; McKinley, G. A.: Stronger winds over a large lake in response to weakening air-to-lake temperature gradient. *Nature. Geosci* . **2009**, *2*, 855-858.

(45) Roberts, L. C.; Hug, S. J.; Dittmar, J.; Voegelin, A.; Kretzschmar, R.; Wehrli, B.; Cirpka, O. A.; Saha, G. C.; Ashraf Ali, M.; Badruzzaman, A. B. M.: Arsenic release from paddy soils during monsoon flooding. *Nature. Geosci* . **2010**, *3*, 53-59.

(46) Shepherd, T. G.: Large-scale atmospheric dynamics for atmospheric chemists. *Chem. Rev.* **2003**, *103*, 4509-32.

(47) Osthoff, H. D.; Roberts, J. M.; Ravishankara, A. R.; Williams, E. J.; Lerner, B. M.; Sommariva, R.; Bates, T. S.; Coffman, D.; Quinn, P. K.; Dibb, J. E.; Stark, H.; Burkholder, J. B.; Talukdar, R. K.; Meagher, J.; Fehsenfeld, F. C.; Brown, S. S.: High levels of nitryl chloride in the polluted subtropical marine boundary layer. *Nature Geosci.* **2008**, *1*, 324-328.

(48) Palakodeti, R. C.; LeBoeuf, E. J.; Clarke, J. H.: Tool for assessment of process importance at the groundwater/surface water interface. *J. Environ. Manag.* **2009**, *91*, 87-101.

(49) Weber, F.-A.; Voegelin, A.; Kaegi, R.; Kretzschmar, R.: Contaminant mobilization by metallic copper and metal sulphide colloids in flooded soil. *Nature Geosci.* **2009**, *2*, 267-271.

(50) Bowman, W. D.; Cleveland, C. C.; Halada, L.; Hresko, J.; Baron, J. S.: Negative impact of nitrogen deposition on soil buffering capacity. *Nature Geosci.* **2008**, *1*, 767-770.

(51) Boxall, A. B. A.; Blackwell, P.; Cavallo, R.; Kay, P.; Tolls, J.: The sorption and transport of a sulphonamide antibiotic in soil systems. *Toxicol. Lett.* **2002**, *131*, 19-28.

(52) Cabana, G.; Rasmussen, J. B.: Modelling food chain structure and contaminant bioaccumulation using stable nitrogen isotopes. *Nature* **1994**, *372*, 255-257.

(53) Fitzgerald, W. F.; Lamborg, C. H.; Hammerschmidt, C. R.: Marine Biogeochemical Cycling of Mercury. *Chem. Rev.* **2007**, *107*, 641-662.

(54) Bouchez, J.; Lajeunesse, E.; Gaillardet, J.; France-Lanord, C.; Dutra-Maia, P.; Maurice, L.: Turbulent mixing in the Amazon River: The isotopic memory of confluences. *Earth Planet. Sci. Lett.* **2010**, *290*, 37-43.

CHAPTER THREE: FABRICATION OF NANO- AND MICROMOTORS

The work discussed in this chapter resulted in the following publications:

Zhao, G.; Ambrosi, A.; Pumera, M. Clean room-free rapid fabrication of roll-up self-powered catalytic microengines. *J. Mater. Chem. A.* **2014, 2**, 1219-1223.
Zhao, G.; Pumera, M., Concentric bimetallic microjets by electrodeposition. *RSC Advances* **2013,** *3,* 3963-3966.
Zhao, G.; Ambrosi, A.; Pumera, M., Self-propelled nanojets via template electrodeposition. *Nanoscale* **2013**, *5*, 1319-1324.

3.1 Introduction

Fabrication, functionalization and application of artificial motors at the nanometer and micrometer scales are one of the most important areas of study in nanomaterials science and technology.[1-8] Considerable amount of research effort has been put into such study as it is of high interest both theoretically and practically.[9-14] It is the ultimate purpose of human being to be able to deploy such ultra-small motors in various systems to carry out different tasks, such as sensing and biosensing,[15-19] environmental remediation,[12,20-22] manipulation of cells,[23,24] and so on. Realization of such applications requires that the

motors must be strongly powered, well-controlled, and effectively functionalized.[1] All of these requirements are based on the effective design and fabrication of the nano-/micromotors. In this Chapter, I would like to introduce the attempts that we made to contribute into the pursuit of better routes for the fabrication of such motors.

Nano-/micromotors are made based on the special properties of nanomaterials. Materials at nanometer and micrometer scales are much more reactive than their macroscale counter parts, because of the increment of the ratio of surface area (SA) to volume. The surface area to volume (V) ratio of a sphere is calculated to be:

$$SA/V = 4\pi a^2/\frac{4\pi a3}{3} = \frac{3}{a}$$

where *a* is the radius of the sphere.

As can be seen from this equation, when the sphere keeps going down in size, this ratio is getting higher and higher, indicating that a higher fraction of atoms are staying at the surface of the structure.[25] Thus, the reactivity of materials at the nanometer and micrometer scales is greatly enhanced since atoms at the surface are responsible for the reactions.[26] This effect can significantly enhance the catalytic effect of platinum materials at nanometer to micrometer sizes, which gives a sufficient power thrust to run the motors in the fluid, as well as for the motors to carry out certain delivery and towing tasks.

When we are to run such nanomotors or micromotors in the running liquid, the motors are experiencing a different phenomenon than the counter parts also: the motors are running under the low Reynolds number scheme.[27] Reynolds number is a unit-less number which describes the special prosperities of the liquid as well as solid particles running in the liquid.[28,29] It is defined as the ratio between the “inertial forces” and viscous forces experienced by the rigid particles moving relative to the fluid, and can be quantified as[30]:

$$Re = \rho vL/\mu$$

where ρ is the density of the liquid, v is the relative velocity, L is the characteristic length of the particle, and μ is the viscosity of the liquid.

The typical Re of a human swimming in a pool is in the order of 10^4, while that of a bacteria swimming in water is at the order of 10^{-4}.[28] This means that, for a bacterium to swim in water, it is almost as hard as for a human to be swimming in honey. In other words, viscous force is the dominate force than the inertial force, and the motion of the particle is stopped immediately once the driving force is gone, with completely no coasting to be observed.[27,28] This is much different from motion at the macroscale as the moving objects generally coast for some observable distances after the driving force is gone. Effects of Reynolds number on the motion of micromotors are to be further discussed in Chapter 5.

The intrinsic small size of motors also determines the way of characterizing the motor structures, as well as the motion itself. Nanomotors and micromotors are only seen with the help of microscopes, and if we would like to see the detailed characterization of such materials, electron microscopes are generally needed, including Scanning Electron Microscape (SEM) and Transmission Electron Microscope (TEM). This is because a high enough resolution is required for us to observe the nano-/micromaterials, and the resolution of the waves can be determined by the Abbes equation[31]:

$$d = \frac{0.612\lambda}{NA}$$

where d is the minimum resolvable distance, λ is the wavelength of the power source, and NA is constant that indicates the numerical aperture.

The wavelength of visible light predetermines that any distances smaller than ~200 nm are not going to be resolved by optical microscopes.[31] Wavelengths of electrons are much short than that of light, and when a high enough accelerating voltage is applied to generate the electron beam, smaller nanoparticles can be resolved with electron microscopes.[31] On the other hand, optical microscopes are primarily required to observe and record the motion of such nano-/micromotors, which place a prerequisite for the fabrication of nano-/micromotors that their smallest dimension must be larger than ~200 nm. Anything with a smaller size is not able to be accurately resolved and seen with the optical microscopes. Thus, current nano-/micromotors are born with their technique size constrains and should be within the range of ~200 nm and above in any dimension.

In this Chapter, I would like to introduce the attempts of developing new routes for the fabrication of nano-/micromotors, including the electrodeposition of metallic tubular nanomotors, simplified rolled-up technique for the production of tubular micromotors, as well as the electrodeposition of tubular micromotors.

3.2 Fabrication of Bimetallic Nanotubular Motors

3.2.1 Synthesis and Characterizations of Bimetallic Nanotubular Motors

Small motors of tubular shapes are currently the most important type of motors in this research, due to their high power output, ease of functionalization, linear motion trajectory.[11] Therefore, extensive work has been put into the study of such tubular nano-/micromotors. The first emerge of the self-propelled bimetallic nanomotors can be dated back to a decade ago,[32,33] and the fabrication of such motors has been based on the template-growth of the metallic nanorods, with a radius of about 150 nm and a typical length of a few μm.[34] Motion of such small motors are powered typically by the disproportionation of H_2O_2 at different metallic parts, which leads to the migration of electrons within the motor and the migration of H_3O^+ at the surrounding of the metallic

surface, efficiently powering the motor to the counter direction to this migration.[34,35] This mechanism is denoted as a self-electrophoresis process, and efforts has been made to increase the mobility of such motors.[36-38] Velocities of such small motors can be from as low as 4-15 body lengths in each second (bl/s) to as high as 30-75 bl/s, relying on the chemical structure of the multimetallic rods.[39]

The tubular-shaped small motors were invented in recent years through the rolling-up of metallic membranes. Such tubular-shaped motors possess a typical diameter of several μm and the length can be around 50 μm.[11] Although using a same fuel source, propulsion mechanism of the motion is principally different. Bubble ejection from the catalytic reaction of H_2O_2 provides the driving force for the motion, and such bubbles are clearly observed under optical microscope, being expelled from only the back end of the tubular motors. Such tubular motors are fabricated with high-end techniques, usually in a clean room to carry out the patterning, deposition and the rolling-up of the films.[40,41] An alternative technique emerged later to fabricate the microtubular motors through the electrochemical deposition route. The tubes made in both methods are concentric in materials composition, and the diameters are usually larger than 2 μm.[42,43] It therefore is determined to be of high importance to scale-down the dimension of the microtubes to nanometer dimensions, as they can be comparable with biological structures.

Sanchez *et al* has reported the fabrication of nanotubular motors through the lithography route, however, it usually takes a few days for the fabrication to complete and high-end facilities are required for the production.[11] In this section, I wish to show a highly parallel, easy, quick and cost-effective production of nanomotors by the template electroplating approach. Such nanomotors are of the sizes of 150 nanometers in radius with a variable length and are lower in dimensions than typical micromotors or nanomotors (sizes of 300–5000 nm by 10–50 μm) and they are considered to be the smallest bubble-propelling

motors artificially made so far.[44] Next, it is to be demonstrated that such nanomotors are able to run at speeds as high as 40 body lengths in each second as well as to illustrate the same kinds of motion styles as their microscale counterparts. Moreover, because of the small dimensions, the motors can have significant cooperative behaviors with the small bubbles that they run into during the course of motion.

Experimental Procedures

The Au/Pt bimetallic nanotubular motors were fabricated with a modified electroplating method on an aluminum oxide (AAO) template membrane. The AAO membranes with channel radius of 100 nm were bought from Whatman (Cat. no. 68096022, Germany). Ag conductive ink (Lot # L18U007, Alfa Aesar, Singapore) was placed on one face of the membrane with commercial cotton rods. A piece of flattened aluminum foil was attached to the ink immediately, which is utilized as the working electrode. The membrane was placed into a customized electroplating cell. A Pt counter electrode and an Ag/AgCl reference electrode were adapted in the setup.

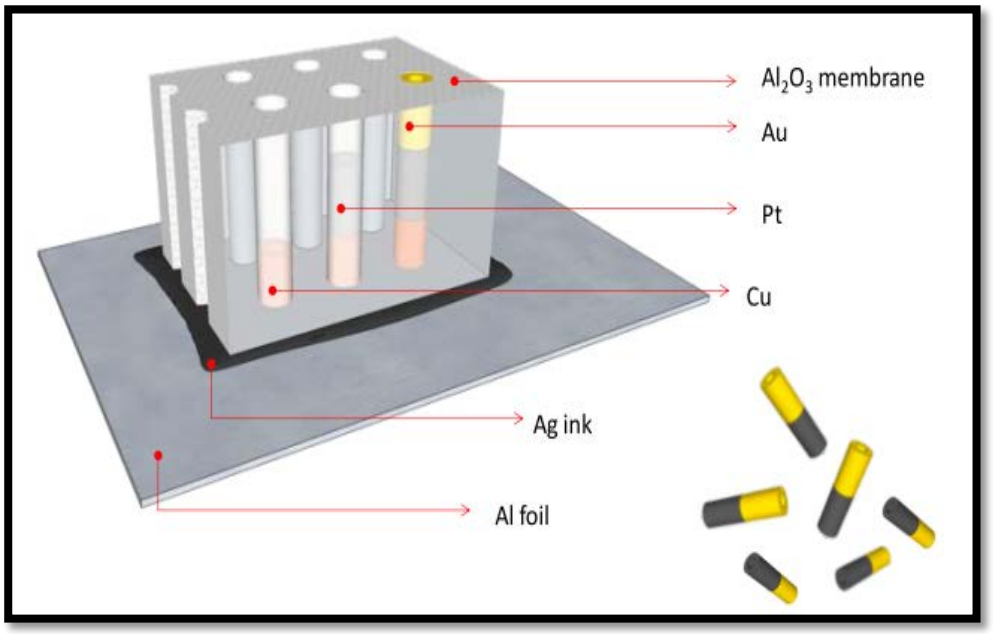

Figure 3-1. Illustration of the fabrication process for the bimetallic nanotubular motors. Silver ink was placed on one face of the aluminum oxide membrane followed by the attachment of flattened Al foil. Sequential electrodeposition of copper, platinum and gold was done under the galvanostatic mode. The Au/Pt bimetallic tubes were released into water after taking off the Ag ink and etching away the AAO membrane.

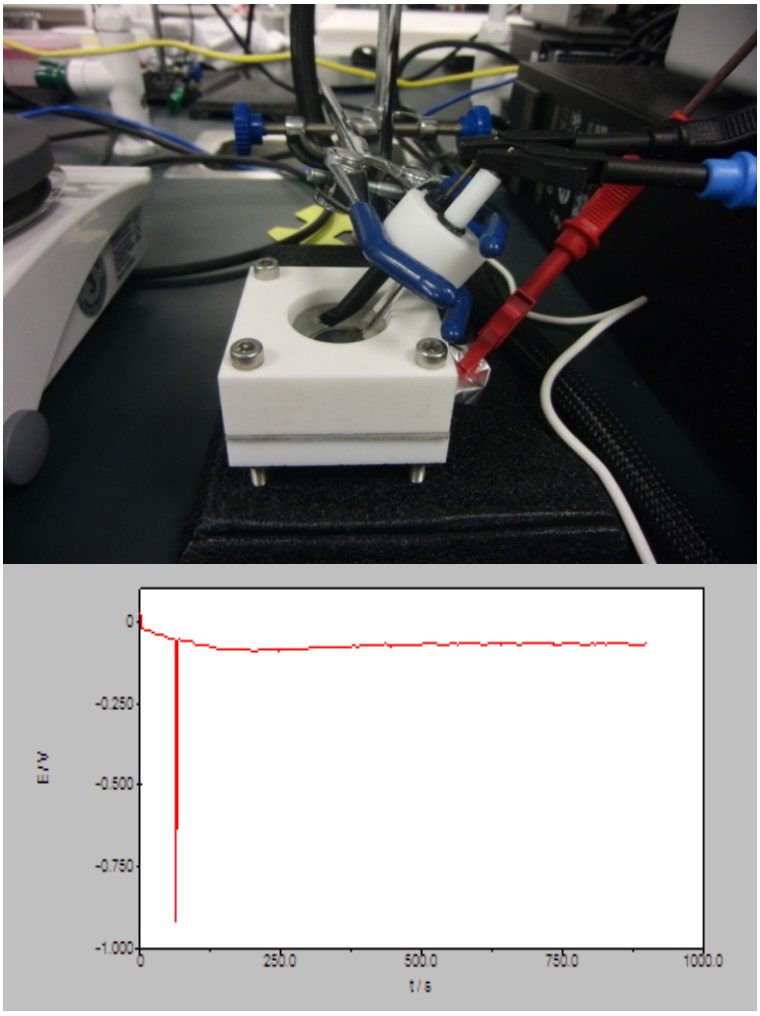

Figure 3-2. Experimental setup for the fabrication of bimetallic nanotubes. Ag ink was placed on one face of aluminum oxide membrane followed by the attachment of flattened Al foil. Sequential electrodeposition of copper, platinum and gold was done under the galvanostatic mode. The Au/Pt bimetallic tubes were released into water after

taking off the Ag ink and etching away the AAO membrane. Top image shows the plating setup and bottom image shows the potential curve.

Electroplating was done with a μAutolab type III electrochemical analyzer (Eco Chemie, The Netherlands) connected to a PC and controlled by General Purpose Electrochemical Systems Version 4.9 Software (Eco Chemie). The membrane was rinsed with 5 ml of DI water (18.2 μΩ cm) for four times, and a copper sacrificial layer was plated under a fixed current of -10 mA for 900 seconds. The plating solution contains 1 mol/L $CuSO_4$. Subsequently, after taking off the copper plating solution, the membrane was rinsed five times with 8 ml of water. Platinum and gold were then plated at five mA for 2700 seconds, respectively, with the commercial plating solutions (Technic, Inc). After rinsing for five times with eight ml of water each, the membrane was ultrasonicated for three times in two ml of diethyleneglycol monoethylether acetate for one minute each time. The Ag ink layer was totally gone during the sonication process. The membrane was then soaked in three ml of 5 mol/L nitric acid until the copper part is no longer seen. After rinsing with H_2O, the membrane was put in an Eppendorf tube with 2 ml of 3 M sodium hydroxide and ultrasonicated until no shards left. The mixture was rinsed and centrifuged at 1,500 rounds per minute for 60 seconds for ten times with two ml of H_2O to thoroughly to eliminate the inorganic impurities. The final aqueous suspension of nanoscale tubes was kept at ambient condition of around 23^oC. Scanning electron microscopy and energy dispersive X-ray spectroscopy (SEM/EDX) were carried out with a JEOL JSM 7600F SEM machine.

Motion of the nanojet engines was investigated in an aqueous solution containing 9 wt % of hydrogen peroxide at constant surfactant concentrations (1 wt % of SDS). Both were obtained from Alfa Aesar. Optical microscope videos and images were obtained with a

Nikon Eclipse TE 2000-E microscope, CFI 10× optics. Video sequences were processed with Nikon NIS-Elements™ software.

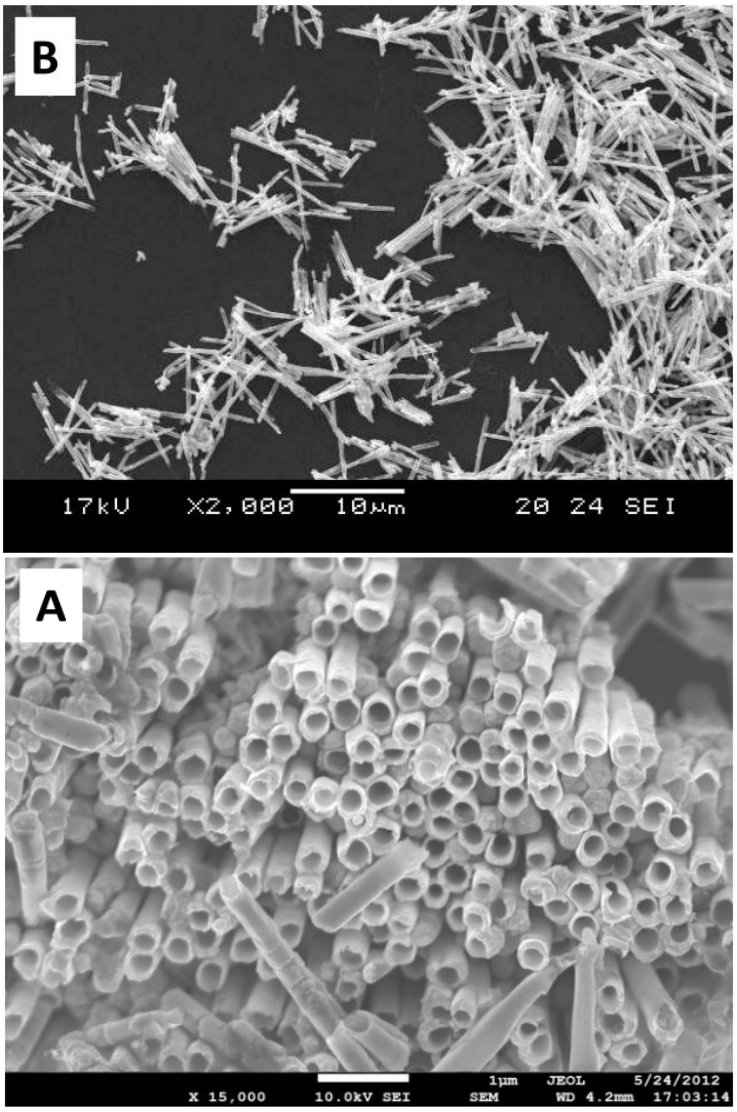

Figure 3-3 Scanning Electron Microscope (SEM) analysis of the Au/Pt bimetallic nanoscale tubes. (A) Top image of the tubes prior to the elimination of the copper sacrificial part; (B) Nanoscale tubes on silicon wafer after the elimination of the copper part. Scale bars indicate 1 µm and 10 µm, respectively.

Results and Discussion

The highly parallel production of bimetallic nanotubular motors by electroplating can be understood from Figure 3-1. This experiment utilized a commercially available AAO membrane as template. Principally, the production procedure started with the application of the Ag conductive ink at one side of the AAO template, followed by the plating of a Cu sacrificial part, with the platinum and the gold segments electrochemical deposited by means of chronocoulometry. After that, the AAO template and sacrificial copper part are etched away, generating the Au/Pt tubes in large arrays, as can be seen from the SEM images in Figure 3-4. Such bimetallic tubes are made up of 2 longitudinal parts, Au and Pt, and their presence can be verified with SEM images as well as the EDX mapping results (Figure 3-4A). It is important to notice that the longitudinal deposition of different element is not feasible with the previously reported methods for the production of nanomotors. SEM/EDX is a preferred approach for the characterizations of the materials, as the individual elements gives a negligible contrast of the image in the SEM viewing setup. The objective for the production of the Au/Pt nanotubes lies that different elements of the structure are able to be specifically functionalized. With a similar approach, bimetallic nanoscale rods are also able to be produced. The key parameter that decides whether the deposited structures are tubular or rod-like morphology is the generation of the initial conductive part (the silver layer) as illustrated previously. If the initial conductive part is electroplated in the way that it ensures the plating only at the walls of the nanochannels of the AAO template, the resulting materials are tubular shaped. If the initial conductive part ensures the plating of materials across the channel, the resulting materials are nanoscale rods. It is of high interest to investigate the geometry and dimension distribution of the mass-produced nanomotors. The length is controlled by the time length of the deposition procedure. On the other hand, at given conditions, the length would change across the same batch of tubes deposited. As shown in Figure 3-5, the typical length is 4.5–5.0 micrometers with about 65% of the nanotubes showing lengths in

the range of 4.0–6.0 micrometers and whole distribution ranging from 2.2 to 7.06 micrometers (n = 50, standard deviation is 1.16 micrometers). The presence of very short (2–3 micrometer) nanotubes can be possibly attributed to the breakage of the longer tubes during the procedure. The average outer radius is 155 nm with distribution from 100 to 205 nm (n = 100; standard deviation 50 nanometers). The average inner radius is 115 nm, whole distribution is ranging from 60 to 165 nm (n = 100; standard deviation 40 nm). The geometry of the tubes is controlled by the membrane channels and their quality. Tubes of curved geometry or merged tubes could also be found in a minor amount.

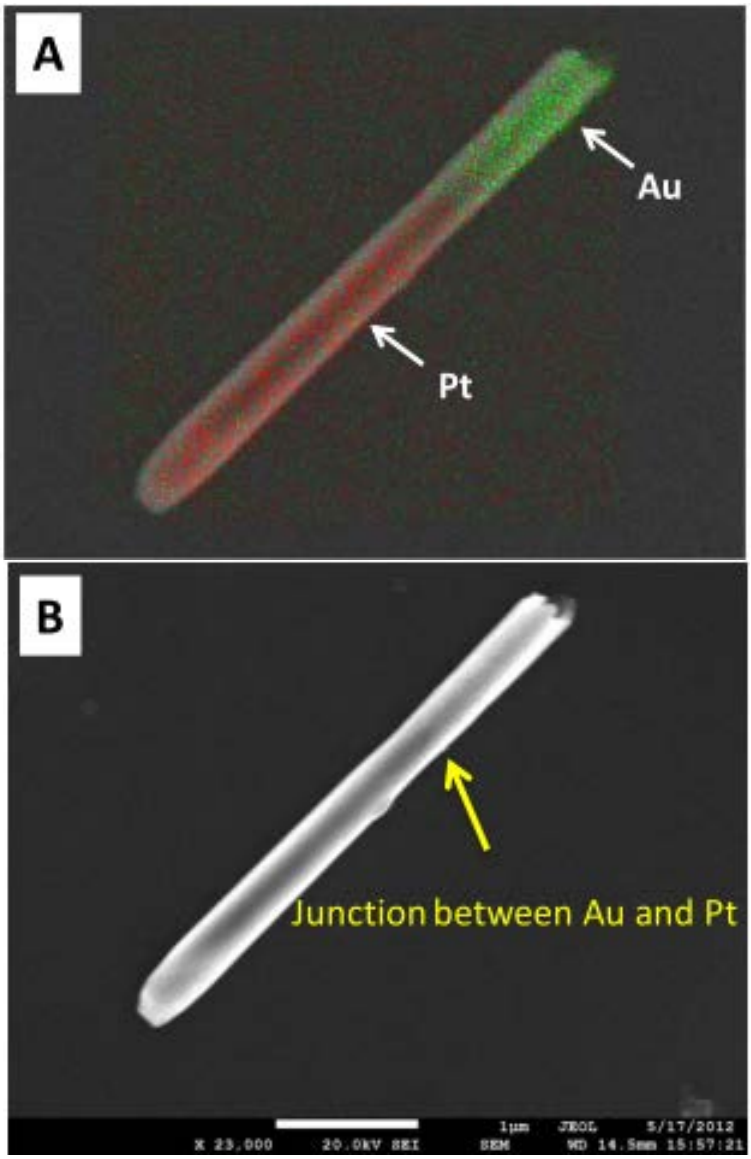

Figure 3-4 (A) Mapping of the elements using SEM/EDX. Red color shows platinum and green color shows gold. (B) SEM image of the same nanotube indicating different contrast of platinum and gold. Scale bars: 2 μm for (A) and 1 μm for (B).

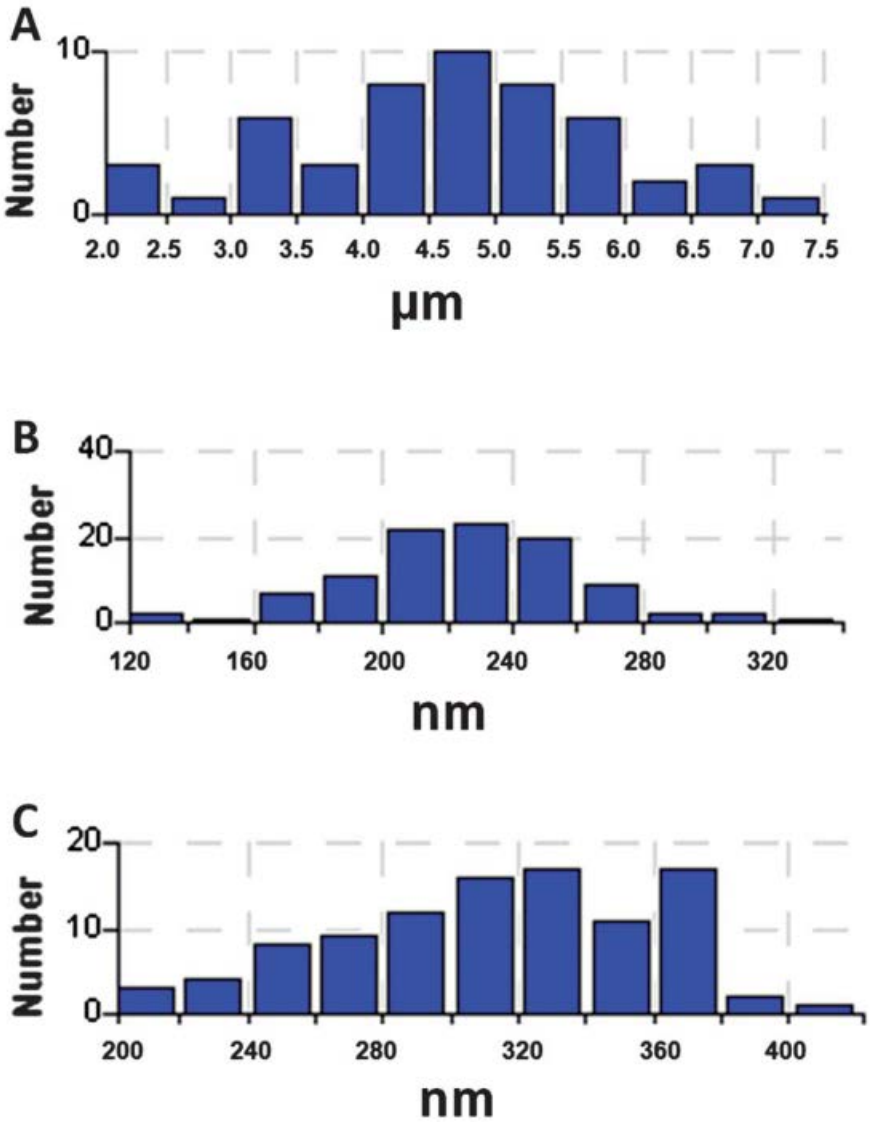

Figure 3-5 Size statistics of nanoscale motors made by electroplating. (A) Length of the tubes (n = 50); (B) inside diameter of tubes (n = 100) and (C) outside diameter of tubes (n = 100).

3.2.2 Motion Study

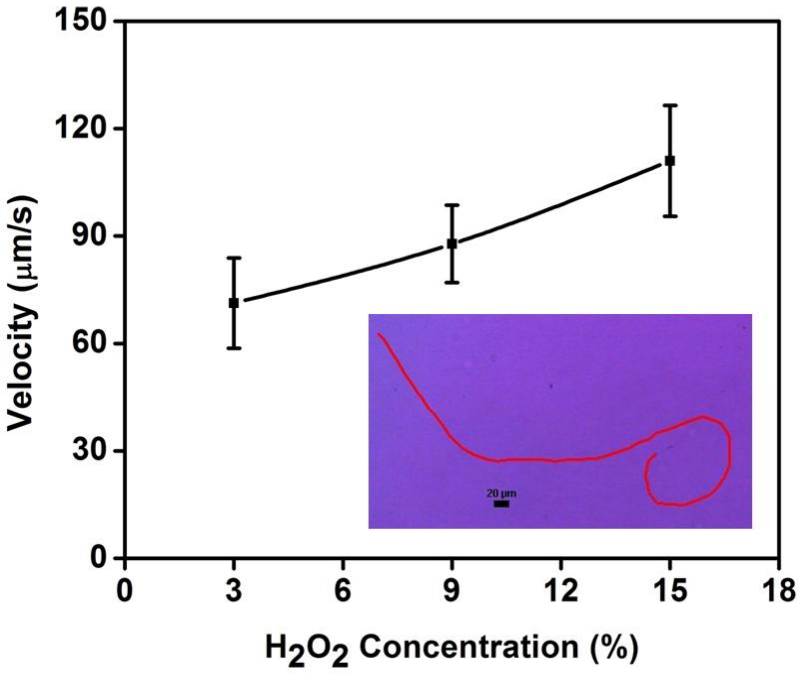

Figure 3-6 Effect of the H_2O_2 concentration on the velocity of the nanomotors. With higher amount of hydrogen peroxide in the liquid, the nanomotors move at faster speeds. The velocities of the motors were measured over a time interval of 10 s from six different experiments. The tracking line presented in the inset illustrates the motion of a nanomotor with 9 wt % of hydrogen peroxide present in the liquid. Scale bar: 20 μm.

Motion study of the Au/Pt bimetallic nanomotors was carried out. The capability of movement arised from the detachment of nanoscale bubbles from the motors was first determined. In Figure 3-7, we illustrate that indeed the Au/Pt nanomotors show motion in 3–15 wt % of hydrogen peroxide, with the speed ranging from 20 to 40 body lengths per second. Such speeds, in body lengths per second, are quite comparable with the speeds of typical tubular micromotors, as well as the speeds of the fastest bimetallic rod-shape nanomotors. It is also apparent that the amount of H_2O_2 significantly affects the movement of these nanomotors. The mean speed for the movement of nanomotors is 71 μm/s (n = 6) at a concentration of 3 wt % for hydrogen peroxide. With the presence of

higher amount of hydrogen peroxide fuel to 15 wt %, the mean speed of the nanomotors accelerated to 111 µm/s.

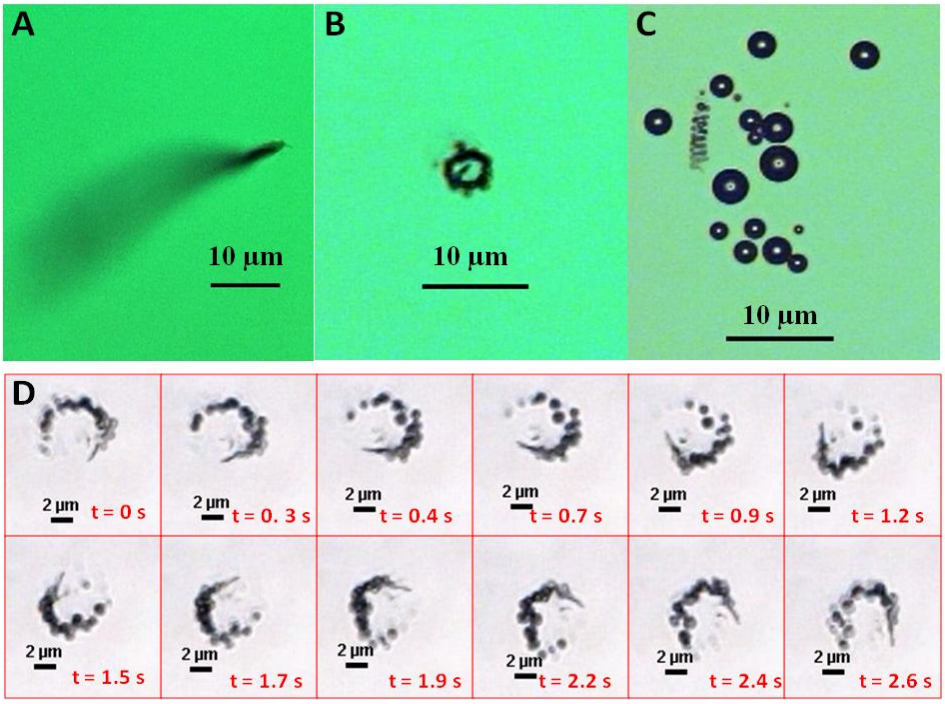

Figure 3-7 Various motion styles were found for the nanomotors. (A) motors moving in a linear translational motion; (B) circular motion of the nanomotors; (C) screw like movement, which is a combination of the linear and circular motions; (D) Images of a motor running in the rotational path of small radius. Scale bars: 10 µm in (A–C) and 2 µm in (D).

It is known that micromotors are able to show different types of movement, including linear, rotational, or the combined motion of a screw like fashion, which is determined by the geometry of the micromotors. In a similar way, it is also illustrated in Figure 3-7 that the nanomotors can have also the abovementioned motion styles similar to the

microtubular motors, including (A) linear, (B) circular and (C) screw like movements. Figure 3-7D gives the time-lapse snapshots of the rotational movement of the nanomotor.

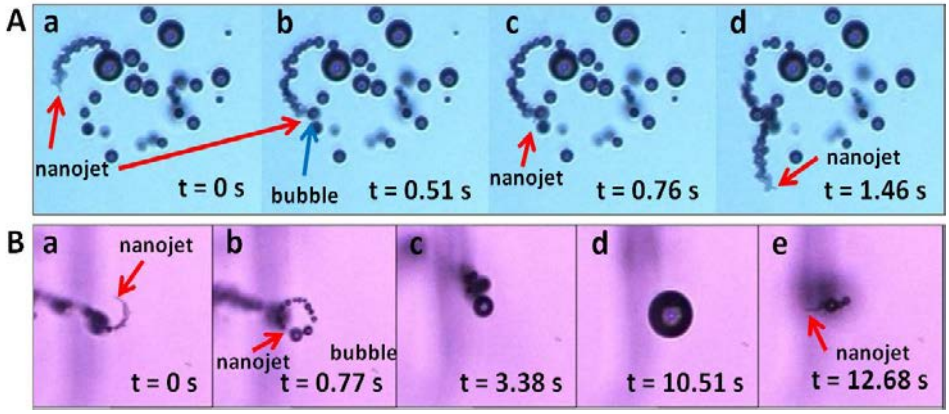

Figure 3-8 Interactions between running nanomotors and the small bubbles. Because of the small dimensions of the nanomotors, their movement is going to be altered by the bubbles released from the inside layer of the motors. (A) Abrupt alteration in the directionality when the nanomotors collides with the bubble; (B) the nanonmotors can be engulfed when colliding with the bubble it previously generated. Scale bars: 10 μm.

The impact of the oxygen bubbles can exert on the motion of the nanomotors can be intriguing. In early studies, the influence of micro-bubbles has been investigated for the microtubular motors. Owing to the nanometer dimension of nanomotors researched in this research and the bubble-ejection principle, it is feasible to see the interactions of such nanomotors with small oxygen bubbles in the liquid in an alternative manner from that with micromotors. Figure 3-8A illustrates time-lapsed microscopic figures of the nanomotors colliding with the small oxygen bubbles, and this collision leads to a significant alteration in the directionality of movement by around 160^{o} (‘‘bouncing back’’). One other case of collision of nanomotors with oxygen bubble can be seen in Figure 3-8B. The nanomotor is constrained at the liquid/oxygen interface of the small bubble released out of the tubular end of the motor and it continues to run at the bubble

surface of the microbubble in a rotational way. The released oxygen molecules lead to an increment in the size of the bubble, which will burst at last when a critical limit is reached. The nanomotor is released from the bubble after the burst and the motion persists in the liquid. Note that these illustrations are qualitative as there is significant difficulty in guiding the motor towards the oxygen bubble in a defined directionality. However, such collisions of nanomotors with the bubbles are often observed throughout the motion of the nanomotors.

3.3 Fabrication of Microscale Tubular Motors

3.3.1 Electrodeposition Route

Inspired by the AAO-templated electrochemical deposition of nanomotors, we continued to study on the feasibility of making the tubular micromotors with the same principle. A cyclopore polycarbonate membrane was adapted and the copper-platinum concentric micromotors were successfully fabricated with an alternative electrochemical deposition process. In an alternative to the sputter-production of sacrificial and conductive layer, as reported by Prof. Wang's group[5], the usage of commercially-available colloidal graphite suspension was chosen.

Experimental Procedures

Materials

Cyclopore polycarbonate membranes with pores of 2 μm in diameter were purchased from Whatman, USA (Cat. No.7060-2511). The pores are conical in shape. Colloidal graphite (isopropanol base) was purchased from Ted Pella, Inc., USA (Lot. No.12009-2). Hydrogen peroxide (27%) was purchased from Alfa Aesar,

Singapore. DMSO, methylene chloride and ethanol were purchased from Tedia, USA. $CuSO_4 \cdot 5H_2O$ (98+%) and sodium dodecylsulfate (SDS, Lot. No. 079K0335) were purchased from Sigma-Aldrich. Platinum plating solution was obtained from Technic Inc., USA (Lot No. 20251001). The chemicals were used as received and ultrapure water (18.2 MΩ cm) from a Millipore Milli-Q purification system was used for all of the experiments.

Apparatus

Electrochemical deposition was carried out using a μAutolab type III electrochemical analyzer (Eco Chemie, The Netherlands) connected to a computer and controlled by General Purpose Electrochemical Systems version 4.9 software (Eco Chemie). The deposition procedure was conducted at room temperature using a three-electrode arrangement. A platinum electrode was utilized as a counter electrode, and Ag/AgCl was used as a reference electrode (CH Instruments, Inc., USA). The ultrasonication process was carried out using a Fisherbrand FB 11203 ultrasonicator, and centrifugation was carried out using a Beckman Coulter Allegra 64R centrifuge. Scanning electron microscopy (SEM/EDX) analysis was conducted using a JEOL JSM 7600F instrument. Optical microscope videos and images were obtained using a Nikon Eclipse TE 2000-E microscope. Video sequences (100 fps) were processed using Nikon NIS-Elements™ software.

Methods

The Cu/Pt concentric bimetallic microtubes were synthesized *via* a modified electrochemical deposition procedure on a cyclopore polycarbonate template, as depicted in Figure 3-9. Colloidal graphite ink was applied to one side of the polycarbonate template using commercial cotton swabs. A piece of flattened aluminium foil was attached to the ink immediately, to serve as a working electrode for the plating

experiments. The template was assembled into a customized electrochemical deposition cell. The template was rinsed with 5 mL of ultrapure water (18.2 MΩ cm) four times, and the Cu outer layer was deposited galvanostatically at −4 mA for 450 s from a deposition solution which contained 1 M $CuSO_4$. Subsequently, after removing the deposition solution, the template was rinsed five times with 8 mL of water. The platinum segment was then electrodeposited at −4 mA for 450 s, using a commercial plating solution. When the deposition of Pt layer on the microtubes was completed, the electrochemical cell was disassembled and the template was washed five times with 8 mL of water each time. After that, the template was ultrasonicated three times in 2 mL of water for 3 min each time. The graphite layer was removed during the ultrasonication procedure. The template was placed in an Eppendorf tube with 2 mL of methylene chloride and ultrasonicated until the whole template was dissolved. The electrochemically deposited microtubes were collected as a pellet after centrifugation at 6000 rpm for 3 min and subsequently washed three times with methylene chloride. The solution was then washed with ethanoland water two times each and centrifuged for 3 min after each washing step. The microtubes were stored in water at room temperature.

The micromotors were set into motion for propulsions in aqueous solutions containing various concentrations of hydrogen peroxide with a fixed surfactant concentration. A mixture of micromotors (5 µL), SDS (1 wt %) and hydrogen peroxide was applied to a glass slide which had been freshly cleaned with N_2 gas. The behavior of the micromotors was then observed under the microscope. Optical microscope videos and images were obtained using a Nikon Eclipse TE 2000-E microscope. Video sequences (100 fps) were processed with Nikon NIS-Elements™ software.

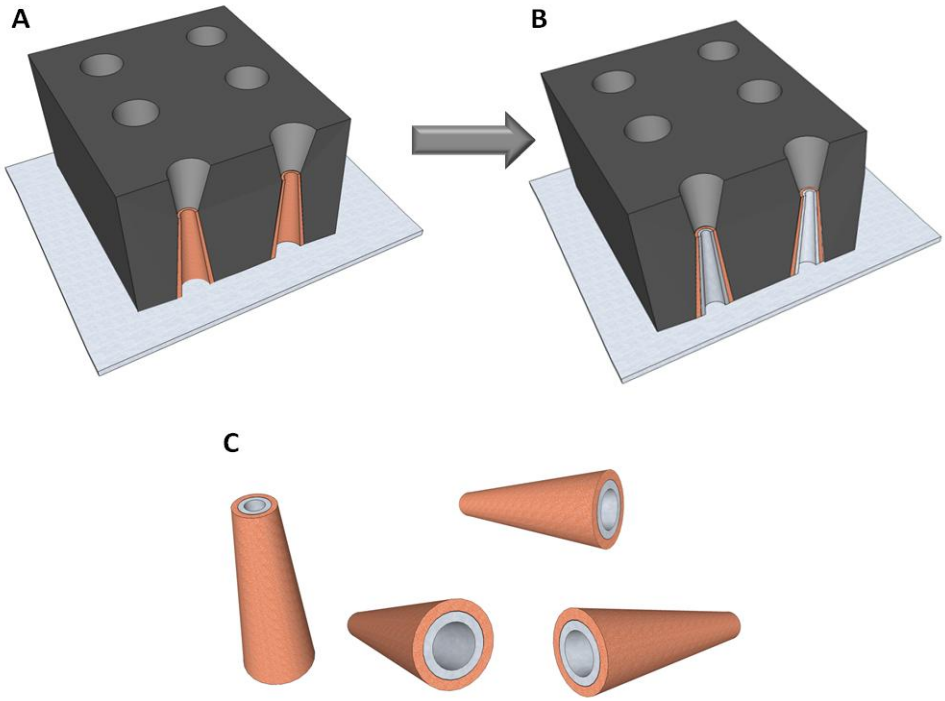

Figure 3-9 Template-directed electroplating of concentric bimetallic micromotors. (A) The Cu segment is deposited in a membrane microchannels linked to a graphite ink electrode. (B) The platinum segment is plated. (C) The polycarbonate membrane is etched and the micromotors are suspended in water.

Results and Discussion

Upon dissolution of the membrane, the micromotors were characterized using scanning electron microscopy (SEM) and were determined to adapt a conical geometry. It was noted that in earlier reports by other authors, the gold outside segment was plated in DMSO solvent. The presence of DMSO resulted into partial dissolving of polycarbonate template and low amount of microtubular motors generated. However, the gold-platinum micromotors produced showed agile movements. Figure 3-10 depicts the template (A) prior to and (B) after the deposition of the micromotors, indicating that this approach does not result in the dissolution of the template; instead it facilitates the large parallel production of concentric bimetallic micromotors.

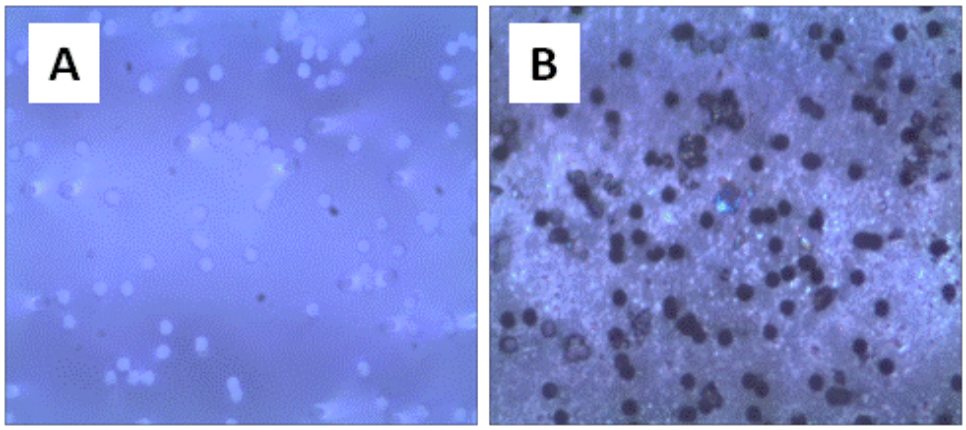

Figure 3-10 Optical microscope images of the polycarbonate template (A) prior to and (B) after electrodeposition fabrication of concentric bimetallic copper-platinum micromotors. Images were taken with 100× magnification.

Figure 3-11 depicts SEM graphs of the produced copper-platinum micromotors at different magnifications. It can be seen from the SEM graphs that the micromotors keep the conical geometry of the polycarbonate template channels; the mean length of the micromotors was around 7 µm and the diameters of the microtubes are around 1.5 and around 2 µm at their opposite ends. Figure 3-11 D and E illustrate the energy dispersive X-ray spectroscopic (EDX) characterization of the fabricated bimetallic microtubular motors. The SEM/EDX graphs clearly illustrate the existence of copper and platinum segments on the tubes. Statistical study of 20 micromotors (n= 20) indicates that the mean length is 10.4 µm (standard deviation 2.6 µm), the diameter at the larger opening end is 1.92 µm (standard deviation 0.34 µm), and the diameter at the smaller opening end is 1.43 µm (standard deviation 0.31 µm).

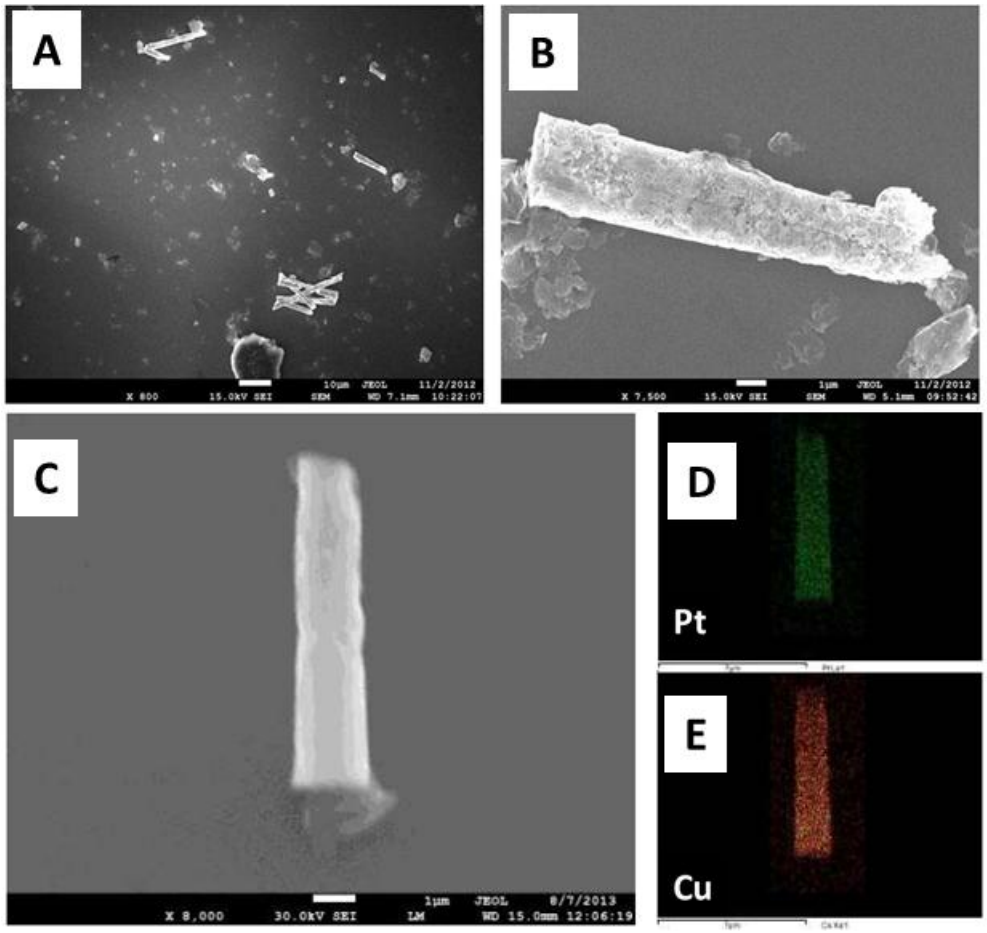

Figure 3-11 (A-C) Scanning electron microscopic images of micromotors suspended in the water suspension. Note that debris around tubes is graphite from the graphite ink (D, E) SEM/EDX elemental characterizations of micromotor composition. Scale bars: 10µm for A, 1 µm for B, and 1 µm for C.

The bimetallic micromotors run in the H_2O_2 solutions at high velocities, similar to previously produced rolled-up micromotors or polymer-platinum micromotors. Such bimetallic micromotors illustrate high speed motion of ~7 body lengths per second (bl/s), even in a very low amount (0.2 wt %) of H_2O_2. Figure 3-12 depicts the micromotors in (A) absence of hydrogen peroxide and (B) in the presence of 1 wt % hydrogen peroxide. The relationship between the micromotor velocities on the amount of hydrogen peroxide is highlighted in the graph shown in Figure 3-12C).

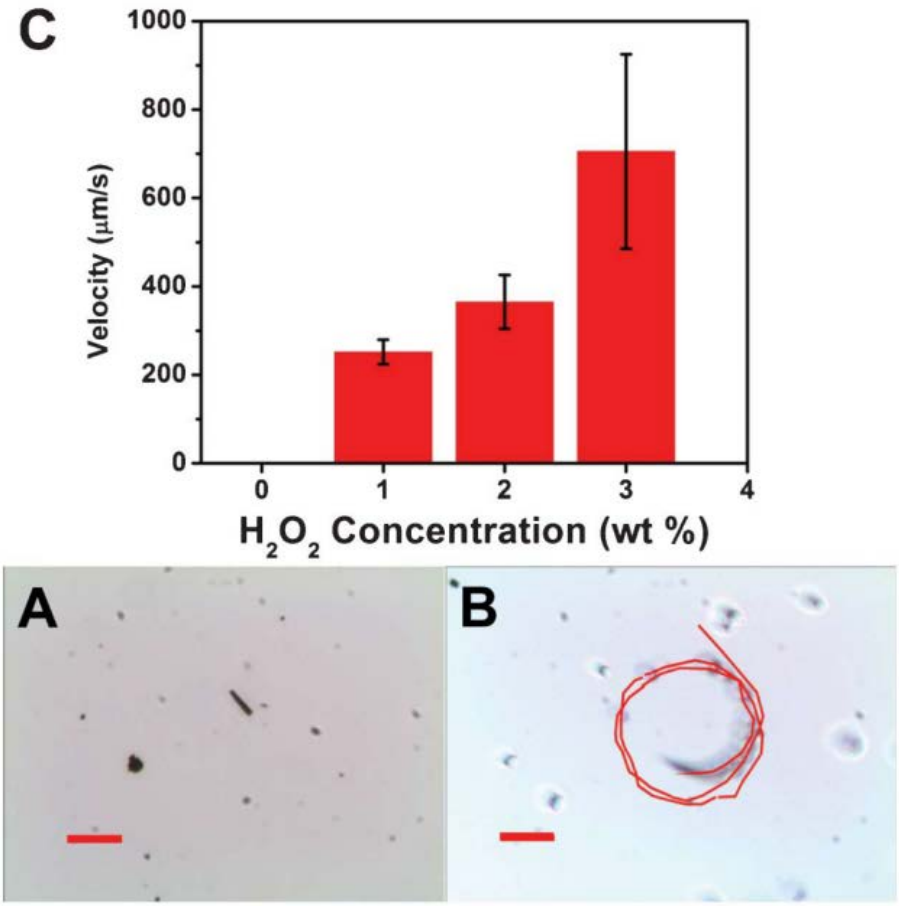

Figure 3-12 Optical micrographs of the micromotors in (A) absence and (B) the presence of 1 wt % hydrogen peroxide. Scale bars of 20 μm; tracking line for 5 seconds. (C) Plot showing dependence of average velocities of micromotors on concentration of hydrogen peroxide.

3.3.2 Lithography Route

Besides the electrochemical deposition route, the rolled-up method by the lift-off of the metallic membrane presents also a highly efficient and reproducible approach to produce the catalytic microtubes. Since its early emerge in 2009,[40] this route of fabrication has been highly adapted and motors of various dimensions, functionalizations and applications have been illustrated extensively in the literature.[5,11,45-48] However, the fabrication of such micro-tubular motors has been a challenging and costly job, as it demands the clean-room conditions and machines, including a mask-aligner, photo-

lithography, and an thermal or electron beam deposition facilities able to tilt the specimen. Implementation of these machines and conditions will cost a huge amount of money. Additionally, it takes several days for the production process to be carried out, making it a considerably time-consuming approach. Thus, I would like to illustrate here our attempt of designing a fast and effective approach for the production of the roll-up micro-tubular motors, which requires a lower amount of high-end facilities as well as a shorter time for the production.

Experimental Procedures

The production processes make use of the Cu TEM sampling grids (300 meshes, referred to as TEM grids in the text) with formvar and carbon support layer, and these TEM grids were bought from Beijing XXBR Technology Co. Initially, such TEM-grids were soaked in chloroform for ten minutes to etch away the formvar polymer part. The glass cover slips were blew with N_2 flow and ultrasonicated in H_2O, acetone and IPA for three minutes each. Consequently, the glass surfaces were put under oxygen plasma for three minutes. A number of 2 distinctive approaches were generated for the production of lift-off microtubes, including the production of lift-off microtubes with H_2O_2 reaction, and the production of lift-off microtubes by etching away the sacrificial part.

For the first approach, poly (methyl methacrylate) (PMMA) was used as the sacrificial part. The PMMA powder was dissolved in dichloromethane (DCM) to form a clear solution of weight concentration of 5.3%. After that, such PMMA in DCM solution was applied (950 μL) on the surface of a pre-treated glass slide. This glass slide has been soaked and ultrasonicated in water, acetone and IPA, 2 minutes each, and subsequently blew clean and put under oxygen plasma for 5 minutes to make the glass surface more hydrophilic. The glass with the solution on top was placed in the spin-coater, and the

spin-coating was done at five thousand rounds per minute for 40 seconds. The acceleration/deceleration duration were set to be 15 and 0 seconds, respectively. After the spin coating, a thin layer of dried PMMA was formed adhering on the surface of glass. It was determined that such polymer layer were stable and suitable for usage within 48 hours of the spin coating. Next, the treated TEM grids were put on top of the polymer layer and the glass slips were put on the hotplate for one minute while slightly pressing the grids to make sure a good contact with the PMMA layer. Afterwards, Pt metal of 5 nanometer thickness was sputter-coated on the PMMA and TEM grids with a current of 10 mA for 45 seconds. The TEM grids were taken off from the glass just by shaking the cover slip, and a droplet of 10 m L acetone was dropped on top of the sputtered place where the TEM grids had been placed. Rolling-up of the Pt membrane into a tubular-structure was achieved as acetone could selectively dissolve the PMMA part. The cover slip was then soaked in EtOH and ultrasonicated for five minutes to release the microtubes into the liquid. The microtubes were kept in EtOH liquid at room temperature.

For the second approach, the chloroform-treated TEM grids were put on top of the freshly cleaned side of the cover glass and Pt metal of 3 nanometer thickness was sputtered on the cover slip with a current of 2 mA for 30 seconds. The TEM grids were removed from the glass surface just by shaking the glass. Then, an amount of 10 μL of H_2O_2 of 7 % concentration was dropped on the surface of the sputtered place, which had not been covered by the TEM grids. A large amount of bubbles were seen and the cover glass was soaked in H_2O once no more bubble appeared. The cover glass was ultrasonicated for five minutes to release the microtubes into the liquid. The cover glass was simply taken off from H_2O and the microtubes were kept in H_2O liquid at room temperature.

Results and Discussion

In this novel approach, to get well-defined metal membrane, the mask-aligner normally utilized in clean room based approaches, has been taken place with commercially purchased TEM grids of defined openings which served as masks. The Si substrate is replaced by a normal cover glass and the metal deposition is carried out with commonly available sputter-coater. Different easy processes are proposed and analyzed in this work: (i) a sacrificial part of PMMA have been spin coated on the glass surface before applying the mask, which is the TEM grid. After that, the deposition of platinum is done with a sputter coater, and lastly the polymer sacrificial part is etched away for the lifting-off and rolling-up of the platinum membrane due to the internal strain. (ii) A TEM grid is put directly on the glass surface without any polymer layer, and platinum is sputtered on top of the glass surface and the microtubes generated by adding H_2O_2 which can trigger the fracture-induced rolling-up of the platinum membrane into the tubes. Figure 3-13 gives a sketch of the procedure.

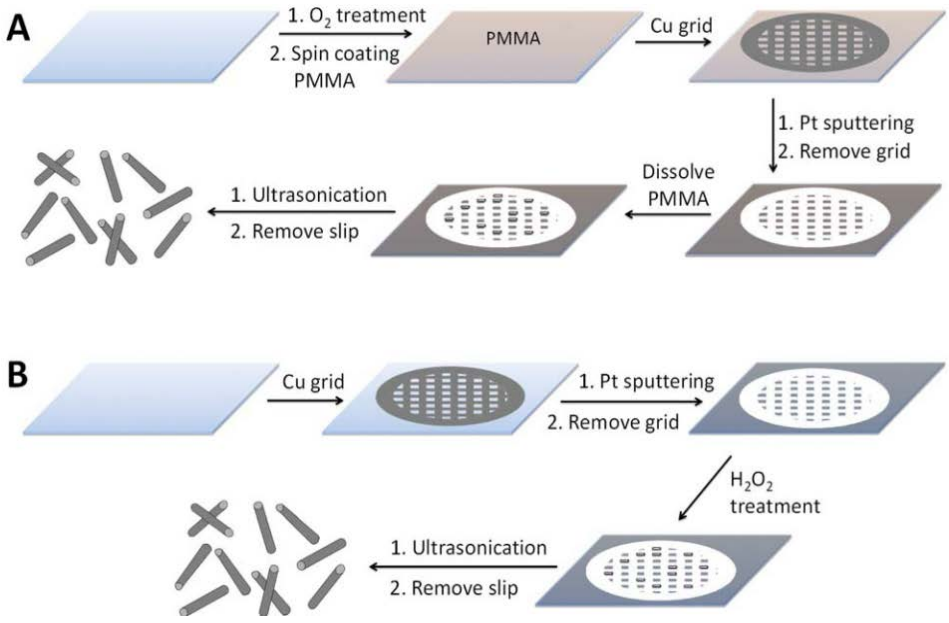

Figure 3-13 Illustration of procedures for the production of platinum microtubes through different routes: (A) TEM grid template/PMMA sacrificial part approach; (B) TEM grid template/hydrogen peroxide assisted rolling up of the microtubes..

TEM grid template/PMMA sacrificial layer production of Pt microtubes

The route utilizing the polymer sacrificial part is shown in Figure 3-13A. A normal cover glass was pretreated in O_2 plasma to eliminate impurities and ensure a hydrophilic surface chemistry at the same time. The cover glass was then spin-coated with a layer of PMMA membrane. The polymer membrane works to facilitate the rolling-up of the microtubes at the last step of the procedure. The polymer part becomes dry immediately after the spin coating, and a TEM Cu grid of defined openings of 60 μm × 60 μm with 23 μm spacing (Fig. 3-14A), is put on the polymer surface. A Pt layer of 5 nanometers is then sputtered on the surface of TEM grids as well as the polymer layer. The taking off of the TEM grid generates a well-defined pattern of platinum part. Lastly, by etching away the PMMA sacrificial part with DCM, the lifting-off of the platinum membrane as well as the generation of platinum tubes from the strain induced rolling (Fig. 3-14B) take place. The whole production route spans about two hours. The determination of the side towards which the membrane rolls to form the microtube could not be manipulated, and for this reason the resulting microtubes are of varied magnitude in length, as can be seen from Figure 3-14C. Most of the tubes show lengths between 30 and 60 micrometers with a relative standard deviation of about 37.2%. It shall be noticed, however, that both the template directed electroplating of micromotors as well as the production of microtubes with the clean room facilities give a similarly wide range of sizes, with relative standard deviation of 21 – 28.5% (determined by the template used) and 13.2%, respectively. Thus, the length range of microtubes produced by this easy approach is comparable to the length range of other alternative approaches. Moreover, as it is hard to manipulate the direction of the rolling, the geometries of the microtube endings also vary. A layered cylindrical microtube with a blunt ending was seen when the platinum layer rolled in a direction parallel to the axis of the tube body, while a layered cylindrical microtube with a

sharp ending was seen when the platinum layer was rolled from the membrane with an angle off the axis. The diameter of the tubes formed through this route was 4.6 µm (17% RSD, n = 20). The rolled-up microtubes were then tested for movement in the presence of H_2O_2 and show an agile bubble-driving motion with velocities close to 100 µm s^{-1} depending on the concentration of H_2O_2.

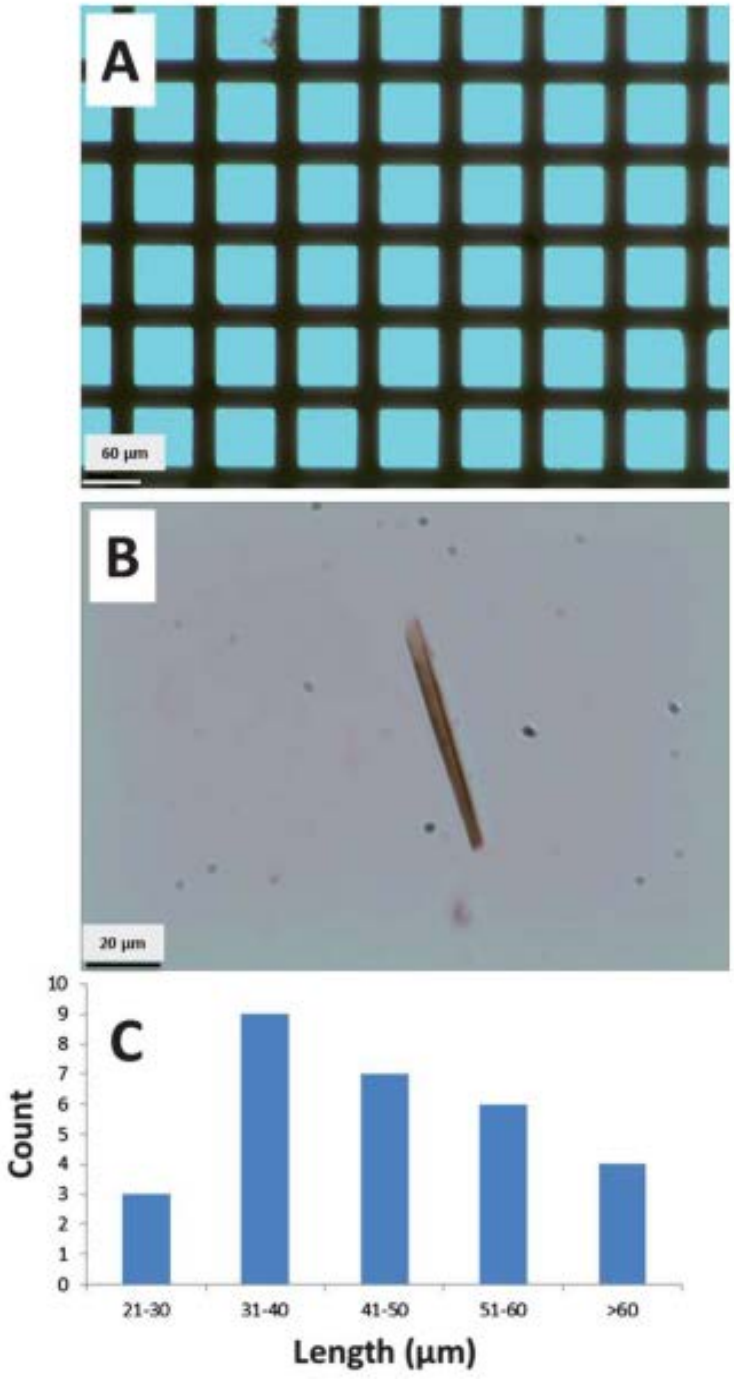

Figure 3-14 (A) Optical image of TEM grids (300-mesh) utilized for the fabrication of rolled up microtubes. The spaces are of sides of 60 μm long; the distances between squares are 23 μm long. Scale bar indicates 60 μm. (B) A typical microscope characterization of the microtube; scale bar indicates 20 μm. (C) Length distribution of the microtubes, n = 30.

TEM grid template/hydrogen peroxide assisted lift-off production of Pt catalytic micromtors

Using route (ii) (see Figure 3-13B), the TEM grid was directly put on the glass cover and no prior coating of the polymer part was carried out. The sputter coating of platinum layer was carried out as in approach (i). After that, the TEM grid was removed and the remaining deposited part was exposed to hydrogen peroxide. The bubbles were out at the edges of the platinum layer and due to the film fracture; the platinum membrane was lifted off, which then rolled up into tubes. The whole procedure spans about two hours. It should be noted that different from the above-mentioned PMMA-based approach, the length of the microtubes produced with this approach is not affected by the TEM grid openings, but can be determined to some extent by the concentration of H_2O_2 which generates varied fracture densities within the 60 μm × 60 μm platinum squares. The size of microtubes was reduced, in fact, from around 20 μm for concentrations of 7 and 14 wt % of hydrogen peroxide to the length of 10 μm for concentrations of 21 and 28 wt % of hydrogen peroxide. Figure 3-15 shows the Pt squares after lifting-off and the length distribution of tubes for different concentrations of hydrogen peroxide.

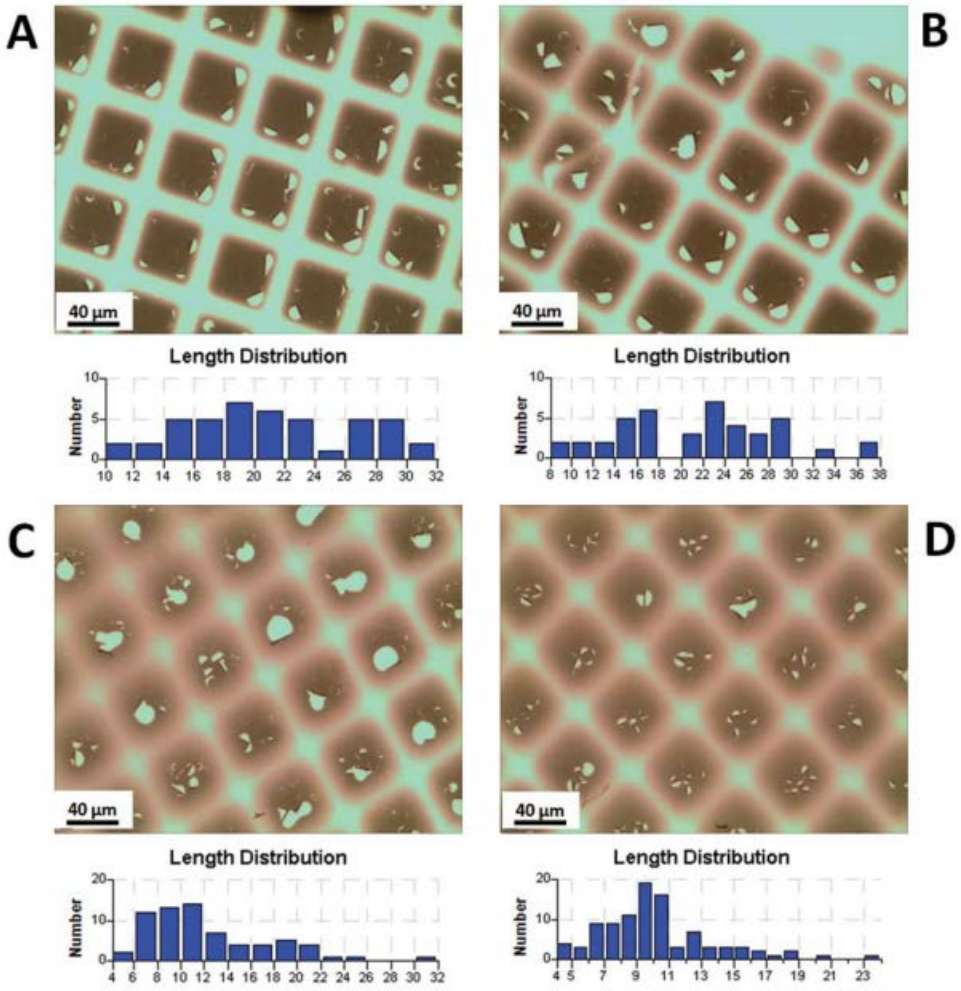

Figure 3-15 Optical micrographs of hydrogen peroxide induced rolling-up of platinum nano-film on glass cover with (A) 7%, (B) 14%, (C) 21% and (D) 28% of H_2O_2. After deposition of platinum with a 60^o tilt of the glass on the copper grid-covered glass, the H_2O_2 solutions were placed on the platinum membrane, leading to the lifting off of platinum nano-film as the oxygen gas was produced. The length distribution idnicates that more uniform microtubes were made when 7% hydrogen peroxide was used.

Tubes generated in different concentrations of H_2O_2 showed a similar diameter of 2.8 µm (14% RSD, n = 20). The produced microtubes possess typically sharp endings, as can be seen in Figure 3-16 SEM images, which have been reported to be good for microsurgeries in earlier work.[49] Such sharp endings were generated because of the irregular shape of the platinum membrane torn off by the oxygen bubbles. Hydrogen peroxide assisted

lifting off of tubes showed a very fast motion of 382 µm s^{-1} in 1% hydrogen peroxide and 740 µm s^{-1} in 3% of hydrogen peroxide, which is equivalent to 20 to 40 bl s^{-1}, respectively (Figure 3-17A) This speed compares well with that of microtubular motors made by the template-based electroplating approach (Figure 3-17B) or the microtubular motors made through the rolled-up procedure with clean room facilities.

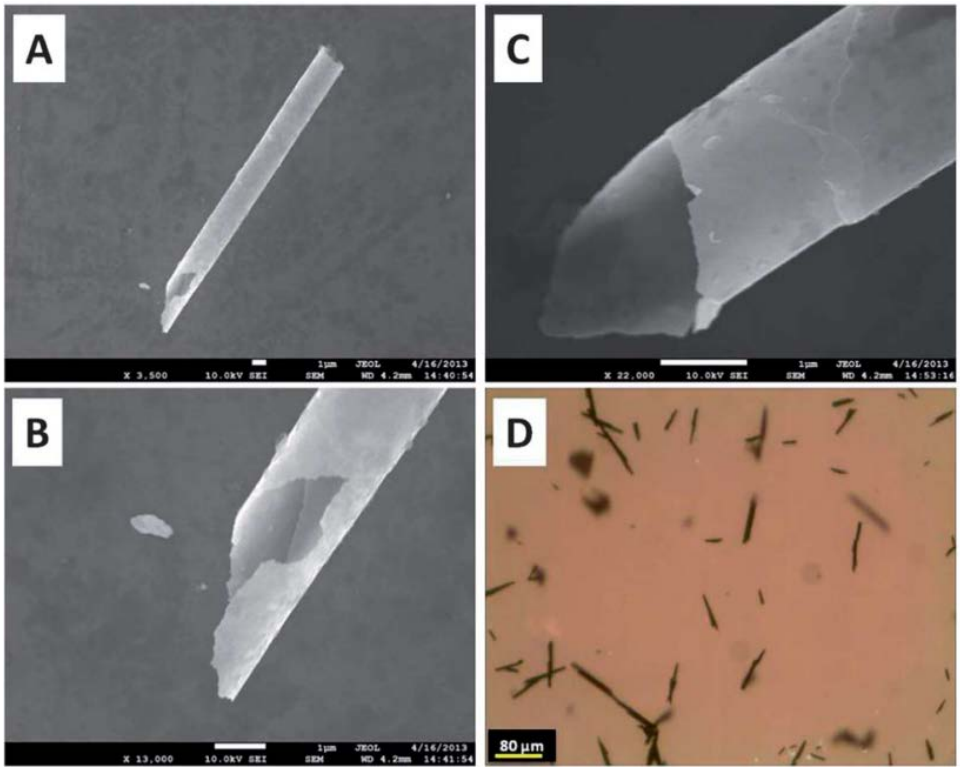

Figure 3-16 (A – C) SEM images of platinum microtubes made from hydrogen peroxide (7%) assisted lifting off of the membrane assisted lift-off process. (D) Optical image of the as formed microtubes in suspension. Scale bars are 1 µm (A – C) and 80 µm (D).

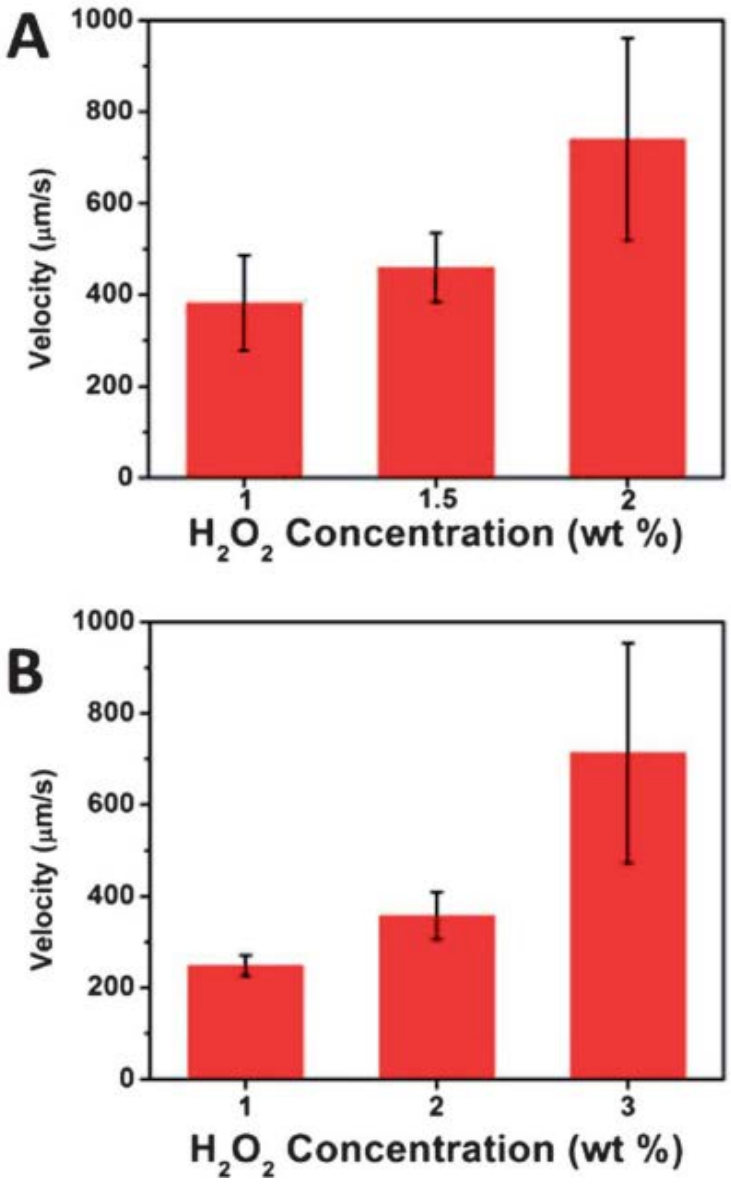

Figure 3-17 Comparison of velocities of microtubular motors fabricated through (A) a roll-up process with 7% hydrogen peroxide and (B) fix-current electroplating with a polycarbonate template. A higher velocity of these rolled-up motors was seen as compared to the electroplated motors.

In summary, a very simple and fast approach for the production of autonomous microtubular motors has been introduced. Such a route eliminates the necessity for clean room condition as well as expensive machines; it utilizes cover glasses rather than Si wafers, a TEM grid as a template mask in place of the mask aligner and a sputter coater

instead of the e-beam evaporator. This is quite a simple approach and can be simply reproduced practically in any materials laboratory around the world, and it has the potential of leading to a significant increment in research in this area.

3.4 References

(1) Wang, J.: *Nanomachines: Fundamentals and Applications*; Wiley-VCH Verlag GmbH & Co. KGaA: Weinheim, Germany, 2013.

(2) Wang, J.: Can man-made nanomachines compete with nature biomotors? *ACS Nano* **2009**, *3*, 4-9.

(3) Wang, J.: Biomolecule-functionalized nanowires: from nanosensors to nanocarriers. *Chemphyschem* **2009**, *10*, 1748-55.

(4) Wang, J.; Manesh, K. M.: Motion control at the nanoscale. *Small* **2010**, *6*, 338-45.

(5) Huang, G.; Wang, J.; Mei, Y.: Material considerations and locomotive capability in catalytic tubular microengines. *J. Mater. Chem.* **2012**, *22*, 6519-6525.

(6) Paxton, W. F.; Sen, A.; Mallouk, T. E.: Motility of catalytic nanoparticles through self-generated forces. *Chemistry* **2005**, *11*, 6462-70.

(7) Paxton, W. F.; Sundararajan, S.; Mallouk, T. E.; Sen, A.: Chemical locomotion. *Angew. Chem. Int. Ed.* **2006**, *45*, 5420-9.

(8) Claridge, S. A.; Castleman, A. W.; Khanna, S. N.; Murray, C. B.; Sen, A.; Weiss, P. S.: Cluster-Assembled Materials. *ACS Nano* **2009**, *3*, 244-255.

(9) Sengupta, S.; Ibele, M. E.; Sen, A.: Fantastic Voyage: Designing Self-Powered Nanorobots. *Angew. Chem. Int. Ed.* **2012**, *51*, 8434-8445.

(10) Patra, D.; Sengupta, S.; Duan, W.; Zhang, H.; Pavlick, R.; Sen, A.: Intelligent, self-powered, drug delivery systems. *Nanoscale* **2013**, *5*, 1273-83.

(11) Mei, Y.; Solovev, A. A.; Sanchez, S.; Schmidt, O. G.: Rolled-up nanotech on polymers: from basic perception to self-propelled catalytic microengines. *Chem. Soc. Rev.* **2011**, *40*, 2109-2119.

(12) Soler, L.; Sanchez, S.: Catalytic nanomotors for environmental monitoring and water remediation. *Nanoscale* **2014**, *6*, 7175-7182.

(13) Gibbs, J. G.; Zhao, Y.-P.: Measurement of driving force of catalytic nanomotors in dilute hydrogen peroxide by torsion balance. *Rev. Sci. Instrum.* **2008**, *79*, *086108.*

(14) Loget, G.; Zigah, D.; Bouffier, L.; Sojic, N.; Kuhn, A.: Bipolar Electrochemistry: From Materials Science to Motion and Beyond. *Acc. Chem. Res.* **2013**, *46*, 2513-2523.

(15) Kagan, D.; Calvo-Marzal, P.; Balasubramanian, S.; Sattayasamitsathit, S.; Manesh, K. M.; Flechsig, G.-U.; Wang, J.: Chemical Sensing Based on Catalytic Nanomotors: Motion-Based Detection of Trace Silver. *J. Am. Chem. Soc.* **2009**, *131*, 12082-12083.

(16) Wu, J.; Balasubramanian, S.; Kagan, D.; Manesh, K. M.; Campuzano, S.; Wang, J.: Motion-based DNA detection using catalytic nanomotors. *Nat. Commun.* **2010**, *1*, 36.

(17) Campuzano, S.; Kagan, D.; Orozco, J.; Wang, J.: Motion-driven sensing and biosensing using electrochemically propelled nanomotors. *Analyst* **2011**, *136*, 4621-30.

(18) Orozco, J.; Garcia-Gradilla, V.; D'Agostino, M.; Gao, W.; Cortes, A.; Wang, J.: Artificial enzyme-powered microfish for water-quality testing. *ACS Nano* **2013**, *7*, 818-24.

(19) Liu, Z.; Li, J.; Wang, J.; Huang, G.; Liu, R.; Mei, Y.: Small-scale heat detection using catalytic microengines irradiated by laser. *Nanoscale* **2013**, *5*, 1345-52.

(20) Orozco, J.; Vilela, D.; Valdés-Ramírez, G.; Fedorak, Y.; Escarpa, A.; Vazquez-Duhalt, R.; Wang, J.: Efficient Biocatalytic Degradation of Pollutants by Enzyme-Releasing Self-Propelled Motors. *Chem. Euro. J.* **2014**, *20*, 2866-2871.

(21) Zhao, G.; Seah, T. H.; Pumera, M.: External-energy-independent polymer capsule motors and their cooperative behaviors. *Chemistry***2011**, *17*, 12020-6.

(22) Soler, L.; Magdanz, V.; Fomin, V. M.; Sanchez, S.; Schmidt, O. G.: Self-propelled micromotors for cleaning polluted water. *ACS Nano* **2013**, *7*, 9611-20.

(23) Sanchez, S.; Solovev, A. A.; Schulze, S.; Schmidt, O. G.: Controlled manipulation of multiple cells using catalytic microbots. *Chem. Commun.* **2011**, *47*, 698-700.

(24) Balasubramanian, S.; Kagan, D.; Jack Hu, C.-M.; Campuzano, S.; Lobo-Castañon, M. J.; Lim, N.; Kang, D. Y.; Zimmerman, M.; Zhang, L.; Wang, J.: Micromachine-Enabled Capture and Isolation of Cancer Cells in Complex Media. *Angew. Chem. Int. Ed.* **2011**, *50*, 4161-4164.

(25) Daniel L. Schodek, P. F., Michael F. Ashby: *Nanomaterials, Nanotechnologies and Design: An Introduction for Engineers*; Butterworth-Heinemann: Burlington, USA, 2009.

(26) Elsevier: *Nanotechnology Safety*; Elsevier: San Diego, USA, 2013.

(27) Gibbs, J. G.; Kothari, S.; Saintillan, D.; Zhao, Y. P.: Geometrically designing the kinematic behavior of catalytic nanomotors. *Nano letters* **2011**, *11*, 2543-50.

(28) Purcell, E. M.: Life at low Reynolds number. *Am. J. Phys.***1977**, *45*, 3-11.

(29) McHenry, M. J.; Azizi, E.; Strother, J. A.: The hydrodynamics of locomotion at intermediate Reynolds numbers: undulatory swimming in ascidian larvae (Botrylloides sp.). *J. Exp.Biol.* **2003**, *206*, 327-43.

(30) Happel J. Brener, H.: *Low Reynolds number hydrodynamics, with special applications to particulate media*; Kluwer: Norwell, MA, , 1983.

(31) Zhou, W., Wang, Z. L *Scanning Microscopy for Nanotechnology: Techniques and Applications*; Springer: New York, USA, 2006.

(32) Kline, T. R.; Paxton, W. F.; Mallouk, T. E.; Sen, A.: Catalytic Nanomotors: Remote-Controlled Autonomous Movement of Striped Metallic Nanorods. *Angew. Chem. Int. Ed.* **2005**, *117*, 754-756.

(33) Paxton, W. F.; Kistler, K. C.; Olmeda, C. C.; Sen, A.; St. Angelo, S. K.; Cao, Y.; Mallouk, T. E.; Lammert, P. E.; Crespi, V. H.: Catalytic Nanomotors: Autonomous Movement of Striped Nanorods. *J. Am. Chem. Soc.* **2004**, *126*, 13424-13431.

(34) Wang, Y.; Hernandez, R. M.; Bartlett, D. J., Jr.; Bingham, J. M.; Kline, T. R.; Sen, A.; Mallouk, T. E.: Bipolar electrochemical mechanism for the propulsion of catalytic nanomotors in hydrogen peroxide solutions. *Langmuir* **2006**, *22*, 10451-6.

(35) Gibbs, J.; Zhao, Y.: Catalytic nanomotors: fabrication, mechanism, and applications. *Front. Mater. Sci.* **2011**, *5*, 25-39.

(36) Laocharoensuk, R.; Burdick, J.; Wang, J.: Carbon-Nanotube-Induced Acceleration of Catalytic Nanomotors. *ACS Nano* **2008**, *2*, 1069-1075.

(37) Demirok, U. K.; Laocharoensuk, R.; Manesh, K. M.; Wang, J.: Ultrafast Catalytic Alloy Nanomotors. *Angew. Chem. Int. Ed.* **2008**, *47*, 9349-9351.

(38) Balasubramanian, S.; Kagan, D.; Manesh, K. M.; Calvo-Marzal, P.; Flechsig, G. U.; Wang, J.: Thermal modulation of nanomotor movement. *Small* **2009**, *5*, 1569-74.

(39) Gao, W.; Sattayasamitsathit, S.; Wang, J.: Catalytically propelled micro-/nanomotors: how fast can they move? *Chem. Rec.* **2012**, *12*, 224-231.

(40) Solovev, A. A.; Mei, Y.; Bermudez Urena, E.; Huang, G.; Schmidt, O. G.: Catalytic microtubular jet engines self-propelled by accumulated gas bubbles. *Small* **2009**, *5*, 1688-92.

(41) Solovev, A. A.; Sanchez, S.; Pumera, M.; Mei, Y. F.; Schmidt, O. G.: Magnetic Control of Tubular Catalytic Microbots for the Transport, Assembly, and Delivery of Micro-objects. *Adv. Func. Mater.* **2010**, *20*, 2430-2435.

(42) Gao, W.; Sattayasamitsathit, S.; Orozco, J.; Wang, J.: Highly Efficient Catalytic Microengines: Template Electrosynthesis of Polyaniline/Platinum Microtubes. *J. Am. Chem. Soc.* **2011**, *133*, 11862-11864.

(43) Gao, W.; Sattayasamitsathit, S.; Uygun, A.; Pei, A.; Ponedal, A.; Wang, J.: Polymer-based tubular microbots: role of composition and preparation. *Nanoscale* **2012**, *4*, 2447-53.

(44) Sanchez, S.; Solovev, A. A.; Harazim, S. M.; Deneke, C.; Feng Mei, Y.; Schmidt, O. G.: The smallest man-made jet engine. *Chem. Rec.* **2011**, *11*, 367-370.

(45) Orozco, J.; Campuzano, S.; Kagan, D.; Zhou, M.; Gao, W.; Wang, J.: Dynamic isolation and unloading of target proteins by aptamer-modified microtransporters. *Anal. Chem.* **2011**, *83*, 7962-9.

(46) Kagan, D.; Campuzano, S.; Balasubramanian, S.; Kuralay, F.; Flechsig, G. U.; Wang, J.: Functionalized micromachines for selective and rapid isolation of nucleic acid targets from complex samples. *Nano lett.* **2011**, *11*, 2083-7.

(47) Solovev, A. A.; Mei, Y.; Schmidt, O. G.: Catalytic Microstrider at the Air–Liquid Interface. *Adv. Mater.* **2010**, *22*, 4340-4344.

(48) Solovev, A. A.; Smith, E. J.; Bof' Bufon, C. C.; Sanchez, S.; Schmidt, O. G.: Light-Controlled Propulsion of Catalytic Microengines. *Angew. Chem. Int. Ed.* **2011**, *50*, 10875-10878.

(49) Xi, W.; Solovev, A. A.; Ananth, A. N.; Gracias, D. H.; Sanchez, S.; Schmidt, O. G.: Rolled-up magnetic microdrillers: towards remotely controlled minimally invasive surgery. *Nanoscale* **2013**, *5*, 1294-1297.

CHAPTER FOUR: MAGNETIC PROPERTIES OF NANO- AND MICROMOTORS

The work discussed in this chapter resulted in the following publications:

Zhao, G.; Sanchez, S.; Schmidt, O. G.; Pumera, M., Micromotors with built-in compasses. *Chem. Commun.* **2012,** *48*, 10090-10092.

Zhao, G.; Wang, H.; Sanchez, S.; Schmidt, O. G.; Pumera, M. Artificial micro-cinderella based on self-propelled micromagnets for the active separation of paramagnetic particles. *Chem. Commun*. **2013,** *49*, 5147-5149.

Zhao, G.; Pumera, M., Magnetotactic artificial self-propelled nanojets. *Langmuire* **2013,** 29, 7411–7415.

4.1 Introduction

The motions of small scale motors all have to do with forces. Initiation of motion, acceleration of speed, changing of moving directions, as well as the pause/resume of the movement are all determined by the net force imposed on the motors. Depending on the effects of the forces, they can be grouped into the driving forces or the resistance forces. For example, the bubble propulsion force is considered to be the driving force for the

catalytic tubular motors; while the friction force from the liquid media is the resistance force. Also, depending on the different ways that forces are exerted on the motors, they can be grouped into the category of contact forces or action-at-a-distance forces. For example, the bubble propulsion force as well as the friction forces mentioned above act by contacting the motors' bodies, thus they belong to the contact forces. While for electric forces, gravitational forces, as well as magnetic forces, a contact with the motors is not necessary, and thus they are the action-at-a-distance forces. Such kind of forces offers a possibility for the remote control of small motors' movements, and they can not only work as the driving force for the motors,[1-8] but also alter the motion direction without changing the driving force or the friction force.[9-13]

Magnetic force, as one of the action-at-a-distance forces, has been utilized in the manipulation of small motors extensively.[14-18] Reports have emerged to show the utilization of magnetic force to power the motion of nano-/micromotors,[19-21] and even the hybrid motors powered by both magnetic field and chemical fuel have been proposed.[6] In some other works, magnetic field was used purely as a guidance to alter the motion direction of the motors.[22] In this case, the magnetic field only affects the direction of motion without affecting the net driving force of the motion.

Although there have been plenty of reports on the magnetic control over the motion directionalities of nano-/micromotors, the study on the magnetization of the motors is lacking. In this chapter, I would like to demonstrate the effort we had made to explore the magnetization of ferromagnetic nano-/micromotors with the presence of external magnetic field. In our work, it was found that when a piece of magnet was placed at the vicinity of the ferromagnetic nano-/micromotors, such motors became magnetized and worked as a magnet with their own north/south poles. The magnetized motors were observed to be attracted or pushed away from the external magnet, and this behavior of such small motors was observed for the first time.

The functionalization and application of the magnetic properties of the micromotors are also to be discussed in this chapter. We successfully demonstrated that the magnetized micromotors are able to selectively catch and deliver the paramagnetic beads from a pool of beads mixture.

4.2 Micromotors with Built-in Compasses

Ferromagnetic materials consist of lots of magnetic domains where the magnetic moments are often randomly oriented, and thus no overall magnetism is exhibited. When such materials are not magnetized, they can only be attracted towards a magnetic field, and no repulsive force is present against the external magnetic field. However when the external magnetic field is strong, such ferromagnetic materials can be magnetized by reorienting of the domains according to the external field. Under this circumstance, the ferromagnetic materials become magnetic with their own north/south poles. Such magnetization process can be frequently seen in the industry, from the recording of the magnetic tape to the production of various kinds of magnets. Depending on the polarity of the magnetized materials, they can be either attracted or repelled by the external magnetic field. In this section, I would like to show that with the presence of external magnetic field, the Fe-containing microtubular motors can be magnetized, with defined north/south poles of their own. When this happened, they can be either attracted or repelled by the external magnetic field. Our work showed for the first time that external magnet can magnetize and repulse the Fe-incorporated micromotors.

Experimental Procedures

Fabrication of such microtubular motors was carried out by our collaborators based on reported procedures. Basically, electron-beam (e-beam evaporation of Ti, Fe, and Cr as

well as the magnetronsputtering (Pt) of thin metallic films on patterned photoresist squares with a single element size of 50 μm ×50 μm were carried out. Initially, the photoresist AR-P 3510 was spin-coated on a piece of 1.5 inch silicon wafer, and the spinning was done at 3,500 rpm for 35 seconds. After that, a soft bake on a hotplate at the temperature of 90^{o}C was carried out for 1 minute. Subsequently, the resist was exposed to ultra-violet light by applying a Karl Suss MA-56 mask aligner (410–605 nm). The patterns were then developed in an AR300-35/H_2O solution (1:1). A tilted deposition of the metallic layers was done at an angle of ~60 degree, with reference to the horizontal axis of the resist surface. The metal nano-films were obtained layer by layer, with a thickness of 3 nm for titanium, 5 nm for iron, and 5 nm for chromium. Thereafter, a layer of 1 nm thickness of Pt was deposited on the structure with magnetron sputtering. The materials were soaked in acetone where rolling-up of the thin metallic membranes into microtubes was achieved by selectively dissolving the photoresist layer. In order to avoid the microtubes from collapsing due to the high surface tension of liquid, the supercritical point drying process was carried out. The microtubes were ready to use and kept at room temperature.

Running of micromotors was studied in aqueous liquid with 9 wt % of H_2O_2 at fixed surfactant concentrations (1 wt% of SDS). A small portion (1%, v/v) of IPA was put into the liquid to facilitate the visibility of the microtubes. Control trials without H_2O_2 hydrogen peroxide carried out in water suspension had the same amount of SDS and IPA present. Magnetic field was applied by placing permanent magnet about 3 cm from the Petri dish in the horizontal plane. For reversing of the magnetic field, the permanent magnet was rotated 180^{o} at the fixed location.

Optical microscope videos and images were received with Nikon Eclipse TE 2000-E microscope, CFI 10× optics. Video sequences were handled with Nikon NIS-Elements^{TM} software.

Results and Discussion

We would like to demonstrate that it is feasible to magnetize microtubular motors incorporated with ferromagnetic materials. The magnetized microtubular motors become permanent magnets and are able to be attracted or repulsed by the external magnet according to the polarity of the magnet whereas non-magnetized microtubes are attracted to the external magnet regardless of the polarity of the external magnetic field. The net force from bubble pushing and compass-needle like effect resulted into magnetotactic micromotors working in a similar way as that of the magnetotactic microorganisms.[23,24] This offers a new approach for the manipulation over direction of micromotors. The directionality of the magnetized microtubular motors is able to be controlled even from a large distance by altering the polarity of the external magnet. This is illustrated different to ferromagnetic non-magnetized microtubular motors which can have merely attractive effect towards the external magnet. These results offer the possibility of long-distance manipulation of self-powered microtubular motors.

With and without the application of external magnet, the motion behaviors of the magnetized microtubular motors and the not magnetized microtubular motors can be significantly distinctive from each other. The micromotors production is through the rolling up of layers of metallic membranes of titanium, iron, chromium and platinum, and their individual thicknesses are three, five, five and one nanometers, respectively. The mean magnitude in terms of tube lengths is around 56 micrometers, and that of the tube diameter is around 3 micrometers. The bubbles can be seen out from the tube opening asymmetrically when put in the aqueous liquid with H_2O_2, and such asymmetry of bubble ejection offers the driving force for the motion of the microtubes. The micromotors run in a unidirectional fashion and if there is no external magnet around, their mean speed can

be roughly 230 micrometers in one second. If a piece of magnet is placed around the running droplet, the motion of the not magnetized microtubes turned to be directed parallel to the magnetic field with the bubble-ejecting end of the tube aligned against the external magnet. The speed of the microtubes was around 300 micrometers per second. Moreover, upon turning the external magnet for 180^o to reverse the north/south poles of it, the directionality of the micromotors wasn't reversed. (Figure 4- 1) However, if the microtubular motors, incorporated with a layer of Fe, was magnetized by putting the magnet near the running droplet at around 2 millimeters distance, the observation was very much different, The external magnet (neodymium) of field strength of B=270 mT was applied for 10 s and the microtubular motors were successfully magnetized longitudinally. Such magnetized micromotors behaved like microscale bubble propelled magnets, and they possessed alternative reaction towards the external magnetic field compared to the not magnetized microtubes. Random motion was seen for the magnetized motors in 9% of hydrogen peroxide when there was no external magnet around; however, when an external magnet of ~2 mT was placed around the running liquid, such motors run with a direction parallel to the magnetic field. For a specific instance illustrated in Figure 4-1B, a, the magnetized motors run towards the magnet with its front end, which is the end without bubble ejection, pointing to the external magnet. The mean speed of the motors under this condition was around 60 micrometers per second. The possible scenario for this speed drop from the external-magnet-absent condition is that the motion is spiral and not linear as in the condition without external magnet. The linear speed was controlled by a mixed effect from both the bubble-propelled force and the magnetic force pulling the tube towards the magnet, and these two forces were towards the same direction. When the external magnet was turned 180^o (Figure 4-1B, b), the magnetized micromotors working as a microscale magnet, re-directed its motion by 180^o also, leaving the front-end of the micromotors faced against the magnet and was propelled by bubble-

propulsion away from the external magnet. However, the force between the magnetic micromotors and the external magnet was still attractive force under this condition. This force was trying to pull the micromotor towards the external magnet, which was opposite from the bubble-pushing force. Thus, the net force along the tube motion direction is the subtraction of the magnet-pulling force from the bubble-pushing force, which lowered the driving force exerted on the micromotor. As a result, a slower motion was recorded, with the mean speed being ~50 μm s^{-1}. When the external magnet was turned for a second time, the magnetized tubes flipped over by around 180^{o} also, with its front end pointing towards the external magnet, as seen in Figure 4-1B, c. The bubble-pushing and magnet-pulling force acted in a synergic fashion and the mean speed was higher to be around 62 micrometer per second. The different speeds for the magnetized microtubular motors when oriented towards or against the external magnet were also partially attributed to the different steepness of the spiral movement with rough steepness (helix angle) of 20^{o} , 10^{o}, and 21^{o} (Figure 4-1B, a, b, c). Figure 4-1B shows that changing the direction of the external magnet would alter the direction of the magnetized motors. The north and south poles of the magnetized microtube illustrated beside the motors as a red and blue bars. The real distance of the neodymium permanent magnet from the running droplet containing the motors was around 3 centimeters. The reproducibility of such observations was confirmed by repeating the experiments on other microtubes (n = 20).

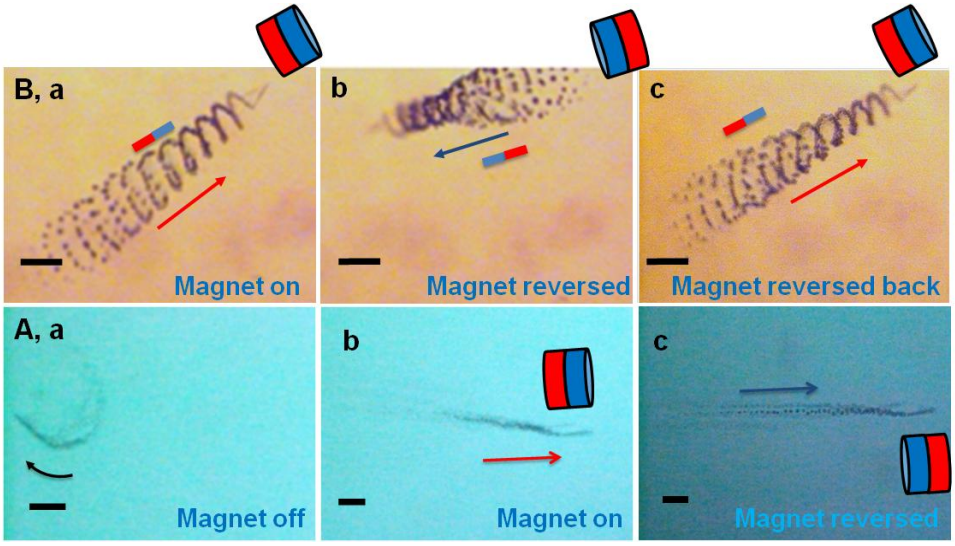

Figure 4-1 Motion of (A) not magnetized and (B) magnetized bubble-pushing microtubular motors under the conditions (a) without (b) with the external neodymium magnet. (c) Direction of the magnetized microtubular motors altered with changing the polarity of the external magnet, which resulted in the reversing of the motion. The external magnet was put around 3 centimeters away from the motors. The small red and blue bars indicate the poles of magnetized tube. The running of motors was carried out at 9 % H_2O_2 and 1 % SDS. Scale bars indicate 40 µm.

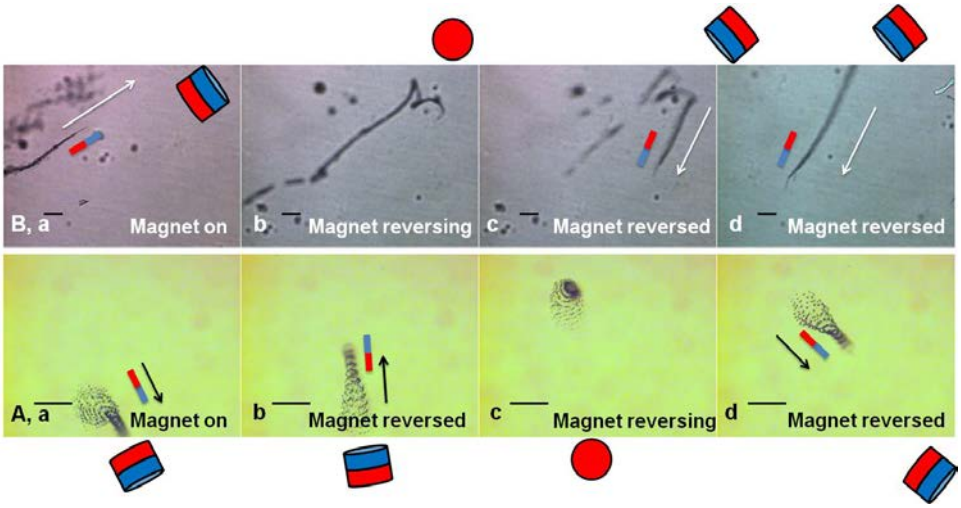

Figure 4-2 Motion of magnetized bubble-ejection microtubular motors in a spiral way (A) and in a linear direction (B). It is observed that the direction of the motion can be manipulated by polarity of the external magnet, which induced the change of the motion. The illustration of a large magnet indicates the direction of the external magnet but not the exact position of the external magnet as it was put around 3 centimeters away from the running droplet. The small red and blue bars indicate the magnetic polarity of magnetized microtubes. Running of the micromotor was done at 9 % H_2O_2, with 1 % SDS as surfactant. Scale bars indicate 100 µm.

Another instance of the spiral motion as well as the linear motion of magnetized microtubular motors was shown in Figure 4-2. Figure 4-2A illustrates the orientation of the magnetized microtube (a) towards the external magnet, (b) against the external magnetic field upon changing the polarity of the external magnet, (c) reversal of the orientation of the magnet by ‘‘flipping” the external magnet and (d) motion of the microtubular motor for a second time towards the magnet. The speeds of the microtubular motors are 37/32/37 micrometers per second for cases a, b and d, respectively. Figure 4-2B demonstrates (a) motion under the impact of the external magnet, (b) the reversal of the polarity of the magnetic field by ‘‘flipping the external magnet and (c, d) the reversed orientation of the magnetized tubes by reversing the orientation of the external magnet. The speeds of motors are 158/114 micrometers per second in cases a and d, respectively.

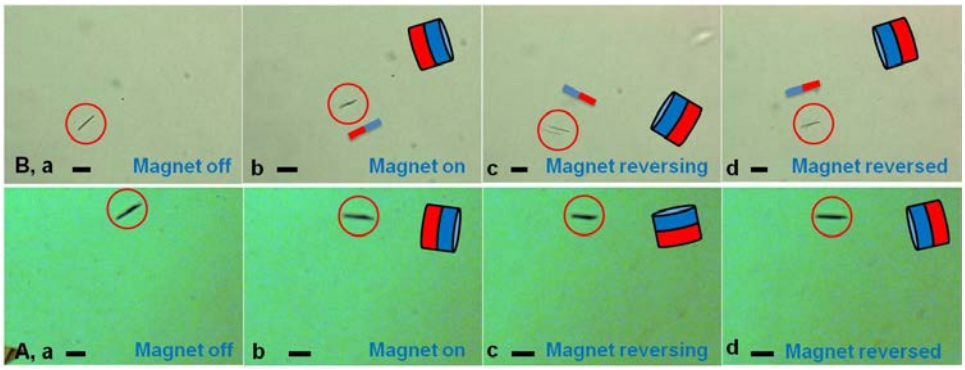

Figure 4-3 Microscope graphs of (A) not magnetized and (B) magnetized self-powered microtubular motors under the condition (a) no external magnet applied and (b) the a strong external magnet put beside the running liquid. (c) Direction of the magnetized microtubes altered with reversing orientation of the external magnet. Experiments were done in water based liquid with 1 % SDS as a surfactant in the absence of H_2O_2. Scale bars indicate 40 µm.

To confirm the theory for the micromotor magnetization, the impact of external magnet on the microtubular motors without hydrogen peroxide was studied. The not magnetized and magnetized microtubes showed no movement without hydrogen peroxide and external magnet (Figure 4-3Aa and Figure 4-3Ba). When an external magnet was placed by the side of the liquid, the not magnetized microtubes rotated according to the orientation of the magnet; on the other hand, when the magnetic field was reversed, direction of the microtubes was not altered (Figure 4-3A, b–d). The microtubular motors migrated slowly towards the external magnet. In the case of the magnetized microtubes, they turned upon the reversal of the external magnet. Such microtubes showed slow migration to the external permanent magnet at a speed of around 8 micrometers per second due to attractive force by the external field (Figure 4-3B, b–d). These observations indicate that the magnetized microtubes behave like a magnetic compass needle as they

can reorient themselves according to the external magnetic field. This capability of magnetized microtubes without hydrogen peroxide is analogous to that of the dead magnetotactic bacteria.

In summary, it was illustrated in this section that microtubular motors incorporated with iron are able to be magnetized and work as small self-powered compass-needles. Such magnetic microtubes can sense the presence and polarity of external magnetic field and redirect themselves. Such observations indicate that magnetic microtubular motors can detect and run towards the external magnet, similar to magnetotactic bacteria.

4.3 Magnetotactic Nanomotors

Based on the catalytic decomposition of H_2O_2, the bubble-propelled microtubular motors can move with a strong power thrust. But it takes more than just the power to efficiently deploy such motors for future development, and one amongst the all the key elements for their operation is the autonomy of such motors. It is reasonable to expect that the nano-/micromotors shall be able to sense the environment that they are running inside, and take some action accordingly. For example, such responses can arise from the changes in light, specific chemicals, temperature, as well as the presence of external magnetic field. Such "sense and act" behavior can be correspondingly termed as thermotaxis, magnetotaxis, phototaxis, or chemotaxis. To date only a limited number of such tactic effects have been reported, such as the chemotactic or magnetotatic behaviors of small objects.[25-27] The word "tactic" indicates that such small motors can detect the presence of chemical or magnetic gradient and respond to run towards or against the origin of such chemicals or magnetic field. Chemotaxis is widely seen and lots of creatures are able to detect the presence of nutrients or harmful molecules, and magnetotatic effect can be seen in

magnetotactic bacteria (i.e., Magneto-spirillum magnetotacticum). Such creatures are able to self-orient according to the external magnetic field due to the presence of ferromagnetic iron oxide crystals within their body. Moreover, such self-aligning capability of the bacteria is still present as a respond to external magnetic field even for dead bacterium, behaving in a similar fashion to the needle of a compass.[23,24]

In the small motors field of study, the magnetotaxis phenomenon has been observed on the self-propelling nanowires. [28,29] In the recent decade, the bubble-ejection self-propelling micromotors have shown a dramatic development. Also, in the size range smaller than micrometer scales, fabrication and testing of motors emerged and received lots of attention in the research field. On the other hand, the observation over the magnetotaxis effect of such nanomotors has been lacking. It was demonstrated in Section 4.2 that that rolled-up microtubular motors incorporated with a layer of Fe metal can be magnetized, and the induced alignment of the magnetic field of the magnetized microtube is along its longitudinal axis. The “Swiss roll” structures of such motors indicate that the iron segment is presented along the whole body of the tube. In this section, I wish to demonstrate a follow up on the earlier study on magnetized microtubular motors by showing similar observations on the nanotubular motors, and there are two principle differences. First, we addressed in principle the possibility to create such an induced magnetic moment in the nanomotors, which can respond the external magnetic field with its own north/south poles. And second, as the nanomotors were electroplated in the templates, the individual metallic segments along the axis of the tube are not present throughout the whole body, which is significantly different from the structure of the microtubular motors shown in Section 4.2. One would wonder naturally that if the short segment within the tubular body is able to be magnetized in the axial direction as the direction of magnetization has a significant impact on the magnetotactic effect of the

nanotubular motors. In this section, I wish to demonstrate the magnetotactic observation of bubble propelled nanotubular motors.

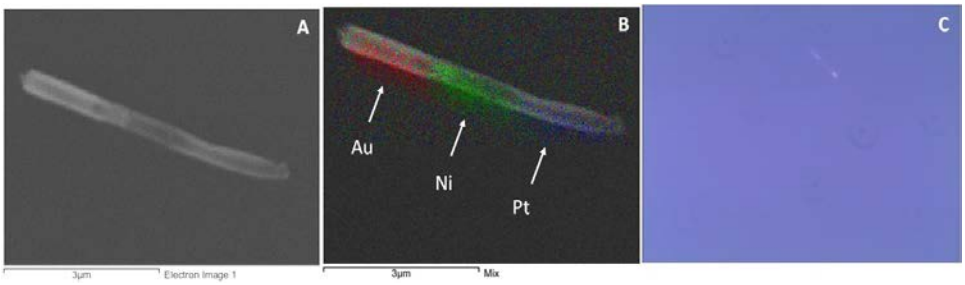

Figure 4-4 Microscopic characterization of Au/Ni/Pt nanotubular motors. (A) Scanning electron microscopy (SEM) characterization of the Au/Ni/Pt nanotubular motor. (B) SEM/EDX characterizations of the Au/Ni/Pt nanotubular motor with a labeling of the elemental composition. (C) Optical image of the Au/Ni/Pt nanotubular motor with the different colors in reflected light from different segments of the nanotubular motors. Scale bars 3 µm.

Experimental Procedures

The Au/Ni/Pt ferromagnetic motors were produced with a modified electroplating process with the AAO membrane as template.[30] Ag conductive paste was put to the branched surface of the membrane using cotton applicators. A piece of flattened Al foil was attached to the silver paste immediately, which works as the working-electrode. The membrane together with the aluminum foil was assembled into a customized electroplating cell. A Pt counter-electrode and Ag/AgCl reference-electrode were used. Electroplating was done using a µAutolab type III electrochemical analyzer linked to a PC and controlled by General Purpose Electrochemical Systems version 4.9 software. The membrane was rinsed thoroughly with five mL of DI water (18.2 mΩ cm) for four times,

and a copper sacrificial layer was grown at a fixed current of − 10 mA for 900 s. The plating solution was made up of 1 M $CuSO_4$ in water solution. After that, after taking out the plating solution, the membrane was washed 5 times with 8 mL of H_2O. Pt, Ni, and Au parts were electroplated separately. Platinum and gold were plated at − 5 mA for 2700 s each using the commercial electrodeposition solutions. The nickel part was also plated at − 5 mA for 2700 s with a home-made Ni plating solution (20 g/L $NiCl_2{\cdot}6H_2O$, 515 g/L $Ni(H_2NSO_3)_2{\cdot}4H_2O$, and 20 g/L H_3BO_3 (buffered to pH 3.4)). When the electroplating steps were done, the plating setup was disassembled and the membrane was rinsed 5 times with 8 mL of H_2O each. Consequently, the membrane was ultrasonicated 3 times in 2 mL of diethyleneglycol monoethylether acetate for one minute each time. The Ag conductive ink was totally dissolved into the solvent in the process of ultrasonication. The sacrificial Cu part was eliminated by the polishing of the Cu surface with cotton applicators soaked with 6.5% of nitric acid. After rinse with H_2O, the membrane was put in an Eppendorf tube with 2 mL of sodium hydroxide and ultrasonicated to totally remove the visible shards. The suspension was washed and centrifuged ten times at 1,500 rounds per mind for one minute with 2 mL of H_2O to thoroughly eliminate the salt impurities. Lastly, the aqueous liquid containing the nanotubular motors were kept at room temperature.

The running of the motors was carried out in an aqueous running liquid with 9 wt % H_2O_2 at a fixed concentration of SDS, which was 1 % in a Petri dish of 1.7 cm in radius. A magnetic field was utilized by putting a permanent magnet about 3 cm from the Petri dish in the horizontal plane. To reverse the magnetic field, the external magnet was reversed at the same distance. The neodymium permanent magnet (~270 mT) was used for magnetic control of the nanomotors at a distance of around three centimeters.

Results and Discussion

The Au/Ni/Pt multi-segmented nanomotors were produced with the electroplating approach as explained above. Such nanomotors contains 3 segments: a platinum part responsible for the catalytic reaction of H_2O_2 and bubble-propulsion, a nickel part to magnetize the nanotubular motors, and a gold part maybe used for chemical modifications of the tube surface and possible functions. The radius of the nanotubues is ~ 150 nm, and the average length is around five micrometers. Figure 4-4A is the SEM characterization for the tubes that gives the morphology of the nanotubes; Figure 4-4B is the EDS mapping that shows the elemental composition of the nanotube, and Figure 4-4B gives an optical microscope image that shows the different colors of different segments of the nanotube. According to the SEM (Figure 4-4A), the difference in color contract could be seen to distinguish the individual segments of the nanotube. The EDS mapping (Figure 4-4B) was present to illustrate the element composition of the nanotubes. According to Figure 4-4B, the nickel part (green) is deposited in between the gold (red) and platinum (blue) parts. According to the optical microscope photo (Figure 4-4C), presence of different elements could also be seen based on the different reflectivity. The Au/Ni/Pt naotubues in the liquid were exposed to a magnetic field of 270 mT for 30 s. The presence of external magnetic field led to the re-alignment of the magnetic domains in the nickel part and the nickel segment became magnetized with its own north/south poles. As the nickel part possessed a longer dimension along the axis of the nanotube than across its axis, the north and south poles of the nickel segment are oriented parallel to the tube axis. As can be seen from Figure 4-4, platinum is just one segment in the trimetallic nanotubes; nickel and gold are not able to catalyze the decomposition of hydrogen peroxide. This is an important difference in configuration from that of all microtubular motors produced either *via* rolling up approach or electroplating process, as the inside layers of the tubular micromotors consist of one uniform platinum element. For the nanotubes reported in this section, platinum takes up only around one third of the length located at the end of the

nanotubes. It can be thus confirmed that even at this structure where only a small segment is catalytically active, the motors are still able to run. H_2O_2 reacted at the platinum site and the O_2 gas is released at this end. Such bubble ejection offers a driving force for the flux of hydrogen peroxide solution at the gold end and its disproportion at the platinum segment, in a similar fashion to the microtubular motors.

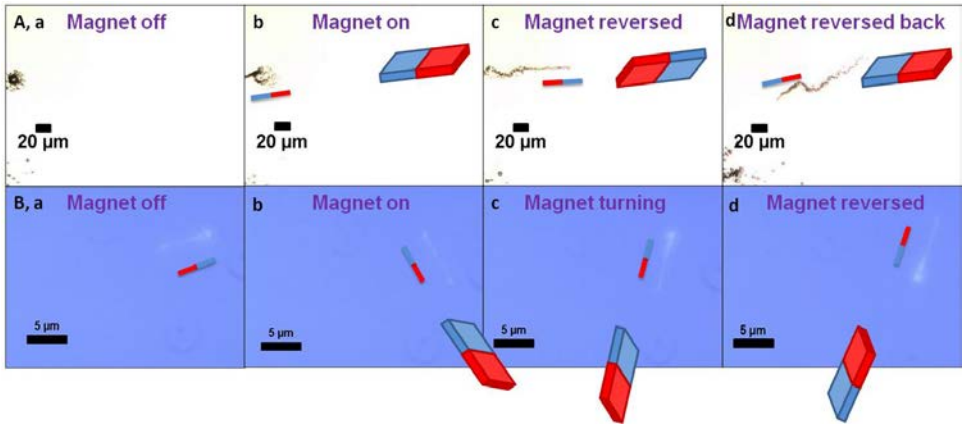

Figure 4-5 Motion of magnetized naotubular motion in (A) the presence of hydrogen peroxide and (B) the absence of hydrogen peroxide. The alignment of the magnetized microtube is altered by reversing the orientation of the external magnet, resulted into a reversing of the running direction. The red and blue bar near the running liquid depicts the magnetic polarity of the nanotubular motor. The magnet was placed around 3 centimeters away from the running liquid. Conditions: (A) 9 % H_2O_2 with 1 % SDS; (B) aqueous liquid with 1 % of SDS.

It is illustrated in this section that the nickel part of a nanotubulars motor are magnetized and respond to the reversing of external magnet as a permagnet magnet themselves. Figure 4-5Aa illustrates that when there is no external magnet placed near the running liquid, the motion of the magnetized nanotubular motors is random. But when the magnetized nanotubular motors are exposed to an external magnetic field, the motion

direction of the motors is parallel to the external magnetic field. In Figure 4-5Ab, it can be found that the nanotube is oriented and the platinum end is pointing to the external magnet and the motor run against the external magnet as it has been previously magnetized. When the external magnetic field is reversed (Figure 4-5Ac), the magnetized nanotubular motor runs toward the external magnet. And upon the repeated rotating of the external magnet (Figure 4-5Ad), the motor reorients its motion direction and runs against the magnet for a second time. The reversion of motion orientation is realized as long as the movement persists. And when the motion is away from the external magnet, the net driving force is the result of subtracting the magnetic attraction from the bubble-ejection. The driving force in this case is weaker and a lower average speed of around 30 micrometers per second. When the motion is towards the magnet, the net driving force is the plus of the bubble-ejection and magnetic attraction, which leads to a faster motion of around 88 micrometers per second in mean speed.

As described previously, the magnetotactic bacteria realign its body due to the external magnetic field even if it is dead, and such reaction can be attributed to the ferromagnetic crystals in the cells. Similarly for the magnetized nanotubes, the realignment can also be observed when they are “dead”, which is when there is no fuel present to power their motion. As can be seen in Figure 4-5B. no movement of the tube happening without external magnet, but when magnet is placed near to the running liquid, the tube realigns and points towards the (Figure 4-5B,b). Upon the turning the magnet, the tube is also seen turning (Figure 4-5B,c) and eventually, when the magnet turns for 180^{o} (Figure 4-5B, d), the orientation of the nanotube reverses too.

4.4 Application: Artificial Micro-Cinderella

In this section, I would like to introduce the work on the application of ferromagnetic material (in this case iron) incorporated microtubular motors. It is shown that such ferromagnetic micromotors can pick up the paramagnetic beads without any attractive interactions with the diamagnetic silica beads. This observation offers the possibility of active separation of specific beads from a pool of beads.

Application of the artificial nano-/micromotors depends on the abilities of such motors to be strongly powered as well as well manipulated. The successful fabrication of such small motors through different routes is reported extensively in the literature, including bimetallic microwires,[28] Janus motors,[31] screw-shaped motors,[32] as well as the nano-/microtubular motors.[33] Among different types of small motors, the tubular motors are of high interest to us as they demonstrated a high power output, linear directionality, ease of manipulation, and convenience of modification and functionality.[16] So far various applications of the tubular motors have been proposed and demonstrated, and one of the important ones is the navigated and selective picking up and delivery of cargoes.[13,34,35] Such capability has been achieved *via* the mechanical-attachment to the front end of the tube,[13] the usage of a bio-recognition element (such as single stranded DNA, protein molecules),[34,35] or the chemical bonds.[36] In the following text, I will present our work on the selective pick-up of paramagnetic cargo by the magnetized microtubular motors, without the aid of any surface modification. It shall be seen that such magnetized motors were equipped with a permanent magnetic moment and were able to selectively catch the targeted beads from a mixture with the diamagnetic beads, in the absence of an external magnetic field, as depicted in Figure 4-6.

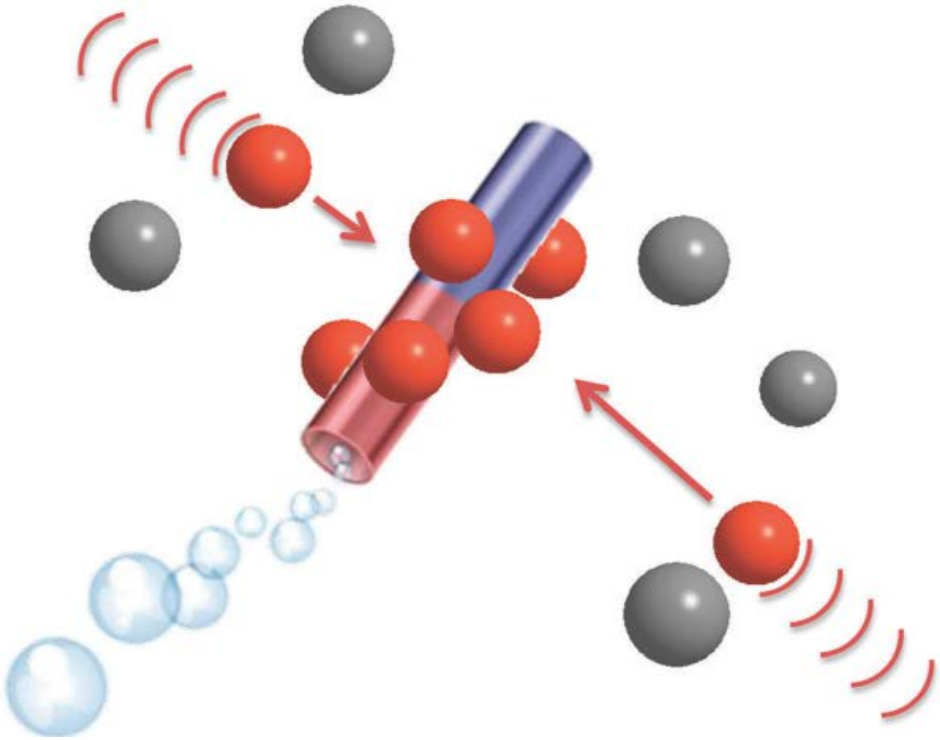

Figure 4-6 Self-propelled microtubular motors with a permanent magnetic moment attract paramagnetic particles (brown, dynabeads) and deliver them, not affecting the diamagnetic (grey, SiO_2) ones.

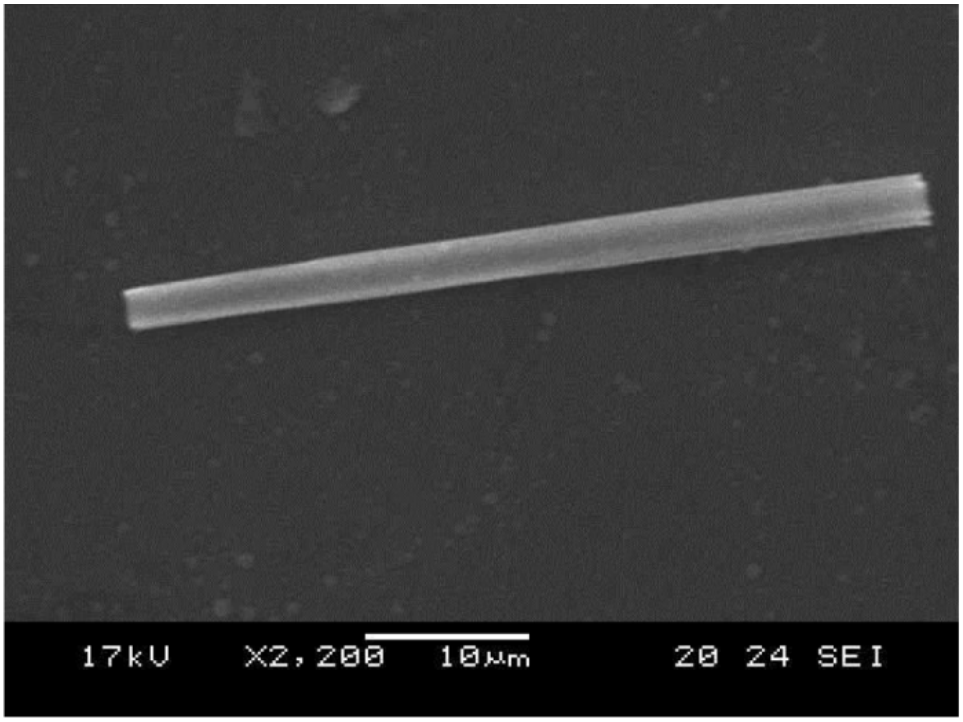

Figure 4-7. Scanning electron micrograph of microtubular motors. Scale bar 10μm.

Experimental Procedures

The microtubular motors (diameter of 5 μm and length of 50 μm, refer to Figure -7 for SEM characterization) were fabricated through a same route as described in Section 4.2. The motion studies of the micromotors with the beads in the running suspension. A concentration of 6 wt % of hydrogen peroxide fuel was used at a constant concentration of SDS (1 wt %) as surfactant. The suspensions of M-270 Dynabeads and the silica beads were diluted with ultrapure water. The running recipe consisted of 5 μL of micromotor suspension, a final concentration of 1 wt % of SDS, 6 wt % of hydrogen peroxide, as well as the pre-diluted bead suspension (1 μL). This running liquid was gently placed on a cover slip freshly cleaned with N_2 gas. The magnetic field was applied by putting a permanent neodymium magnet at about one centimeter away from the running liquid.

Results and Discussion

After being exposed to an external magnetic field with an intensity of ~270 mT for a few seconds, the Fe-incorporated tubes become magnetized. Such ‘‘micromagnets’’ are able to responds to changes in the external magnetic field by realigning its tubular body. When such microtubes are put into a running liquid with H_2O_2, the decomposition of the fuel molecules provides a power source for the tubes to run. The magnetized micromotors running in the hydrogen peroxide containing liquid can attract and catch the paramagnetic microscale particles. Figure 4-8A shows the motion of a micromotor that is not magnetized in a liquid with paramagnetic beads of 2.7 micrometers diameter. These micromotors won’t have any interaction with the paramagnetic beads and they were found to run at a mean speed of 130 μm/s. When such micromotors are exposed to a magnetic field of neodymium for 10 s, they became magnetized and were able to attract

and carry a large volume (>30 beads) of paramagnetic beads to its surface (Figure 4-8B). Dynal paramagnetic beads with a streptavidin functionalized surface were utilized in this study. The surface of such beads can be modified with many different types of biological molecules, which offers a great potential for future applications of the magnetized micromotors. Moreover, an on-the-fly paramagnetic bead capture is also shown without the presence of an external magnet as the micromotor works as a permanent magnet.

The ordered ‘‘chain’’ structures of paramagnetic beads seen in Figure 4-8B are remnant structures after placing of an external magnet near the running liquid to magnetize the micromotors. Figure 4-8 shows the experiments carried out without the presence of external magnet. It was noted that self-electrophoretically driven nanomotors could also pick up and transport the iron oxide containing payloads. However, such pick-up and transport of payloads were possible only with the constant presence of an external magnet, which is quite different from the behavior of the micromotors described here.

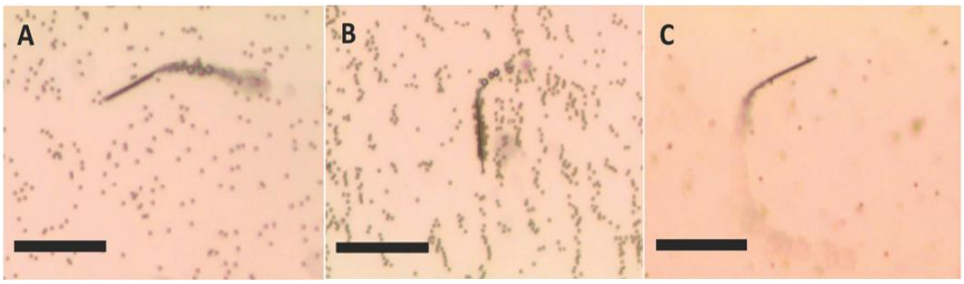

Figure 4-8 Motion of (A) not magnetized and (B) magnetized micromotors in a running liquid with the presence of paramagnetic beads. (C) On-the-fly catching of paramagnetic beads by magnetized micromotors. Scale bar of 50 μm. Conditions: 6% hydrogen peroxide, 1% SDS, beads concentration approximates to 3×10^{5} mL^{-1}.

The capability to selectively catch the paramagnetic beads from a pool with diamagnetic beads was also illustrated for the magnetized micromotors. Figure 4-9 illustrates the motion of self-running magnetized micromotors in a mixture of paramagnetic beads and diamagnetic SiO_2 beads. The magnetized micromotors were able to selectively pick up the paramagnetic beads while not affecting the diamagnetic beads at the same time.

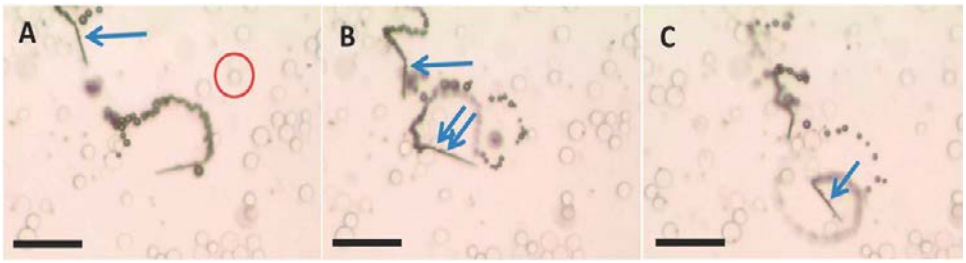

Figure 4-9 Magnetized micromotors can selectively pick up of paramagnetic beads (see arrow, dark spots: dynabeads of 2.7 µm in diameter) while not catching the diamagnetic beads (see one example as highlighted in the red circle, diamagnetic with maximum diameter of 20 µm). A, B and C represent time 0, 2 and 4 s of time frame. Scale bar of 50 µm. Conditions: 6% hydrogen peroxide, 1% SDS, beads concentration approximates to 3×10^4 mL^{-1} for the silica diamagnetic beads and 1×10^4 mL^{-1} dynabeads.

Control experiments (Figure 4-10) using not magnetized micromotors indicated that such micromotors were not able to distinguish between the paramagnetic and diamagnetic beads and run through their dispersion without any sign of magnetic interactions.

Figure 4-10 Not magnetized micromotors are not able to pick up the paramagnetic beads (dark spots) from a mixture with the paramagnetic beads. The motor runs through the

beads mixture without catching any of the beads. A, B and C represent time 0, 3 and 5 s of time frame. Scale bar of 50 μm. Conditions: 6% hydrogen peroxide, 1% SDS, beads concentration approximates to 3×10^4 mL^{-1} for the silica beads and 1×10^4 mL^{-1} dynabeads.

4.5 References

(1) Loget, G.; Kuhn, A.: Propulsion of Microobjects by Dynamic Bipolar Self-Regeneration. *J. Am. Chem. Soc.* **2010**, *132*, 15918-15919.

(2) Sentic, M.; Loget, G.; Manojlovic, D.; Kuhn, A.; Sojic, N.: Light-Emitting Electrochemical "Swimmers". *Angew. Chem. Int. Ed.* **2012**, *51*, 11284-11288.

(3) Loget, G.; Kuhn, A.: Bipolar electrochemistry for cargo-lifting in fluid channels. *Lab Chip* **2012**, *12*, 1967-71.

(4) Loget, G.; Zigah, D.; Bouffier, L.; Sojic, N.; Kuhn, A.: Bipolar Electrochemistry: From Materials Science to Motion and Beyond. *Acc. Chem. Res.* **2013**, *46*, 2513-2523.

(5) Loget, G.; Kuhn, A.: Electric field-induced chemical locomotion of conducting objects. *Nat. Commun.* **2011**, *2*, 535.

(6) Tottori, S.; Zhang, L.; Qiu, F.; Krawczyk, K. K.; Franco-Obregón, A.; Nelson, B. J.: Magnetic Helical Micromachines: Fabrication, Controlled Swimming, and Cargo Transport. *Adv. Mater.* **2012**, *24*, 811-816.

(7) Zhang, L.; Petit, T.; Peyer, K. E.; Nelson, B. J.: Targeted cargo delivery using a rotating nickel nanowire. *Nanomedicine* **2012**, *8*, 1074-80.

(8) Peyer, K. E.; Zhang, L.; Nelson, B. J.: Bio-inspired magnetic swimming microrobots for biomedical applications. *Nanoscale* **2013**, *5*, 1259-1272.

(9) Kline, T. R.; Paxton, W. F.; Mallouk, T. E.; Sen, A.: Catalytic Nanomotors: Remote-Controlled Autonomous Movement of Striped Metallic Nanorods. *Angew. Chem.* **2005**, *117*, 754-756.

(10) Sundararajan, S.; Lammert, P. E.; Zudans, A. W.; Crespi, V. H.; Sen, A.: Catalytic Motors for Transport of Colloidal Cargo. *Nano lett.* **2008**, *8*, 1271-1276.

(11) Sundararajan, S.; Sengupta, S.; Ibele, M. E.; Sen, A.: Drop-Off of Colloidal Cargo Transported by Catalytic Pt–Au Nanomotors via Photochemical Stimuli. *Small* **2010**, *6*, 1479-1482.

(12) Solovev, A. A.; Sanchez, S.; Pumera, M.; Mei, Y. F.; Schmidt, O. G.: Magnetic Control of Tubular Catalytic Microbots for the Transport, Assembly, and Delivery of Micro-objects. *Adv. Func. Mater.* **2010**, *20*, 2430-2435.

(13) Sanchez, S.; Solovev, A. A.; Schulze, S.; Schmidt, O. G.: Controlled manipulation of multiple cells using catalytic microbots. *Chem. Commun.* **2011**, *47*, 698-700.

(14) Sanchez, S.; Solovev, A. A.; Harazim, S. M.; Schmidt, O. G.: Microbots swimming in the flowing streams of microfluidic channels. *J. Am. Chem. Soc.* **2011**, *133*, 701-3.

(15) Solovev, A. A.; Xi, W.; Gracias, D. H.; Harazim, S. M.; Deneke, C.; Sanchez, S.; Schmidt, O. G.: Self-propelled nanotools. *ACS Nano* **2012**, *6*, 1751-6.

(16) Mei, Y.; Solovev, A. A.; Sanchez, S.; Schmidt, O. G.: Rolled-up nanotech on polymers: from basic perception to self-propelled catalytic microengines. *Chem. Soc. Rev.* **2011**, *40*, 2109-2119.

(17) Gao, W.; Kagan, D.; Pak, O. S.; Clawson, C.; Campuzano, S.; Chuluun-Erdene, E.; Shipton, E.; Fullerton, E. E.; Zhang, L.; Lauga, E.; Wang, J.: Cargo-Towing Fuel-Free Magnetic Nanoswimmers for Targeted Drug Delivery. *Small* **2012**, *8*, 460-467.

(18) Garcia-Gradilla, V.; Orozco, J.; Sattayasamitsathit, S.; Soto, F.; Kuralay, F.; Pourazary, A.; Katzenberg, A.; Gao, W.; Shen, Y.; Wang, J.: Functionalized Ultrasound-Propelled Magnetically Guided Nanomotors: Toward Practical Biomedical Applications. *ACS Nano* **2013**, *7*, 9232-9240.

(19) Gao, W.; Sattayasamitsathit, S.; Manesh, K. M.; Weihs, D.; Wang, J.: Magnetically powered flexible metal nanowire motors. *J. Am. Chem. Soc.* **2010**, *132*, 14403-5.

(20) Xi, W.; Solovev, A. A.; Ananth, A. N.; Gracias, D. H.; Sanchez, S.; Schmidt, O. G.: Rolled-up magnetic microdrillers: towards remotely controlled minimally invasive surgery. *Nanoscale* **2013**, *5*, 1294-1297.

(21) Baraban, L.; Streubel, R.; Makarov, D.; Han, L.; Karnaushenko, D.; Schmidt, O. G.; Cuniberti, G.: Fuel-free locomotion of Janus motors: magnetically induced thermophoresis. *ACS Nano* **2013**, *7*, 1360-7.

(22) Solovev, A. A.; Mei, Y.; Bermudez Urena, E.; Huang, G.; Schmidt, O. G.: Catalytic microtubular jet engines self-propelled by accumulated gas bubbles. *Small* **2009**, *5*, 1688-92.

(23) Blakemore, R.: Magnetotactic bacteria. *Science* **1975**, *190*, 377-9.

(24) Simmons, S. L.; Bazylinski, D. A.; Edwards, K. J.: South-seeking magnetotactic bacteria in the Northern Hemisphere. *Science* **2006**, *311*, 371-4.

(25) Ibele, M.; Mallouk, T. E.; Sen, A.: Schooling behavior of light-powered autonomous micromotors in water. *Angew. Chem. Int. Ed.* **2009**, *48*, 3308-12.

(26) Hong, Y.; Blackman, N. M.; Kopp, N. D.; Sen, A.; Velegol, D.: Chemotaxis of nonbiological colloidal rods. *Phys. Rev. Lett.* **2007**, *99*, 178103.

(27) Zhao, G.; Seah, T. H.; Pumera, M.: External-energy-independent polymer capsule motors and their cooperative behaviors. *Chemistry* **2011**, *17*, 12020-6.

(28) Kline, T. R.; Paxton, W. F.; Mallouk, T. E.; Sen, A.: Catalytic nanomotors: remote-controlled autonomous movement of striped metallic nanorods. *Angew. Chem. Int. Ed.* **2005**, *44*, 744-6.

(29) Dhar, P.; Cao, Y.; Kline, T.; Pal, P.; Swayne, C.; Fischer, T. M.; Miller, B.; Mallouk, T. E.; Sen, A.; Johansen, T. H.: Autonomously Moving Local Nanoprobes in Heterogeneous Magnetic Fields. *J. Phys. Chem. C.* **2007**, *111*, 3607-3613.

(30) Banholzer, M. J.; Qin, L.; Millstone, J. E.; Osberg, K. D.; Mirkin, C. A.: On-wire lithography: synthesis, encoding and biological applications. *Nat. Protocols.* **2009**, *4*, 838-848.

(31) Baraban, L.; Makarov, D.; Streubel, R.; Monch, I.; Grimm, D.; Sanchez, S.; Schmidt, O. G.: Catalytic Janus motors on microfluidic chip: deterministic motion for targeted cargo delivery. *ACS Nano* **2012**, *6*, 3383-9.

(32) Zeeshan, M. A.; Grisch, R.; Pellicer, E.; Sivaraman, K. M.; Peyer, K. E.; Sort, J.; Özkale, B.; Sakar, M. S.; Nelson, B. J.; Pané, S.: Hybrid Helical Magnetic Microrobots Obtained by 3D Template-Assisted Electrodeposition. *Small* **2014**, *10*, 1284-1288.

(33) Li, J.; Zhang, J.; Gao, W.; Huang, G.; Di, Z.; Liu, R.; Wang, J.; Mei, Y.: Dry-Released Nanotubes and Nanoengines by Particle-Assisted Rolling. *Adv. Mater.* **2013**, *25*, 3715-3721.

(34) Orozco, J.; Campuzano, S.; Kagan, D.; Zhou, M.; Gao, W.; Wang, J.: Dynamic Isolation and Unloading of Target Proteins by Aptamer-Modified Microtransporters. *Anal. Chem.* **2011**, *83*, 7962-7969.

(35) Balasubramanian, S.; Kagan, D.; Jack Hu, C.-M.; Campuzano, S.; Lobo-Castañon, M. J.; Lim, N.; Kang, D. Y.; Zimmerman, M.; Zhang, L.; Wang, J.: Micromachine-Enabled Capture and Isolation of Cancer Cells in Complex Media. *Angew. Chem. Int. Ed.* **2011**, *50*, 4161-4164.

(36) Kuralay, F.; Sattayasamitsathit, S.; Gao, W.; Uygun, A.; Katzenberg, A.; Wang, J.: Self-propelled carbohydrate-sensitive microtransporters with built-in boronic acid recognition for isolating sugars and cells. *J. Am. Chem. Soc.* **2012**, *134*, 15217-20.

CHAPTER FIVE: MOTION OF NANO- AND MICROMOTORS IN REAL ENVIORNMENTS

The work discussed in this chapter resulted in the following publications:

Zhao, G.; Wang, H.; Khezri, B., Sanchez, S.; Schmidt, O. G.; Webster, R. D.; Pumera, M. Corrosion of self-propelled catalytic microengines. *Chem. Commun.*, **2013,** *49*, 9125-9127.

Zhao, G.; Khezri, B., Webster, R. D.; Pumera, M. Influence of real-world environments on the motion of catalytic bubble-propelled micromotors. *Lab Chip* **2013,** *13*, 2937-2941.

Zhao, G.; Viehrig, M.; Pumera, M., Challenges of the movement of catalytic micromotors in blood. *Lab Chip* **2013,** *13*, 1930-1936.

Zhao, G.; Sanchez, S.; Schmidt, O. G.; Pumera, M., Poisoning of bubble propelled catalytic micromotors: the chemical environment matters. *Nanoscale* **2013,** *5*, 2909-2914.

Zhao, G.; Nguyen, N. T.; Pumera, M. Reynolds numbers influence the directionality of self-propelled macrojet engines in the 10^{-4} regime. *Nanoscale* **2013,** *5*, 7277-7283.

5.1 Introduction

The design and development of small motors have received increasing attention in recent years, and one of the most outstanding nano-/micromotors, the catalytic tubular motors, have demonstrated strong power thrusts as well as desirable motion manipulations.[1-11] Also, such catalytic nano-/micromotors have been shown to perform a wide range of tasks, including environmental remediation,[12-14] drug delivery,[15,16] manipulation of cells,[17,18] or microsurgeries.[19] However, the presence of H_2O_2 is a must for the motion of these small motors and it would hamper any working of the motors in real life environments, especially for biological fluids as hydrogen peroxide is very toxic even at small amount. Significant amounts of efforts were devoted to replace H_2O_2 with other chemical fuels, especially with blood and biological fluid abundant glucose, but little success has been made to date. In our research work, instead of seeking alternative fuels, it is the hope to pose another important issue on the motion of catalytic small motors in real-world environments. We would like to address the concern that whether the catalytic small motors are able to move in the real environments, what is their capability to move, as well as how they are affected by the surrounding medium that they are running inside. This is by no means trivial, because it could possibly turn out that even with the ideal biocompatible fuel readily available, such small motors might not be capable of running in some real-world environments due to the advert effects from the medium.

In this chapter, I would like to present the work we have done to deploy the catalytic microtubular motors in running suspensions with various recipes to mimic the real environments. Different kinds of medium of interest were selected and it is our aim to study the environment effects on the motion, and thus the performance, of the micromotors.

5.2 Influence of Reynolds Number on Motion of Micromotors

Since the propulsive force generated by the catalytic micromotors is sufficiently high to transport heavy payloads, it can be foreseen that such motors can offer potential breakthroughs for eventually real applications. The running of such micromotors can be classified into 3 different types: (i) linear or quasi-linear, by this definition, the micromotors move along a curved trajectory with big radius, typically with a radius of one order magnitude larger than the length of the micromotors; (ii) circular/rotational, where the radius of the circular trajectory is in the same order of magnitude as the length of the motors; and (iii) screw like, where the self-running motors show a movement in the way that the back end is doing circular motion while the tip or front end of the micromotor is running forward along the axis radial to the plane of circular motion, leading to a conical-shaped or screw like trajectory. All the three categories of movement are commonly seen and in this section, cases (ii) and (iii) are collectively termed as "circular motion" to carry out the motion investigation. As such, the motion styles of the motors could be grouped into linear or circular motions in the following text. Figure 5-1 shows an illustration.

In Chapter 2, it is shown that the motion styles of millimeter-sized self-propelled capsule motors moving at an intermediate Re regime (Reynolds number in the range of 1– 100) can be significantly affected by viscosity of the fluid and speed of the motors.[20] Sanchez *et al* looked into the influence of velocity on the motion styles of bubble propelled micromotors with lengths of 50 μm.[21] In their work, it was found that when the micromotors showed a faster motion, the directionality of the micromotors altered from

linear-fashion to a circular path. Such change in directionality possesses major implications for the usage of micromotors, because even when they are running faster, eventually it might not mean that a longer path will be covered as they can circulate around. Such issue is intriguing since Re of such micromotors is at a much smaller regime, typically in the 10^{-4} or 10^{-5} order of magnitude.

In this section, I would like to show our effort on the extension on the study done by Sanchez *et al* to more generalized scenarios, in which not only the fluid viscosity but also the speed of micromotors were altered to vary the Reynolds number. Such parameters that define the Re are carefully investigated, and their influence on the Re can be seen in the following equation:

$$\mathrm{Re} = \frac{\rho v L}{\mu}$$

where ρ is density of the fluid, v is the mean speed of the motors, L is the characteristic linear dimension of the motors and μ is the dynamic viscosity of the fluid.[22]

In our study, it was determined that at a higher viscosity (lower Re), the motors run more likely in a linear fashion while at a lower viscosity (larger Re), the motors tend to run in a circular fashion. This is important for the movement of micromotors in real world environments (blood/oil), where the viscosity of the running media can be significantly higher than that of the aqueous fluid.

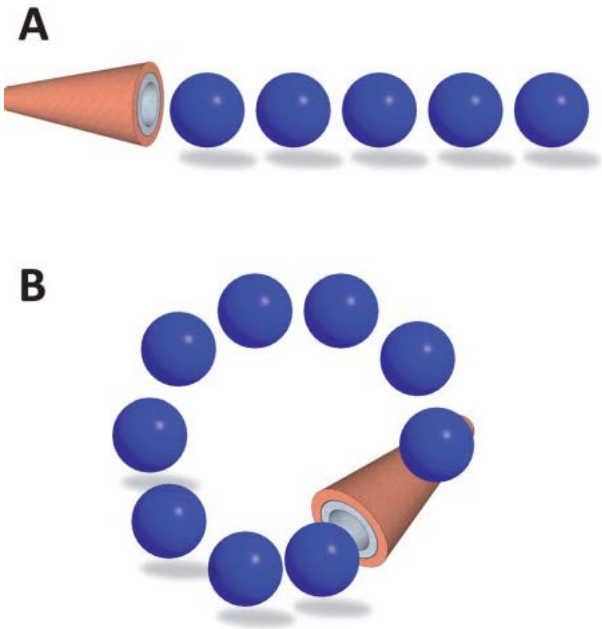

Figure 5-1 Motion directionality of micromotors is affected by Reynolds numbers. (A) Linear movement of micromotors; (B) Circular movement of micromotors.

Experimental Procedures

In this study, micromotors fabricated through the template electrodeposition route were used, whose fabrication process can be found in details in Section 3.3.1. The microtubular motors were running in the aqueous fluids of varying recipes. In order to investigate the motion directionality by changing the concentration of H_2O_2, the liquid containing micromotors (5 µL), SDS (1 wt%) and H_2O_2 of concentrations from 1 wt % to 3 wt % were mixed to form the aqueous running liquids; in order to investigate the motion directionality by changing the concentration of glycerol, the liquid containing micromotors (5 µL), SDS (1 wt %), H_2O_2 (fixed concentration of 6 wt %) and glycerol were mixed to form the aqueous running liquids with different concentrations of glycerol. A 5 µL drop of the running liquid was placed gently on a cover glass freshly blew with N_2 gas. The motion of the micromotors was then studied under the microscope (Nikon Eclipse TE 2000E). Videos and images were analyzed with Nikon NIS-Elements software,

and five videos were tracked to get the average speed of micromotors. The linear or circular trajectories were seen under microscope, and a number of 50 (n = 50) micromotors were counted to get the ratio of motors in terms of linear/circular trajectories.

The morphology and structure of the microtubular motors were characterized. Their average length is roughly 7 micrometers, and the tip diameter is averaged to be 1.5 micrometers while the end average diameter is 2 micrometers.

Results and Discussion

In order to study the influence of motion speed on directionality, the velocity was altered by varying the amount of hydrogen peroxide in the running liquid, from 1 wt % to 3 wt % in 0.5 wt % steps. As shown in Figure 5-2, the mean velocity became higher, from 220 to 650 μm/s as the fuel amount was made higher from 1% to 3% (number of experiments, n = 5). According to Equation 1, the Reynolds numbers also increased from 5×10^{-4} to 14×10^{-4}.

The directionality was seen to be significantly affected by the velocity of the motors. The data shows that around 55% of the motors were running in a linear fashion with 1% of hydrogen peroxide, and the ration was much less that only 7% of the microtubular run with a linear trajectory when 3% of hydrogen peroxide is present in the running liquid. Showcases for micromotors running in a linear fashion at 1 wt% of hydrogen peroxide and in a circular fashion at 3 wt% of hydrogen peroxide are shown in Figure 5-3.

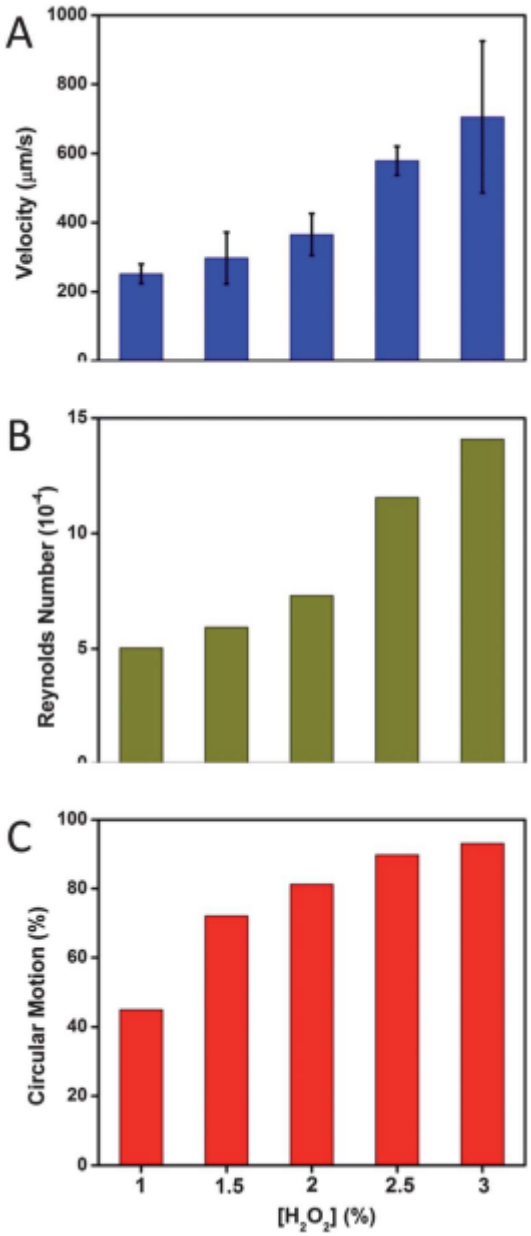

Figure 5-2 The motion styles of the microtubular motors can be dependent on how fast the motors are running. (A) With higher amount of hydrogen peroxide in the running liquid, higher speeds can be seen for the motors. (B) The Reynolds number of the motors is also higher as calculated from Equation 1. (C) The ratio of motors running in a circular trajectory was also found to be higher with higher concentrations of hydrogen peroxide present.

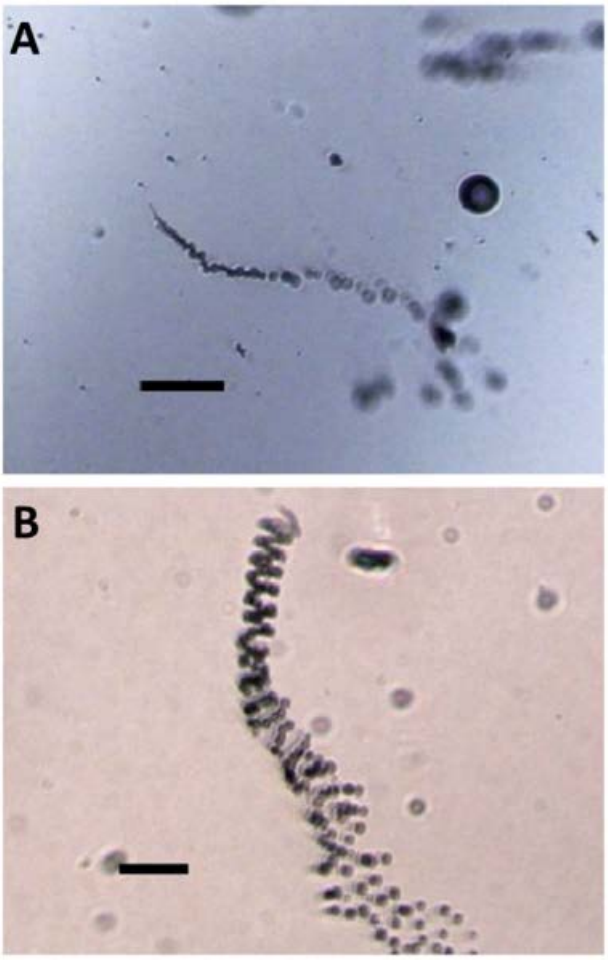

Figure 5-3 Showcases of the impact of amount of hydrogen peroxide on motion style of the micromotors. (A) Quasi-linear motion was seen at 1% of H_2O_2 and (B) A circular trajectory at 3% of H_2O_2. Scale bar of 50 µm.

Next, the impact of fluid viscosity on the trajectory of the micromotors was investigated. The viscosity of the running liquid was made higher from 1.0 mPa s for H_2O to 14.3 mPa s for 64% of glycerol by mixing glycerol with H_2O.[23] The amount of H_2O_2 was maintained at a fixed concentration (6 wt %) in the entire study. As shown in Figure 5-4, with higher amount of glycerol in the running liquid from 16% to 64%, the motion of the micromotors was slower, with mean speeds dropped from 240 µm/s to 31 µm/s. It was also noteworthy to mention that at 0% of glycerol, the velocity of the motors was not able

to be tracked as all the micromotors showed an extremely high speed circular motion and it inhibited the measuring of the speed.

With higher amount of glycerol in the running liquid, the Re was found lower from 3.16×10^{-4} to 0.05×10^{-4}.The motion style of the micromotors was significantly influenced by enhancing the viscosity and reducing the Re of the system. At 0% glycerol, only circular motions were seen (n = 50). When the amount of glycerol was made higher to 64%, the viscosity was also higher, and the ratio of motors running in a linear fashion was seen to be higher and became 55% in total. Examples of a micromotor running in a circular fashion at 0% of glycerol and in a linear fashion at 64% of glycerol can be seen in Figure5-5.

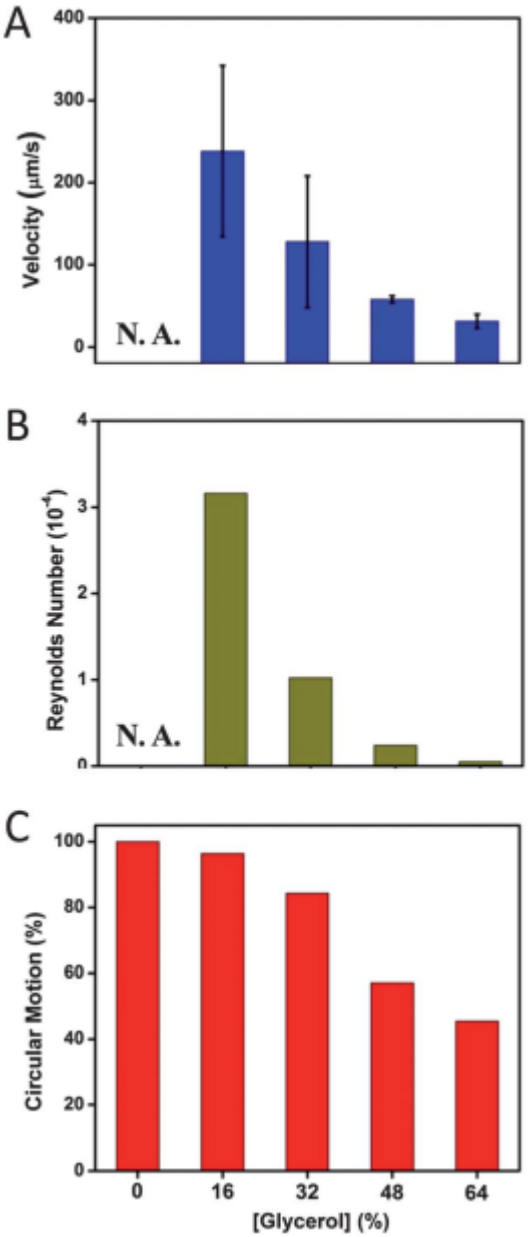

Figure 5-4 Motion styles have to do with the fluid viscosity of the running liquid, which is controlled upon varying the amount of glycerol in the liquid. (A) Reduced motion speed was observed as more glycerol was mixed in the liquid. (B) Reynolds number of the system was also found lower (C) A less percentage of motors running with a circular trajectory can be seen for running liquids containing more glycerol. N.A. means that the velocity couldn't be measured due to the fast circular motion of the micromotors. The running liquids contain 6% of hydrogen peroxide and 1% of SDS.

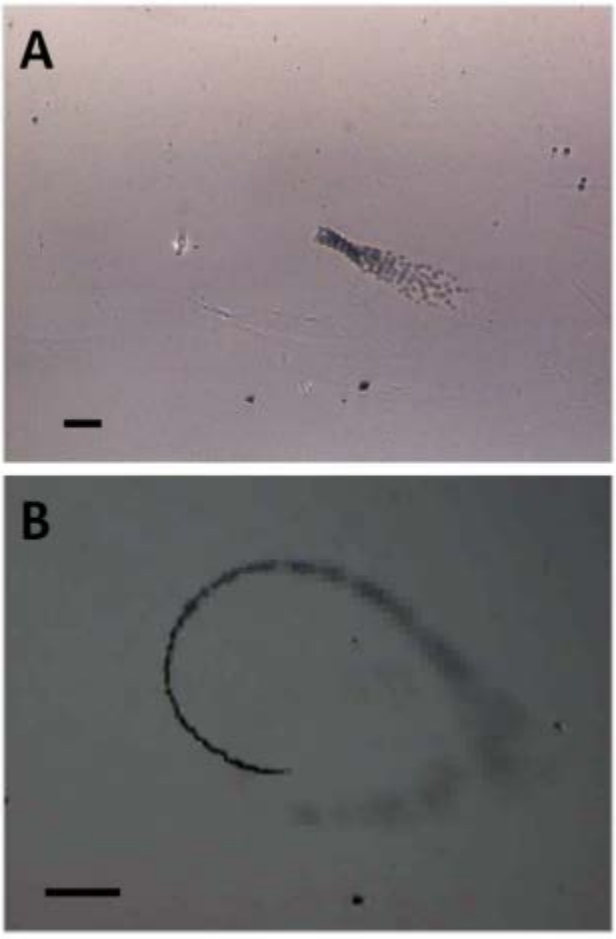

Figure 5-5 Showcases of impact of fluid viscosity on motion styles of micromotors. (A) Circular motion of micromotors in running liquid contains no glycerol; (B) Quasi-linear trajectory of the motors running in the liquid containing 64 wt% of glycrol. Scale bar: 50

μm. The amounts of hydrogen peroxide and SDS were fixed to be 6 wt% and 1 wt%, respectively.

5.3 Corrosion of Micromotors

In this section, I will illustrate that the rolled-up tubular micromotos and electroplated micromotors are undergoing a strong corrosion effect in the running suspension, as well as in the suspension with only SDS surfactant, or even in the suspension with only water. The metal components are dissolved and released into the liquid medium, and this effect was observed for Pt, Cu, Fe, Ti and Au elements. The observed corrosion behavior of such micromotors has strong implications for applications of the motors in real environments, because the abovementioned ions are toxic. Moreover, lifetime of the motors are shortened due to the corrosion of the tube body, which is different from the notion that such motors can run in the suspension forever as long as hydrogen peroxide is available in the liquid.

As H_2O_2 molecules are highly oxidative, they are utilized as the fuel in most of the reported small motor systems, including the millimeter scale platelets,[24] or in nano-/micromotors.[25] It has been reported that molecules of H_2O_2 facilitate the corrosion process of metals or their alloys.[26] Moreover, not only restricted to hydrogen peroxide, presence of other molecules, even H_2O can deliver a highly corrosive media for a few metallic components. The galvanic corrosion of contacting different metals happens at a high speed in H_2O, resulting in a significant challenge to protect the metals in water, especially in the shipbuilding or water pipe industries. When water is present, the metals in contact possess different electrochemical potentials, which are the key reason for the fast corrosion of such metals as in the process; they work as anode/cathode. A current will

be generated with the presence of aqueous liquid and flow between different metals. A dissolution or corrosion of the anode metal is expected due to this current flow.

In our study, as is the case in most of the nano-/micromotor studies, the small motors consist of two or more different metals. To make things worse, these motors are deployed in aqueous medium and hydrogen peroxide is the fuel in most case for their propulsion. Thus, it is of high interest for us to look into the extent of corrosion, if happening, of the nano-/micromotors. The consequence due to the corrosion would be significant if they are to work in real applications, as the corroded nano-/micromotors may lose their functionality or generate toxic heavy ions into the system.

Experimental Procedures

In order to investigate the corrosion of the micromotors, 2 different kinds of bubble-propelled motors were used. The first kind of motors are the rolled-up micromotors fabricated through the lithography route, containing the elements of Pt, Cr, Fe and Ti, and they are the same tubes described in Section 4.2. The second kind of motors was made through a template electroplating process, containing an inner platinum layer and an outside copper layer. Figure 5-6 and Figure 5-7 present the SEM and EDX characterizations of the first and second kinds of tubes, respectively.

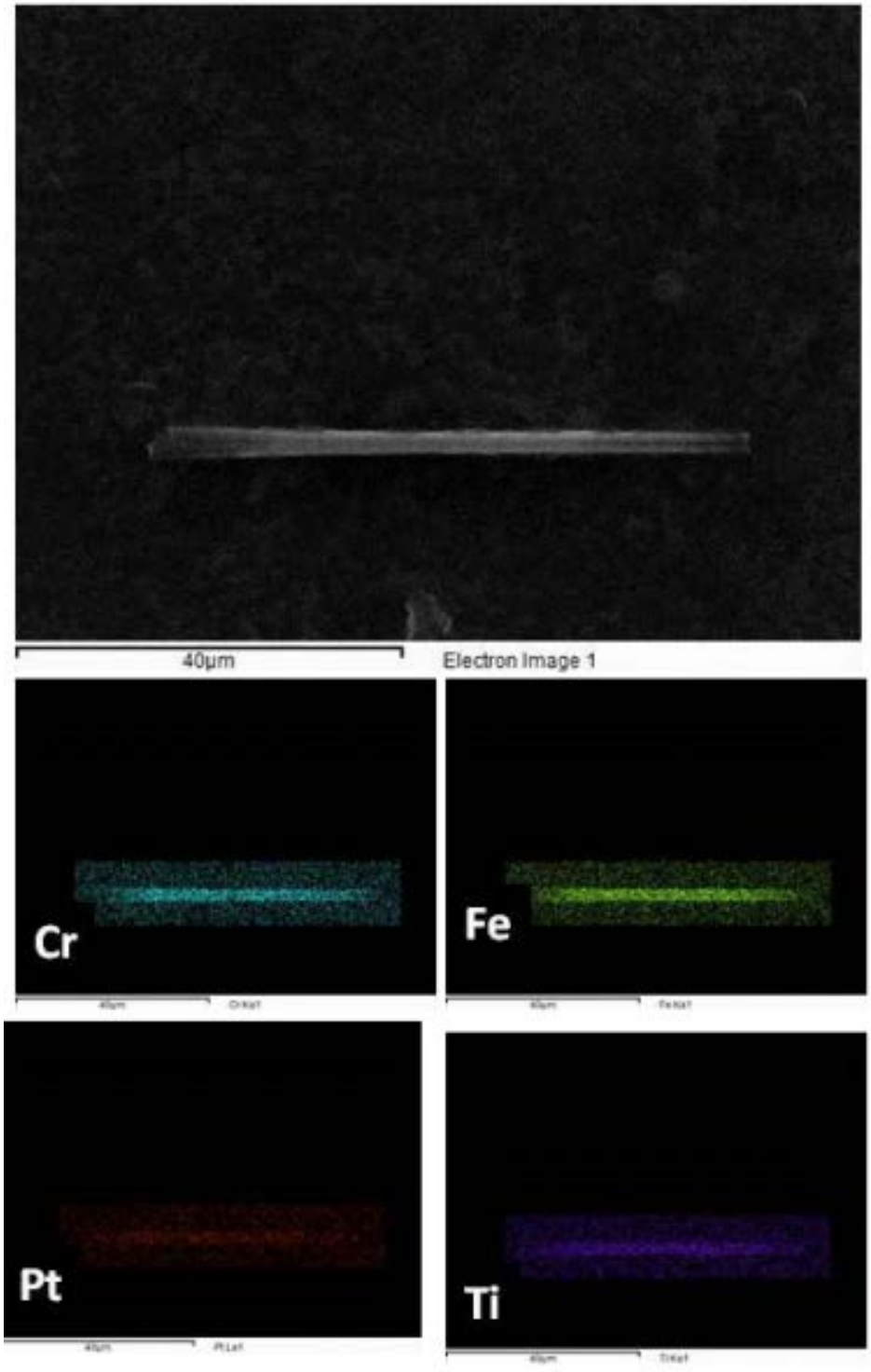

Figure 5-6 SEM/EDX analysis of roll-up technology fabricated micromotors. Scale bars of 40 µm.

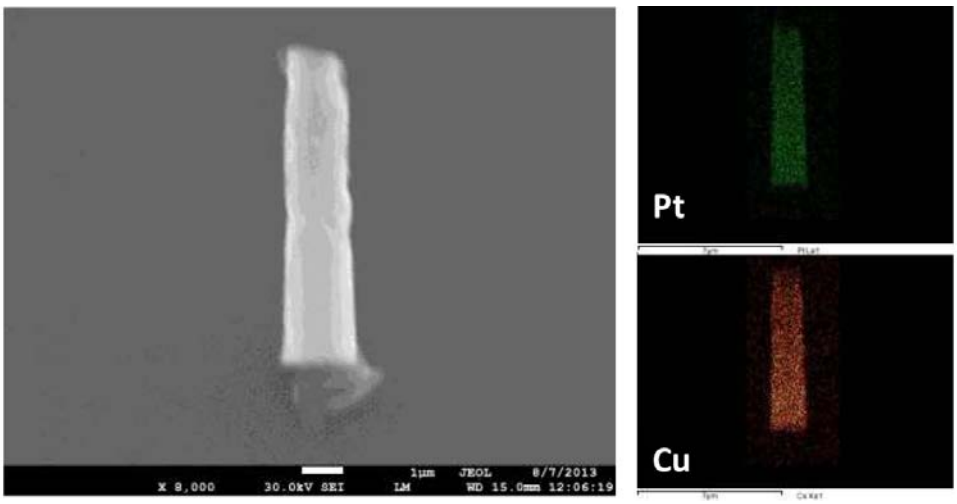

Figure 5-7 SEM/EDX analysis of Cu/Pt electrodeposited micromotors.

These micromotors were mixed in the liquids in which they have been illustrated to run, such as 7.76 wt % hydrogen peroxide and 1.15 wt % SDS for 168 hours. After that, the liquid was filtered through a nanoporous AAO and the elemental composition of the filtrate was analyzed *via* an ultra-trace analysis involving ion conductive plasma-mass spectrometry analysis (ICP-MS). Corrosion study in liquid mixture with only SDS, or only H_2O was also carried out, as shown in Figure 5-8 and 5-9. Moreover, control studies on the ICP-MS measurement of metallic elements in the blank liquids which were not exposed to micromotors were also done in the following mixtures: (i) 7.76 wt % hydrogen peroxide and 1.15 wt % SDS; (ii) 1.15 wt % SDS only and (iii) H_2O only.

Results and Discussion

For the Pt/Fe/Cr/Ti rolled-up micromotors. (i) When soaked to H_2O for 168 hours, the composition of the filtrate was 3.63 ppb platinum, 6.08 ppb titanium, 0.98 ppb chromium and iron ＜D.L. (detection limit). This corresponds to a corrosion of the micromotors segments, specifically 1.29 % of the platinum, 2.73 % of titanium and 1.04 % of chromium. (ii) When mixed in 1.15 % SDS, the corrosion speed was doubled with 6.41 ppb platinum, 8.3 ppb titanium, 2.54 ppb chromium and 5.10 ppb iron, corresponding to a

corrosion of 2.29 % platinum, 3.72 % titanium, 2.70 % chromium and 1.47 % iron (percentage calculations are based on the concentration of metals in the filtrate with subtracted control experiment of liquid without the presence of micromotors). With the presence of H_2O_2, the corrosion speed accelerated again, leading to 10.99 ppb platinum, 23.97 ppb titanium, 27.56 ppb chromium and a startling amount of 272.57 ppb iron in the filtrate, which corresponds to 3.93 % platinum, 10.76 % titanium, 29.27 % chromium and 78.65 % iron of the original micromotors being corroded. The control experiments were done by the ICP-MS analysis of the elemental composition of the liquids in the absence of micromotors. In H_2O, there was 0.07 ppb platinum while iron, titanium, chromium and copper were under the detection limit (D.L. ≈ 10 ppt);[27] The liquid with 1.15 % SDS was measured to have 0.89 ppb platinum, 5.08 ppb titanium, 0.68 ppm chromium, as well as iron and copper with amounts less than the detection limit. The liquid with 7.76 % hydrogen peroxide and 1.15 % SDS had 3.22 ppb platinum, 5.03 ppb titanium, 12.92 ppb chromium, 52.27 ppb iron and 0.87 ppb copper. The control liquids were found to have much less metallic ions than the corresponding filtrates of corrosion liquids of micromotors. Thus it is evident that significant amounts of the metallic segments of the micromotors were corroded in the liquids.

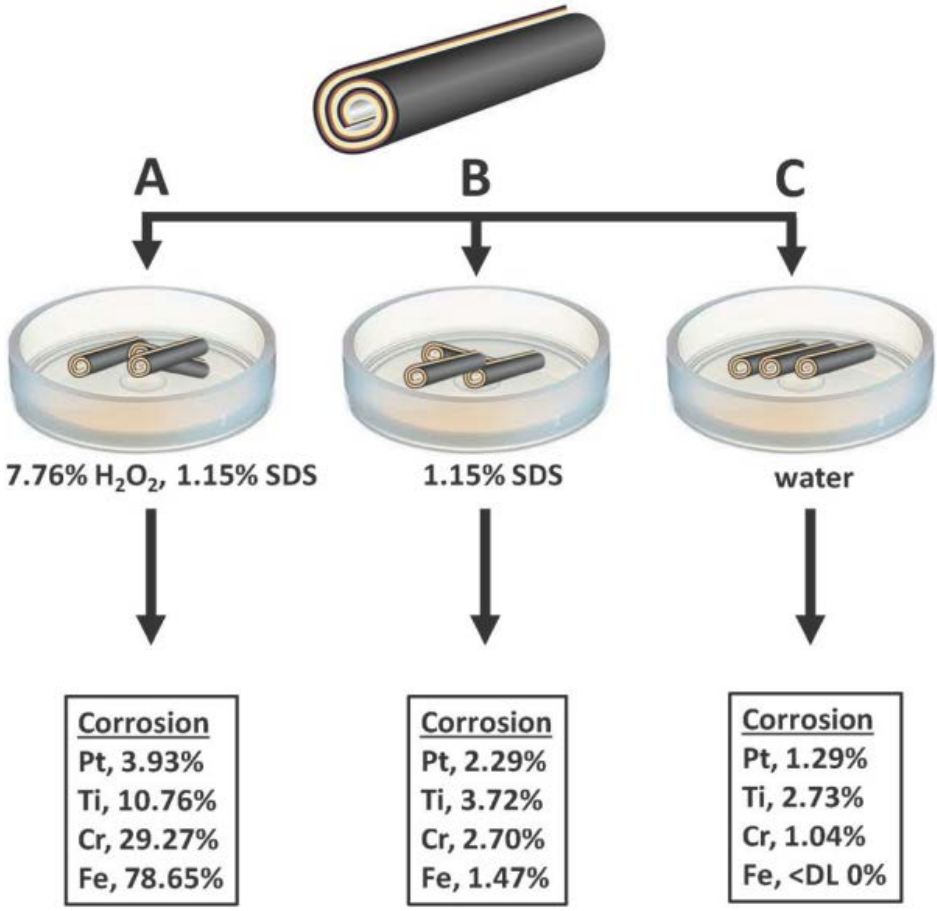

Figure 5-8 Corrosion of self-running rolled up micromotors in different liquids: (A) 7.76 % hydrogen peroxide and 1.15 % SDS; (B) 1.15 % SDS and (C) H_2O. Amounts shown in the columns show the concentrations of the metallic parts of the micromotors corroded during the 168 hours.

For the electroplated micromotors, only platinum and copper elements are present in the body of tubes. The microtubes are conical in shape, and their average length was determined to be ~7 µm and diameters were found to be 1.5 and 2 µm in the tip and tail. In a similar approach to the experiments done for the rolled up micromotors, the electroplated micromotors were put into 3 different liquids, (i) H_2O, (ii) 1.15 % SDS in H_2O and (iii) 7.76 % hydrogen peroxide and 1.15 % of SDS in H_2O for 168 hours. The liquid containing the microtubes were filtered with AAO membrane and analyzed for platinum and copper concentrations. It was measured in the filtrate of micromotors that

had been soaked in H_2O, 18.93 ppb platinum and 646.23 ppb copper were present, corresponding to 0.1 % platinum and 15.96 % copper from the original micromotors (after eliminating the background platinum and copper concentrations). In the filtrate of micromotors soaked in liquids containing SDS, an amount of 62.53 ppb of platinum and 677.76 ppb of copper was determined, corresponding to the corrosion of such elements by 0.32 % for platinum and 16.74% for copper. Moreover, hydrogen peroxide was also shown to facilitate the corrosion of the metallic elements in micromotors; it was determined that 246.52 ppb of platinum and 2194.45 ppb of copper were present in the filtrate of micromotors which were soaked in 7.76 % hydrogen peroxide and 1.15 % of SDS; this corresponds to 1.28 % platinum and 54.21 % copper of the original micromotors being corroded.

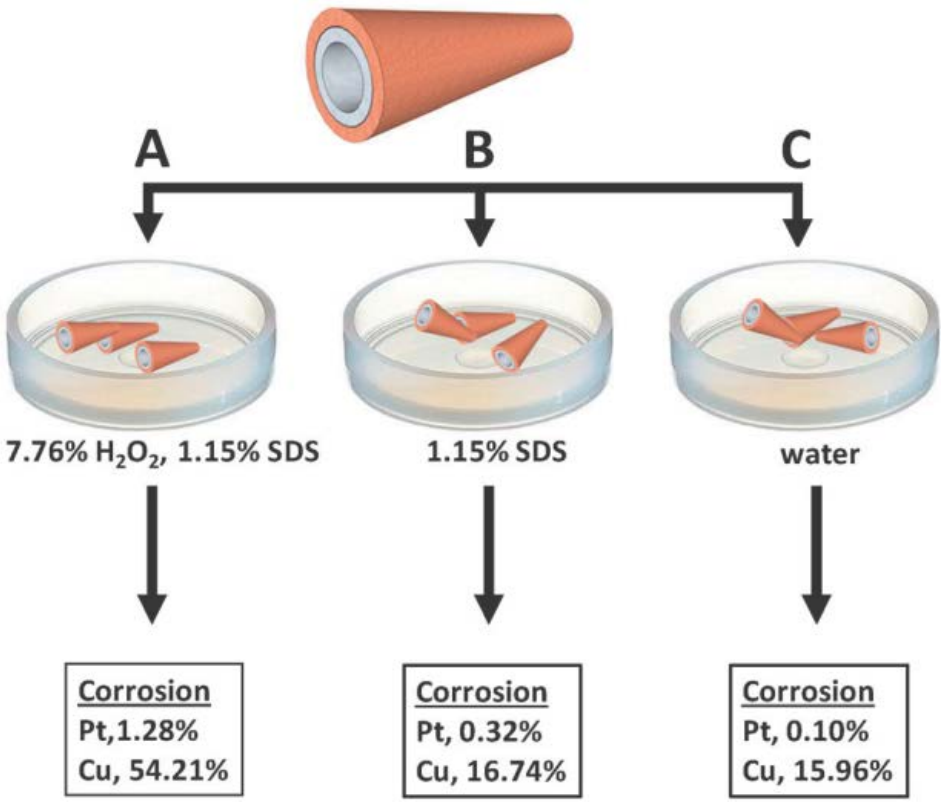

Figure 5-9 Corrosion of self-running electroplated micromotors consist of copper and platinum in different liquids: (A) 7.76 % hydrogen peroxide and 1.15 % SDS; (B) 1.15%

SDS and (C) H_2O only. Amounts shown the columns indicate how much of the micromotors were corroded during the 168 hours.

5.4 Poisoning of Bubble Propelled Catalytic Micromotors

In recent years, the bubble-propelled tubular motors have been extensively studied because of their good performance and ease of operation.[21,28] The mechanism of such motors is simply the asymmetric ejection of O_2 from the tail of the microtubes, and yet it allows the motors to run at very high speeds while performing powerful works like cargo transport,[29] cell-manipulation,[18] biomolecules isolation,[17] cell/tissue penetration[11,19,30] or oil removal.[31] However, the operation of such motors in different environments may show some degree of impact on the motion of the motors. For example, the platinum metal are easily poisoned by the sulphur element when it is working as a catalyst, and the presence of sulphur containing amino acids or peptides is of high amount in blood or cells. Inorganic sulphur containing molecules may also be present in natural water samples. It is our interest to determine the effect of molecules that present in the environment on the platinum catalytic motors.

In this section, I would like to show that at a fixed amount of H_2O_2 (9%), the movement of the micromotors are possible to be significantly affected by molecules in the running liquid. The running of the micromotors is determined by how fast the O_2 bubbles are produced,[32] thus if some chemicals in the liquid can influence the decomposition of H_2O_2, they could also strongly affect the movements of the catalytic small motors. For example, certain organic or biomolecules can quench the platinum-catalyzed disproportionation of hydrogen peroxide. In this section, it is shown that dimethyl sulfoxide (DMSO) can quench the •OH radical from the disproportionation of hydrogen peroxide and thus

reducing the mobility of the catalytic micromtors. Moreover, biological molecules with sulphur-containing moieties can also affect the catalytic reactions by poisoning the platinum surface, and thus such molecules were used to investigate the toxic effect on the motion of catalytic micromotors. As sketched in Figure 5-10, when there is–SH or $–SCH_3$ moiety in the molecules, the movement of the micromotor was hampered in both the velocity and the number of motors that are able to run. It is also found that higher amount would be required for the $–SCH_3$ containing methionine to reduce the movement of the micromotors, suggesting that platinum is much more sensitive to –SH moieties. These findings indicate that organic molecules and biomolecules in the natural or biological liquids are able to significantly reduce the movement of platinum-catalyzed micromotors.

In this section, it is found that some biological molecules and organic chemicals with S-containing moieties are able to strongly reduce the movements of the micromotors. Such reduction in mobility can happen in 2 approaches: (i) quenching of •OH radicals produced by the platinum catalyzed decomposition of H_2O_2, and (ii) the toxic effect of such molecules on the platinum inner surface. Both of these approaches are to be illustrated in the following text, and microtubular motors fabricated in the rolled up process or electroplating process were both used to study the poisoning effects.

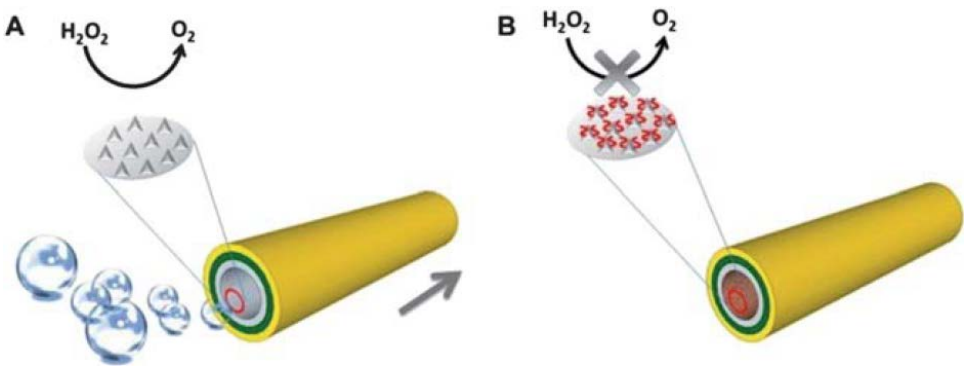

Figure 5-10 Poisoning of platinum micromotors with sulphur-containing molecules. (A) Without the poisoning chemicals, strong reaction of hydrogen peroxide happens at the platinum surface to power the motion of the microtubular motor; (B) With the poisoning molecules in the running liquid, catalyzed disproportionation of hydrogen peroxide was quenched/inhibited to some extent, and less O_2 gas was produced to give a lower or none mobility of the micromtors.

Experimental Procedures

In order to investigate the poisoning effect of molecules on the micromotors, two different kinds of bubble-ejection motors were used. The first kind of motors is the rolled-up micromotors fabricated through the lithography route, and they are the same tubes described in Section 4.2. The second kind of motors is made through a template electroplating process, and they consist of a platinum inner catalytic layer and a copper outside layer. Please refer to Figure 5-6 and Figure 5-7 for the SEM and EDX images of the tubes characterizations of the first and second kinds of tubes, respectively.

To investigate the poisoning effect, micromotors were mixed in the running liquid with fixed SDS amount of 1%, and the concentration of H_2O_2 was set to be 9% for rolled up tubes and 2% for electrodeposited tubes. A mixture of micromotors (5 μL), SDS (1 % final concentration), hydrogen peroxide and various amounts of “poisonous” chemicals were gently placed on a cover slip surface freshly cleaned with N_2 gas. Optical microscope videos and images were obtained with a Nikon Eclipse TE 2000E microscope. Videos (100 fps) and images were processed with Nikon NIS-Elements software. For each of the data points, at least 32 measurements were taken into account.

Results and Discussion

Quenching of O_2 gas production with DMSO

Platinum metal can catalyze the decomposition reaction of H_2O_2 to produce oxygen as product, and a radical process is adapt for such decomposition.[33] In this reaction, the hydroxyl radical •OH is important for the generation of oxygen molecules.[34] Therefore, with the presence of molecules that can quench the radical reaction, (DMSO in this study), the rate of O_2 production is determined by the following equation:[34]

$$\frac{\mathrm{d}[\mathrm{O_2}]}{\mathrm{d}t} = k_{1S}\,[\mathrm{S}][\mathrm{H_2O_2}]\left[1 - \frac{k_D[\mathrm{DMSO}]}{K_{2S}[\mathrm{H_2O_2}] + k_D[\mathrm{DMSO}]}\right]$$

where [S] is the active metal surface, k_D , k_{1S} and k_{2S} are the constants in the reaction processes and [DMSO] and [H_2O_2] are the concentrations of DMSO and H_2O_2 in the running liquid. The production of O_2 is dependent on 3 aspects: the amount of H_2O_2, the concentration of DMSO (or other chemical quenchers for the radical process) as well as the active surface area of the platinum. As the production of oxygen bubbles is based on the radical mechanism, the movement of the micromotors is highly sensitive to chemicals that can quench such radicals. In order to run the micromotors in a chemically complex environment – which is the situation for natural samples, there is a high possibility that such chemical quenchers are present in the samples. Here, DMSO was utilized as it is a well-known quencher for the •OH radicals.[35]

In the running liquid containing 9 wt % of hydrogen peroxide, the impact of DMSO amount on the movement of the micromotors (fabricated via the rolled up process, if not described otherwise) was investigated.[36] Figure 5-11 shows that in the presence of 20 mM of DMSO, 56.25% (n = 32) of the micromotors were not able to run at all and became thoroughly inactivate due to the quenching effect. DMSO can quench the radicals generated in situ, even at a large amount of H_2O_2 (9%, equivalent to a ratio of ~145 hydrogen peroxide molecules for each DMSO molecule). Because of the homogenous

presence in the liquid; DMSO molecules were fluxed into the tube by the micromotors inlet together with the hydrogen peroxide molecules, effectively quenching the radicals as soon as they are generated. No motion could be observed at all when the concentration of DMSO was as high as 80 mM. Besides the less numbers of micromotors that able to show motion, DMSO molecules can also reduce the mobility of the micromotors that were still showing some motion, as illustrated in Figure 5-11B. An obvious decrease in motion speed could be seen with DMSO concentration being as low as 20 mM. The average velocity was reduced from around 180 micrometers per second to 99 micrometers per second. Such reduction in mobility is attributed to the quenching of the •OH radicals which resulted in a less amount of O_2 generated, and thus a weaker thrust to power the motion.

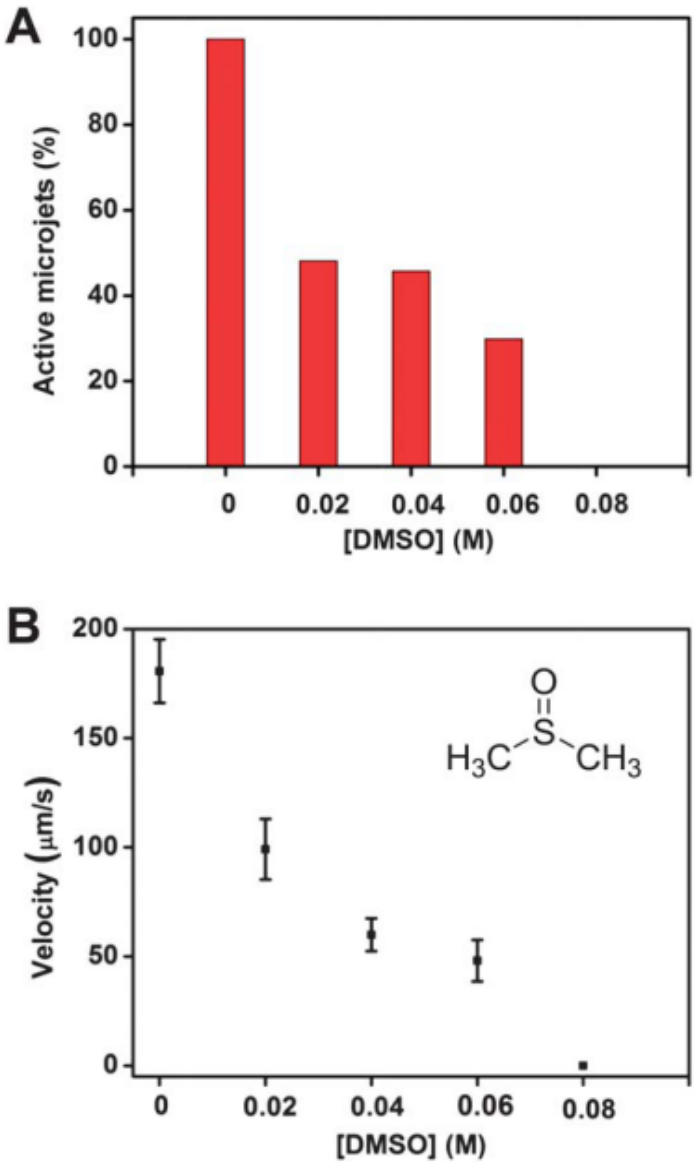

Figure 5-11 DMSO molecules in the running liquid can drastically influence the mobility of micromotors. (A) Impact of the DMSO concentration on the percentage of the micromotors that were able to run. More than 50% of the motors showed no motion at all at 20 mM of DMSO (number of running motors in liquids without DMSO was set as 100%), and not a single microtube was found moving if the concentration was higher to be 80 mM; (B) Impact of the amount of DMSO on the velocities of running micromotors. Tracking results were done for 10 s from 5 independent running experiments to obtain the average velocity.

Poisoning of the micromotors with extracellular-thiols

Molecules with sulphur moiety (H_2S, RSH, RSSR) have been shown to show toxic effect on platinum catalyst even at a very low concentration, and such effect is attributed to the generation of bonds between platinum and the sulphur moieties.[37] Sulfur can chemisorb onto the active sites of the platinum, blocking the catalytic-active surfaces. Additionally, other side-reactions are also possible as a result of the strong chemical bonds between platinum and the adsorbed molecules, which are even able to change the surface characteristics of the platinum to a higher degree.[38] Some of the extracellular thiols, such as cysteine, methionine and glutathione, are of high physiological importance. Such molecules are present in extracellular/intracellular fluids. The concentrations of such molecules in biological liquids, such as plasma and urine, can be useful biomarkers in many clinical situations and the physiological concentrations are normally in 1–10 mM range.[39-41] Such molecules possess either an R – SH or R – S – S – R moiety. It is our interest to see whether such molecules can poison the inside surface of the micromotors as platinum is the material for such surface. The first molecule studied is one of the simplest of these thiols, cysteine, and poisoning studies from serine molecules were also studied to serve as control experiments to see if the –SH group is the reason for the inhibition. The serine molecules possess the same structure as the cysteine molecules with the exception of the side chain moiety, which is –SH for cysteine and –OH for serine. The cysteine molecules can be oxidized by H_2O_2 to generate a disulfide bond.[42] The presence of such bonds and the possible residual –SH groups in the liquid are responsible for the poisoning effect on the platinum surface,[37] and the poisoning effect can be seen from Figure 5-12. Experiments on the liquids containing cysteine and serine molecules were carried out under the same condition.

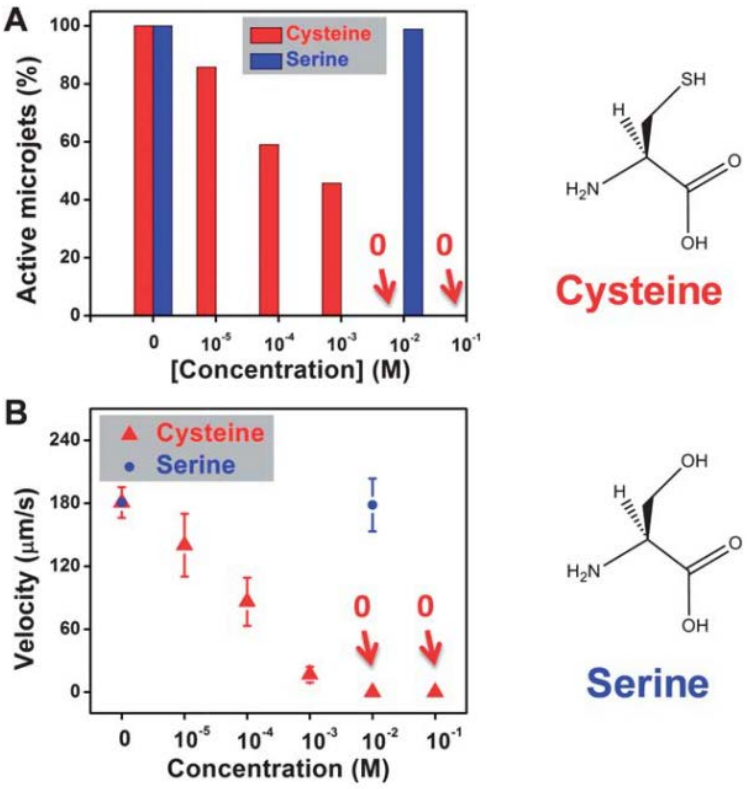

Figure 5-12 The amount of cysteine in the running liquid can drastically decrease the mobility of the rolled up micromotors. (A) More than half of the micromotors were deactivated with the presence of 0.001 M of cysteine, and all the micromotors were deactivated with the amount of cysteine increased to 0.01 M. Almost 100% of the micromotors showed mobility in the serine containing running liquid; (B) Obvious decrement in velocity was recorded for the micromotos that were able to run, from ~180 μm/s without cysteine to ~16.7 μm/s with 0.001 M of cysteine present. The speed was still ~180 μm/s for micromotors moving in the serine containing liquid with 0.001 M of serine present. Tracking of the videos were carried out for a time interval of 10 s from 5 independent-experiments to get the mean velocity.

Figure 2-11A shows that even the concentration was as low as 1×10^{-5} M for cysteine, there is still an amount of 15% of the micromotors that were deactivated, and a dramatic decrement of the velocity was also recorded. Such effects can be attributed to the

coverage of the inner platinum surface of these micromotors with an active R–SH group, and such coverage can significantly inhibit the decomposition of hydrogen peroxide catalyzed by the platinum. With the presence of 1 mM cysteine in the running liquid, merely less than 50% of the micromotors exhibited motion, and when the amount of cysteine was made higher to be 10 mM, 0% of the micromotors moved. On the other hand, nearly 100% of the micromotors showed motion in the liquid containing 10 mM of serine. Moreover, the presence of cysteine can both deactivate the micromotors and also decrease the driving force for the active micromotors, similar to DMSO. The mean velocity was found to be reduced from ~180 μm/s to ~86 μm/s with the presence of 0.1 mM cysteine in the running liquid, and the velocity was further reduced to ~17 μm/s for 1 mM of cysteine and eventually to 0 μm/s at 10 mM concentration of cysteine. The speed of the micromotors was not changed regardless there is no serine molecules or in the presence of 10 mM of serine (180 μm s^{-1}).

It was observed for the cysteine containing running liquid that partial deactivation of the platinum catalytic sites resulted into less amount of O_2 generated, which led to a reduced driving force for the micromotors, and thus lower speed was recorded. As a comparison, such decrement of speed was not seen for the serine containing running liquid. As the difference between the structures of a cysteine and a serine molecule lies only in the –SH and –OH side-chain moiety, it can be confirmed that the –SH moieties are responsible for the observed poisoning effects.

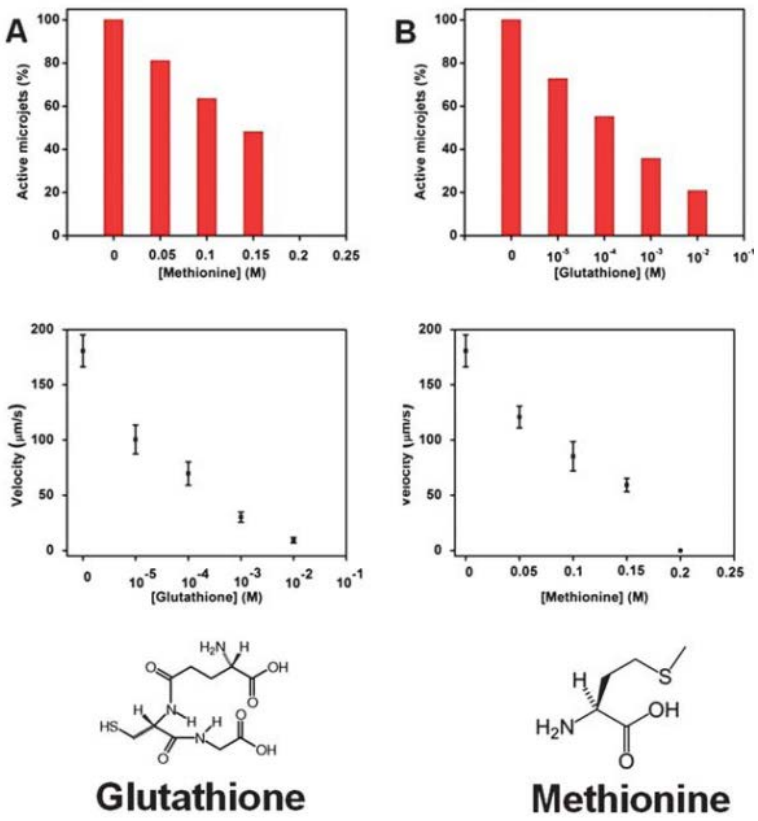

Figure 5-13 Differences in the poisoning capabilities for glutathione and methionine molecules in the running liquids (A) only <40% of rolled up microtubes showed mobility with only 0.001 M of glutathione in the running liquid, and a dramatic decrement of velocity was also seen, from ~180 μm/s without glutathione to ~30 μm/s at 0.001 M concentration of glutathione; (B) >50% of the motors were deactivated at 0.15 M of methionine and no more running micromotors found when the concentration was 0.2 M, and an obvious decrement of velocity was also seen for the motors, from ~180 μm/s without methionine to ~60 μm/s at 0.15 M concentration of methionine; tracking data were taken for a time length of 10 seconds from 5 independent running experiments in order to get the mean velocity.

Next, poisoning effects from more complex thiols were also studied. Glutathione is a very important tripeptide which contains the –SH moiety responsible for its antioxidative capability. It is present in ~5 mM concentration in the mammalian cells.[39] The platinum

micromotors were very susceptible to be poisoned by glutathione at a concentration much lower than the physiological concentrations of this tripeptide. At 0.1 mM (10^{-4} M) concentration, nearly 50% of the micromotors were deactivated and the speed of the remaining running motors was significantly decreased from ~180 to ~70 μm/s (Figure 5-13A). At the physiological concentrations of glutathione, which are in the 1 –10 mM range, about 65 – 80% of the micromotors got deactivated and the remaining micromotors showed a reduced mobility at 10–30 μm/s. Other than the R – SH and RS – SR' moiety, the R – SR' moiety is also able to poison platinum. As can be seen in Figure 5-13, almost 50% of the micromotors were deactivated at 0.15 M of methionine. It is evident that the R – S – CH_3 moiety of methionine is weaker in poisoning effect than that of the R – SH moiety in cysteine (note that the -R portion of cysteine molecule and that of methionine are very close in structure) and in glutathione, even though it is still significantly poisoning the platinum catalytic micromotors at 0.1 M levels. Such weaker effect can be attributed to the difference in structure, that methionine (in contrast to cysteine) does not have the – SH moiety but only the – SCH_3 moiety, which can form a weaker bond to platinum (via chelation), in a similar manner as in methionine platinum dichloride.[43]

To confirm that the poisoning of motion is not present only for the rolled up micromotors,[44] similar experiments were carried out on motors of smaller sizes made through the electroplating process. Such micromotors were made up of microtubes with platinum inside layer and a copper outside layer. Similar to the rolled up motors, the electroplated motors could also be poisoned by the presence of sulphur containing molecules in the running liquid. As can be seen from Figure 5-14, with the presence of 50 mM glutathione, more than 70 % of the micromotors were deactivated and the speed of the remaining active micromotors was significantly lowered from ~380 to 80 μm/s. The mechanism of poisoning is the same as that for the rolled up micromotors.

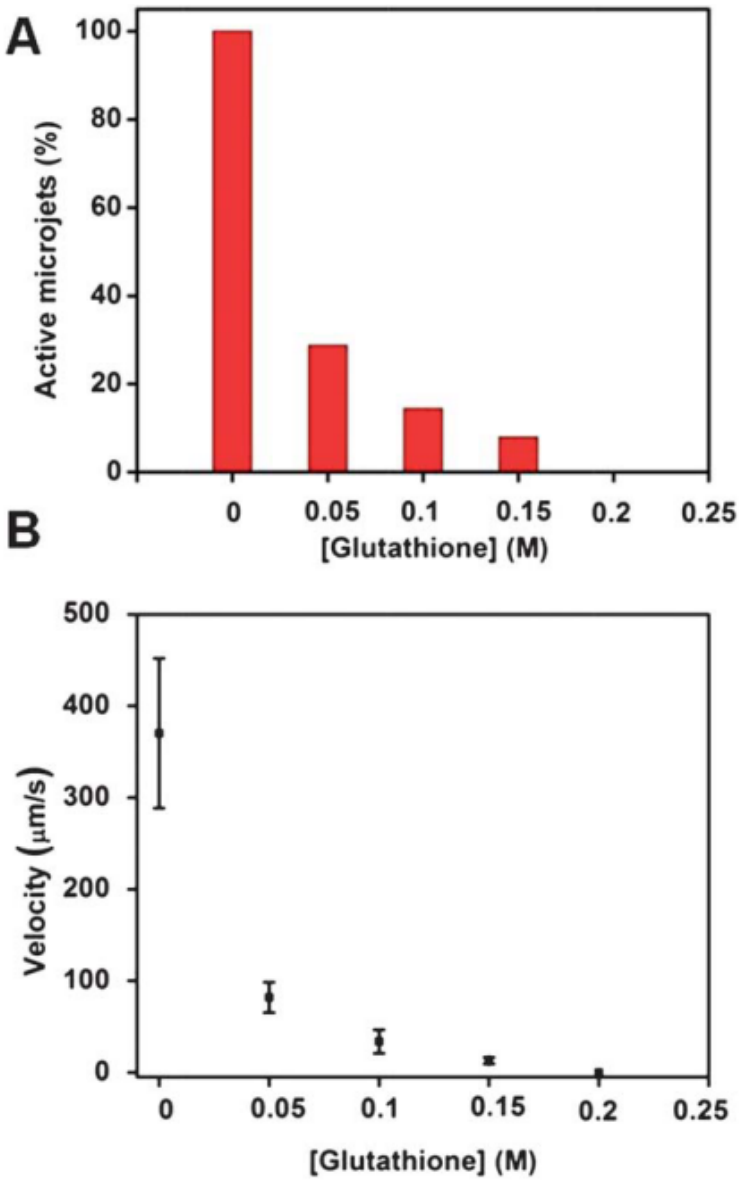

Figure 5-14 Glutathione molecules in the running liquid can decrease also the mobility of electroplated micromotors. (A) Impact of the glutathione concentration on the percentage of the active micromotors. When the amount of glutathione was 0.2 M in the running liquid, no more micromotors were found running. (B) Impact of the concentration of glutathione on the speeds of the active micromotors. Tracking data were taken for a time length of 10 s from 5 independent running experiments in order to get the mean velocity.

5.5 Motion of Micromotors in Different Water Samples

Various applications of the catalytic tubular micromotors have been demonstrated so far, ranging from biomedicine,[17,18,45-48] environmental clean-up[12,13,49,50] to natural resource discovery.[51] However, such reported works were mostly carried out in deionized water, which represent an ideal medium rather than practical. Having investigated the hampering effect from extracellular thiols or organic solvents, it is our interest to see how the real-world water samples can affect the motions of the micromotors. It was found that the mobility of the motors are seriously and negatively affected by the water samples. Differences in such impacts were also observed for tap water, lake water, rain water and sea water samples.

Experimental Procedures

The electrodeposited microtubular motors were utilized in this study, whose synthesis can be find in Section 3.3.1.Water samples were all collected in Singapore: sea water sample was collected from the East Coast of Singapore, lake water was from the Nanyang Lake in Nanyang Technological University (NTU) campus, Singapore, rain water was collected on a building roof of 30 meters high in the western area of Singapore, and tap water was from the laboratory tap water in Nanyang Technological University, Singapore.

The micromotors were set into motion for propulsions in aqueous solutions containing various concentrations of water samples, a fixed concentration of hydrogen peroxide (3%) and a fixed surfactant concentration (SDS, 1 wt %). A mixture of micromotors (5 mL), SDS (1 wt %), H_2O_2 (3 wt %) together with the tested water samples were applied on a glass slide freshly cleaned with nitrogen gas. The behaviors of the motors were then observed under a microscope. Optical microscope videos and images were obtained with Nikon Eclipse 50i microscope. Video sequences were processed with Nikon NIS-

Elements^{TM} software. Ion Chromatography (IC). Cation IC experiments were performed with a Dionex ISC-900 utilizing an Ion Pac CS12A 4 mm × 250 mm analytical column. For cation IC, the eluent consisted of 20 mM methanesulfonic acid, and the chemical regenerant consisted of 100 mM tetrabutylammonium hydroxide. Anion IC experiments were performed with a Dionex ICS-1100 utilizing an Ion Pac AS22 4 mm × 250 mm analytical column. For anion IC, the eluent consisted of 4.5 mM sodium carbonate and 1.4 mM sodium bicarbonate, and an electrochemical suppressor was used. Conductivity measurements were performed with a Radiometer IONcheck 30 probe.

Results and Discussion

As the micromotors are propelled by the catalytic decomposition of H_2O_2 at the inner surface of the tubes, the liquid medium was fluxed into the tube from the front end of tube as it runs. In this way, chemical composition of the liquid can affect the motion of the tubes. In our study, the distilled water was used in the control experiment, and motion of motors in tap water, lake water, rain water, as well as sea water was compared to the behavior of the motors in the distilled water. In particular, we decided to focus on the ratio of the micromotors expelling bubbles in the given environment, as well as on the ratio of motors moving in the given media. In addition, for the motors which exhibited motion, their average velocities were also determined. In all of the experiments, the concentration of fuel used is 3 wt % in all cases. We first evaluated the motion of the micromotors in tap water. As shown in Figure 5-15, while 100% of the micromotors ejected bubbles and showed mobility in distilled water; only 19% of them ejected bubbles in tap water and only 15% exhibited motion. The average velocity of the micromotors in distilled water is 365 μm s^{-1}, while the velocity of the micromotors in a maximum concentration (71.5%) of tap water is merely 54 μm s^{-1}. Note that the fuel used is 3% H_2O_2 in tap water prepared from a 27% (wt.) stock solution and later added to the tap

water, therefore the maximum concentration of tap water was 71.5% (indicated in the Figures as ‘‘Max’’). In order to investigate whether the decrease in the mobility of the micromotors takes places gradually or in a single step, we prepared mixtures of tap water with distilled water at different concentrations (v/v). We found that the decrease in mobility of the micromotors was gradual over the concentration range, as shown in Figure 5-15A. Next, we turned our attention to the rain water sample. Similar to the previous example, the viability of the micromotors in rain water (with 3% H_2O_2) was much lower than that in distilled water, with only 27% of the motors ejecting bubbles and 23% of the motors exhibiting motion. The average velocity of the mobile micromotors in rain water was 117 μm s^{-1}, which is significantly lower than that in the distilled water (365 μm s^{-1}). As in the case of tap water, when rain water was mixed with distilled water, the viability and mobility decreased gradually with a corresponding increase in the fraction of rain water present (Figure 5-15B). The exact levels of organic compounds in the water samples are currently not available. Nevertheless, the tap water is purified to high standards with organic compounds having values in the very low ppm to ppt levels. A recent study on atmospheric gaseous compounds identified 48 volatile organic compounds in Singapore, but these are not likely to enter the water to a significant amount (compared to the concentrations of inorganic ions). Subsequently, we investigated the motion of the micromotors in natural fresh water reservoir. The mobility of the micromotors in lake water is lower when compared with distilled water; only 28% of them ejected bubbles and 23% were observed to show motion (Figure 5-15C). The velocity of the micromotors in lake water is 97 μm s^{-1}. Interestingly, the mobility of the micromotors in lake water is somewhat similar to that of the rain water sample. The mobility of micromotors was also shown to gradually decrease upon increasing the fraction of lake water in distilled water. It should be noted that mobility of the micromotors is higher in rain or lake water than in tap water. We will discuss the reasons

in the following text. Relative standard deviations (RSD) for velocity data points in Figure 5-15A are 36.6%, 27.7%, 27.7%, 21% and 8.7% for 0, 15, 30, 45 and 60% (v/v) of tap water, respectively. RSD for data presented in Figure 5-15B are 36.6%, 20.8%, 31%, 48% 57% for 0, 15, 30, 45 and 60% (v/v) rain water, respectively. RSD for data presented in Figure 5-15C are 36.6%, 25%, 21%, 40%, 41.4% for 0, 15, 30, 45 and 60% (v/v) lake water, respectively.

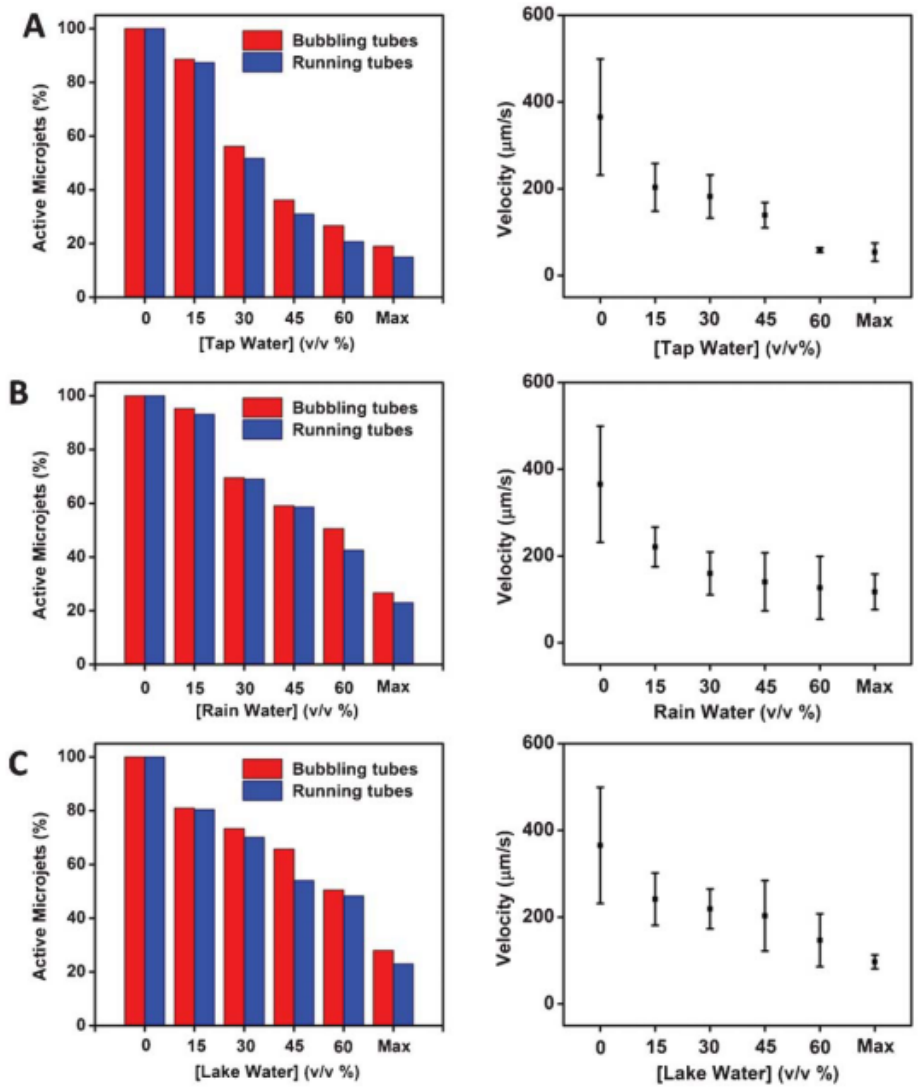

Figure 5-15 Motion of the catalytic micromotors (prepared by electrochemical template deposition method) in various real-world waters. (A) tap water, (B) rain water and (C) lake water. Left: Graph showing the influence of the natural water concentration (as

diluted with distilled water) on the activity of the micromotors, which exhibited either bubble ejection (red bar) or micromotors motion (blue bar). Right: Graph showing the influence of the concentration of natural waters on the velocity of the moving micromotor. Conditions in the all experiments: temperature of 23^{o}C, 3% (wt.) H_2O_2 and 1 (wt.) % SDS.

Lastly, we investigated the mobility of micromotors in the seawater sample. It was previously suggested that bubble-propelling micromotors are capable of performing environmental clean-up of oil spills,[31] which strongly implies that such operation takes place in seawater. However, when we immersed the micromotors in seawater (containing 3% wt of H_2O_2), we observed no motion. When we examined the influence of seawater content in seawater/distilled water mixture, we observed a dramatic decrease of the mobility of micromotors, at 6% (v/v) seawater whereby only 47% of motors ejected bubbles and no more than 41% move with an average velocity of 63 μm s^{-1} (compared to 365 μm s^{-1} in distilled water), see Figure 5-16A. At 9% (v/v) of seawater, only 8.6% of the catalytic motors ejected bubbles, and 1% exhibited motion. The striking differences between the motions of the micromotors in the fresh-water sources and in seawater led us to the hypothesis that the motion of the micromotors is influenced by the amount of inorganic ions present in the environment. To test this hypothesis, we first performed the experiment in a NaCl solution. As seawater contains NaCl at a large concentration of approximately 35 g L, NaCl itself is sometimes used to simulate an “artificial seawater” environment (Figure 5-16B); hence we studied whether the micromotors move in a 35 g L^{-1} NaCl solution. We did not observe any bubble ejection or motion of micromotors, leading us to study how diluted NaCl solutions can influence the motions of the micromotors. We observed a very similar decrease in the viability of the micromotors in diluted seawater, with bubble ejection being reduced to 30% in 6% of NaCl solution (35 g

L^{-1} NaCl being considered as 100%) and only 20% of micromotors were moving, with a reduced speed of 84 μm s^{-1} (Figure 5-16B). At 9% NaCl solution, only 3.8% of micromotors produced bubbles and 3.4% move at a velocity that is nearly 0 μm s^{-1}; and at 12% NaCl, no motion of micromotors was observed. Therefore we have demonstrated that in contrary to previous observations, the motion of the Pt catalytic bubble micromotor is highly influenced by the salt concentration in the environment, which is similar to the motion of self-electrophoretically propelled microrods. It should be noted that a similar experiment with rolled-up micromotors was also performed, and no motion was observed in seawater at 3% H_2O_2 either. Note that the decreased mobility of micromotors is not caused only by the NaCl solution, but by solution of other salts as well. Figure 5-17 shows a similar trend for KNO_3 solution.

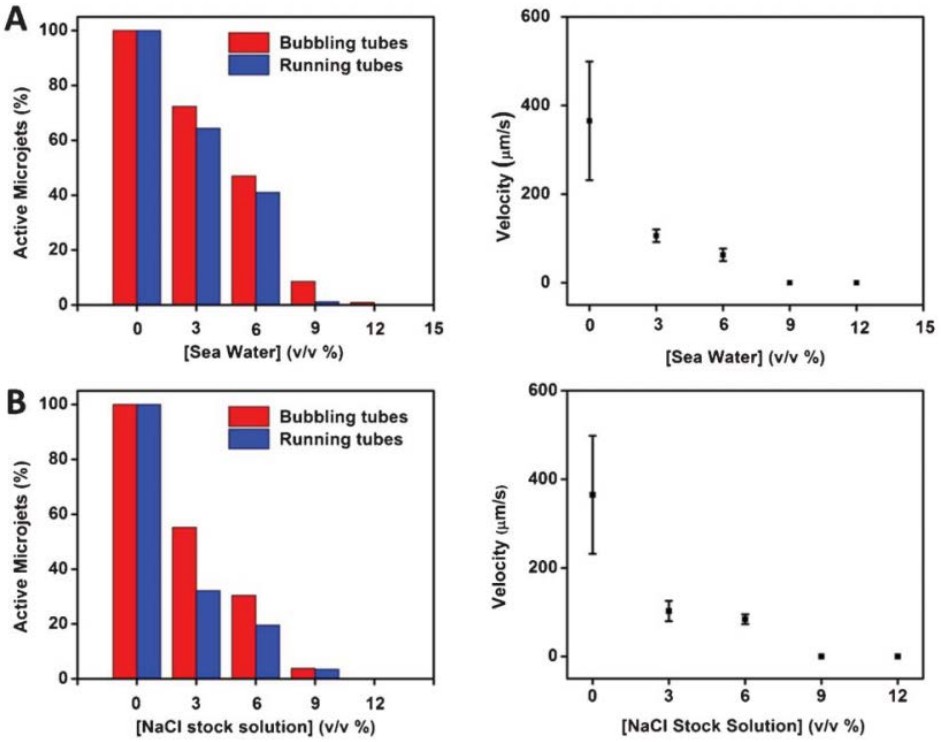

Figure 5-16 Motion of the catalytic micromotors (prepared by electrochemical template deposition method) in various fractions of (A) seawater, (B) 35 g L^{-1} NaCl stock solution. Left: A graph showing the influence of the seawater or NaCl stock solution concentration

(as diluted with distilled water) on the activity of the micromotors, which exhibited either bubble ejection (red bar) or micromotors motion (blue bar). Right: A graph showing the influence of the concentration of seawater or NaCl stock solution on the velocity of the moving micromotors. Conditions in all of the experiments: temperature 23^{o}C, 3% (wt.) H_2O_2 and 1 (wt.) % SDS.

Table 5-1 Mean concentration of ions is in mg L^{-1} (equivalent to ppm) of the common chemical compositions in water samples measured by ion chromatography.

[Ion] (mg L^{-1})	Tap water	Rain water	Lake water
F^-	0.46	0.05	0.028
Cl^-	14.39	1.44	3.80
NO_3^-	2.02	1.48	0
SO_4^-	19.49	3.08	2.36
Na^+	6.99	0.47	2.49
NH_4^+	0.51	0.28	0.44
K^+	3.67	0.37	0.58
Mg^{2+}	0.96	0.080	0.47
Ca^{2+}	13.89	0.73	6.32

To explore this issue in a greater detail, and in order to explain the differences in the decrease of the mobility of micromotors in fresh water sources, we determined the inorganic ion compositions of the water samples using ion chromatography and conductivity measurements. It can be observed from Table 5-1 that tap water contains the largest amounts of inorganic ions, such as F^-, Cl^-, SO_4^{2-}, Na^+, K^+, Ca^{2+}, Mg^{2+} etc., much more than in lake water or rain water. This is also reflected in the higher conductivity reading of 137 µS cm^{-1} for tap water, as compared to the rain and lake water conductivities of 33 and 41 µS cm^{-1}, respectively. The amount of ionic components of the solution directly correlates to the decreased viability and mobility of micromotors.

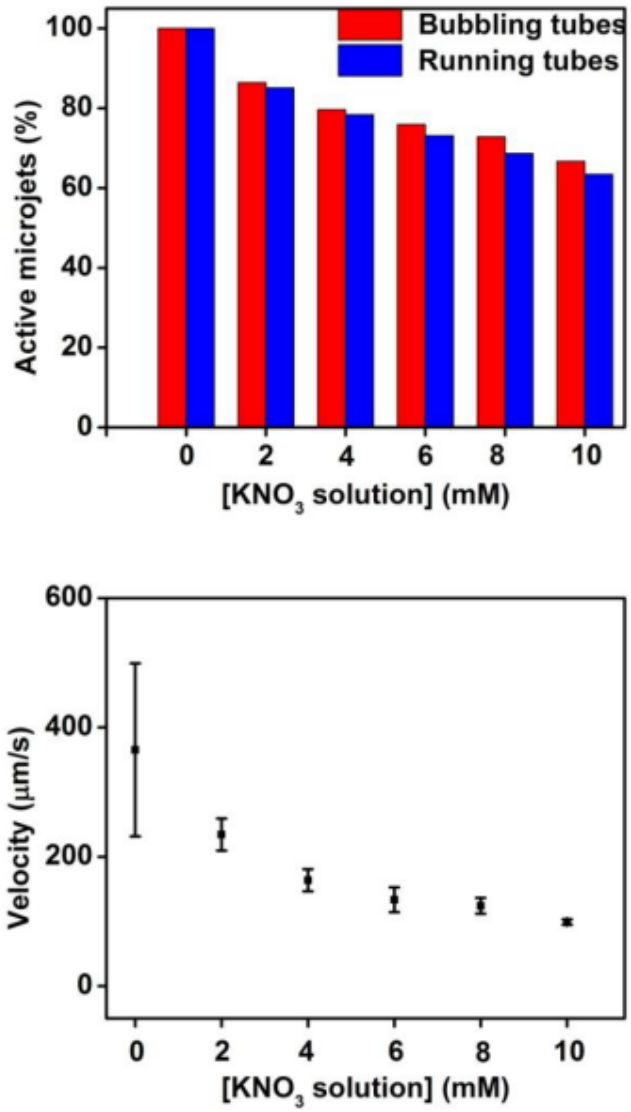

Figure 5-17 Motion of the catalytic micromotors (prepared by electrochemical template deposition method) in KNO_3 solution at different concentrations. Top: Graph showing the influence of the KNO_3 solution concentration on the activity of the micromotors, which exhibited either bubble ejection (blue bar) or micromotor motion (red bar). Bottom: Graph showing the influence of the concentration of KNO_3 solution on the velocity of the moving motors. Conditions in the all experiments: temperature of 23^{o}C, 3% (wt.) H_2O_2 and 1 (wt.) % SDS.

5.6 Motion of Micromotors in Blood

It is one of the ultimate goals for the research community to utilize the artificial small motors in real biological environments, among which blood is of high expectation. We believe that with a sufficient power thrust and precise manipulation of motion to run the motors in blood vessel, site-specific drug delivery and microsurgeries can be envisioned, which will benefit the medical technology as well as human heath in a great deal. Thus, it is of importance to investigate the behavior of such motors running in blood, although the biocompatible and yet powerful chemical fuel is not readily available in the current era.

The blood itself is very complex in terms of composition. The main components of blood are blood cells that are suspended in a liquid medium, called the blood plasma. Blood cells take up around 45% of the volume of blood, whilst blood plasma takes up roughly 55% of it. Blood cells can be further differentiated as the red blood cells (RBC, or named erythrocytes; with a typical concentration of ~5- 6× 10^6 cell mL^{-1} , and they account for 99% of the cellular components), white blood cells, and platelets.[52] The distances among the RBCs are extremely short as there is a space boundary in blood vessels. Thus, the blood is a highly packed system. As for the plasma, there is up to 92% of water and 8% of other components, including different kinds of electrolytes (mainly Na^+ and Cl^-), various protein molecules (immunoglobulin, albumin, as well as the clotting factors), and the nutrient molecules. Without the blood clotting factors, the plasma can be termed as serum.[52]

If we are to deploy the artificial nano-/micromotors in blood, effects of different components in blood might have some impacts on the motion of the motors. For example, running in the RBC-packed liquid medium can exert high amount of frictional forces on the motors, and thus significantly reducing their velocities. Moreover, the inlets of tubular

micromotors might be blocked by the cells or protein clusters, and the hampering effect over the catalytic decomposition of fuel molecules might present. Furthermore, absorption of protein or other molecules at the inside surface of the motors can passivate the catalytic effect and greatly reduce their motion. And thus, I wish to introduce here our work on the observations that how the blood components can affect the motion of catalytic tubular micromotors.

Experimental Procedures

Materials and apparatus

Hydrogen peroxide (27 wt%, Lot # 10151507) was purchased from Alfa Aesar, Singapore. Colloidal graphite (isopropanol base) was purchased from Ted Pella, Inc. (Lot # 12009-2, USA). Sodium dodecyl sulfate (SDS, Lot # 079K0335), human serum (from human male AB plasma) and red blood cells (dry powder, glutaraldehyde treated, from sheep) were purchased from Sigma-Aldrich. Phosphate buffer saline (PBS, pH 7.2) was from Gibco. PBS buffer was prepared from potassium phosphate monobasic (1.54 mM), sodium chloride (155.17 mM) and sodium phosphate dibasic (2.71 mM). Chemicals were used as received and solutions were prepared using ultrapure water (18.2 MΩ cm) from a Millipore Milli-Q purification system. Counting red blood cells for reconstitution was carried out with a hemacytometer (Hausser Scientific, USA) and centrifugation was carried out with a Beckman Coulter® Allegra® 64R centrifuge. Viscosity was measured using CONTRAVES low shear 40 viscometer. Electrochemical deposition was carried out with a μAutolab type III electrochemical analyzer (Eco Chemie, Netherlands) connected to a computer and controlled by General Purpose Electrochemical Systems version 4.9 software (Eco Chemie). Optical microscope videos and images were obtained

with a Nikon Eclipse TE 2000-E microscope. Video sequences (100 fps) were processed with Nikon NIS-Elements^{TM} software.

Methods

Fabrication of Ti/Fe/Cr/Pt microtubes was carried out using the previously reported protocol. Briefly, a layer of AR-P 3510 photoresist was spin-coated on silicon wafers (1.5 inch) at 3500 rpm for 35 s. After that, a soft bake using a hotplate was carried out at 90 °C for 1 min. The wafer was then exposed to UV light with a Karl Suss MA-56 mask aligner (410–605 nm). The exposed patterns of the photoresist were developed in an AR300-35/H_2O solution (1:1). Microtubes were obtained by a tilted deposition at an angle of about 60° (measured from the horizontal axis) on the photoresist. Metal films with thicknesses of 3 nm (Ti), 5 nm (Fe) and 5 nm (Cr) were deposited layer by layer on the tilted samples. Using magnetron sputtering, a layer of Pt with 1 nm thickness was deposited onto the Ti/Fe/Cr samples. Rolling-up of films into a tubular structure was done by immersing the sample into acetone, as it could selectively etch the photoresist layer. Finally, supercritical point drying was used to keep the tubes from collapsing due to the high fluid surface tension.

The Cu/Pt concentric bimetallic microtubes were synthesized with a modified electrochemical deposition procedure on a cyclopore polycarbonate template. Colloidal graphite ink was applied on one side of the polycarbonate template with commercial cotton swabs. A piece of flattened aluminium foil was attached to the ink immediately, which serves as the working electrode for the plating experiments. The template was assembled into a customized electrochemical deposition cell. A platinum counter electrode and the Ag/AgCl reference electrode were utilized. Electrochemical deposition was carried out with a μAutolab type III electrochemical analyser connected to

a computer and controlled by General Purpose Electrochemical Systems Version 4.9 Software. The template was rinsed with 5 mL of ultrapure water (18.2 MΩ cm) 4 times, and the Cu outer layer was deposited galvanostatically at −4 mA for 450 s. The deposition solution contained 1 M $CuSO_4$. Consequently, after removing the solution, the template was rinsed 5 times with 8 mL of water. A platinum segment was subsequently electrodeposited at −4 mA for 450 s using the commercial plating solutions. When the deposition of microtubes was finished, the electrochemical cell was disassembled and the template was washed 5 times with 8 mL of water each time. After that, the template was ultrasonicated 3 times in 2 mL of ultra-pure water for 3 min each time. The graphite layer was removed during the sonication procedure. The template was placed in an Eppendorf tube with 2 mL of methylene chloride and ultrasonicated until the whole template dissolved. The electrochemically deposited microtubes were collected by centrifugation at 6000 rpm for 3 min and washed repeatedly 3 times with methylene chloride. The liquid was subsequently washed with ethanol and water two times each and centrifuged for 3 min after each washing step. The tubes were stored in water at room temperature.

Motion studies of the micromotors in various biological samples were carried out in an aqueous solution containing 3 wt % of hydrogen peroxide at constant surfactant concentrations (1 wt % of SDS). Solutions of the red blood cells (~5 × 106 cell μL−1) were reconstituted and diluted with 1×PBS buffer saline solution (pH 7.2). A mixture of the micromotors (5 μL), SDS (1 wt %), hydrogen peroxide (3 wt %) and the tested sample were applied on a glass slide freshly cleaned with N_2 gas.

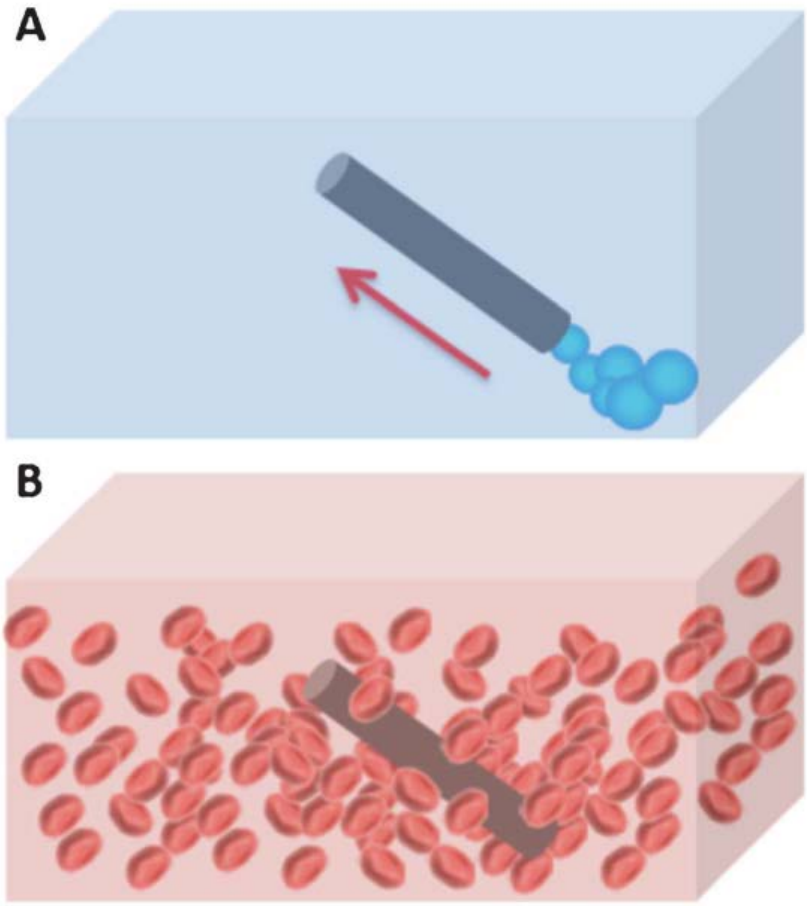

Figure 5-18 Schematic representations of the concept demonstrated in this section, showing the motion studies of the micromotors in (A) phosphate buffer saline solution and (B) the red blood cells and serum mixture in a concentration corresponding to that of human blood. Both solutions contained 3 wt % H_2O_2 as fuel and 1% SDS.

Results and Discussion

We first investigated if the catalytic micromotor engines are able to move in the artificial blood suspensions (in the presence of added fuel, H_2O_2 and surfactant (SDS), see Figure 5-18 for schematics). Figure 5-19 shows that catalytic micromotors prepared by rolled-up technology are able to move in phosphate buffer saline solutions containing 3% H_2O_2 and 1% SDS (both in wt %), at a typical velocity of ~1.2 bl s; however, one can observe in

Figure 5-19B that the micromotors do not exhibit any motion in a red blood cell and serum mixture at a concentration of 3% H_2O_2.

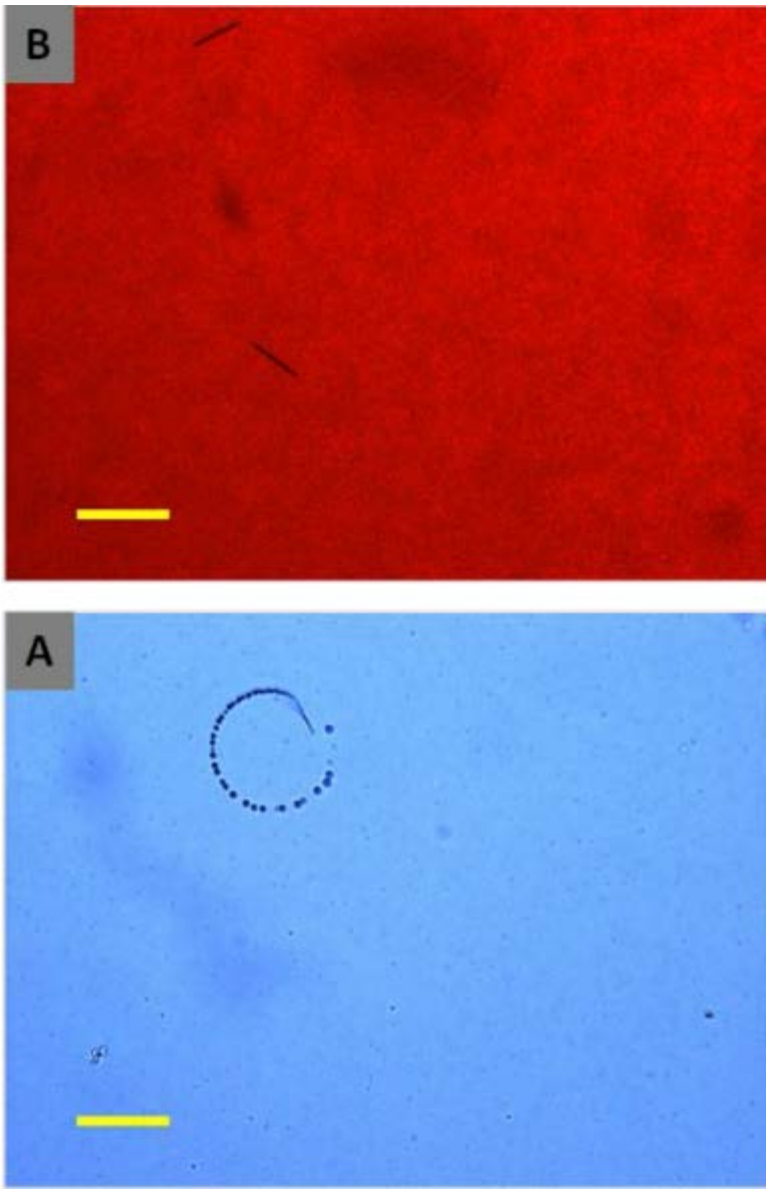

Figure 5-19 Schematics of the concept demonstrated in this section. Motions of the micromotors in (A) phosphate buffer saline solution (pH 7.2) and (B) red blood cell (~5×10^6 cell μL^{-1}) and serum mixture of concentration corresponding to that of the blood. Both solutions contained 3% (wt) H_2O_2 as fuel and 1% SDS. The micromotors were prepared by rolled-up technology. Scale bar indicates 100 µm.

Even when the concentration of fuel was increased to 6% and 9%, the motion of the micromotors remained non-existent in the red blood cell and serum mixture (Figure 5-20). In the following text, we wish to address the question of whether the lack of movement from the catalytic engines is due to the presence of red blood cells or the presence of the components of serum.

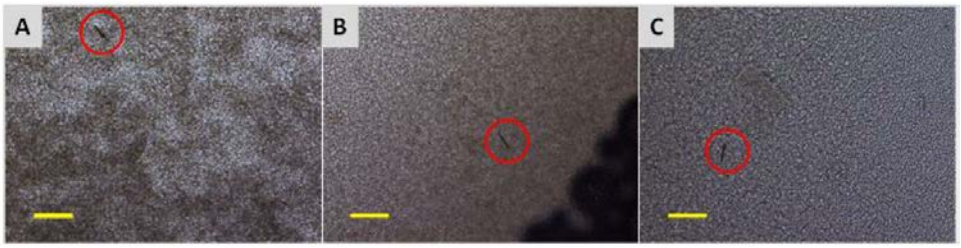

Figure 5-20 Motion of the rolled-up micromotors in red blood cell (~5×10^6 cell μL^{-1}) and serum mixture of concentration corresponding to the concentration in the blood. (A) 3% (B) 6% and (C) 9% (wt) H_2O_2 as fuel and 1% SDS. Scale bars indicate 100 µm.

We dispersed the red blood cells in phosphate buffer saline solution at concentrations corresponding to the one found in human blood, as well as at concentrations of 10×, 100×, 1000×, 10 000× and 100 000× dilutions of the one in blood. We investigated the motion of the micromotors in these dispersions, in the presence in red blood cell dispersions of concentrations corresponding to natural blood, as well as the subsequent dilutions. It was observed that while none of the micromotors showed bubble ejection at non-diluted and 10× diluted concentrations of red blood cells, 90% of the observed micromotors showed bubble ejection at 100 000× dilution. Correspondingly, 0% of micromotors showed motion in the solutions containing non-diluted to 100× diluted suspension of red blood cells, while 50% of micromotors showed movements at 100 000× dilution of the red blood cells (for detailed data, see Figure 5-21).

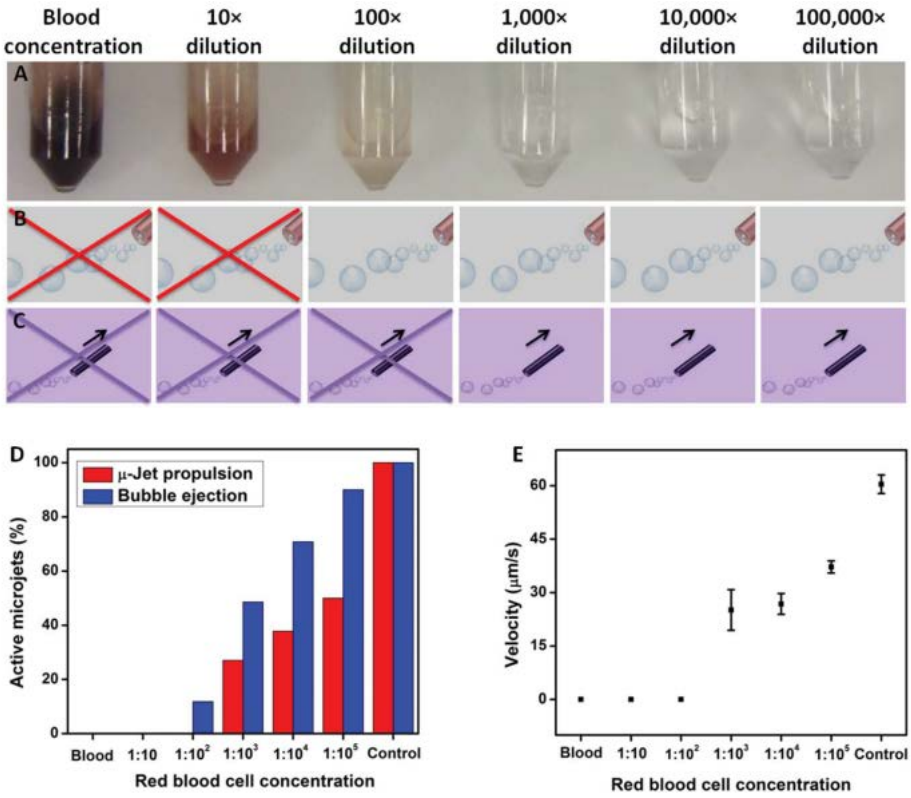

Figure 5-21 Motion of the rolled-up micromotors in red blood cell dispersions. (A) Photographs illustrating the color of consecutively diluted suspensions of red blood cells. (B) Schematic illustrations of whether the bubble ejection from micromotors was observed and (C) whether the motion of micromotors was observed in given suspensions. (D) A graph showing the influence of red blood cell concentration on the percentage of micromotors found to exhibit either bubble ejection (blue bar) or motion (red bar). Note that 10× diluted RBC solution is denoted as 1: 10, 100× diluted as 1: 10^2 etc. in the graph. (E) A graph showing the influence of red blood cell concentration on the velocity of the moving micromotors. Note that a ‘‘Control’’ experiment was carried out in phosphate buffer saline solution (pH 7.2), while the notation ‘‘Blood’’ means the concentration of red blood cells typical for blood (~5× 10^6 cell μL^{-1}). Conditions in all of the experiments: temperature of 23^{o}C, 3 wt % H_2O_2 and 1 wt % SDS.

For each suspension, we observed at least 45 micromotors ($n \geq 45$) and the data are normalized to the motion of the micromotors in phosphate buffer saline solutions without the presence of cells. It is to be noted that there were only a portion of micromotors moving in the solution containing red blood cells, and in addition the motors that in fact did move actually exhibited much lower velocities than those running in the phosphate buffer, as shown in Figure 5-21E. Clearly, these micromotors were unable to exhibit any motion whatsoever at concentrations of red blood cells close to the concentration of real blood. No motion can be observed even at 100× dilution of the red blood cell concentration and at greater dilutions, only some of the micromotors move at velocities that were lower than those in the phosphate buffer saline solution. Possible factors contributing to the crippling effect on the ability of the micromotors to move are to be discussed in a later section.

Consequently, we shifted our attention to the motion of the micromotors in serum, which is essentially blood without the presence of cellular components and clotting factors. We varied the concentrations of serum in phosphate saline buffer solution (v/v) from 70% to 0% (with 3% of hydrogen peroxide and 1% SDS in all discussed cases in the following text) and observed the micromotors' behavior in such media. It should be noted that it is not principally possible to prepare 100% serum with H_2O_2 as the fuel, as the stock solution of hydrogen peroxide has a concentration of 27%, so there is always dilution factors present in the preparation of serum solutions containing H_2O_2. Figure 5-22 summarizes the observed motion of the rolled-up micromotors in serum. Figure 5-22 A shows snapshots of typical micromotors in the media, while Figure 5-22, B and C schematically show whether there are any generation of bubbles and/or motions (B and C, respectively). No bubble generation was observed in 70% serum solutions, but at a concentration of 50% (v/v) serum, we observed bubbles being generated (without

observed motion of the micromotor). The motion of the micromotors can be observed only at concentrations of serum at 30% (v/v) or lower. Bubble ejection is observed to be 0% for cases of 70% serum, 32.8% for cases of 50% serum, 65.5% for cases of 30% serum and 77.4% for cases of 10% serum. Likewise, motion of the micromotors was not observed in 70% and 50% serum, and 46.8% of the micromotors exhibited motion for 30% serum and 77.4% for 10% serum solution (Fig. 3, D). For each suspension, we recorded the motion for at least 45 micromotors ($n \geq 45$) and the data were normalized to that of the micromotors in phosphate buffer saline solution. Not only does a fraction of the micromotors exhibit motion in 30% and 10% serum, but the velocity of the micromotors was also lower than those in phosphate buffer saline solution, as shown in Figure 5-22, E. The velocity decrease in diluted serum solutions is dramatic and could hardly be explained simply by viscosity changes. In fact, it could also be due to the components of serum adsorbing onto the catalytic sites of the jets, hampering the propulsion.

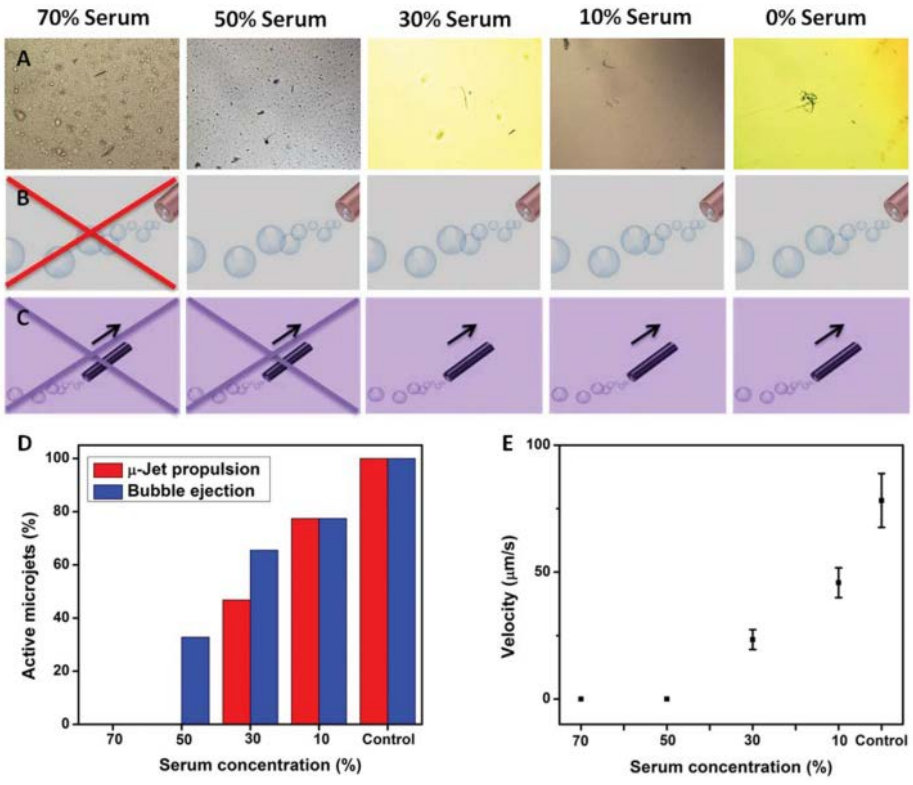

Figure 5-22 The motion of the rolled-up micromotors in serum. (A) Typical micrographs of the micromotors in the serum. (B) Schematic representations illustrating whether bubble ejection from the micromotors was observed and (C) whether the motion of micromotors was observed in a given serum solution. (D) A graph showing the influence of the serum concentration on the percentage of the micromotors found to exhibit either bubble ejection (blue bar) or motion (red bar). (E) A graph showing the influence of serum concentration on the velocity of the moving micromotors. Note that the ‘‘Control’’ experiment was carried out in phosphate buffer saline solution (pH 7.2). Conditions in all of the experiments: temperature of 23^{o}C, 3 wt % H_2O_2 and 1 wt% SDS.

We consequently investigated the behavior of micromotors prepared *via* template-electrochemical deposition. These micromotors are smaller than the ones prepared via rolled-up technology (rolled-up micromotors have typical dimensions of 50μm in length and 5 μm in diameter), with average dimensions of 10 μm in length and 2 μm in diameter. These electrodeposited micromotors behave in a similar way as the rolled-up micromotors described above. While these electro-deposited micromotors show agile mobility in 3% H_2O_2 and 1% SDS in phosphate buffer with velocities of 74 μm s^{-1}, they neither move nor eject bubbles in a mixture of red blood cells and serum, as shown in Figure 5-23.

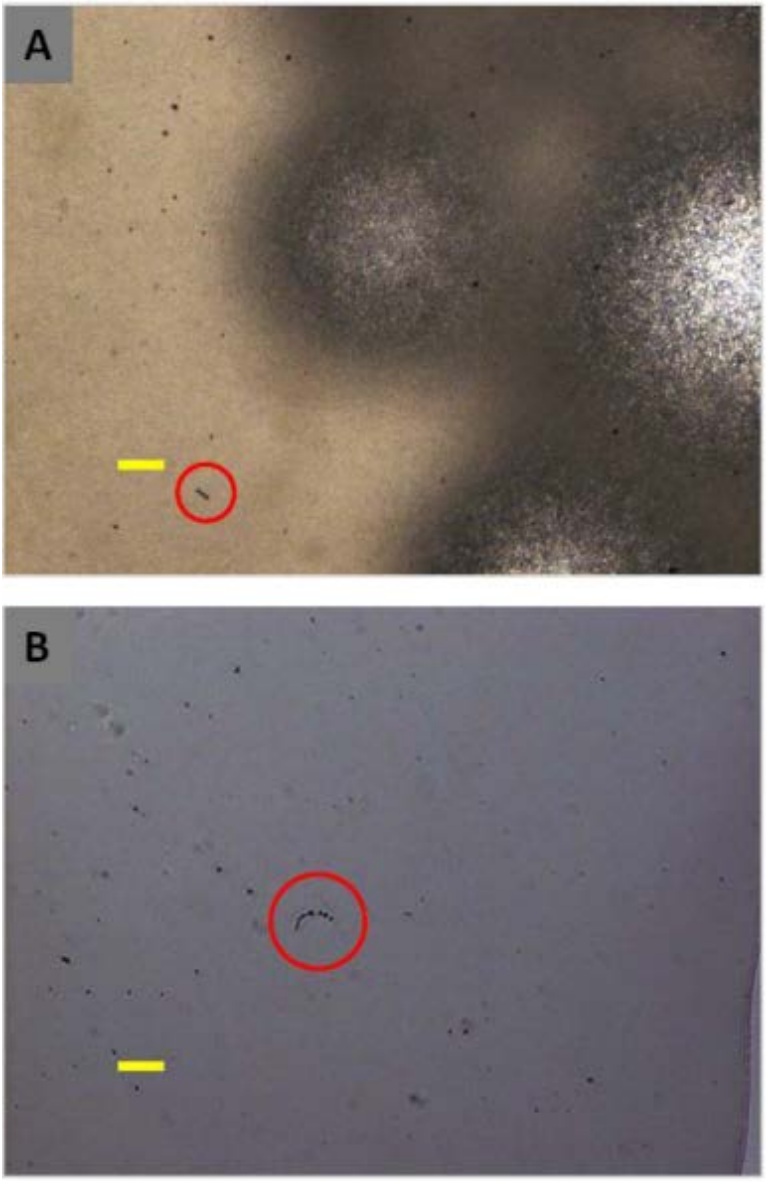

Figure 5-23 Motion of the template- electrochemical deposition technology prepared micromotors in (A) red blood cell (~5×10^6 cell μL^{-1}) and serum mixture of concentration corresponding to the concentration in the blood and (B) phosphate buffer saline solution (pH 7.2). Both solutions contained 3% (wt) H_2O_2 as fuel and 1% SDS. Scale bars indicate 50 µm.

We consequently investigated the influence of the blood components, the red blood cells and serum on their movement. Not surprisingly, these micromotors behaved similarly to the rolled-up micromotors described in the previous section, as shown in Figure 5-24, A

and B. At a blood concentration of red blood cells, none of these micromotors produced bubbles and no movement of the jet was observed. At 10× dilution of red blood cells, ~10% of the jets ejected bubbles, while none of them exhibited any motion. At 100× dilution of the red blood cells, 62% of micromotors ejected bubbles and ~24% exhibited motion. The micromotors, which showed movement at 100× dilution of red blood cells, demonstrated a reduced velocity of 34 μm s^{-1} when compared to a velocity of 74 μm s^{-1} in the phosphate buffer solution. A similar trend can be observed in the serum as well, whereby at 70% serum (containing 3% of H_2O_2 as fuel and 1% SDS) only 9.2% of micromotors exhibited bubble ejection and only 4.9% showed movement. The micromotors, which did move, displayed very low velocities of 5.9 μm s^{-1} (compared to 74 μm s^{-1} in phosphate buffer). With a decreasing concentration of serum, the viability of the micromotors increases. However, at 30% serum, 71.5% of the electroplated micromotors ejected bubbles, but only 26.4% exhibited motion at an average velocity of 32.1 μm, which is still less than half of the velocity in the buffer solution. The reasons for the decreased/crippled mobility of micromotors in a solution of red blood cells and in serum are complex. First, one should take into account the size compatibility of micromotors with blood components. The internal diameter of rolled up micromotors is ~4.5 μm, while the internal diameter of Cu/Pt electrodeposited micromotors is ~1μm. The diameter of a red blood cell is ~6–8 μm, while the size of a capillary in the human body is 5–10 μm.[53] Even though the red blood cell has developed evolutionary to be very flexible and move in small capillaries, the openings of electrodeposited micromotors are too small for red blood cells to enter them. It is likely that the inlet of micromotor becomes blocked by red blood cells, effectively limiting the inlet of fuel, and thus crippling the micromotor's movement. In cases of rolled-up micromotors the mechanisms can be the same; or in addition, it is possible that a red blood cell enters the microtube cavity and due to adhesion to Pt it clogs the opening and therefore debilitates the micromotor's movement.

The other components, such as proteins and amino acids present in serum are too small (maximum size of tens of nanometers) to mechanically disable the micromotors by clogging them up. Second, it is possible that small molecules, such as proteins, enzymes, peptides or hormones interact with the inner Pt surface of the micromotor and passivate it. Thirdly, blood, consisting of a red blood cell solution and serum, has higher dynamic viscosities than phosphate solution. Therefore, the drag force will be higher and the movement of the micromotor slower. In particular, for particles moving in the solution at small velocities without turbulence (therefore at low Reynolds numbers; note that Re for micromotors studied here is 10^{-5}–10^{-4}) the drag force (F_{frict}) can be calculated using Stokes' equation:[54]

$$F_{frict} = 6\pi\eta r v$$

where η is dynamic viscosity, r is the radius of a particle and v is velocity. If we assume that the propulsion force (F_{prop}) is constant in all solutions for a fixed H_2O_2 concentration and the fact that $F_{prop} = F_{frict}$, it is clear that the velocity of the micromotor indirectly decreases with an increase in viscosity. To address the above mentioned questions why the motion of the micromotors is crippled in the red blood cell and serum solutions, we measured the viscosity of the various solutions. We found that the dynamic viscosity in 10× diluted red blood cell solution is 5.07 mPa s, in 100× diluted solution is 3.00 mPa s, in 1,000× diluted solution is 2.06 mPa s, in 10 000× diluted solution is 1.81 mPa s, and in phosphate buffer 0.90 mPa s. It is possible to observe that when increasing viscosity ~26 from 0.90 to 1.81 mPa s (for red blood cells at 10 000× dilution), the velocity of the motors decreases about 2 times, following Stokes' equation. With a further increase of viscosity to 2.06 mPa s for 1000× diluted red blood cells solution, the velocity of micromotors further decreases, still following Stokes' equation. However, with increasing concentration of red blood cells (and increasing viscosity) to 100× and 10× diluted red

blood cells solution, the micromotors do not show any motion and there is a sudden break in the dependence of velocity on viscosity. This is likely due to the fact that in a concentration range from free solution to 1000× diluted red blood cells solution the governing factor of the solution is viscosity, while with increasing concentration of red blood cells, other factors, such as blockage of microtube by red blood cells is taking place. A similar study of viscosity has been carried out for serum. We found that 70% serum has a viscosity of 2.10 mPa s, about two times higher than phosphate buffer. However, no motion was observed in 70% serum. Therefore we deduce that the components of serum inhibit evolution of O_2 bubbles by their chemo/physisorption on the Pt inner walls of micromotors; blockage of micromotors in serum is not possible as serum contains only proteins and smaller molecules.

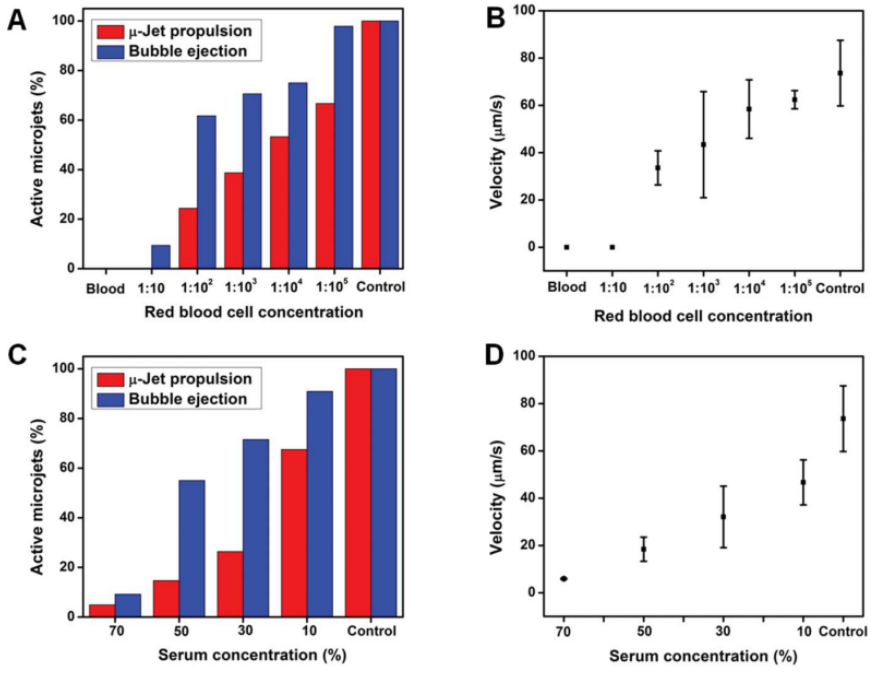

Figure 5-24 Movement of the electrochemical deposition-prepared micromotors in (A, B) red blood cell dispersion and (C, D) serum solutions. (A) A graph showing the influence of the red blood cells concentration on the percentage of the micromotors found in the suspension, which exhibited either bubble ejection (blue bar) or motion (red bar). Note

that 10× diluted RBC solution is denoted as 1: 10, 100× diluted as 1: 10^2 etc. in the graph. (B) A graph showing the influence of the red blood cells concentration on the velocity of the moving micromotos. (C) A graph showing the influence of serum concentration on the percentage of micromotors found in the serum solution which exhibited either bubble ejection (blue bar) or motion (red bar). (D) A graph showing the influence of the serum concentration on the velocity of the moving micromotors. Note that the ‘‘Control’’ experiment was carried out in phosphate buffer saline solution (pH 7.2), while notation the ‘‘Blood’’ means the concentration of red blood cells typical for blood (~ 5×10^6 cell μL^{-1}). Conditions in all of the experiments: temperature of 23^oC, 3 wt % H_2O_2 and 1 wt % SDS.

In summary, we have discussed the challenges facing the motion of micromotors in blood. It was discovered that catalytic micromotors in fact show no motion in blood, which is contrary behavior to the very agile micromotors in phosphate buffer solution. By investigating the major components of blood, such as red blood cells and serum separately, it was found that both components, independently of each other, cripple the ability of the micromotors to move even at very high dilutions. For the case of red blood cells, the possible reason for such motion inhibition can be due to the blocking of tube ends with the cells; for the case of blood serum, attachment of serum protein molecules onto the Pt surface may reduce the available surface and also poison the Pt catalyst. Therefore, such motion inhibition can be originated from both chemical and physical reactions. While it is possible that future micromotors with higher propulsion strength will be developed and their viability in blood may exhibit higher magnitude, it is very likely that qualitatively, the general trends of suppressing the motion/viability of micromotors would be persistent. These findings suggest that future research in the area of biomedical applications of these autonomous devices should focus not only on the

search for new fuels, but also on overcoming the problems related to the impact on the motion of these micromotor systems due to the presence of the red blood cells and serum proteins. Furthermore, future studies should also take into account specific and non-specific reactions of the immune system to micromotors caused by components of the blood, that were not taken into account during this study.

5.7 References

(1) Orozco, J.; Campuzano, S.; Kagan, D.; Zhou, M.; Gao, W.; Wang, J.: Dynamic isolation and unloading of target proteins by aptamer-modified microtransporters. *Anal. Chem.* **2011**, *83*, 7962-9.

(2) Balasubramanian, S.; Kagan, D.; Jack Hu, C.-M.; Campuzano, S.; Lobo-Castañon, M. J.; Lim, N.; Kang, D. Y.; Zimmerman, M.; Zhang, L.; Wang, J.: Micromachine-Enabled Capture and Isolation of Cancer Cells in Complex Media. *Angew. Chem. Int. Ed.* **2011**, *50*, 4161-4164.

(3) Orozco, J.; Jurado-Sánchez, B.; Wagner, G.; Gao, W.; Vazquez-Duhalt, R.; Sattayasamitsathit, S.; Galarnyk, M.; Cortés, A.; Saintillan, D.; Wang, J.: Bubble-Propelled Micromotors for Enhanced Transport of Passive Tracers. *Langmuir* **2014**, *30*, 5082-5087.

(4) Garcia, M.; Orozco, J.; Guix, M.; Gao, W.; Sattayasamitsathit, S.; Escarpa, A.; Merkoci, A.; Wang, J.: Micromotor-based lab-on-chip immunoassays. *Nanoscale* **2013**, *5*, 1325-31.

(5) Gao, W.; Sattayasamitsathit, S.; Orozco, J.; Wang, J.: Efficient bubble propulsion of polymer-based microengines in real-life environments. *Nanoscale* **2013**, *5*, 8909-14.

(6) Orozco, J.; Cortés, A.; Cheng, G.; Sattayasamitsathit, S.; Gao, W.; Feng, X.; Shen, Y.; Wang, J.: Molecularly Imprinted Polymer-Based Catalytic Micromotors for Selective Protein Transport. *J. Am. Chem. Soc.* **2013**, *135*, 5336-5339.

(7) Liu, Z.; Li, J.; Wang, J.; Huang, G.; Liu, R.; Mei, Y.: Small-scale heat detection using catalytic microengines irradiated by laser. *Nanoscale* **2013**, *5*, 1345-52.

(8) Solovev, A. A.; Sanchez, S.; Schmidt, O. G.: Collective behaviour of self-propelled catalytic micromotors. *Nanoscale* **2013**, *5*, 1284-1293.

(9) Baraban, L.; Harazim, S. M.; Sanchez, S.; Schmidt, O. G.: Chemotactic Behavior of Catalytic Motors in Microfluidic Channels. *Angew. Chem. Int. Ed.* **2013**, *52*, 5552-5556.

(10) Soler, L.; Magdanz, V.; Fomin, V. M.; Sanchez, S.; Schmidt, O. G.: Self-Propelled Micromotors for Cleaning Polluted Water. *ACS Nano* **2013**, *7*, 9611-9620.

(11) Solovev, A. A.; Xi, W.; Gracias, D. H.; Harazim, S. M.; Deneke, C.; Sanchez, S.; Schmidt, O. G.: Self-propelled nanotools. *ACS Nano* **2012**, *6*, 1751-6.

(12) Orozco, J.; Garcia-Gradilla, V.; D'Agostino, M.; Gao, W.; Cortes, A.; Wang, J.: Artificial enzyme-powered microfish for water-quality testing. *ACS Nano* **2013**, *7*, 818-24.

(13) Soler, L.; Magdanz, V.; Fomin, V. M.; Sanchez, S.; Schmidt, O. G.: Self-propelled micromotors for cleaning polluted water. *ACS Nano* **2013**, *7*, 9611-20.

(14) Paxton, W. F.; Sundararajan, S.; Mallouk, T. E.; Sen, A.: Chemical locomotion. *Angew. Chem. Int. Ed.* **2006**, *45*, 5420-9.

(15) Gao, W.; Kagan, D.; Pak, O. S.; Clawson, C.; Campuzano, S.; Chuluun-Erdene, E.; Shipton, E.; Fullerton, E. E.; Zhang, L.; Lauga, E.; Wang, J.: Cargo-Towing Fuel-Free Magnetic Nanoswimmers for Targeted Drug Delivery. *Small* **2012**, *8*, 460-467.

(16) Kagan, D.; Laocharoensuk, R.; Zimmerman, M.; Clawson, C.; Balasubramanian, S.; Kang, D.; Bishop, D.; Sattayasamitsathit, S.; Zhang, L.; Wang, J.:

Rapid delivery of drug carriers propelled and navigated by catalytic nanoshuttles. *Small* **2010**, *6*, 2741-7.

(17) Balasubramanian, S.; Kagan, D.; Hu, C. M.; Campuzano, S.; Lobo-Castanon, M. J.; Lim, N.; Kang, D. Y.; Zimmerman, M.; Zhang, L.; Wang, J.: Micromachine-enabled capture and isolation of cancer cells in complex media. *Angew. Chem. Int. Ed.* **2011**, *50*, 4161-4.

(18) Sanchez, S.; Solovev, A. A.; Schulze, S.; Schmidt, O. G.: Controlled manipulation of multiple cells using catalytic microbots. *Chem. Commun.* **2011**, *47*, 698-700.

(19) Xi, W.; Solovev, A. A.; Ananth, A. N.; Gracias, D. H.; Sanchez, S.; Schmidt, O. G.: Rolled-up magnetic microdrillers: towards remotely controlled minimally invasive surgery. *Nanoscale* **2013**, *5*, 1294-1297.

(20) Zhao, G.; Pumera, M.: Reynolds numbers exhibit dramatic influence on directionality of movement of self-propelled systems. *Phys. Chem. Chem. Phys.* **2012**, *14*, 6456-6458.

(21) Sanchez, S.; Ananth, A. N.; Fomin, V. M.; Viehrig, M.; Schmidt, O. G.: Superfast motion of catalytic microjet engines at physiological temperature. *J. Am. Chem. Soc.* **2011**, *133*, 14860-3.

(22) Happel, J., Brener, H.: *Low Reynolds number hydrodynamics, with special applications to particulate media*; Kluwer: Norwell, MA, 1983.

(23) Lide, D. R.: *CRC Handbook of Chemistry and Physics*; 92 ed.; CRC, 2011.

(24) Ismagilov, R. F.; Schwartz, A.; Bowden, N.; Whitesides, G. M.: Autonomous Movement and Self-Assembly. *Angew. Chem. Int. Ed.* **2002**, *41*, 652-654.

(25) Mei, Y.; Solovev, A. A.; Sanchez, S.; Schmidt, O. G.: Rolled-up nanotech on polymers: from basic perception to self-propelled catalytic microengines. *Chem. Soc. Rev.* **2011**, *40*, 2109-2119.

(26) Craig, B. D., Aderson, D. S.: *Handbook of Corrosion Data*, 1995.

(27) Nham, T. T.: American Spectroscopy Laboratory: Typical Detection Limits for an ICP-MS. *Am. Lab.* **1998**, *30*, 17A.

(28) Gao, W.; Sattayasamitsathit, S.; Wang, J.: Catalytically propelled micro-/nanomotors: how fast can they move? *Chem. Rec.* **2012**, *12*, 224-31.

(29) Solovev, A. A.; Sanchez, S.; Pumera, M.; Mei, Y. F.; Schmidt, O. G.: Magnetic Control of Tubular Catalytic Microbots for the Transport, Assembly, and Delivery of Micro-objects. *Adv. Func. Mater.* **2010**, *20*, 2430-2435.

(30) Kagan, D.; Benchimol, M. J.; Claussen, J. C.; Chuluun-Erdene, E.; Esener, S.; Wang, J.: Acoustic droplet vaporization and propulsion of perfluorocarbon-loaded microbullets for targeted tissue penetration and deformation. *Angew. Chem. Int. Ed.* **2012**, *51*, 7519-22.

(31) Guix, M.; Orozco, J.; Garcia, M.; Gao, W.; Sattayasamitsathit, S.; Merkoci, A.; Escarpa, A.; Wang, J.: Superhydrophobic alkanethiol-coated microsubmarines for effective removal of oil. *ACS Nano* **2012**, *6*, 4445-51.

(32) Solovev, A. A.; Mei, Y.; Bermudez Urena, E.; Huang, G.; Schmidt, O. G.: Catalytic microtubular jet engines self-propelled by accumulated gas bubbles. *Small* **2009**, *5*, 1688-92.

(33) Weiss, J.: The Free Radical Mechanism in the Reactions of Hydrogen peroxide. In *Advances in Catalysis*; W.G. Frankenburg, V. I. K., Rideal, E. K., Eds.; Academic Press, 1952; Vol. Volume 4; pp 343-365.

(34) Foroutan-Nejad, C.; Badri, Z.; Shahbazian, S.; Rashidi-Ranjbar, P.: The Laplacian of electron density versus NICSzz scan: measuring magnetic aromaticity among molecules with different atom types. *J. Phys. Chem. A.* **2011**, *115*, 12708-14.

(35) Yoshimura, Y.; Inomata, T.; Nakazawa, H.; Kubo, H.; Yamaguchi, F.; Ariga, T.: Evaluation of free radical scavenging activities of antioxidants with an

H(2)O(2)/NaOH/DMSO system by electron spin resonance. *J. Agric. Food Chem.* **1999**, *47*, 4653-6.

(36) Sanchez, S.; Solovev, A. A.; Harazim, S. M.; Deneke, C.; Mei, Y. F.; Schmidt, O. G.: The smallest man-made jet engine. *Chem. Rec.* **2011**, *11*, 367-70.

(37) Grove, D. E.: Catalysts — Myths and Realities. *Platinum Metals. Rev.* **2003**, *47*.

(38) Dunleavy, J. K.: Final Analysis: Sulfur as a Catalyst Poison. *Platinum Metals Rev.* **2006**, *50*, 110-110.

(39) Oktyabrsky, O. N.; Smirnovam, G. V.; Muzyka, N. G.: Role of glutathione in regulation of hydroperoxidase I in growing Escherichia coli. *Free Radic. Bio.l Med.* **2001**, *31*, 250-5.

(40) Toussaint, B.; Pitti, C.; Streel, B.; Ceccato, A.; Hubert, P.; Crommen, J.: Quantitative analysis of N-acetylcysteine and its pharmacopeial impurities in a pharmaceutical formulation by liquid chromatography-UV detection-mass spectrometry. *J. Chromatogr. A* **2000**, *896*, 191-9.

(41) Nekrassova, O.; Lawrence, N. S.; Compton, R. G.: Analytical determination of homocysteine: a review. *Talanta* **2003**, *60*, 1085-95.

(42) Luo, D.; Smith, S. W.; Anderson, B. D.: Kinetics and mechanism of the reaction of cysteine and hydrogen peroxide in aqueous solution. *J. Pharm. Sci.* **2005**, *94*, 304-16.

(43) Erickson, L. E.; Bailey, P. D.; Kimball, T. L.; Morgan, B. R.: Stereochemistry of platinum complexes of the neutral amino acids allylglycine, S-methylcysteine, methionine, and corresponding sulfoxides. *Inorg. Chim. Acta* **2003**, *346*, 169-180.

(44) Mei, Y.; Huang, G.; Solovev, A. A.; Ureña, E. B.; Mönch, I.; Ding, F.; Reindl, T.; Fu, R. K. Y.; Chu, P. K.; Schmidt, O. G.: Versatile Approach for Integrative

and Functionalized Tubes by Strain Engineering of Nanomembranes on Polymers. *Adv. Mater.* **2008**, *20*, 4085-4090.

(45) Wang, J.; Gao, W.: Nano/Microscale motors: biomedical opportunities and challenges. *ACS Nano* **2012**, *6*, 5745-51.

(46) Kuralay, F.; Sattayasamitsathit, S.; Gao, W.; Uygun, A.; Katzenberg, A.; Wang, J.: Self-propelled carbohydrate-sensitive microtransporters with built-in boronic acid recognition for isolating sugars and cells. *J. Am. Chem. Soc.* **2012**, *134*, 15217-20.

(47) Kuralay, F.; Sattayasamitsathit, S.; Gao, W.; Uygun, A.; Katzenberg, A.; Wang, J.: Self-Propelled Carbohydrate-Sensitive Microtransporters with Built-In Boronic Acid Recognition for Isolating Sugars and Cells. *J. Am. Chem. Soc.* **2012**, *134*, 15217-15220.

(48) Campuzano, S.; Orozco, J.; Kagan, D.; Guix, M.; Gao, W.; Sattayasamitsathit, S.; Claussen, J. C.; Merkoci, A.; Wang, J.: Bacterial isolation by lectin-modified microengines. *Nano lett.* **2012**, *12*, 396-401.

(49) Orozco, J.; Vilela, D.; Valdés-Ramírez, G.; Fedorak, Y.; Escarpa, A.; Vazquez-Duhalt, R.; Wang, J.: Efficient Biocatalytic Degradation of Pollutants by Enzyme-Releasing Self-Propelled Motors. *Chem. Eur. J.* **2014**, *20*, 2866-2871.

(50) Soler, L.; Sanchez, S.: Catalytic nanomotors for environmental monitoring and water remediation. *Nanoscale* **2014**, *6*, 7175-7182.

(51) Sen, A.; Ibele, M.; Hong, Y.; Velegol, D.: Chemo and phototactic nano/microbots. *Faraday Discuss.* **2009**, *143*, 15-27; discussion 81-93.

(52) Mueller, M. M.; Seifried, E.: Blood transfusion in Europe: basic principles for initial and continuous training in transfusion medicine: an approach to an European harmonisation. *Transfus. Clin. Biol.* **2006**, *13*, 282-5; quiz 286-9.

(53) Alberts, B., Johson, A., Lewis, J., Raff, M., Roberts, K., Walter, P.: *Molecular biology of the cell*; 4 ed.; Taylor & Francis: New York, 2002.

(54) Batchelor, G. K.: *An Introduction to Fluid Dynamics*; Cambridge University Press: Cambridge, England, 1967.

Chapter 6 Summary and Outlook

6.1 Summary

The design and development of small motors have received significant advancement in the past decades. These motors offer a great potential for lots of real-world applications that will eventually benefit all mankind. Therefore, although the research in small motors is still at early stage and some distance from real performances, it is of high value and importance to push forward this research field and develop more state-of-art motors. Scientists have strived to improve the power thrust, explore more biocompatible fuels, achieve better manipulation of motion, as well as to functionalize the motors with higher ability for applications. The projects involved in this thesis were all focused on the design, fabrication, motion study and showcase of applications of the small motors.

In the development of millimeter scale motors, the polymer capsule structures were adapted. Fabrication of such motors is simply based on the phase-inversion of polysulfone molecules, and the mechanism of motion is originated from the Marangoni effect, whereby a difference in surface tension leads to a net force, which drives the motors to move forward. Methods in the motion investigation of such motors are significantly different from the nano-/micromotors – a microscope is not required for the record of videos. Instead, a normal video recorder is used. These motors were observed to show a high velocity in their motion, and the motion can last for as long as around half an hour, effectively covering a long path length. Different factors affecting the motion were also explored, including the solvents in the running medium, composition of the capsule itself,

as well as the temperature or viscosity of the medium. Also, interactions between the normal and SDS-incorporated capsules were also shown. The latter was found to repulse the oil droplets, leading to a practical application of cleaning the water surface contaminated with oil. Moreover, the capsule motors were also test in different running schemes, namely the oil-water interface, and in a maze channel. Magnetic manipulation of motion and sense/act against chemicals were also illustrated. Finally, the observed enhanced diffusion of pollutants was also shown, which was also based on the Marangoni effect to run.

For the research in nano-/micromotors, the tubular-shaped motors were the center of our focus. Such motors are powered by the chemical decomposition of the fuel molecule: hydrogen peroxide. The catalytic decomposition of hydrogen peroxide at the platinum surface of the motors generates oxygen bubbles, which provide a pushing force while ejected from the end of tubes. As this pushing force works as the driving force for their motion, it is thus the driving force for this type of motors, which are therefore named as the bubble-propelled nano-/micromotors. Two different routes were developed for the fabrication of such motors, namely the electrodeposition route, and the lithography route, both were developed based on the previously report methodologies. The effect of fuel concentration on motion velocity of these tubes was reported. And the impact of viscosity of the running medium and the Reynolds number on the motion styles of micromotors was also seen. Moreover, the ferromagnetic properties of such tubular motors were utilized to a great extent in the research projects, and magnetization of the ferromagnetic materials in the tubes was observed for both the micromotors and the nanomotors. What's more, the magnetized micromotors were even found capable of selective catching of large amount of paramagnetic beads from a pool of different beads, and this can be one of the practical applications of such tubular motors. The environment for the motors was seen to

show negative effects on the motors. Firstly, corrosion of metallic materials in the tubes was detected and illustrated. Secondly, presence of certain organic/inorganic molecules in the liquid can significant hamper the motion of the tubes, and the influence at different concentrations was shown in this thesis. Thirdly, there is some reduction of motion ability, in terms of both amount of running motors and velocity of the motors, while trying to run such tubular micromotors in real environments, ranging from tap water, lake water, sea water, rain water, to human blood, red blood cell suspensions, as well as serum.

6.2 Outlook

Small motors have been shown to possess the potential for a wide range of applications. Nevertheless, a few limitations are still present that stopped these motors from deployed into real-world applications. Thus, more efforts in the research and development of such small motors are needed and it can be foreseen that the whole society can be benefited in many ways.

Currently, the development of small motors is faced with many challenges. Firstly, a powerful and bio-compatible fuel is desired so that such motors can be run in biological systems. Hydrogen peroxide has been used extensively as it can be easily decomposed with the presence of catalyst to generate oxygen bubbles. However, the toxic effect towards biological systems is significant as hydrogen peroxide is an oxidizing agent. Therefore, in order to deploy the motors in the real applications, especially in the biological systems, powerful fuel molecules that are harmless to the environment are demanded. Other than hydrogen peroxide, possible candidates for such fuels can be glucose or adenosine triphosphate (ATP), as such molecules are all present in the biological system. Thus we can see in the future work that the catalytic utilization of such molecules should be achieved with high efficiency. Secondly, the poisoning or hampering

effect from molecules present in the running medium can significantly reduce the mobility of motors, which places another serious challenge on the research in this field. The factors affecting the motion can be both physical and chemical. For the physical inhibition, adsorption of molecules or materials onto the active surface plays a key role; for the chemical inhibition, poisoning of catalyst or quenching of radicals were shown to significantly affect the reaction and reduce the mobility of motors. Better design of the motor structures should be sought to reduce the possibility of both of these two inhibiting routes. Thirdly, control of the motion in speed, direction, as well as the styles is highly desirable, to ensure that such motors can reach desired destinations in a timely manner. The manipulation of speed has been mainly focused on the available amount of fuel molecules, which can be limited by the composition of the running liquid. Future directions should consider pre-loading the fuel molecules into the motors so that a more efficient control of speed can be achieved. In terms of motion direction, other than utilizing the magnetic field to control the motors, it is also possible to expand the possibilities and study on other action-at-a-distance forces or fields, such as the electric force or the ultrsonication energy. Lastly, more bio-compatible materials for the motors should also be developed that can not only counter the corrosion by the surrounding liquid, but are also not generating any toxic elements to the environments.

It is hoped that small motors of different sizes are moving smartly in different environments, carrying with them the cargoes or tasks, to the future destinations that human beings are looking forward to.